

**Disequilibrium melting of plagioclase during biotite fluid-absent
anatexis of metapelites in the South Marginal Zone of the
Limpopo belt, South Africa**

by
Nonkuselo Madlakana

*Thesis presented in partial fulfilment of the requirements for
the degree of Master of Science in the Department of Earth
Sciences at Stellenbosch University*



Supervisor: Prof Gary Stevens

March 2016

DECLARATION

By submitting this thesis electronically, I declare that the entirety of the work contained therein is my own, original work, that I am the sole author thereof (save to the extent explicitly otherwise stated), that reproduction and publication thereof by Stellenbosch University will not infringe any third party rights and that I have not previously in its entirety or in part submitted it for obtaining any qualification.

Signature:

Date: March 2016

ABSTRACT

This study investigated the behaviour of plagioclase during fluid-absent biotite melting in a metapelitic source from which peraluminous granite magma had segregated. The study focused on the Bandelierkop Quarry (South Marginal Zone of the Limpopo belt), where stromatic and discordant nebulous leucosomes contain peritectic garnet crystals produced by the following melting reactions; $Bt + Sil + Qtz + Pl = Grt + Ilm + Melt$; and, $Bt + Qtz + Pl = Grt + Ilm + Opx + Crd + Melt$. In rare cases, large (10 to 20mm) garnet crystals within both leucosome types are growth zoned. These garnet crystals host plagioclase inclusions, which are commonly euhedral and occur as single crystals, clusters of crystals and as polymineralic inclusions which typically consist of biotite, rutile and orthopyroxene. The inclusions display considerable chemical heterogeneity. Matrix plagioclase in both leucosome types ranges in composition from An_{27} to $_{35}$, whilst that in the residuum adjacent to the leucosomes ranges from An_{32} to $_{39}$. Euhedral plagioclase inclusions are considerably more calcic with compositions that range from An_{50} to $_{83}$. Composition of the inclusions shows no relationship with position within the garnet crystal, or with size of the plagioclase crystal. These crystals are also significantly zoned, yet their zoning is not systematic, with inclusions displaying both Na- and Ca-enriched rims. Garnet zonation around the inclusions was investigated in detail and demonstrates that the Ca-rich nature of the inclusions is not a consequence of Ca-uptake from garnet. In contrast, anhedral plagioclase within large amoeboid polymineralic inclusions displays compositions similar to the matrix plagioclase. Garnet also hosts very small ($\leq 10\mu m$) inclusions of quartz + plagioclase \pm biotite. These micro-granite inclusions are interpreted as melt inclusions.

The complexity of plagioclase behaviour recorded within the peritectic garnet crystals is interpreted to reflect disequilibrium during anatexis due to slow diffusion in plagioclase; only the outer portions of the plagioclase crystals participate in the melting reaction and they do so by combined dissolution and precipitation of new, Ca-rich crystals. Modelling demonstrates that the Ca-contents of these new crystals is inversely proportional to the amounts of plagioclase that participate in the reaction. Consequently, the euhedral plagioclase inclusions are interpreted to be peritectic, where these occur as polymineralic inclusions they are small and plagioclase is volumetrically dominant, so the melt volume in the inclusion was low. The more Ca-rich rims in euhedral plagioclase inclusions may reflect zonation produced by the melting reaction, whilst Na-rich rims may reflect crystals that are too calcic to equilibrate with melt within the time-scale available for melting, the volume of equilibrium is extremely locally controlled, which in turn induces Na-rich rims. The preservation of these garnet

crystals, possibly due to rapid and efficient melt loss from the leucosome structures, provides a rare insight into the details of the anatectic process. In the vast majority of migmatitic granulites these are lost due to comprehensive extensive recrystallization and homogenization of mineral compositions.

UITTREKSEL

Hierdie studie ondersoek die gedrag van plagioklaas gedurende vloeistof-vrye biotiet smelting in 'n metapelitiese bron vanwaar peraluminous graniet magma geskei het. Die studie fokus op die Bandelierkop Steengroef (Suid Marginale Zone van die Limpopo belt), waar stromatiese en afwykende newelagtige leukosome peritektiese granaatkristalle bevat wat produseer is deur die volgende smeltingsreaksies; $Bt + Sil + Qtz + Pl = Grt + Ilm + Smelt$; en, $Bt + Qtz + Pl = Grt + Ilm + Opx + Crd + Smelt$. In seldsame gevalle is groot (10 tot 20mm) granaatkristalle vanuit beide leukosoom tipes gesoneer tydens die groeiproses. Hierdie granaatkristalle bevat plagioklaas insluitings wat in die algemeen euëdries is en as enkel kristalle, kristal clusters en as polimineraliese insluitings wat tipies bestaan uit biotiet, rutiel en ortopirokseen. Die insluitings vertoon aansienlike chemiese heterogeniteit. Matriks plagioklaas in beide leukosoom tipes vertoon 'n reeks komposisies van An 27 tot 35, waaartydens die in die residium aangrensend tot die leukosome verskil van An 32 tot 39. Euëdriese plagioklaaskristalle is aansienlik meer kalies met 'n reeks komposisies van An 50 tot 83. Komposisies van die insluitings wys geen verhouding met posisie binne die granaat kristal of met die grootte van die plagioklaas kristal nie. Hierdie kristalle is ook merkwaardiglik gesoneer maar die sonering is nie sistematies nie, waar die insluitings beide Na en Ca-ryke vellings vertoon. Granaat sonering rondom die insluitings was in detail ondersoek en dit demonstreer dat die Ca-ryke natuur van die insluitings nie 'n oorsaak van Ca-opname vanaf granaat is nie. In kontras vertoon die oneievormige plagioklaas vanbinne groot amobidale polimineraliese insluitings komposisies soortgelyk aan die matriks plagioklaas. Granaat bevat ook baie fyn ($\leq 10\mu m$) isometriese insluitings van quartz + plagioklaas \pm biotiet. Hierdie mikrogranietinsluitings word as smeltingsinsluitings geïnterpreteer.

Die kompleksiteit van die gedrag van plagioklaas is aangeteken vanbinne die peritektiese granaatkristalle en is geïnterpreteer as die refleksie van onewewigtigheid gedurende anateksis as gevolg van stadige diffusie in plagioklaas. Slegs die buitenste gedeelte van die plagioklaaskristalle neem deel aan die smeltingsreaksie en hul doen dit deur gekombineerde ontbinding en presipitasie van nuwe Ca-ryke kristalle. Modelling demonstreer dat die Ca-inhoud van hierdie nuwe kristalle omgekeerd eweredig is tot die hoeveelheid plagioklaas wat deel neem aan die reaksie. Gevolglik is die euëdriese plagioklaas insluitings as peritekties geïnterpreteer. Waar hierdie voor kom as polimineraliese insluitings, is hulle klein en plagioklaas is volumeries dominant, so die smelt volume in die insluiting was klein. Die meer Ca-ryke vellings in euëdriese plagioklaasinsluitings mag sonering as gevolg van die smeltingsreaksie reflekteer, waartydens Na-ryke vellings die kristalle reflekteer wat te kalies is om

te ekwilibreer met die smelt. Die volume van ewewig is uiters plaaslik beheer wat dan Na-ryke vellings insluit. The bewaring van hierdie unieke granaatkristalle, moontlik as gevolg van spoedige en effektiewe verlies aan smelt van die leukosoomstrukture, bied 'n rare insig in die proses van anatekse. In die oorweldigende meerderheid van magmatiese granuliete is hierdie kirstalle verlore as gevolg van omvattende uitgebreide herkristallasie en homogenisering van mineraalkomposisies.

ACKNOWLEDGMENTS

This research was supported by the South African National Research Foundation (NRF) in the form of grant to Professor Gary Stevens via SARChI programme and an MSc bursary to Nonkuselo Madlakana. I would like to acknowledge support from my supervisor Prof. Gary Stevens for his continuous ideas and for providing invaluable insight into the findings of this study. This thesis would not have been completed without your continuous ideas. Special thanks go to: Sara Burness for providing your time on proofreading my thesis, Dr. Marcos Garcia Arias your assistance during the modelling calculations, Dr. Nicoli Gautier for providing some diagrams used in this study and Dr. Jeanne Taylor for providing trace element data. Thank you to Priscilla L. Ramphaka, Madelaine Frazenburg and Prof. Dirk Frei for your help with my analytical acquisitions.

I would also like to thank Worship Mugido for his invaluable support from the day I started Geology to this day. You have been more than a friend to me, thank you for your time and support, life will be meaningless without plagioclase, thanks Mr. Ostrich. I would like to thank all my friends for their support. I would also like to thank my family particularly my late father Nonteki for believing in me. Ndiyabulela Ntlane wanga umphefumlo wakho ungalala ngoxolo. To my mom Nonagethi enkosi Tshawekazi ngemfundiso zakho, ngothando lwakho nange mithandazo ngaphandle kwakho ngendinekho apha ngoku. Ndibulela bonke abantwana basekhaya ngenxaso yabo.

TABLE OF CONTENTS

DECLARATION	i
ABSTRACT	ii
UITTREKSEL	iv
ACKNOWLEDGMENTS	vi
TABLE OF CONTENTS	vii
LIST OF FIGURES	x
LIST OF TABLES	xvi
LIST OF EQUATIONS	xvii
1. INTRODUCTION	1
2. GEOLOGICAL SETTING	6
2.1. <i>Geology of the SMZ</i>	6
2.1.1. <i>Previous studies on the SMZ granulites facies rocks</i>	9
2.1.1.1. <i>Timing of metamorphism in the Bandelierkop formation</i>	10
2.1.2. <i>Partial melting of the Bandelierkop metasediments</i>	12
2.1.2.1. <i>The composition of the leucosomes</i>	13
3. DETAILS OF THE PLAGIOCLASE INCLUSIONS IN GARNET	17
3.1. <i>General petrography of the large poikiloblastic garnet crystals</i>	17
3.2. <i>Stromatitic leucosomes</i>	20
3.2.1. <i>L2t-6</i>	20
3.2.2. <i>L2t-7</i>	22
3.3. <i>Nebulitic leucosomes</i>	23
3.4. <i>Residues</i>	25
4. ANALYTICAL METHODS	26
4.1. <i>Electron beam analyses</i>	26
4.2. <i>LA-ICP-MS</i>	27
4.3. <i>Modelling</i>	30
5. CHEMISTRY OF THE GARNET	31
5.1. <i>Major element chemistry</i>	31

5.1.1.	<i>Stromatitic leucosomes</i>	32
5.1.1.1.	<i>L2t-6</i>	32
5.1.1.2.	<i>L2t-7</i>	34
5.1.2.	<i>Nebulitic leucosomes</i>	35
5.2.	<i>LA-IC PMS</i>	38
5.2.1.	<i>L2t-6</i>	40
5.2.2.	<i>Nebulitic leucosomes</i>	42
5.2.3.	<i>Residues</i>	44
6.	CHEMISTRY OF PLAGIOCLASE INCLUSIONS	46
6.1.	<i>Stromatitic leucosomes</i>	50
6.1.1.	<i>L2t-6</i>	50
6.1.2.	<i>L2t-7</i>	51
6.2.	<i>Nebulitic leucosomes</i>	52
6.3.	<i>Residues</i>	54
6.4.	<i>The relationship between plagioclase inclusion sizes and their anorthite content</i>	55
7.	DETAILS OF GARNET AND PLAGIOCLASE ZONATION IN THE VICINITY OF ZONED PLAGIOCLASE INCLUSIONS	57
7.1.	<i>Inclusions that increase in anorthite towards the rims</i>	57
7.2.	<i>Inclusions that decrease in anorthite towards the rims</i>	62
8.	DISCUSSION	64
8.1.	<i>Origin of garnet</i>	64
8.2.	<i>Major element zoning in garnet</i>	64
8.3.	<i>Trace element disequilibrium in garnet</i>	66
8.4.	<i>Biotite inclusions within garnet</i>	69
8.5.	<i>The origin of the plagioclase inclusions within garnet</i>	70
8.6.	<i>Plagioclase petrogenesis and disequilibrium melting</i>	71
8.7.	<i>Are the compositions of the plagioclase inclusions affected by Ca exchange with garnet</i>	76
8.8.	<i>The composition of plagioclase inclusions</i>	78
9.	GENERAL CONCLUSIONS	80
10.	REFERENCES	82
11.	APPENDICES	90

APPENDIX A	91
APPENDIX B.....	93
APPENDIX B-1	104
APPENDIX C.....	110
APPENDIX D	112
APPENDIX E.....	122
APPENDIX F.....	164

LIST OF FIGURES

Figures	Pages
1. A simplified geological map of the SMZ modified from Stevens et al., 1997. The locality of the Bandelierkop quarry (Ba) is indicated by the red dot.....	9
2. P-T-t path for the SMZ metasedimentary rocks (modified from Nicoli et al., 2014). The P-T path for the metapelites of the Bandelierkop quarry is adapted from Taylor et al. (2014) and has been added for comparison. Comparatively, the Matok age from Laurent et al. (2013) and the retrograde age from Kreissig et al. (2001) are also portrayed.....	11
3. (a) A photograph of the western face of the Bandelierkop Quarry, illustrating the relationship between the metapelitic and semipelitic layers which host the stromatic and nebulitic leucosomes (modified from Taylor et al., 2014). The stars indicate where the samples were taken. (b) Large garnet enclosed by cordierite within a stromatic leucosomes. (c) Garnet crystals within nebulitic leucosomes.	13
4. (a-b) The composition of the BQ leucosomes from Taylor et al. (2014) relative to fluid-absent experimental melt compositions produced from a wide range of metasedimentary starting materials between 775 and <900°C and 1-15 kbar (Montel & Vielzeuf, 1997; Patiño Douce and Beard, 1996; Patiño Douce & Harris, 1998; Patiño Douce and Johnston, 1991; Pickering and Johnston, 1998; Stevens et al., 1997; Vielzeuf and Holloway, 1988). Also shown are the natural glass compositions that show homogenized melt inclusions and glassy inclusions within peritectic minerals from natural migmatites, generated between 700 and 860°C and 5-8 kbar (Acosta-Vigil et al., 2007; Bartoli et al., 2013; Ferrero et al., 2012). (a-b) Also illustrates granulite-facies leucosome compositions from metasedimentary migmatites, where partial melting is well understood through fluid-absent incongruent melting of biotite (at >750-900°C and 4-12kbar). Other compositions were excluded to avoid uncertainties related to partial melting of UHT, or the amphibolite facies (from Taylor et al., 2014). (c) Two models for the behaviour of plagioclase during incongruent biotite breakdown in the BQ (modified from Taylor et al., 2014). In the first scenario, peritectic, more calcic plagioclase is produced at the site of plagioclase melting in the source rock. A proportion of the peritectic plagioclase, together with peritectic garnet is entrained to the magma and transported to the site of magma accumulation. The melt is lost from the leucosomes, resulting in low K ₂ O leucosomes. The remaining melt crystallizes quartz, plagioclase and K-feldspar and may also participate in biotite producing retrograde reactions with ferromagnesian minerals in the residuum. In this scenario, K and Si contents of the leucosomes prior to retrograde reactions in the residuum are linked in that both reflect the volume of melt remaining in the leucosome. Thus, the Si content of the leucosomes is low. The second scenario, the melting of plagioclase in the source produces more calcic melt than in the scenario described above. Peritectic plagioclase precipitates within the leucosomes. Quartz co-precipitation from the melt is induced by the precipitation of	

- plagioclase, as the content of Si increases in the melt. Most of the melt escape from the leucosomes producing low K₂O leucosomes with no correlation between the quartz and K-feldspar mode (Fig. 4d-e). The latter scenario, peritectic garnet is grown in the source and entrained to the magma. The leucosome compositions are low in K, but have Si values similar to those of the experimental melts.....16
5. Thin section photomicrographs illustrating the occurrence and textural characteristic of mineral assemblages in the leucosomes. (A) Garnet is partially replaced by cordierite within the stromatic leucosomes. Cordierite is subsequently replaced by a fine-grained fibrous intergrowth of kyanite, orthoamphibole, biotite and quartz. (B) Garnet on the stromatic leucosomes margins. (C) Sample L5GR-3, showing the replacement of garnet by orthopyroxene and cordierite. Two generations of orthopyroxene are identified; a coarse-grained orthopyroxene surrounding garnet and a symplectitic intergrowth of orthopyroxene and cordierite. Cordierite is replaced by biotite, orthoamphibole and kyanite. Mineral abbreviation from Kretz (1983).19
 6. BSE images showing textural characteristics of plagioclase inclusions in garnet. (A) A single euhedral plagioclase inclusion in garnet. Zonation is seen in this BSE image; brighter = higher average atomic mass, and represents a more Ca-rich domain within the plagioclase. (B) Plagioclase in association with other polymineralic inclusions. (C-D) Euhedral plagioclase inclusions in contact with quartz. (E) Anhedral plagioclase crystals within garnet. (F) Fine-grained euhedral inclusion in garnet. Mineral abbreviations from Kretz (1983).21
 7. BSE image illustrating the locality of mineral inclusions within garnet. Mineral abbreviation from Kretz (1983). (A) Show magnified image of the melt inclusions within garnet.22
 8. BSE images displaying textural features between plagioclase inclusions and the garnet host. (A) Plagioclase inclusion with complex zonation. Brighter = higher average atomic mass, and represents a more Ca-rich domain within the plagioclase. (B) Euhedral plagioclase inclusion in contact with quartz. (C) Plagioclase crystal that mimics the garnet symmetry. (D) Euhedral plagioclase inclusion. Mineral abbreviation from Kretz (1983).....23
 9. BSE images illustrating the textural relationships between the plagioclase inclusions in garnet. (A) Euhedral plagioclase inclusion in contact with quartz. (B-C) Monomineralic euhedral plagioclase crystals within garnet. (D-E) Euhedral plagioclase crystals clustered with other polymineralic inclusions. (F) Larger anhedral plagioclase crystal in contact with and enclosing quartz. (G) Anhedral plagioclase inclusion partially enclosed by quartz. Mineral abbreviation from Kretz (1983).24
 10. BSE images presenting textural relationships between plagioclase inclusions and the garnet host. (A) Larger anhedral plagioclase crystals enclosing a quartz inclusion. (B) Euhedral plagioclase inclusion. (C) Euhedral plagioclase inclusion enclosing fine-grained biotite inclusions. (D) Euhedral plagioclase inclusion. Mineral abbreviation from Kretz (1983).....25

11. Normalized rem preferred values of the USGS reference materials; BCR-2 and NIST SRM 612, relative to the original standard values of BCR-2 and NIST SRM 612. Values deviating ± 0.5 from the normalized rem preferred standard values (1.0) are considered good values i.e. Ti. in b. Most element concentrations agree within uncertainty limits of $\sim 1-5\%$29
12. Details of compositional variation in garnet from sample L2t-6. (a) A quantitative spot analysis of a garnet traverse. (b-c) Ca and Mg elemental maps showing qualitative 2D X-ray mapping of a garnet from the stromatitic leucosomes (traverse indicated by dotted line). The warm colours indicated on the colour bar show the highest concentration of an element.....33
13. Details of compositional variation in garnet from sample L2t-7. (a) A quantitative spot analysis of a garnet traverse. (b-c) Mg and Ca elemental maps showing qualitative 2D X-ray mapping of a garnet from the Stromatitic leucosomes (traverse indicated by dotted line). The warm colours show the highest concentration of an element.....35
14. Details of the compositional variation in garnet in sample L5GR-3. (a) A quantitative spot analysis of a garnet traverse. (b-c) Ca and Mg elemental maps showing qualitative 2D X-ray mapping of a garnet from the nebulitic leucosomes (traverse indicated by dotted line). The warm colours indicated on the colour bar show the highest concentration of an element.....37
15. (a) Chondrite-normalized REE pattern of a garnet grain from sample L5GR-3. This garnet is strongly zoned in terms of HREE, enriched in the HREE and has a negative pronounced Eu anomaly in the rims. (b) Y, Yb, Er, Gd, Dy in ppm plotted as proxy for REE zonation from the same sample. The analysis is along the same traverse as in a. (c) Cr, Ti, V and Zr in ppm plotted as proxy for trace elements zonation in sample L5GR-3. The analysis is along the same traverse as in a. (e) A core to rim analysis traverse is illustrated by a yellow dotted line on the BSE image.....43
16. (a) Chondrite-normalized REE pattern of a garnet grain from sample CR1a. This garnet is strongly zoned in terms of HREE, enriched in the HREE and has a negative pronounced Eu anomaly in the rims. (b) Y, Yb, Er, Gd, Dy in ppm plotted as proxy for REE zonation from the same sample. The analysis is along the same traverse as in a. (c) Cr, Ti, V and Zr in ppm plotted as proxy for trace elements zonation in sample CR1a. The analysis is along the same traverse as in a. (d) A core to rim analytical traverse is illustrated by a yellow dotted line on the BSE image.....45
17. The diagram illustrates the relationship between the plagioclase anorthite content and Sr concentration in sample L2t-6. Each colour represents a traverse across an individual crystal. Euhedral and anhedral plagioclase inclusions as well as the plagioclase crystals from the matrix around garnet are illustrated by the different symbols as indicated in the legend. The vertical dotted line indicates the Sr detection limit. Sr content within individual plagioclase was highly variable. In some crystals all the points analysed had Sr above the detection limit. In others, only about 40 % of the points analysed had Sr above the detection limit. The points with Sr content below the detection limit are not plotted. The plagioclase

- anorthite range is kept constant from figure 18 to 21 to allow for direct comparison between the figures. The typical uncertainty for anorthite concentration is ~ 0.26 and that for Sr is 315.85ppm using the standard deviation values (Ca = 0.05, Na = 0.09 and K = 0.05).51
18. The diagram illustrates the relationship between the plagioclase anorthite content and Sr concentration in sample L2t-7. Each colour represents a traverse across an individual crystal. Euhedral and anhedral plagioclase inclusions as well as the plagioclase crystals from the matrix around garnet are illustrated by the different symbols as indicated in the legend. The vertical dotted line indicates the Sr detection limit. Sr content within individual plagioclase was highly variable. In some crystals all the points analysed had Sr above the detection limit. In others, only about 40 % of the points analysed had Sr above the detection limit. The points with Sr content below the detection limit are not plotted. The typical uncertainty for anorthite concentration is ~ 0.26 and that for Sr is 315.85ppm using the standard deviation values (Ca = 0.05, Na = 0.09 and K = 0.05). The plagioclase anorthite range is kept constant from figure 18 to 21 to allow for direct comparison between the figures.52
19. The diagram illustrates the relationship between the plagioclase anorthite content and Sr concentration in sample L5GR-3. Each colour represents a traverse across an individual crystal. Euhedral and anhedral plagioclase inclusions as well as the plagioclase crystals from the matrix around garnet are illustrated by the different symbols as indicated in the legend. The vertical dotted line indicates the Sr detection limit. Sr content within individual plagioclase was highly variable. In some crystals all the points analysed had Sr above the detection limit. In others, plagioclase crystals only about 40 % of the points analysed had Sr above the detection limit. The points with Sr content below the detection limit are not plotted. The typical uncertainty for anorthite concentration is ~ 0.26 and that for Sr is 315.85ppm using the standard deviation values (Ca = 0.05, Na = 0.09 and K = 0.05). The plagioclase anorthite range is kept constant from figure 18 to 21 to allow for direct comparison between the figures.53
20. The diagram illustrates the relationship between the plagioclase anorthite content and Sr concentration in sample CR1a. Each colour represents a traverse across an individual crystal. Euhedral and anhedral plagioclase inclusions as well as the plagioclase crystals from the matrix around garnet are illustrated by the different symbols as indicated in the legend. The vertical dotted line indicates the Sr detection limit. Sr content within individual plagioclase was highly variable. In some crystals all the points analysed had Sr above the detection limit. In others, plagioclase crystals only about 40 % of the points analysed had Sr above the detection limit. The points with Sr content below the detection limit are not plotted. The typical uncertainty for anorthite concentration is ~ 0.26 and that for Sr is 315.85ppm using the standard deviation values (Ca = 0.05, Na = 0.09 and K = 0.05). The plagioclase anorthite range is kept constant from figure 18 to 21 to allow for direct comparison between the figures.55
21. Plot showing the average composition of individual inclusions analysed in this study against their crystal size and morphology.....55

22. Schematic diagram illustrating the locality of the plagioclase crystals within garnet from sample L2t-6 against their composition.....56
23. BSE images illustrating detailed electron microprobe analyses of cross-sections (dotted white lines) through the host garnet into the plagioclase inclusion in sample L2t-6. (A-E) Show magnified inclusions within garnet.....58
24. (A-E) Plots which highlight the detailed electron microprobe analyses of possible garnet zonation around the plagioclase inclusions. The orange shaded areas represent the position of the plagioclase crystals within garnet in sample L2t-6. The light grey shaded area represents garnet around the plagioclase inclusions. Traverses are indicated in the magnified images in Fig. 24.59
25. BSE images illustrating detailed electron microprobe analyses of cross-sections (dotted white lines) through the host garnet into the plagioclase inclusion in sample L5GR-3. (A-D) Show magnified inclusions within garnet.....60
26. Plots which highlight the detailed electron microprobe analyses of possible garnet zonation around the plagioclase inclusions. The orange shaded areas represent the position of the plagioclase crystals within garnet in sample L5GR-3. The light grey shaded area represents garnet around the plagioclase inclusions. Traverses are indicated in the magnified images in Fig. 26.61
27. BSE images illustrating detailed electron microprobe analyses of cross-sections (dotted white lines) through the host garnet into the plagioclase inclusion in sample L2t-7. (A-D) Show magnified inclusions within garnet.....62
28. Plots which highlight the detailed electron microprobe analyses of possible garnet zonation around the plagioclase inclusions. The orange shaded areas represent the position of the plagioclase crystals within garnet in sample L2t-7. The light grey shaded area represents garnet around the plagioclase inclusions. Traverses are indicated in the magnified images in Fig. 28.63
29. Comparison of chondrite-normalized REE zonation profiles within garnet crystals from: the metapelitic residuum and the granitic sheet in melanosomes of the MVS of Swaziland (from Taylor and Stevens, 2010, Fig. 8) to chondrite-normalized REE zonation profiles within garnet crystals from: the stromatic leucosome (sample L2t-6) and the garnet-bearing residuum (sample CRa1). (a) Comparison of REE zonation profiles of garnet from the metapelites of the MVS to the garnet crystals from the stromatic leucosome. (b) Comparison of REE zonation profiles of garnet from the granitic sheet of the MVS to REE zonation patterns of garnet crystal from the stromatic leucosome. (c) Comparison of REE zonation profiles of garnet from the metapelites of the MVS to REE zonation profiles of garnet crystal from the residuum. (d) Comparison of REE zonation profiles of garnet crystal from granitic sheet to REE zonation patterns of garnet crystal in the residuum. r = rim and c = core. The red, green and purple profiles represent REE zonation patterns from this study. The black patterns represent REE zonation patterns from Taylor and Stevens (2010).67

30. Thin section photomicrographs illustrating an optical continuity of biotite inclusions within garnet. (a) A magnified photograph illustrating optical continuity of biotite inclusions within garnet.....70
31. (A-C) Calculated P-T pseudosections investigating the consequences of changing effective bulk rock composition that is caused by slow diffusion in plagioclase. The composition of plagioclase within the different assemblage fields is illustrated by the plotted X_{An} isopleths. The modelling methodology is described in Table 2. Plagioclase out reaction is indicated by the red line. (A) A pseudosection where all of the plagioclase is available to participate in the melting reaction. Within this hypothetical rock that consists of quartz, plagioclase and biotite the plagioclase proportion is 20% of the rock. Plagioclase is stable everywhere in the diagram and the plagioclase anorthite content varies inversely with the amount of melt in the system. The onset of the fields where biotite reacts out marks a very strong variation over a narrow temperature band. (B) A pseudosection illustrating slow diffusion in plagioclase. Hypothetically restricting the amount of plagioclase in the rock to 10 % the formed peritectic plagioclase is more calcic. In this pseudosection the fields where biotite is reacting out marks a tighter variation in plagioclase composition, within this field plagioclase anorthite content is higher than in B. (C) A pseudosection illustrating only 5% proportion of plagioclase hypothetically present in a rock because of slow diffusion. In this pseudosection the plagioclase anorthite content is higher than in A-B, and plagioclase is not stable everywhere in the diagram.75
32. BSE image of the experimental results illustrating the lack of complete re-equilibration of plagioclase crystals during melting (from Johannes, 1989).77
33. A model for the behaviour of plagioclase during biotite incongruent melting in the BQ migmatites that seem to encounter the requirement for the generation of peritectic plagioclase crystals with different compositions (indicated as different colours in the figure) during partial melting. Different peritectic plagioclase crystals results from the fact that the entire plagioclase crystal is not equilibrated with the melt. (T1) Peritectic more calcic plagioclase with different compositions is produced at the site of melting reaction in the source rock, due to the diffusion constrains in the source plagioclase. (T2) Garnet crystals trap peritectic minerals and remnant of biotite as they grow. The crystallisation of peritectic plagioclase induces co-precipitation of peritectic quartz. (T3) A proportion of this peritectic plagioclase together with peritectic garnet, quartz and remnant of biotite, is entrained to the magma and transported into the leucosomes. (T3) Melt (or less crystal-rich magma that segregated from the source) is lost from the structure producing K_2O depleted leucosomes. The remaining melt crystallizes quartz, plagioclase and K-feldspar and may also contribute in biotite producing retrograde reactions with ferromagnesian minerals in the source.81

LIST OF TABLES

Tables	Pages
1. Plagioclase standard compositional variability	27
2. Mineral compositions taken from Stevens et al. (1997) as well as the synthetic bulk compositions used for modelling.	30
3. Representative compositions of individual garnet crystals (wt. %) from specific localities in the leucosomes. The stromatic leucosomes are indicated as L2t-6 and L2t-7 in Table (1) and the nebulitic leucosome is indicated as L5GR-3.	32
4. Representative LA-ICPMS data of garnet from sample L2t-6, L5GR-3 and CRa1. bdl = below detection limits, δ =sigma 1 error.....	38
5. Representative electron beam analyses (EDS for major element and WDS for trace element) of plagioclase inclusions within garnet. L2t-6, L2t-7, L5GR-3 and CR1a are analysed in the same manner. Representative BSE images for quantitative spot analyses from rim to rim of Plag A-G are shown in the petrography section, the compositional data can be seen in Table 5.....	47

LIST OF EQUATIONS

Chemical equations	Pages
Equation 1: $Ms + Qtz + Pl = Sil + Melt$	12
Equation 2: $Bt + Sill + Pl = Grt + melt$	12
Equation 3: $.Bt + Qtz + Pl = Opx \pm Grt \pm Crd + melt$	12
Equation 4: $Bt + Sil + Pl1 + Qtz = Grt + Pl2 + Ilm + melt$	63
Equation 5: $Ca_3Al_2Si_3O_{12} + 2Al_2SiO_5 + SiO_2 = 3CaAl_2Si_2O_8$	75

LIST OF ABBREVIATIONS

Minerals

Pl	Plagioclase
Grt	Garnet
Bt	Biotite
Crd	Cordierite
Qtz	Quartz
Rt	Rutile
Opx	Orthopyroxene
Ilm	Ilmenite
Sil	Sillimanite
Ky	Kyanite
Oamp	Orthoamphibole

Terminology

P-T	Pressure Temperature
Alm	Almandine
Sps	Spessartine
Grs	Grossular
Pyr	Pyrope
An	Anorthite

1. INTRODUCTION

Earth's continental crust is composed largely of granitic rocks, which formed through fluid-absent partial melting reactions within the lower crust (Clemens, 1990; Stevens and Clemens, 1993; Clemens and Watkins, 2001). Although produced within the lower crust, granitic magmas migrate into the upper crust, leaving the lower crust refractory and enriching the upper crust in heat producing elements (Clemens, 1990). A primary expression of this process is the formation of granites (e.g. I-and-S-types) most of which are inherently derived from the crust (e.g. S-type) (Chappell and White, 1974, 2001), and the generation of granulite-facies metamorphic rocks that reflect the residuum left behind after segregation of granitic melts (Clemens, 1990). The volume of granitic melt produced depends strongly on the proportion of hydrous (biotite and hornblende) and anhydrous (feldspar and quartz) reactant phases, the chemical composition of the source and the P-T conditions (Clemens and Vielzeuf, 1987). The source can be either; chemically fertile and produce a relatively large volume of melt, for example most pelitic rocks as they host large volumes of hydrous phases, or it may be less fertile and produce small volumes of melt, as is the case for most greywacke, igneous and previously melt-depleted (residuum) rocks (Stevens et al., 1997; Yakymchuk and Brown, 2014). It has been established that S-type granites originate by partial melting of a metasedimentary source, due to their strongly peraluminous and K₂O-rich character (Chappell and White, 1974). However, I-type granites originate from arc volcanic rocks of intermediate composition (rich in biotite and hornblende) such as the dacites and high-K andesites (Roberts and Clemens, 1993; Clemens et al., 2011).

S-type granites have a wide compositional range from leucogranites to granodiorites (Clemens, 2003; Stevens et al., 2007). The origin of such variation remains a subject of substantial discussion. Some studies (e.g., De Paolo, 1981; Perugini and Poli, 2012; Poli and Tommasini, 1999) claim that processes that occur during magma ascent and crystallization are important in modifying the compositions of granitic magmas. Such processes include magma mixing; assimilation of wall rock; and crystal-liquid fractionation. In contrast, others argue that source processes are important in shaping the chemistry of granites. For example, the entrainment of either the un-melted residual fraction of the source (White and Chappell, 1977) or the peritectic assemblage produced by the melting reaction (Stevens et al., 2007). The processes that occur during magma ascent and crystallization have been effectively refuted by thermal and dynamic limitations (Glazner, 2007) and by the geochemical considerations (Stevens et al., 2007). For example, assimilation may take place either by dissolution of solid crustal rocks into the magma, by the disaggregation of ingested xenoliths, or by partial melting of

wall rocks and mixing with the melt that formed. The energy consumed during this process results in extensive cooling, crystallization, and the formation of a viscous magma unable to undergo further magmatic evolution. In addition, these models have been proposed to account for the linear major element trends in Harker diagrams (magma mixing). The importance of these models in producing geochemical variations in granitic rocks is still a subject of substantial debate (Stevens et al., 2007). These models cannot adequately account for the large-scale major-element compositional trends defined by S-type granites, particularly those depicted by Ti and K as a function of maficity (Fe + Mg) (Stevens et al., 2007). The excellent tight correlation between Ti and maficity matches that defined by stoichiometry of high-temperature biotite. Ti in S-type granites is typically hosted in more than one mineral i.e. ilmenite and biotite. These minerals show noticeably density contrast and appear at different stages in the crystallization sequence. The tight correlation between Ti: maficity requires that the relevant phases are always present in the same proportion in the magma. This is highly unlikely in the case of magma mixing, crystal liquid fractionation and assimilation of wall rock.

The restite unmixing model proposed by Chappell and White (1977) and Chappell et al. (1987) is centred on the idea that granitic magmas represent a mixture between melt and the whole residual assemblage (restite). The term 'restite' includes phases that are not involved in the melting reaction (e.g. pre-anatectic anhydrous ferromagnesian and accessory phases), the remnant of the minerals which are partially consumed by the melting reaction (e.g. plagioclase), the crystals produced by the incongruent melting reaction (e.g. peritectic garnet, cordierite and orthopyroxene), and the un-melted or less molten fractions of the source. The latter usually occurs as amphibolite-facies enclaves in granites, and has led to the idea that such magmas originate by fluid-present melting at low temperature (Chappell et al., 2000). This opposes the general view that most granites originate by incongruent biotite breakdown at high temperature (Patiño Douce and Johnston, 1991; Stevens and Clemens, 1993, Stevens et al., 1997), which produces peritectic sillimanite, garnet, cordierite and orthopyroxene (Brown, 2007; Taylor et al., 2014). The unmixing part of the restite model originates from the fact that the full residual material segregates and ascends and at some point the melt progressively fractionates from the entrained residual material to produce compositional variation in granites. The implication of this model is that for the magma to mobilise, the melt fraction must be high enough so the rheology of the source changes from solid-like to a liquid-like. A major limitation of this model is that it requires diapiric transport of granitic magmas (e.g. Clemens and Mawer, 1992). Diapirism has been refuted as the main model of magma extraction, not because of energy constraints, but because of mechanical

considerations as well as the lack of field evidence in support of the diapirism (Clemens and Mawer, 1992).

Stevens et al. (2007) proposed that to explain the chemistry of granites of the Peninsula pluton of the Cape Granite Suite, only the peritectic and accessory assemblage is entrained into the magma and not the whole partial molten source, i.e. the peritectic assemblage entrainment (PAE) model. Evidence for this model is the strong positive correlation between Ti and maficity in all S-type granites, while elements which are more soluble in the melt (K, Al, and Na) show a wider scatter with maficity. The tight positive correlation between Ti and maficity reflects the co-entrainment of garnet and ilmenite into the magma, both peritectic products of incongruent biotite breakdown. Stevens et al. (2007) also noted that Ti, Fe and Mg within biotite have low solubility in the granitic melts produced by incongruent biotite breakdown. Therefore, this insoluble proportion of biotite must express itself as an assemblage of peritectic minerals produced by the following incongruent melting reaction: $Bt + Qtz + Pl + Sil = Grt + melt + Ilm$. They therefore, proposed that the composition of S-type granites is shaped in the source, by the entrainment of peritectic assemblages into the magma. In addition, the increase in Ca and Al with maficity is proposed to reflect the entrainment of peritectic plagioclase as part of peritectic assemblage (Clemens et al., 2009, 2011). The tight correlation between Zr and maficity is proposed to reflect the co-entrainment of accessory zircon, which also explains the abundance of inherited cores of zircon in granites even in those subsaturated in Zr (Stevens et al., 2007; Clemens et al., 2011). Further evidence for this model shows that melt and the peritectic minerals concentrate in the same melting sites, and that peritectic minerals form new crystals that are small in size than its complementary residue (Clemens et al., 2012). The extraction of the melt facilitates segregation of the accessory and peritectic assemblage and the ratios of individual peritectic phases in the entrained assemblage remains fixed in the ratio decreed by the stoichiometry of the melting reaction. Therefore, the PAE model successfully explains the major element ratios and chemical trends defined by S-type granites with increasing maficity. The most leucocratic granites are considered to entrain extremely small amounts of peritectic minerals, so their chemistry is controlled mainly by the composition of the melts, which in turn depends on the composition of the source (Patiño Douce, 1999; Stevens et al. 2007).

Peritectic assemblage entrainment has not been systematically investigated in many migmatitic environments. However, a study by Taylor and Stevens (2010) is one of the few studies that have considered the peritectic assemblage entrainment model in understanding the origin of peritectic garnet

in the melt transfer and accumulation structures (leucosomes) of the Mkhondo Valley Metamorphic Suite (MVS) in Swaziland. They established that peritectic garnet as small as $< 1\text{mm}$ in size, contains inclusions of melt, quartz and biotite. These peritectic garnet crystals were entrained into the melt and segregated with the magma into the leucosomes. They further hypothesised that the structures that preserved melt longer allowed the garnet to amalgamate and recrystallize by a dissolution-precipitation process, to adopt a more magmatic character. Garnet crystals contained in structures that lost melt more efficiently and rapidly than other structures preserved their peritectic character. In addition, White et al. (2004) published a study on the Broken Hill block in south-eastern Australia. They proposed that the migration of melt along peritectic garnet boundaries has the potential to facilitate peritectic assemblage entrainment. While it is well understood that the entrainment of source components is important in shaping the chemistry of granites, the details of how this process works in the source is unclear. A strong factor contributing to the uncertainty is that the details of the partial melting processes are not completely understood. Experimental, theoretical, and field considerations around partial melting show that it is an incongruent process, and because it is incongruent it produces melt plus solid peritectic phases (Patiño Douce and Johnston, 1991; Stevens and Clemens, 1993). To understand the details of partial melting, a comprehensive study of peritectic minerals particularly garnet that are most likely to preserve evidence of the details of the partial melting process is essential.

One important locality in South Africa, that provides an opportunity to conduct such a study, is the Southern Marginal Zone (SMZ) of the Limpopo belt. Here, stromatic and discordant nebulitic leucosomes contain large peritectic garnet crystals produced by the incongruent breakdown of biotite (Nicoli et al., 2014a; Stevens and van Reenen, 1992; Taylor et al., 2014). A recent study by Taylor et al. (2014) identified an additional aspect of partial melting of the metasedimentary crust, which possibly involves disequilibrium behaviour of plagioclase in the source. Plagioclase behaviour during fluid-absent incongruent partial melting is complex. The details of how plagioclase behaves during the incongruent biotite breakdown are not well understood. Plagioclase is one of the minerals that are extremely resistant to compositional change through diffusion, suggesting that, in some cases, disequilibrium processes play a significant role in shaping the composition of granites (Farina and Stevens, 2011). Disequilibrium melting of plagioclase usually occurs when only the outermost zone of plagioclase melts, due to slow diffusion in plagioclase (Johannes, 1989; Morse, 1984; Taylor et al., 2014), leaving a significant portion of the core unaffected. In addition, Taylor et al. (2014) noted that the stromatic leucosomes in the Bandelierkop Quarry (BQ) are particularly high in $\text{CaO}/\text{Na}_2\text{O}$ and depleted in K_2O . They suggested that the CaO -rich nature of the leucosomes is a consequence of

disequilibrium melting of plagioclase. This study examines the same samples as used by Taylor et al. (2014), to better understand the behaviour of plagioclase during fluid-absent anatexis of metapelites in the SMZ of the Limpopo belt, South Africa. The results of this study may provide a better insight into the processes that shape the chemistry of granites in the source.

2. GEOLOGICAL SETTING

The Limpopo Belt is a high-grade metamorphic terrain that crops out between the Kaapvaal Craton (KC) and Zimbabwe Craton (ZC). It is distinguished from the adjacent cratons by its granulite-facies metamorphism relative to the generally amphibolite- to greenschist-facies rocks of the neighbouring cratons (de Wit et al., 1992; Roering et al., 1992a, b). The belt is made up of three distinct domains that are separated by complex shear zones: the Northern Marginal Zone (NMZ), the Central Zone (CZ) and the SMZ (van Reenen et al., 1990, 1992). The NMZ and the SMZ are segregated from the surrounding granite-greenstone cratons by ca. 2.68 Ga inward-dipping shear zones, termed the North Marginal Thrust Zone (NMTZ) in the north and the Hout River Shear Zone (HRSZ) in the south (Blenkinsop et al., 2004; Roering et al., 1992a, b; van Reenen et al., 1987, 1988, 1990). The CZ is separated from the marginal zones by the 2.0 Ga Triangle Shear Zone (TSZ) in the north and Palala Shear Zone (PSZ) in the south (McCourt and Vearncombe, 1987, 1992; Schaller et al., 1999).

The CZ is interpreted to be an epicontinental, polymetamorphic, exotic, crustal block that has experienced a number of high-grade metamorphic events at 3.2-3.1 Ga and at 2.65-2.52 Ga (Holzer et al., 1998), followed by a younger granulite-facies overprint at ca. 2.0 Ga (Buick et al., 2006; Kreissig et al., 2001; Zeh et al., 2010). While, the NMZ is suggested to represent reworked, high-grade equivalents of the granite-greenstone sequences of the neighbouring Cratons, the SMZ was previously interpreted to represent equivalents of the granite-greenstone sequences of the KC. The study by Nicoli et al. (2014a) has demonstrated that the SMZ contains sediments deposited along an active margin during lateral convergence and is proposed to have been deformed and metamorphosed as a consequence of continental collision along the northern margin on the Kaapvaal craton at ca. 2.7 Ga (Du Toit et al., 1983; Kreissig et al., 2001; Nicoli et al., 2014a; Stevens and van Reenen, 1992a, b; van Reenen et al., 1990). To date, what the SMZ represent is still uncertain and is a subject of an ongoing research. None of the metamorphic events experienced by the CZ are recorded in the SMZ rocks. The CZ and the SMZ are interpreted to have followed different metamorphic histories prior to and during the 2.0 Ga events (Nicoli et al., 2014a).

2.1. *Geology of the SMZ*

The SMZ (Fig. 1) which is bounded in the south by HRSZ and in the north by PSZ is further subdivided into two subzones: a granulite subzone in the north and a retrograde zone in the south, separated by a well-defined retrograde orthoamphibole isograd (van Reenen, 1986). The granulite

subzone is an extensive area of strongly deformed granulites with a dominant ENE-WSW trending foliation in which extremely attenuated metasedimentary rocks occur within tectonically and metamorphically reworked gneissic and migmatitic granitoids. The granulite-facies assemblage is used to define the distribution of high-grade rocks. The retrograde zone forms the southern part of the SMZ. This area occurs between the retrograde orthoamphibole isograd and the HRSZ. The HRSZ boundary separates the granulite terrane from the KC. This structure dips steeply northwards with rehydrated granulites on the northern side having been emplaced against granite-greenstones along its southern contact (Kreissig et al., 2001; Roering et al., 1992a).

Different lines of evidence are proposed to explain the origin of the retrograde southern zone. Van Reenen (1986) proposed hydration of the granulite-facies rocks by H₂O-CO₂-rich fluids, which infiltrated the granulite rocks along HRSZ to produce orthoamphibolite gneiss. Conversely, Vennemann and Smith (1992) suggested that a layer-scale variation in carbon isotope ratios in the graphitic metasedimentary rocks ruled out reactions with externally derived CO₂-rich fluids, and proposed the formation of orthoamphibole on the prograde path, as an alternative explanation.

On the basis of a petrographic study, Stevens (1997) suggested that the retrograde zone results from the interaction between graphite, in the metasedimentary graphite-bearing granulites, with fluids internally derived from crystallizing anatectic leucosomes. As a consequence, the retrograde zone is proposed to represent an area of the SMZ where the bulk of the melt remained in the source, while the granulite subzone represents an area which lost most of the melt formed at peak metamorphism (Stevens, 1997).

The geology of the granulite subzone is dominated by two main rock units: grey banded and migmatized trondhjemitic to tonalitic gneisses termed the Baviaanskloof Gneiss and mafic, ultramafic and metasedimentary units of the Bandelierkop formation (Du Toit et al., 1983). The Bandelierkop formation was previously interpreted to represent a dismembered and metamorphosed equivalent of the greenstone belt sequences on the KC, which occurs as discontinuous infolded keels within the Baviaanskloof grey gneisses, with the metasedimentary rocks representing the most dominant unit of the Bandelierkop formation. The Baviaanskloof Gneiss is proposed to represent the granulite-facies metamorphosed trondhjemites and tonalites on the Kaapvaal craton (Kramers et al., 2006; Kreissig et al., 2000; Roering et al., 1992a; van Reenen et al., 1992; Zeh et al., 2009).

A recent study noted that the sediments of the Bandelierkop formation do not represent equivalents of any of the greenstone belt sedimentary sequences on the KC. This is because these rocks have a maximum sedimentation U-Pb age of ca 2.730 Ga obtained from detrital zircon, with most zircon crystals indicating source rocks younger than ca. 3.00 Ga (Nicoli et al., 2014a). This wide range of ages is different to what is predicted for sediments derived from erosion of the northern KC, and is also different to the ages of the metasedimentary rocks in the greenstone belts metasedimentary succession on the KC. The reason for this is because this portion of the Craton ranges in age between 3.5 and 3.0 Ga, with a big peak at 3.1 Ga (Zeh et al., 2013). The ages post-date the formation of the Dominion and Witwatersrand sedimentary succession on the KC (Nicoli et al., 2014a) and are likely obtained from a different source, which is still debated. However, Nicoli et al. (2014) have postulated the existence of an unnamed block which collided with the Kaapvaal craton, or that the Bandelierkop sediments could also have formed through erosion of the non-preserved Ventersdorp volcanic rocks deposited along the northern boundary of the Kaapvaal craton (Nicoli et al., 2014a). Although, the possible sources for the metasedimentary rocks are assumed, the protolith for the mafic and ultramafic rocks remains unknown.

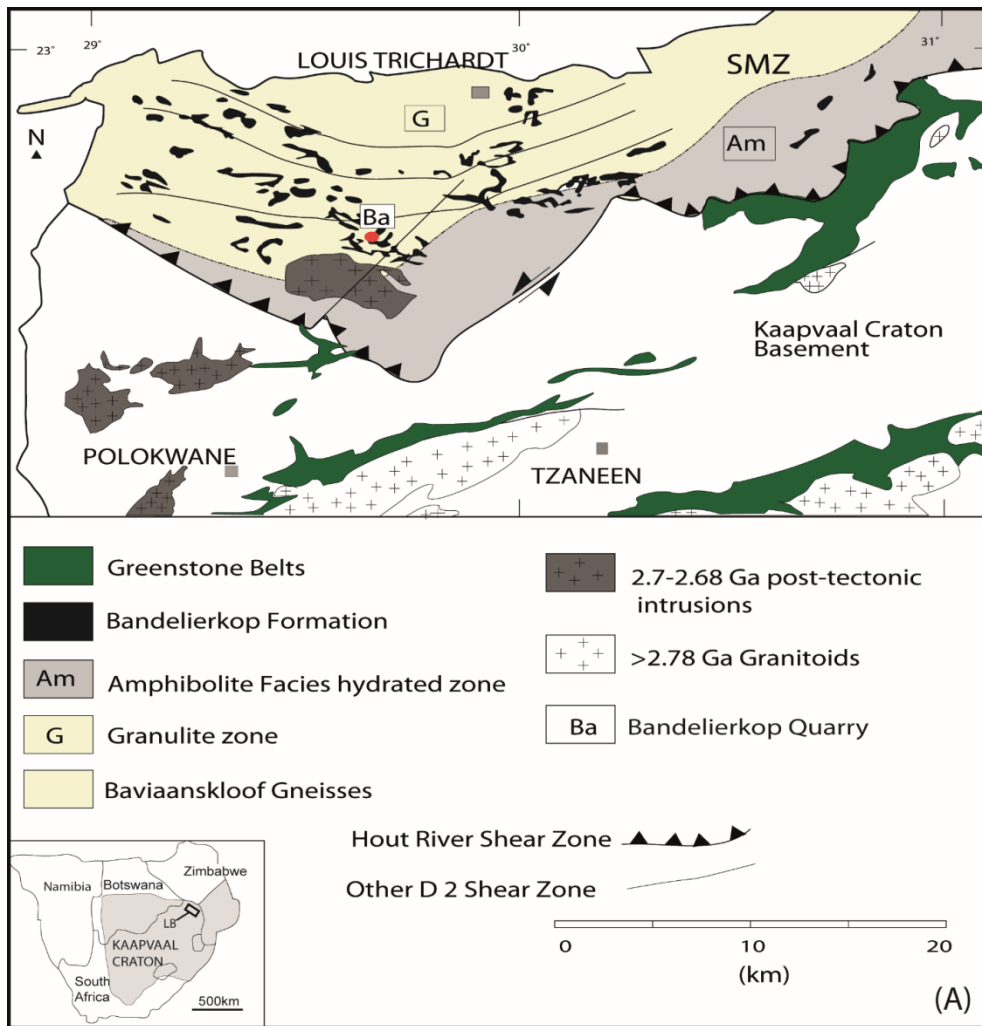


Figure 1: A simplified geological map of the SMZ modified from Stevens et al., 1997. The locality of the Bandelierkop quarry (Ba) is indicated by the red dot.

2.1.1. Previous studies on the SMZ granulites facies rocks

Previous studies on the SMZ granulites concluded that these rocks have experienced a clockwise P-T path evolution. The P-T evolution involves peak metamorphism at 800 to 850°C and at 8.0 to 11.0 kbar, followed by near-isothermal decompression at peak temperature; and finally near-isobaric cooling to retrograde amphibolite-facies conditions below 650°C at 6.0 kbar (Nicoli et al., 2014a; Stevens and van Reenen, 1992a; Taylor et al., 2014). Until recently, the clockwise P-T paths have been based on petrographic studies using cation exchange geothermometry-barometry centred on garnet-cordierite geobarometry and on biotite-garnet geothermometry (Stevens and van Reenen, 1992a). Recent studies have used phase equilibrium modelling to calculate P-T pseudosections from a

number of different rocks in the Bandelierkop formation (Nicoli et al., 2014a; Taylor et al., 2014). Taylor et al. (2014) proposed that the peak metamorphism of the BQ metasediments is in the range of 820 to 890°C and 8.0 to 12.0 kbar. This finding is consistent with a peak metamorphism of approximately 850°C and 11.0 kbar for the rocks of the Brakspruit quarry, a locality some 15 km north of BQ, proposed by Nicoli et al. (2014a).

In comparison, Belyanin et al. (2012) proposed different peak metamorphic conditions in excess of 1000°C at approximately 12 kbar, on the basis of Al-rich orthopyroxene thermometry and ternary feldspar thermometry. They used reintegrated feldspar compositions from a single locality which hosts unusual aluminous layers in the metasedimentary granulites. These Ultrahigh-temperature (UHT) conditions are difficult to reconcile with the widespread existence of peak biotite in both the Baviaanskloof Gneiss and the Bandelierkop Formation metapelites. In the Baviaanskloof Gneiss, biotite and hornblende have not melted. For this reason, the SMZ rocks are unlikely to have undergone a regional peak metamorphic temperature above 900°C, as in such conditions biotite would not have survived (Nicoli et al., 2014b). In the metamorphic conditions proposed by Belyanin et al. (2012), the metasedimentary rocks of the Bandelierkop formation would have been changed into residuum-rich diatexitic, peraluminous, dioritic to granodioritic plutons. Also, a significant proportion of biotite defines a strong foliation in these rocks and orthopyroxene is aligned in this fabric (Nicoli et al., 2014b). As a result, UHT metamorphism in the SMZ is impossible because the rocks do not record the obvious macroscopic evidence consistent with the whole SMZ terrain being 40-85% melt (Nicoli et al., 2014b).

2.1.1.1. Timing of metamorphism in the Bandelierkop formation

Kreissig et al. (2001) reported the timing of peak metamorphism for the BQ leucosomes at 2.69 ± 7 Ga using U-Pb dating of two monazite crystals. In comparison, Taylor et al. (2014) reported a slightly older age on peak metamorphism using U-Pb zircon ages of 2.714 ± 6.4 Ga and 2.713 ± 54 Ga in the BQ leucosomes. This age is in agreement with the age of 2.713 ± 8 Ga obtained from 40 zircon crystals in the metasedimentary rocks of the Brakspruit quarry (Nicoli et al., 2014a). However, it is worth noting that zircon in leucosomes commonly crystallizes close to peak temperature, while monazite generally crystallizes at lower temperature conditions (Parrish, 1990; Lee et al., 1997). After peak metamorphism, the metasedimentary rocks of the SMZ underwent isothermal decompression

followed by isobaric cooling to retrograde conditions. Following this view, Nicoli et al. (2014a) interpreted the monazite age in the BQ leucosomes obtained by Kreissig et al. (2001) to mark the timing of retrograde assemblage formation, and complete solidification of the melt in the leucosomes. In addition, the Matok intrusive complex (Fig. 1) intruded the SMZ rocks a few kilometres north of HRSZ at 2.686 ± 7 Ga. This age is within error identical with the intrusion of undeformed pegmatites at 2.680 ± 6 Ga in the Brakspruit quarry, which marks the end of penetrative deformation in this locality (Nicoli et al., 2014a).

In summary, the fast burial rate of the Bandelierkop sedimentary rocks to more than 30 km depth, the clockwise P-T path evolution, together with the post-peak metamorphic rapid decompression provides strong evidence that the SMZ contains sediments deposited along an active margin during lateral convergence (Nicoli et al., 2014a).

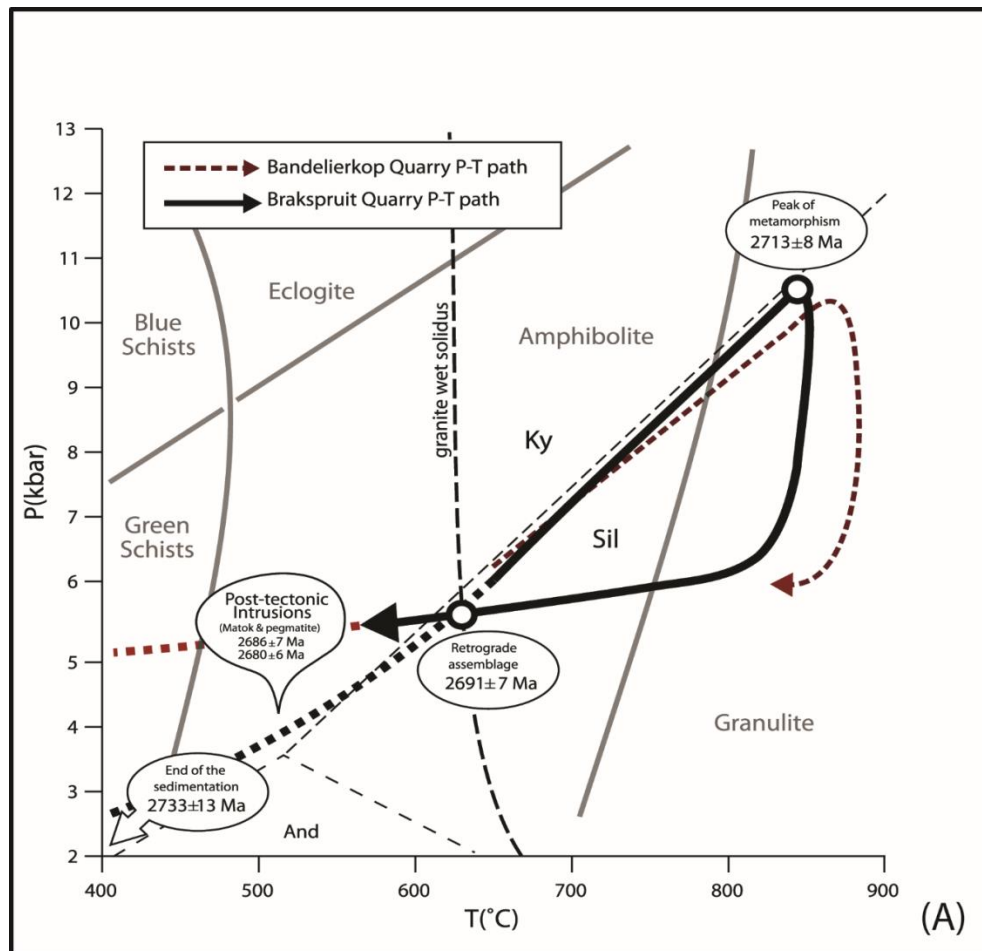


Figure 2: P-T-t path for the SMZ metasedimentary rocks (modified from Nicoli et al., 2014). The P-T path for the metapelites of the Bandelierkop quarry is adapted from Taylor et al. (2014) and has been added for comparison. Comparatively, the Matok age from Laurent et al. (2013) and the retrograde age from Kreissig et al. (2001) are also portrayed.

2.1.2. *Partial melting of the Bandelierkop metasediments*

Bandelierkop formation contains different metasedimentary rocks i.e. the semipelites and metapelites that contain features consistent with *in situ* anatexis. Partial melting of these metasediments occurred by muscovite and biotite breakdown reactions, to produce melt together with peritectic sillimanite, garnet, orthopyroxene and cordierite according to the following simplified melting reactions (Stevens and van Reenen, 1992; Taylor et al., 2014): (1). $Ms + Qtz + Pl = Sil + Melt$; (2). $Bt + Sill + Pl = Grt + melt$; (3). $Bt + Qtz + Pl = Opx \pm Grt \pm Crd + melt$. The first two reactions produced stromatitic leucosomes within the metapelite layer, which experienced solid-state deformation along the prograde path. The third reaction produced undeformed nebulitic leucosomes within the semipelite layer. Stromatic leucosomes are characterized by the presence of sillimanite, whereas the nebulitic leucosomes are marked by the presence of orthopyroxene. An age of 2.714 ± 6 Ga is obtained for the stromatitic leucosomes and 2.713 ± 5 Ga for the nebulitic leucosomes (Taylor et al., 2014).

The semipelite layer is light-grey, medium-grained, and has a granoblastic texture (Taylor et al., 2014). This layer consists of quartz, plagioclase, biotite, garnet and orthopyroxene. The semipelite layer is distinguished from the metapelite layer by a lack of cordierite and sillimanite, and less abundant stromatic leucosomes (Fig. 3a). In places, discordant nebulitic, orthopyroxene-bearing leucosomes and garnet-bearing leucosomes (with associated coarse-grained orthopyroxene-bearing residuum) occur as disseminated, leucocratic patches within the semipelitic layer (Fig. 3c). The nebulitic leucosomes contain blocky peritectic orthopyroxene and quartz + plagioclase + biotite + garnet \pm cordierite, which indicates formation by reaction (3). In contrast, the metapelitic-residue occurs as grey-brown, medium- to coarse-grained, strongly deformed rock layers that host quartz, plagioclase, biotite, 2-5mm-sized garnet, orthopyroxene and cordierite. This layer contains abundant *in situ*, garnet and sillimanite-bearing stromatic leucosomes that range from cm to mm in size. Stromatic leucosomes are the most dominant type in the BQ and are characterized by a metatextitic structure. They occur as deformed veins and are characterized by medium to coarse-grained quartz + plagioclase + garnet \pm sillimanite. The metapelitic-residue layers hosts rare orthopyroxene + cordierite + garnet-bearing nebulitic leucosomes, and associated coarse-grained orthopyroxene-bearing residuum, which destroy the pre-existing foliation in these rocks.

Both leucosomes and the residuum contain peritectic garnet that is proposed to have been generated by reactions (2 and 3, Taylor et al., 2014). Stromatic leucosomes contain peritectic poikiloblasts of garnet, which host euhedral plagioclase inclusions, some of which are more calcic than the plagioclase in the matrix. A detailed investigation of plagioclase contained within the peritectic garnet crystals in the stromatitic leucosomes, garnet-bearing residues, and garnet in the nebulitic leucosomes is necessary, as they most likely to reveal the details of the melting processes and contribute to the chemistry of the leucosomes, as discussed below.

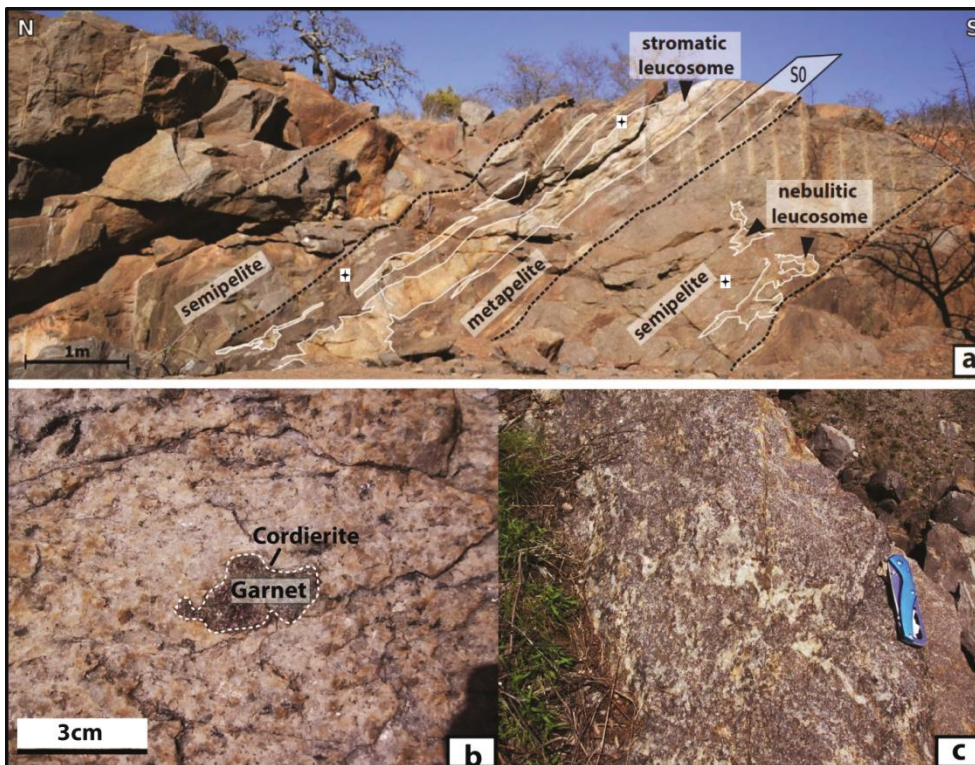


Figure 3: (a) A photograph of the western face of the Bandelierkop Quarry, illustrating the relationship between the metapelitic and semipelitic layers which host the stromatic and nebulitic leucosomes (modified from Taylor et al., 2014). The stars indicate where the samples were taken. (b) Large garnet enclosed by cordierite within a stromatic leucosomes. (c) Garnet crystals within nebulitic leucosomes.

2.1.2.1. The composition of the leucosomes

The bulk composition of the stromatic leucosomes in the BQ, when compared to experimental melts from similar sources are strongly K-depleted; their SiO_2 content is similar to the experimental melts; and their Ca/Na ratios are higher than the experimental melts (Taylor et al., 2014). Two possible

models have been proposed to account for the Ca-rich nature of the leucosomes. Both models consider only the outermost zones of the plagioclase crystal in the source participating in the melting reaction, a significant portion of the plagioclase crystal is not involved in the melting reaction due to slow diffusion (Taylor et al., 2014). In the first scenario, the outer zones of plagioclase in the source melt incongruently, producing CaO-rich peritectic plagioclase at the site of melting reaction. The CaO-rich peritectic plagioclase is entrained into the segregating magma, together with peritectic sillimanite and garnet, and is deposited in the accumulated magma to form leucosomes. The leucosome structures became rheologically solid due to melt loss while the source rocks were undergoing heating. As a result, the chemistry of the leucosomes is interpreted to reflect the amount of peritectic minerals precipitated within the leucosomes and the volume of melt that remained to crystallize in the leucosomes. Quartz and K-feldspar were not entrained into the leucosomes, but crystallized directly from the melt. Therefore, for this model to be viable, the modes of quartz and K-feldspar should correlate positively. However, this is not the case, as the leucosomes are depleted in K_2O and have SiO_2 contents similar to those of the melt (Fig. 4c). The second model proposes a disequilibrium congruent melting of plagioclase in the source. Both models depend on a slow diffusion rate of plagioclase but in the second model plagioclase does not precipitate at the melting site. This model produces CaO-enriched melt, with the crystallization of CaO-rich peritectic plagioclase after the melt has segregated from the source. The melt SiO_2 content increases as a consequence of plagioclase crystallization inducing the co-precipitation of quartz. The latter model is proposed to fit well with the entire spectrum of field, textural and chemical data of the BQ presented by Taylor et al. (2014).

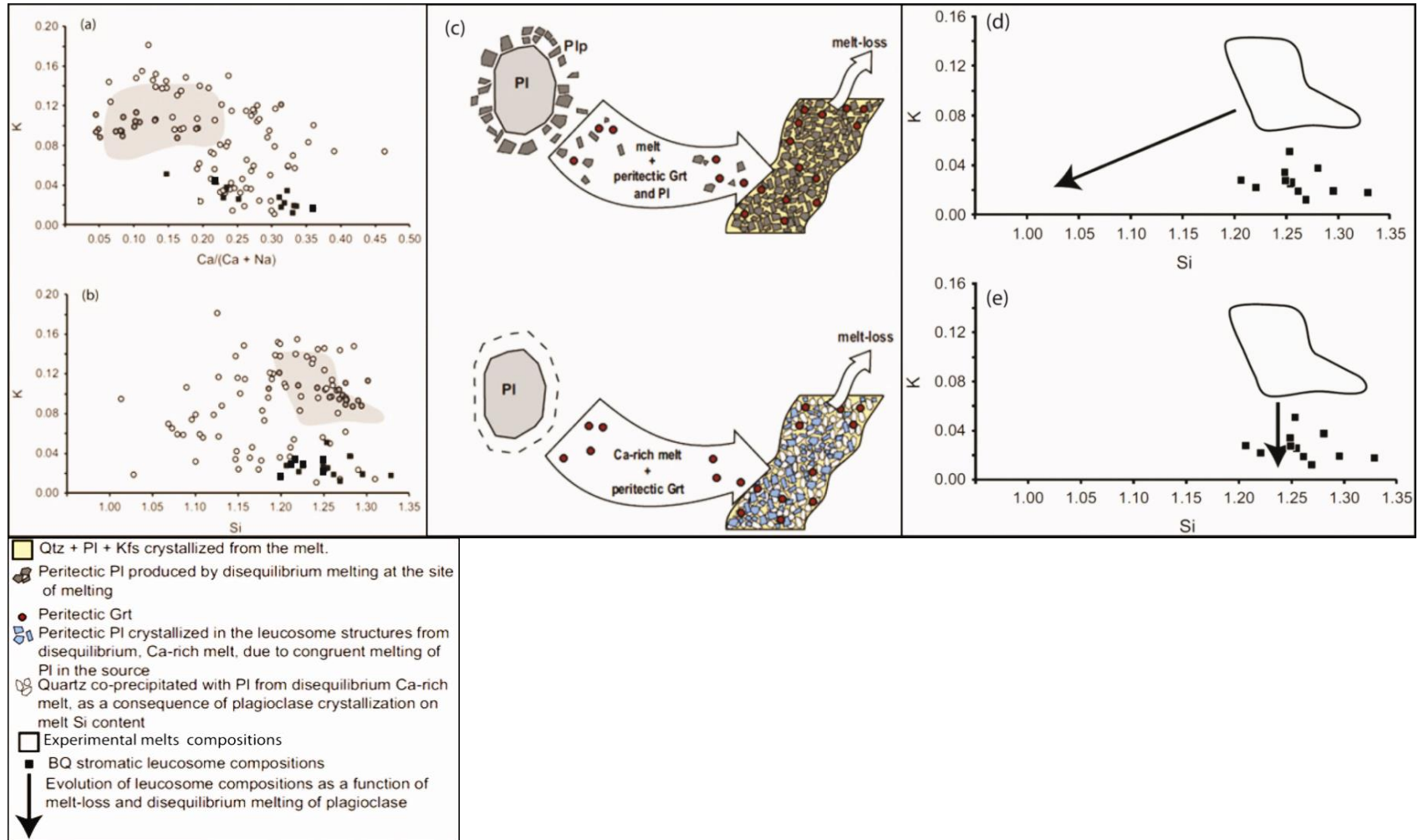


Figure 4: (a-b) The composition of the BQ leucosomes from Taylor et al. (2014) relative to fluid-absent experimental melt compositions produced from a wide range of metasedimentary starting materials between 775 and <900°C and 1-15 kbar (Montel & Vielzeuf, 1997; Patiño Douce and Beard, 1996; Patiño Douce & Harris, 1998; Patiño Douce and Johnston, 1991; Pickering and Johnston, 1998; Stevens et al., 1997; Vielzeuf and Holloway, 1988). Also shown are the natural glass compositions that show homogenized melt inclusions and glassy inclusions within peritectic minerals from natural migmatites, generated between 700 and 860°C and 5-8 kbar (Acosta-Vigil et al., 2007; Bartoli et al., 2013; Ferrero et al., 2012). (a-b) Also illustrates granulite-facies leucosome compositions from metasedimentary migmatites, where partial melting is well understood through fluid-absent incongruent melting of biotite (at >750-900°C and 4-12kbar). Other compositions were excluded to avoid uncertainties related to partial melting of UHT, or the amphibolite facies (from Taylor et al., 2014). (c) Two models for the behaviour of plagioclase during incongruent biotite breakdown in the BQ (modified from Taylor et al., 2014). In the first scenario, peritectic, more calcic plagioclase is produced at the site of plagioclase melting in the source rock. A proportion of the peritectic plagioclase, together with peritectic garnet is entrained to the magma and transported to the site of magma accumulation. The melt is lost from the leucosomes, resulting in low K₂O leucosomes. The remaining melt crystallizes quartz, plagioclase and K-feldspar and may also participate in biotite producing retrograde reactions with ferromagnesian minerals in the residuum. In this scenario, K and Si contents of the leucosomes prior to retrograde reactions in the residuum are linked in that both reflect the volume of melt remaining in the leucosome. Thus, the Si content of the leucosomes is low. The second scenario, the melting of plagioclase in the source produces more calcic melt than in the scenario described above. Peritectic plagioclase precipitates within the leucosomes. Quartz co-precipitation from the melt is induced by the precipitation of plagioclase, as the content of Si increases in the melt. Most of the melt escape from the leucosomes producing low K₂O leucosomes with no correlation between the quartz and K-feldspar mode (Fig. 4d-e). The latter scenario, peritectic garnet is grown in the source and entrained to the magma. The leucosome compositions are low in K, but have Si values similar to those of the experimental melts.

3. DETAILS OF THE PLAGIOCLASE INCLUSIONS IN GARNET

3.1. General petrography of the large poikiloblastic garnet crystals

The petrography of these rocks is well documented by previous researchers (e.g. Stevens and van Reenen, 1992a, b; Stevens, 1997; Taylor et al., 2014), so this study only focuses on plagioclase inclusions within the large, poikiloblastic garnet crystals associated with the leucosomes, the garnet morphology and the garnet compositional zonation. The previous studies noted that metasedimentary rocks contain two different types of garnet crystals, small (typically $\leq 4\text{mm}$), subhedral poikiloblastic garnet crystals in the semipelitic layer, and large (typically 10-20mm), anhedral poikiloblastic crystals in the metapelitic rocks adjacent to the leucosomes and within the leucosomes. These garnet crystals contain sillimanite, plagioclase and biotite inclusions, which suggest formation by breakdown reactions of biotite, in a process that also produced the leucosomes. For this study, samples were taken from the stromatitic leucosomes, garnet-bearing residuum hosting the stromatic leucosomes and nebulitic leucosomes (Fig. 3a).

Stromatic leucosomes contained within the metapelitic layer contain anhedral to rounded peritectic garnet poikiloblasts of ~20mm in diameter (Fig. 3b). These garnet crystals contain abundant inclusions of rounded quartz, rounded biotite and plagioclase (Taylor et al., 2014), that formed during the prograde path of the rock's history (Stevens and van Reenen, (1992). Garnet relics have embayed margins, rimmed, and partially replaced by symplectic intergrowths of orthopyroxene and cordierite, which record the decompression history of these rocks at peak temperatures (Stevens and van Reenen, 1992). Orthopyroxene and cordierite, formed on the decompression path, are partially replaced in the subsequent hydration reactions (Stevens and van Reenen, 1992; Stevens, 1997). Orthopyroxene is partially replaced by biotite and quartz, and cordierite is extensively replaced along its grain boundaries by fine-grained fibrous intergrowth of biotite, kyanite, orthoamphibole and quartz. The decompression reactions changed the sizes and shapes of the garnet, leaving little evidence for the presence of the inclusion-free outer zones in some of the garnet crystals.

Similarly, anhedral peritectic garnets in the nebulitic leucosomes have embayed margins rimmed by coarse-grained orthopyroxene and cordierite (Fig. 4a). In these rocks, a symplectic intergrowth of orthopyroxene and cordierite is present in some places. In others, cordierite is completely replaced by orthoamphibole. Orthopyroxene is partially replaced by fine-grained fibrous intergrowth of kyanite biotite and quartz. These garnet crystals have cores that contain many

inclusions, whereas the rims are inclusion-free. In addition, garnet crystals from the garnet-bearing residuum display the same embayment as described above. The garnet crystals in the garnet-bearing residuum have embayed rims defined by moats of orthoamphibole, biotite and kyanite after cordierite and orthopyroxene.

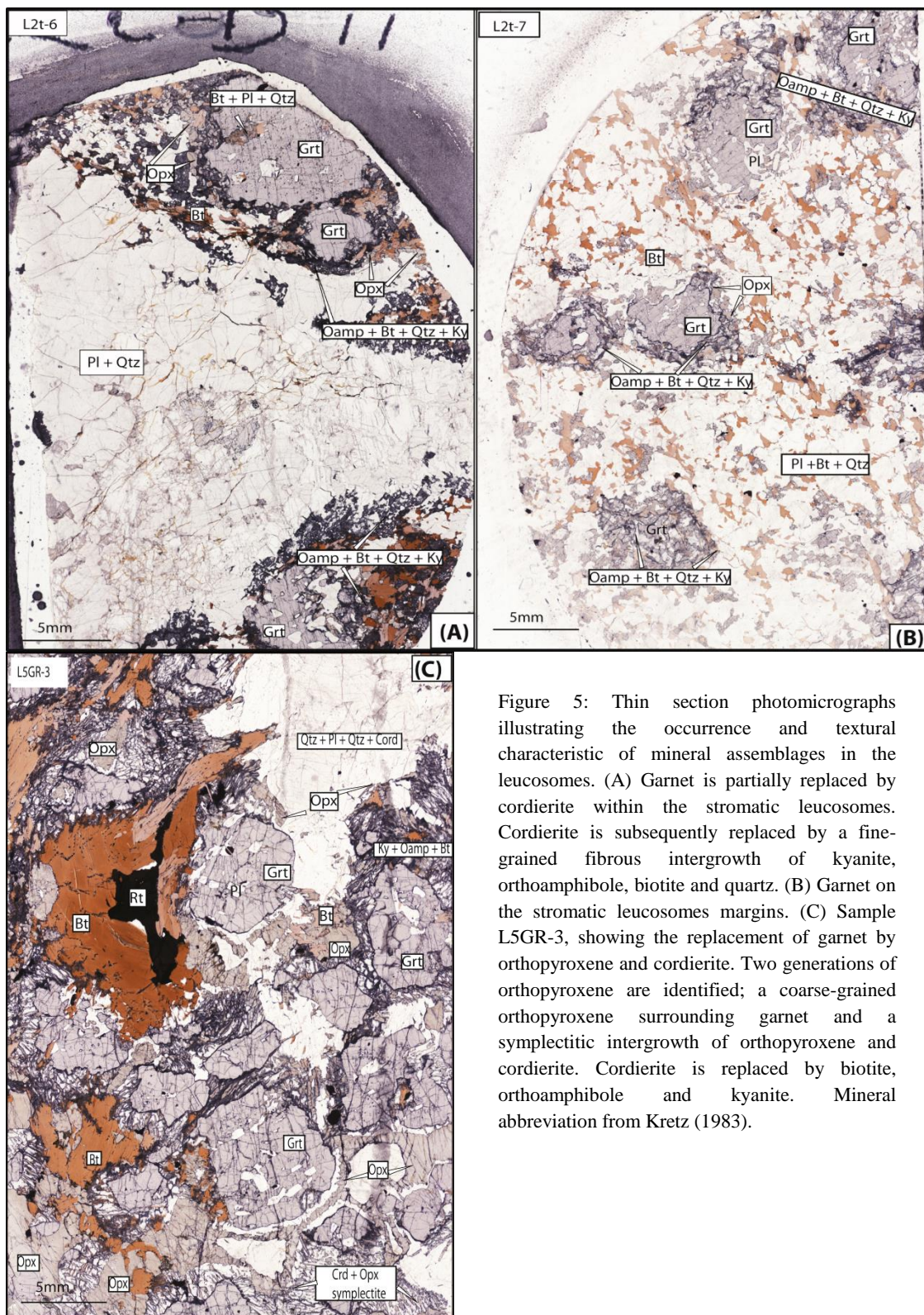


Figure 5: Thin section photomicrographs illustrating the occurrence and textural characteristic of mineral assemblages in the leucosomes. (A) Garnet is partially replaced by cordierite within the stromatic leucosomes. Cordierite is subsequently replaced by a fine-grained fibrous intergrowth of kyanite, orthoamphibole, biotite and quartz. (B) Garnet on the stromatic leucosomes margins. (C) Sample L5GR-3, showing the replacement of garnet by orthopyroxene and cordierite. Two generations of orthopyroxene are identified; a coarse-grained orthopyroxene surrounding garnet and a symplectitic intergrowth of orthopyroxene and cordierite. Cordierite is replaced by biotite, orthoamphibole and kyanite. Mineral abbreviation from Kretz (1983).

3.2. *Stromatitic leucosomes*

3.2.1. *L2t-6*

Garnet in sample L2t-6 occurs as a large poikiloblast of ~ 20mm in diameter and is typically replaced by relatively fine-grained orthopyroxene and cordierite. This indicates that the original garnet crystal was > 20mm in diameter. The garnet is commonly rounded in shape, and set in a matrix, dominated by plagioclase and quartz. Biotite is generally absent in the rock matrix, except a minor amount rimming orthopyroxene and cordierite, and larger crystals around garnet porphyroblast replacing orthopyroxene (Fig. 5A).

This garnet contains various inclusions of plagioclase, biotite, quartz, rutile and apatite (Fig. 6). The plagioclase inclusions show a bimodal distribution and a random scattering within the garnet. These plagioclase inclusions are unusual in that they are generally small in size and are the most abundant inclusions within garnet. Plagioclase inclusions range in crystal form from euhedral to anhedral, and in size from 50 to 500µm. Plagioclase crystals commonly occur as single crystals, clusters of crystals and crystals that typically form polymineralic inclusions that consist of quartz, biotite and rutile. Biotite inclusions range in size from µm to mm (<5µm to 2mm). The larger biotite crystals (mm) are polymineralic, typically consist of plagioclase with or without quartz. The µm inclusions show optical continuity that is not related to the matrix foliation. The optical continuity is interpreted to represent growth of garnet in the source while biotite was melting, rather than crystallization of garnet from the leucosomes. Quartz commonly occurs as both euhedral crystals which display a perfect hexagonal crystal form and rounded crystals within plagioclase. The euhedral quartz crystals occur as single crystals as well as inclusions in plagioclase. Garnet also hosts very fine-grained, up to 10µm clusters of quartz + plagioclase ± biotite (Fig. 7). This assemblage is interpreted as crystallized pure melt inclusions, and follows interpretation of (Cesare et al., 2011).

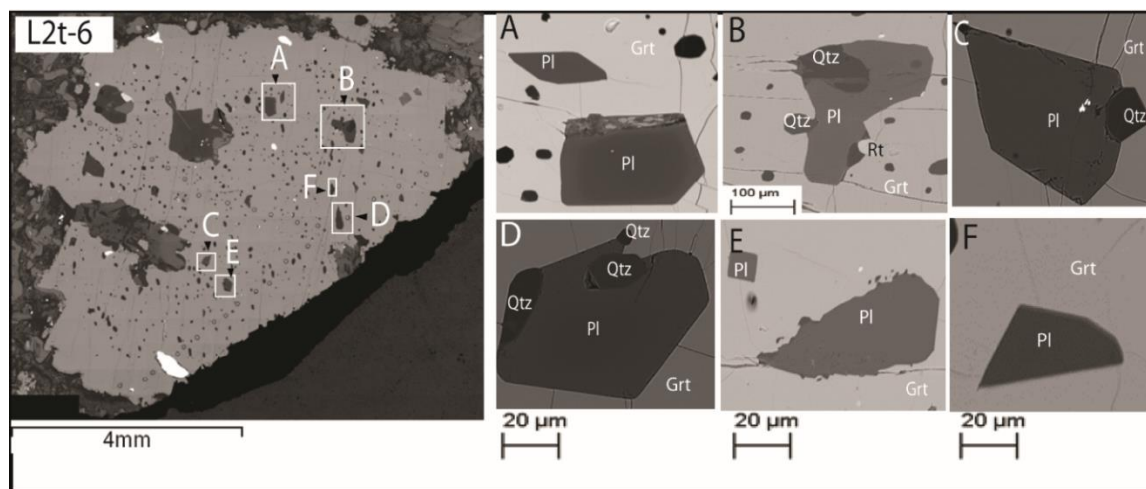


Figure 6: BSE images showing textural characteristics of plagioclase inclusions in garnet. (A) A single euhedral plagioclase inclusion in garnet. Zonation is seen in this BSE image; brighter = higher average atomic mass, and represents a more Ca-rich domain within the plagioclase. (B) Plagioclase in association with other polymineralic inclusions. (C-D) Euhedral plagioclase inclusions in contact with quartz. (E) Anhedral plagioclase crystals within garnet. (F) Fine-grained euhedral inclusion in garnet. Mineral abbreviations from Kretz (1983).

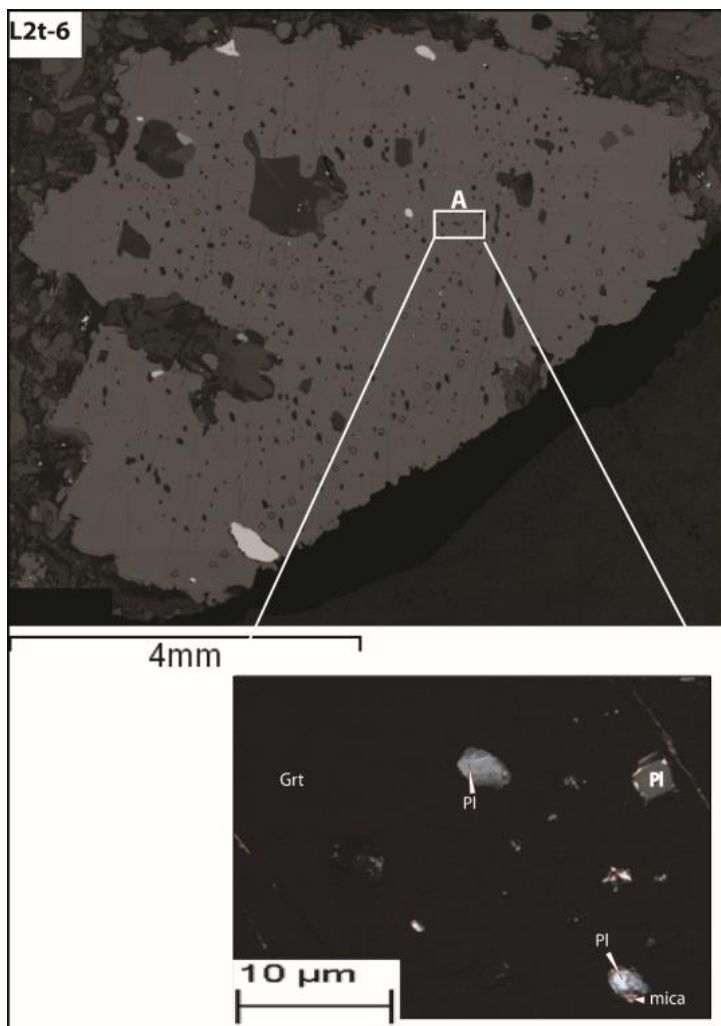


Figure 7: BSE image illustrating the locality of mineral inclusions within garnet. Mineral abbreviation from Kretz (1983). (A) Show magnified image of the melt inclusions within garnet.

3.2.2. L2t-7

This sample was taken from the margin of the stromatitic leucosome. Garnet in this sample is commonly rounded in shape and occurs as relatively large crystal up to 6mm in diameter. This garnet is set in a strongly foliated matrix characterized by biotite, plagioclase, quartz, cordierite and orthopyroxene. The garnet is rimmed, and partially replaced by cordierite and orthopyroxene indicating that this garnet was > 10mm in diameter.

This garnet contains inclusions of plagioclase, quartz, biotite, and rutile in descending abundance (Fig. 8). These inclusions are less abundant than in sample L2t-6, and occur mostly towards the garnet rims. Plagioclase inclusions range in crystal habit from euhedral to crystals that mimic the

garnet symmetry. This form will be referred to as ‘negative garnet form’ Moyen et al. (2006) hereafter. In addition, these plagioclase crystals are commonly clustered in two distinct domains toward the garnet rims. In one domain, the plagioclase inclusions have a negative garnet form, commonly contain rounded quartz inclusions, and some are in contact with euhedral quartz. While, in the second domain plagioclase inclusions are euhedral single crystals. Polymineralic crystals are rare in the second domain. However, when observed, they occur as small crystals $\sim 53\mu\text{m}$ that also typically consist of quartz towards the garnet rims. Quartz inclusions commonly occur as both single crystals and inclusions in plagioclase.

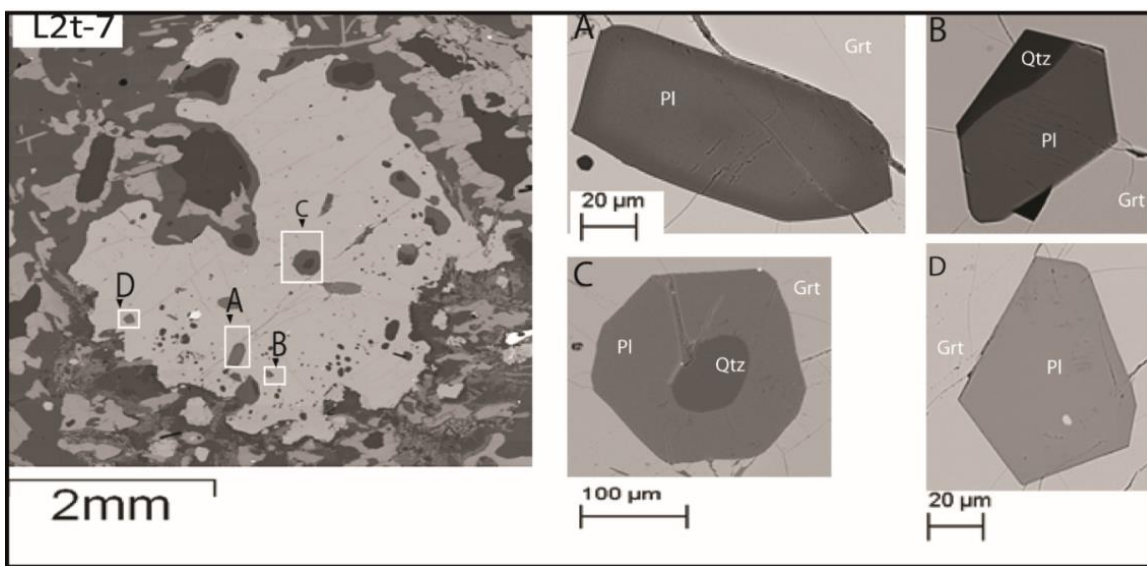


Figure 8: BSE images displaying textural features between plagioclase inclusions and the garnet host. (A) Plagioclase inclusion with complex zonation. Brighter = higher average atomic mass, and represents a more Ca-rich domain within the plagioclase. (B) Euhedral plagioclase inclusion in contact with quartz. (C) Plagioclase crystal that mimics the garnet symmetry. (D) Euhedral plagioclase inclusion. Mineral abbreviation from Kretz (1983).

3.3. *Nebulitic leucosomes*

The nebulitic leucosomes contain large subhedral garnet poikiloblasts, orthopyroxene, cordierite, biotite, quartz and plagioclase. A second generation of orthopyroxene is present as fine-grained orthopyroxene + cordierite symplectic intergrowths. This symplectic intergrowth partially replaces large former garnet. Biotite occurs as both large crystals rimming orthopyroxene, and small intergrowths with kyanite + orthoamphibole + quartz replacing cordierite (Fig. 4C).

A subhedral peritectic garnet (up to 8mm in diameter) contains various inclusions of plagioclase, quartz, rutile, orthopyroxene and biotite, with a decreasing abundance towards garnet rims. Inclusions in this sample are larger than those in the stromatitic leucosomes. Plagioclase inclusions are typically large polymineralic inclusions that contain quartz, orthopyroxene, rutile and biotite. In some cases, plagioclase inclusions occur as small anhedral to euhedral crystals that range in size from 80 to 900 μm . The smaller (80 μm) euhedral plagioclase crystals commonly occur in the interiors of the garnet, and are in contact with quartz, but never contain quartz as inclusions. The relatively larger (> 80 μm) euhedral plagioclase crystals occur as single grains towards the garnet rims. In addition, some euhedral crystals occur as larger (typically 900 μm) polymineralic crystals, which consist of clusters of orthopyroxene, rutile and biotite. Conversely, the anhedral inclusions range in size from 80-600 μm . These plagioclase crystals commonly contain quartz inclusions and usually occur towards the garnet rims. In some cases the plagioclase is partially enclosed by large quartz crystals. The rims of garnet, typically 1.4mm from the inclusion-rich core are inclusion-free (Fig. 8).

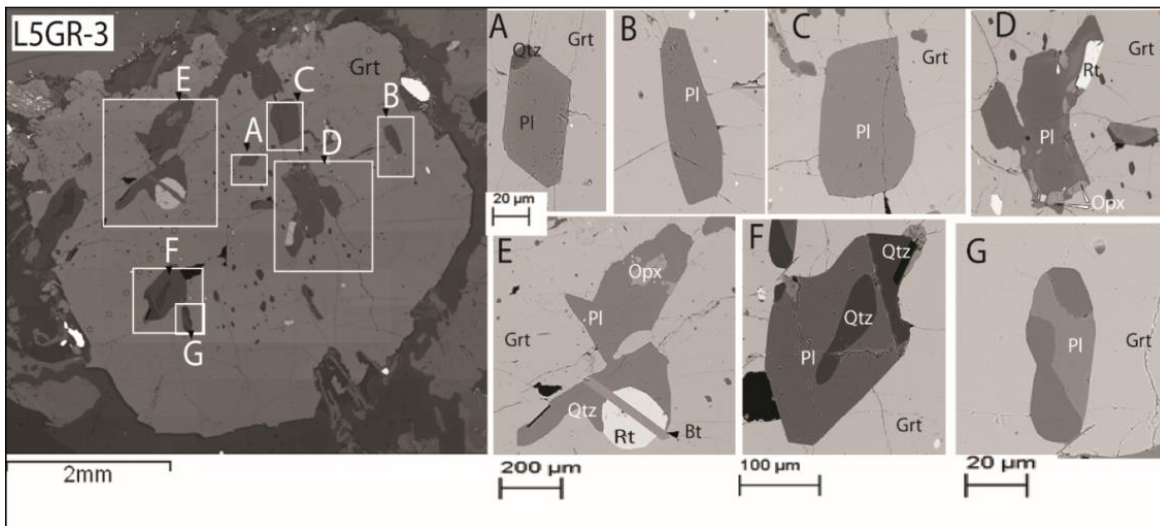


Figure 9: BSE images illustrating the textural relationships between the plagioclase inclusions in garnet. (A) Euhedral plagioclase inclusion in contact with quartz. (B-C) Monomineralic euhedral plagioclase crystals within garnet. (D-E) Euhedral plagioclase crystals clustered with other polymineralic inclusions. (F) Larger anhedral plagioclase crystal in contact with and enclosing quartz. (G) Anhedral plagioclase inclusion partially enclosed by quartz. Mineral abbreviation from Kretz (1983).

3.4. Residues

Garnet contained in the residuum of the metapelitic layer commonly occurs as rounded crystal up to 5mm in diameter. These garnet crystals occur in a matrix dominated by plagioclase and quartz. One garnet crystal contains inclusions of plagioclase, quartz, biotite and rutile (Fig. 9). Plagioclase inclusions vary in crystal form from anhedral to euhedral, and in size from 40 to 500 μ m. The inclusions are randomly distributed within the garnet. The smaller crystals (up to 100 μ m) are euhedral, and are commonly clustered within the garnet core. Some of the smaller crystals only contain biotite inclusions. One large anhedral crystal (up to 500 μ m) occurs near the garnet rim and contains rounded quartz inclusion.

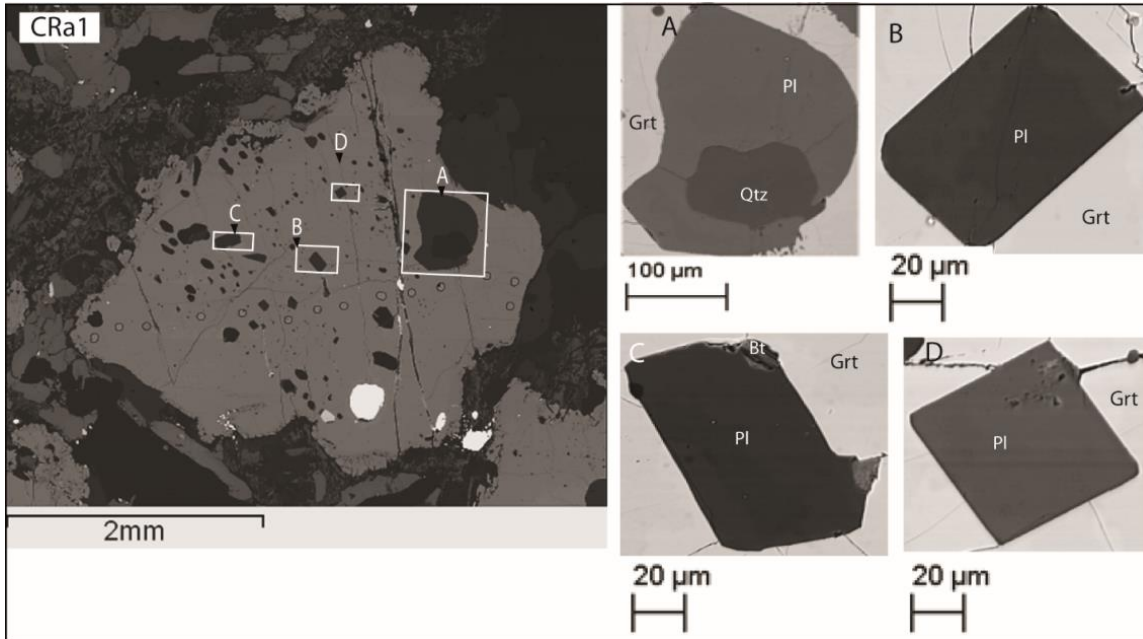


Figure 10: BSE images presenting textural relationships between plagioclase inclusions and the garnet host. (A) Larger anhedral plagioclase crystals enclosing a quartz inclusion. (B) Euhedral plagioclase inclusion. (C) Euhedral plagioclase inclusion enclosing fine-grained biotite inclusions. (D) Euhedral plagioclase inclusion. Mineral abbreviation from Kretz (1983).

4. ANALYTICAL METHODS

4.1. Electron beam analyses

Plagioclase and garnet major element compositions were analysed by quantitative EDS and WDS analysis using a Zeiss EVO MA 15 Scanning Electron Microscope (SEM) at the Central Analytical Facility (CAF) of Stellenbosch University, South Africa. Mineral major element compositions were quantified by EDX (Energy Dispersive X-ray) analysis using an Oxford Instruments® X-Max 20mm² detector and Oxford INCA software. Sr was selectively quantified by WDS analysis using the same instrument and software setup. The acquisition time for the Sr peak was 60s on-peak and 30s off-peak and for EDS mineral analyses, 10 second live-time per analyses. The beam conditions used during quantitative analyses were 20 Kv accelerating voltage, 1.5 nA probe current, with a working distance of 8.5mm and a specimen beam current of -20.00nA. Analyses were quantified using natural mineral standards. Subsequently, the quality of the analytical data was verified by using a mineral standard of known composition as an unknown (Table 1, appendix A). The composition of the known composition was then compared to its actual published composition (Astimex Scientific limited, MINM25-53 #05-010). Mineral chemical compositions were recalculated to their mineral stoichiometries to obtain resultant structural formulae. The resultant stoichiometry was used to evaluate the quality of the analysis. The analyses falling below ± 0.02 of ideal stoichiometry were rejected (i.e. cation totals for plagioclase = 5 ± 0.02 , garnet = 8 ± 0.02 on the basis of 8 oxygens for plagioclase and 12 oxygens for garnet). This system is designed to perform high-resolution imaging concurrently with quantitative analyses, with errors ranging from ± 0.6 to 0.1 wt. % on the major elements using EDS and ± 0.01 to 0.03 wt. % on the trace element (Sr) using WDS. However, no major element garnet data was obtained for the residuum sample because the sample was lost.

Table 1: Plagioclase standard compositional variability

Mineral	PI	PI	PI	PI	Avg(#)	STD	Published standard
Measured standard spot#	1	2	3	4			
SiO₂	53.03	52.54	52.43	52.62	52.66	0.24	53.00
TiO₂	-	-	0.15	-	0.04	0.03	-
Al₂O₃	29.57	29.56	29.48	29.60	29.55	0.72	28.53
FeO	0.38	0.39	0.43	0.48	0.42	0.03	0.37
MgO	-	-	-	0.14	0.03	0.07	0.13
CaO	11.86	11.96	11.84	11.85	11.88	0.05	11.80
BaO	-	-	-	-	-	0.01	0.01
Na₂O	4.59	4.51	4.37	4.42	4.47	0.09	4.35
K₂O	0.38	0.33	0.28	0.37	0.34	0.05	0.41
Total	99.81	99.29	98.98	99.47	99.39	0.56	98.60
Number of anions on the basis of XO⁻²							
Si⁴⁺	2.40	2.40	2.40	2.40	2.40	0.03	2.44
Ti³⁺	-	-	0.01	-	-	1.10	1.55
Al³⁺	1.58	1.59	1.59	1.59	1.59	1.12	-
Fe²⁺	0.01	0.01	0.02	0.02	0.02	-	0.01
Mg²⁺	-	-	-	0.01	-	0.01	0.01
Ca²⁺	0.58	0.58	0.58	0.58	0.58	0.00	0.58
Na⁺	0.40	0.40	0.39	0.39	0.40	0.00	0.39
K⁺	0.02	0.02	0.02	0.02	0.02	0.00	0.02
Σcat.	5.00	5.00	5.00	5.00	5.00	0.00	5.00
Anions	7.98	7.98	8.00	7.98	7.99	0.01	8.00
Sr(ppm)	339.66	240.81	332.79	500.00	353.32	315.85	800.00

STD = standard deviation, Avg = Average, # = number

4.2.LA-ICP-MS

In-situ garnet trace-element analyses were obtained from polished thin sections by Laser-Ablation-Inductively-Coupled-Mass Spectrometry (LA-ICPMS) at CAF. The LA-ICP-MS system consists of an excimer laser ablation system emitting at 193nm (Resonetics Resolution S155) coupled to an Agilent 7500ce quadrupole ICP-MS. Trace element data have been obtained by single spot analysis using a 67µm beam diameter. Ablation was performed using a double-helix ablation cell (Laurin Technic, Canberra, Australia) in helium that was mixed in a conical ablation cup into the Ar sample gas (with approximately 3.5ml/min added N₂) of the mass spectrometer. NIST SRM 610 glass (values from Pearce et al., 1997) was used as a primary calibration standard and measured garnet (by EDS) SiO₂ contents (39 wt. %) was used as an internal standard. In a typical analytical sequence one standard was analysed, followed by 10 unknowns, and then repeated as necessary. For each analysis an ablation time of 20s was applied. Background was measured for 20s prior to ablation. Data acquisition was performed by peak, hopping to measure one sample per peak. Reduction of time-resolved data and

concentration calculations were subsequently performed off-line using the GLITTER software package. One analysis of the NIST SRM 612 and USGS basalt Columbia River (BCR-2) glass standard was performed with every ten unknowns for quality control (Fig. 11). In addition, the results are consistently within 2s of the average concentrations reported by Pearce et al. (1997) and the USGS, respectively. The detection limit for most of the elements is in the lower to mid ppb range. The trace element patterns are normalized to the C1 chondrite values employed by the GLITTER software package.

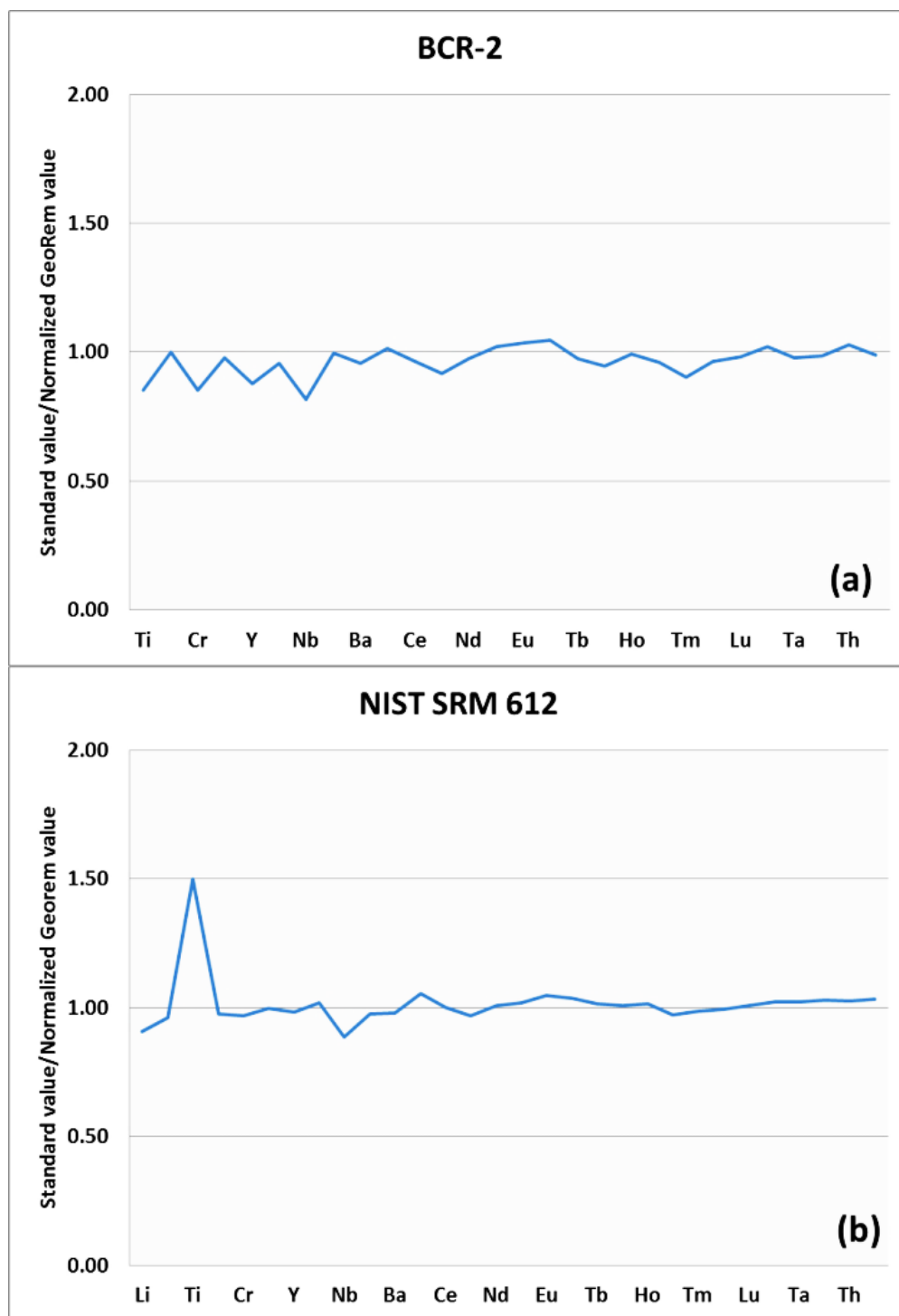


Figure 11: Normalized rem preferred values of the USGS reference materials; BCR-2 and NIST SRM 612, relative to the original standard values of BCR-2 and NIST SRM 612. Values deviating ± 0.5 from the normalized rem preferred standard values (1.0) are considered good values i.e. Ti. in b. Most element concentrations agree within uncertainty limits of ~ 1-5%.

4.3. Modelling

Phase equilibria modelling was undertaken using the chemical system Na₂O-CaO-K₂O-FeO-MgO-Al₂O₃-SiO₂-H₂O-TiO₂-O₂ (NCKFMASHTO) using the THERIAK/DOMINO software package (de Capitani and Petrakaki, 2010), in combination with the updated database model of Holland and Powell (1998). The following models were used: biotite, garnet (White et al., 2005), melt (White et al. (2007), orthoamphibole (Diener and Powell, 2012), muscovite (Coggon and Holland, 2002), ilmenite (White et al., 2005), cordierite (Holland and Powell, 1998), orthopyroxene (White et al., 2002), feldspar (Holland and Powell, 2003). Pseudosections were calculated using three different synthetic bulk rock compositions based on the mineral compositions published by (Stevens et al., 1997), over the same range of temperatures and pressures previously investigated by Taylor et al. (2014) on the metapelite exposures at the BQ. For the purpose of the modelling, the rock was regarded as a mixture of biotite, quartz and plagioclase. The compositions used are provided in (Table 2).

Table 2: Mineral compositions taken from Stevens et al. (1997) as well as the synthetic bulk compositions used for modelling.

Starting compositions				SiO ₂	TiO ₂	Al ₂ O ₃	Fe ₂ O ₃	FeO	MgO	CaO	Na ₂ O	K ₂ O	H ₂ O	Total
Biotite				38.18	2.29	20.21	-	15.34	12.07	-	-	8.99	2.92	100
Plagioclase				59.76	-	25.5	-	-	-	6.41	8.33	-	-	100
Quartz				100	-	-	-	-	-	-	-	-	-	100
Bulk (wt. %)	Pl	Bt	Qtz	SiO ₂	TiO ₂	Al ₂ O ₃	Fe ₂ O ₃	FeO	MgO	CaO	Na ₂ O	K ₂ O	H ₂ O	Total
1	5%	38%	57%	74.5	0.87	8.95	-	5.83	4.59	0.32	0.42	3.42	1.11	100
2	10%	36%	54%	73.72	0.82	9.83	-	5.52	4.35	0.64	0.83	3.24	1.05	100
3	12%	35%	52%	73.41	0.81	10.17	-	5.4	4.25	0.77	1	3.16	1.03	100
4	20	32%	48%	72.17	0.73	11.57	-	4.91	3.86	1.28	1.67	2.88	0.93	100

5. CHEMISTRY OF THE GARNET

5.1. Major element chemistry

Garnet rim-core-rim zonation profiles are illustrated in Figs 10-12. The analysed garnet crystals are an almandine-pyrope solid solution, with minor amounts of grossular and spessartine. Representative garnet major element mineral compositions are summarized in Table 2. The full data set is provided in the appendix B. The calculated end-members discussed below are almandine, pyrope, grossular and spessartine. These are defined as; $X_{alm} = Fe^{2+} / (Fe^{2+} + Mg + Ca + Mn)$, $X_{pyr} = Mg / (Mg + Fe^{2+} + Ca + Mn)$, $X_{sps} = Mn / (Mn + Mg + Fe^{2+} + Ca)$ and $X_{grs} = Ca / (Ca + Fe^{2+} + Mg + Mn)$ respectively.

Table 3: Representative compositions of individual garnet crystals (wt. %) from specific localities in the leucosomes. The stromatic leucosomes are indicated as L2t-6 and L2t-7 in Table (1) and the nebulitic leucosome is indicated as L5GR-3.

Sample	L2t-6	L2t-6	L2t-7	L2t-7	L5GR-3	L5GR-3	L5GR-3
Mineral	Garnet	Garnet	Garnet	Garnet	Garnet	Garnet	Garnet
Generation	Rim	Core	rim	Core	outer-rim	inner-rim	Core
SiO ₂	39.58	39.05	39.41	38.89	39.44	39.23	39.75
Al ₂ O ₃	22.53	22.29	22.44	22.15	22.50	22.30	22.42
Cr ₂ O ₃	0.24	0.00	0.14	0.00	0.42	0.29	0.24
Fe ₂ O ₃	0.14	0.19	0.00	0.06	0.00	0.38	0.00
FeO	25.69	24.98	24.76	24.52	23.39	23.10	21.92
MnO	0.67	0.58	0.62	0.73	0.42	0.48	0.32
MgO	10.83	9.43	10.92	9.34	11.70	12.22	11.86
CaO	1.29	3.38	1.22	3.59	1.45	1.20	2.81
Total	100.97	99.89	99.50	99.28	99.31	99.20	99.31
Number of anions on the basis of 12 oxygen atoms							
Si ⁴⁺	2.99	2.99	3.01	2.99	3.00	2.98	3.01
Al ³⁺	2.00	2.01	2.02	2.01	2.02	2.00	2.00
Cr ³⁺	0.01	0.00	0.01	0.00	0.02	0.02	0.01
Fe ³⁺	0.01	0.01	0.00	0.00	0.00	0.02	0.00
Fe ²⁺	1.62	1.60	1.58	1.58	1.49	1.47	1.39
Mn ²⁺	0.04	0.04	0.04	0.05	0.03	0.03	0.02
Mg ²⁺	1.22	1.08	1.24	1.07	1.33	1.38	1.34
Ca ²⁺	0.10	0.28	0.10	0.30	0.12	0.10	0.23
Σ Cat	8.00	8.00	8.00	8.00	8.00	8.00	8.00
Anions	12.00	12.00	12.02	12.00	12.02	12.00	12.02
Xalm	0.54	0.53	0.53	0.53	0.50	0.49	0.47
Xpyr	0.41	0.36	0.42	0.36	0.45	0.46	0.45
Xgrs	0.03	0.09	0.03	0.10	0.04	0.03	0.08
Xsps	0.01	0.01	0.01	0.02	0.01	0.01	0.01

5.1.1. Stromatitic leucosomes

5.1.1.1.L2t-6

Garnet in sample L2t-6 shows chemical zoning with respect to Ca, Fe and Mg (Fig. 12a), which is also confirmed by the X-ray elemental mapping of the garnet (Fig. 12b-c). The amount of almandine and pyrope increases from core to rim, while the amount of grossular exhibits a general decrease from core to rim. Grossular shows high values in the core ($X_{\text{grs}} = 0.08$), dropping to the compositions similar to that of the rims in the intermediate between the core and the rim ($X_{\text{grs}} = 0.04$) in association with

cracks. The minor component of spessartine is homogeneous from core to rim. The typical compositional ranges are: X_{alm} varies from 0.53 to 0.57, whereas the concentration of X_{pyr} and X_{grs} varies from 0.36 to 0.41 and from 0.09 to 0.03 respectively. An increase in grossular at the rims is accompanied by a decrease in pyrope.

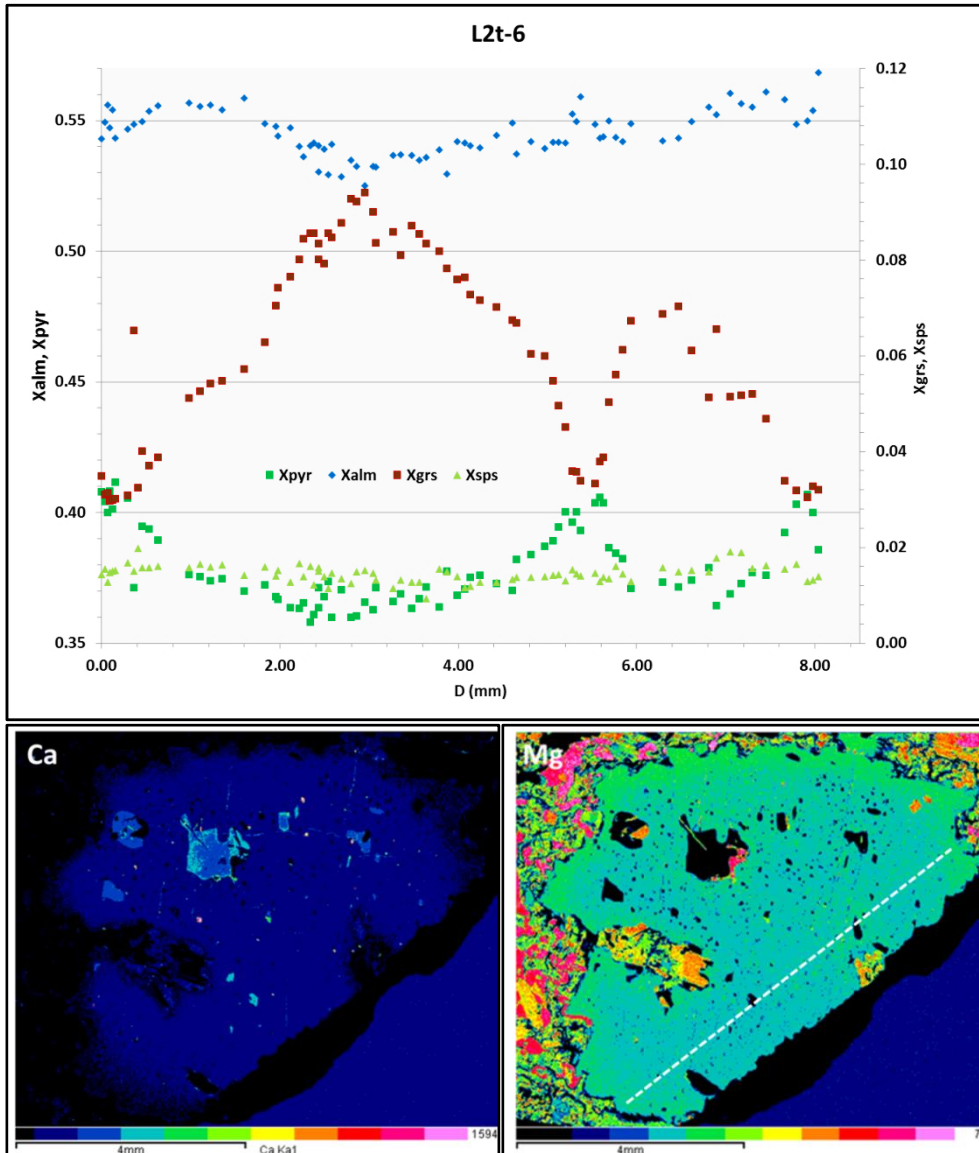


Figure 12: Details of compositional variation in garnet from sample L2t-6. (a) A quantitative spot analysis of a garnet traverse. (b-c) Ca and Mg elemental maps showing qualitative 2D X-ray mapping of a garnet from the stromatolitic leucosomes (traverse indicated by dotted line). The warm colours indicated on the colour bar show the highest concentration of an element.

5.1.1.2.L2t-7

Garnet in sample L2t-7 is compositionally similar to garnet in sample L2t-6. This garnet is zoned with respect to almandine, pyrope and grossular, and unzoned with respect to spessartine. The minor grossular component shows two bell-shaped profiles with the central linear structure through the centre of the crystal. This structure possibly represents a plane along which two separate crystals have been amalgamated with fused grain-boundaries in support of Taylor and Stevens (2010) observations on similar features. Pyrope and almandine show opposite trends with respect to grossular. Grossular displays high values in the intermediate ($X_{\text{grs}} = 0.09$) dropping to low values ($X_{\text{grs}} = 0.03$) in the central portion of the crystal to compositions similar to that of the rim. Pyrope ranges from 0.35 to 0.42 and almandine varies from 0.55 to 0.51. Additional qualitative X-ray elemental mapping of the garnet verified this zonation (Fig. 13b-c).

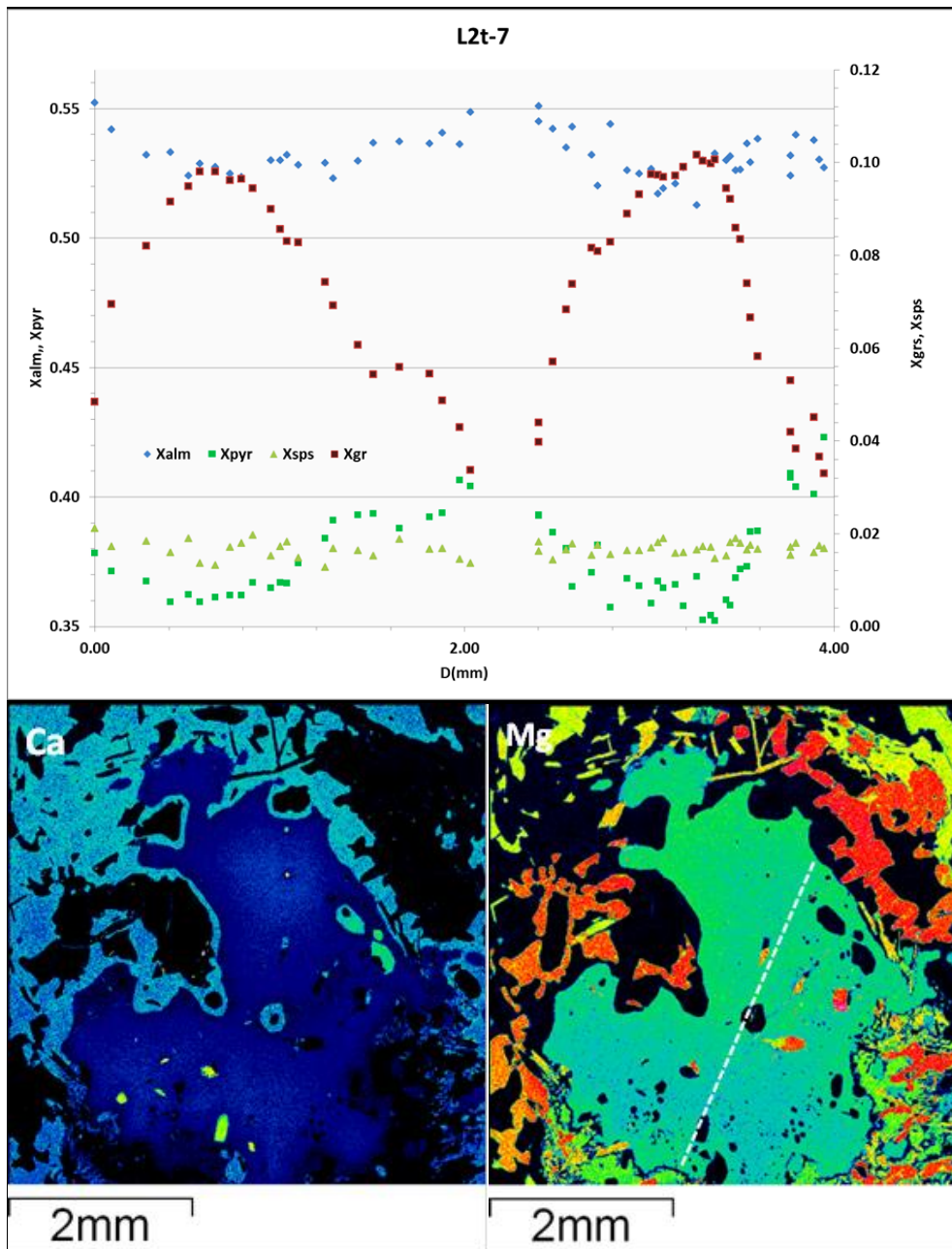


Figure 13: Details of compositional variation in garnet from sample L2t-7. (a) A quantitative spot analysis of a garnet traverse. (b-c) Mg and Ca elemental maps showing qualitative 2D X-ray mapping of a garnet from the Stromatitic leucosomes (traverse indicated by dotted line). The warm colours show the highest concentration of an element.

5.1.2. Nebulitic leucosomes

Garnet in sample L5GR-3 has the same compositional zoning as garnet crystals in samples L2t-6 and L2t-7. This garnet is zoned with respect to almandine, pyrope and grossular, and unzoned with

respect to spessarntine (Fig. 14a). Additional qualitative X-ray elemental mapping of this garnet confirmed this zoning (Fig. 14b-c). Grossular generally decreases from the core to the rim, while pyrope and almandine increases. Grossular shows high values in the core ($X_{\text{grs}} = 0.08$), dropping to compositions similar to that of the rims in the intermediate ($X_{\text{grs}} = 0.04$) in association with cracks. Pyrope and almandine varies from 0.42 to 0.47 and 0.46 to 0.50 respectively. Spessarntine is homogeneous ($X_{\text{sps}} = 0.01$) across garnet crystal. A portion typically 1.4mm from the garnet edge does not contain inclusions. This portion is characterized by a rapid increase in grossular followed by a drop in pyrope and almandine.

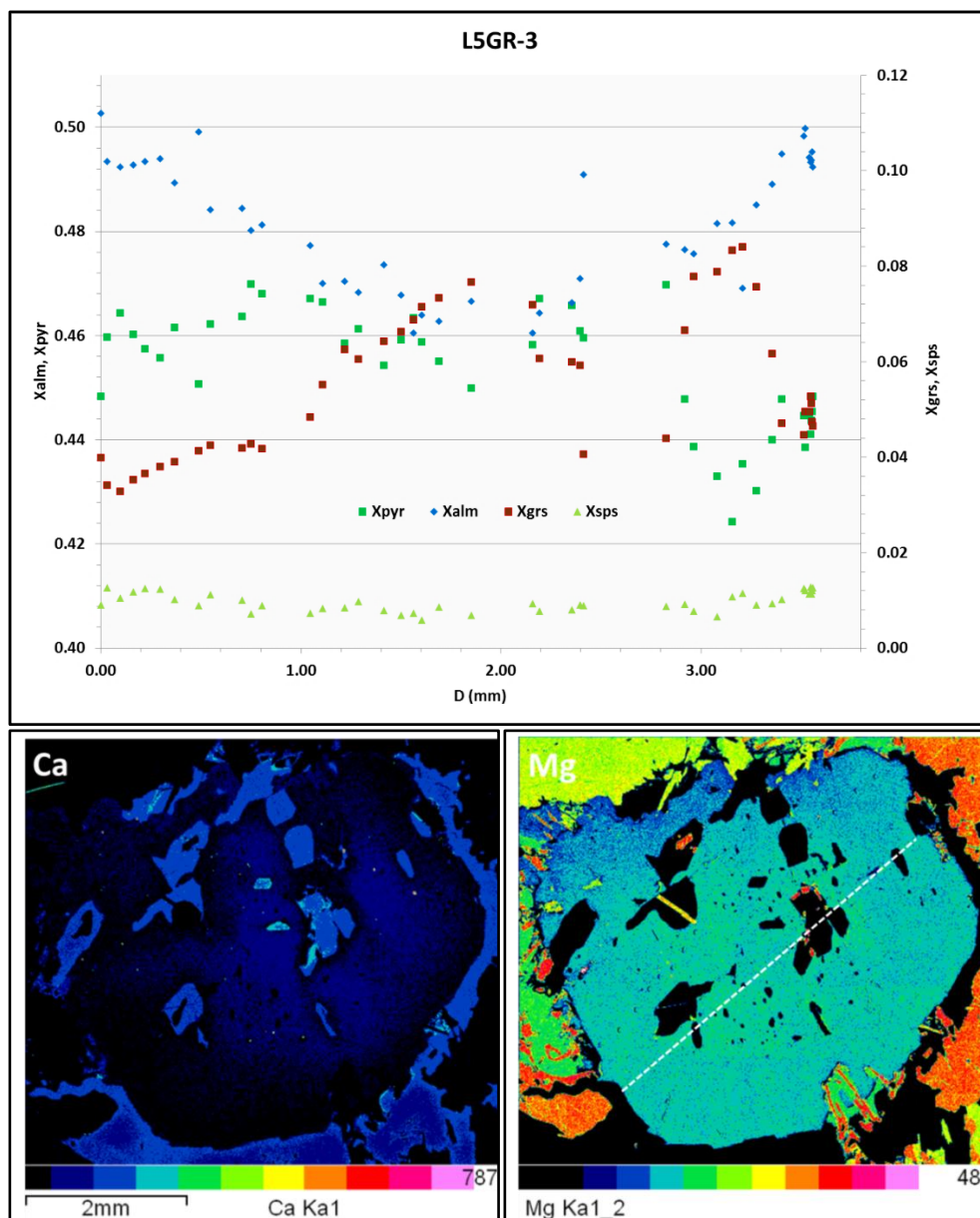


Figure 14: Details of the compositional variation in garnet in sample L5GR-3. (a) A quantitative spot analysis of a garnet traverse. (b-c) Ca and Mg elemental maps showing qualitative 2D X-ray mapping of a garnet from the nebular leucosomes (traverse indicated by dotted line). The warm colours indicated on the colour bar show the highest concentration of an element.

5.2.LA-IC PMS

Table 4: Representative LA-ICPMS data of garnet from sample L2t-6, L5GR-3 and CRa1. bdl = below detection limits, δ =sigma 1 error

	L2t-6				L5GR-3			
	1δ	Grt rim	1δ	Grt core	1δ	Grt rim	1δ	Grt core
Concentration (ppm)								
Li	22.9	bdl	12.0	bdl	8.4	20.6	22.5	118
P	26.9	225	14.4	54.1	16.5	220	11.3	64.0
Sc	7.1	218.9	6.9	211	7.9	237	7.0	205
Ti	5.3	104.1	6.1	125	4.1	79.6	6.2	130
V	2.2	65.0	2.9	83.5	1.8	51.0	5.6	161
Cr	32.8	914	29.2	797	52.3	1386	48.2	1221
Sr	0.04	0.16	0.02	bdl	0.01	0.02	0.01	0.02
Y	3.0	88.8	23.1	712	2.1	60.2	6.7	193
Zr	0.34	5.8	0.42	7.3	0.34	6.1	0.38	6.9
Nb	0.006	0.01	0.004	bdl	0.003	0.0029	0.004	bdl
Cs	0.02	0.066	0.01	bdl	0.006	bdl	0.009	bdl
Ba	0.31	bdl	0.08	bdl	0.07	bdl	0.10	bdl
La	0.009	bdl	0.005	bdl	0.006	bdl	bdl	0.001
Ce	0.02	0.06	0.01	0.016	0.006	0.010	0.009	0.02
Pr	0.0084	0.02	0.0096	0.016	0.005	0.008	0.01	0.02
Nd	0.10	0.45	0.15	0.85	0.08	0.37	0.11	0.69
Sm	0.23	2.0	0.29	2.4	0.18	1.4	0.25	2.5
Eu	0.03	0.16	0.07	0.479	0.04	0.23	0.03	0.15
Gd	0.65	11.1	0.72	11.8	0.45	6.7	0.58	9.2
Tb	0.15	3.1	0.27	5.8	0.09	1.5	0.16	3.1
Dy	0.86	18.8	2.9	73.9	0.51	9.7	1.4	29.3
Ho	0.14	2.8	0.87	22.5	0.11	1.9	0.36	7.8
Er	0.31	5.6	2.7	71.2	0.28	5.1	0.96	21.2
Tm	0.05	0.64	0.43	10.3	0.05	0.74	0.17	3.1
Yb	0.26	4.1	2.5	65.8	0.27	4.5	0.90	19.8
Lu	0.05	0.54	0.32	7.5	0.05	0.56	0.14	2.6
Hf	0.05	0.18	0.06	0.213	0.04	0.09	0.04	0.11
Ta	0.006	0.01	0.01	bdl	0.006	bdl	0.005	bdl
Pb	0.09	bdl	0.03	bdl	0.02	bdl	0.02	bdl
Th	0.04	bdl	0.006	bdl	0.01	0.03	0.010	bdl
U	0.01	0.02	0.009	bdl	0.009	bdl	0.01	bdl

Table 4 (continued)

CRA1				
	1δ	Grt rim	1δ	Grt core
Concentration (ppm)				
Li	5.8	bdl	12	0.01
P	14.5	172	23	39.6
Sc	4.2	118	0.3	11.7
Ti	5.8	109	1.8	bdl
V	3.8	106	0.15	bdl
Cr	79.8	1982	1.4	bdl
Sr	0.05	0.19	bdl	0.006
Y	3.6	99.4	bdl	0.05
Zr	0.54	10	bdl	0.02
Nb	0.008	bdl	0.01	0.58
Cs	0.005	0.005	0.01	3.3
Ba	0.24	1.4	0.15	0.08
La	bdl	0.001	bdl	6.7
Ce	0.006	0.009	bdl	1
Pr	0.009	0.009	bdl	6.5
Nd	0.07	0.19	bdl	1.6
Sm	0.28	2.4	0.07	6.2
Eu	0.04	0.16	0.02	1.1
Gd	0.79	12.2	0.06	9.9
Tb	0.15	2.6	0.01	1.5
Dy	0.94	17.7	bdl	0.21
Ho	0.2	3.7	0.01	bdl
Er	0.49	8.8	0.05	bdl
Tm	0.08	1.1	0.02	bdl
Yb	0.41	7	bdl	bdl
Lu	0.07	0.79	0.02	0.54
Hf	0.05	0.15	bdl	0.09
Ta	0.006	bdl	0.02	bdl
Pb	0.06	0.286	0.06	bdl
Th	0.006	0.006	0.02	bdl
U	0.01	bdl	0.01	0.04

The location for the LA-ICPMS spot analyses is indicated by the yellow dotted line in the BSE images (Figs. 15-17d). Chondrite-normalized REE patterns for individual analysis points are shown in Figs. 15-17a-c. Representative garnet trace element mineral chemistry is presented in Table 3. The full data set is provided in the appendix C.

5.2.1. L2t-6

As expected of garnet from granulite-facies conditions (e.g. Otamendi et al., 2002), garnet in sample L2t-6 displays a typical bell-shaped trace element zonation patterns. The cores are preferentially enriched in Y (plotted as proxy for HREEs) and Dy than the rims (Fig. 15b). The garnet shows no zonation with respect to Zr. V and Ti show a decrease in abundance towards the rim, while Cr increases (Fig. 13c). Y abundance ranges from (700-400ppm in cores) to (< 50ppm in the rims, Fig. 13b). The heavy REEs (Yb and Er) follow spatial distribution patterns that are almost identical to those of Y, although at lower concentrations (70-20 ppm in cores, < 5ppm in the rims). Among the middle REEs, Dy and Gd (which is the most light of the middle REEs) follow a pattern similar to that of Y and the heavy REEs, but with concentrations that are higher than those of heavy REEs (Fig. 15b).

Negative Eu/Eu^* ($\text{Eu}_N / (\text{Sm}_N + \text{Gd}_N)/2$) referred to as Eu/Eu^* hereafter, are considerably more negative in the rim ($\text{Eu}/\text{Eu}^* = 0.01$) than the core ($\text{Eu}/\text{Eu}^* = 0.30$). Sm/Gd ratio shows a decrease (0.38 to 0.15) from core to rim. The $(\text{Lu}/\text{Gd})_N$ values are used as a differentiation index. This garnet has slightly negative chondrite-normalized Gd-Lu slopes $(\text{Lu}/\text{Gd})_N = 5.06 - 0.41$ core to rims (Fig. 15a).

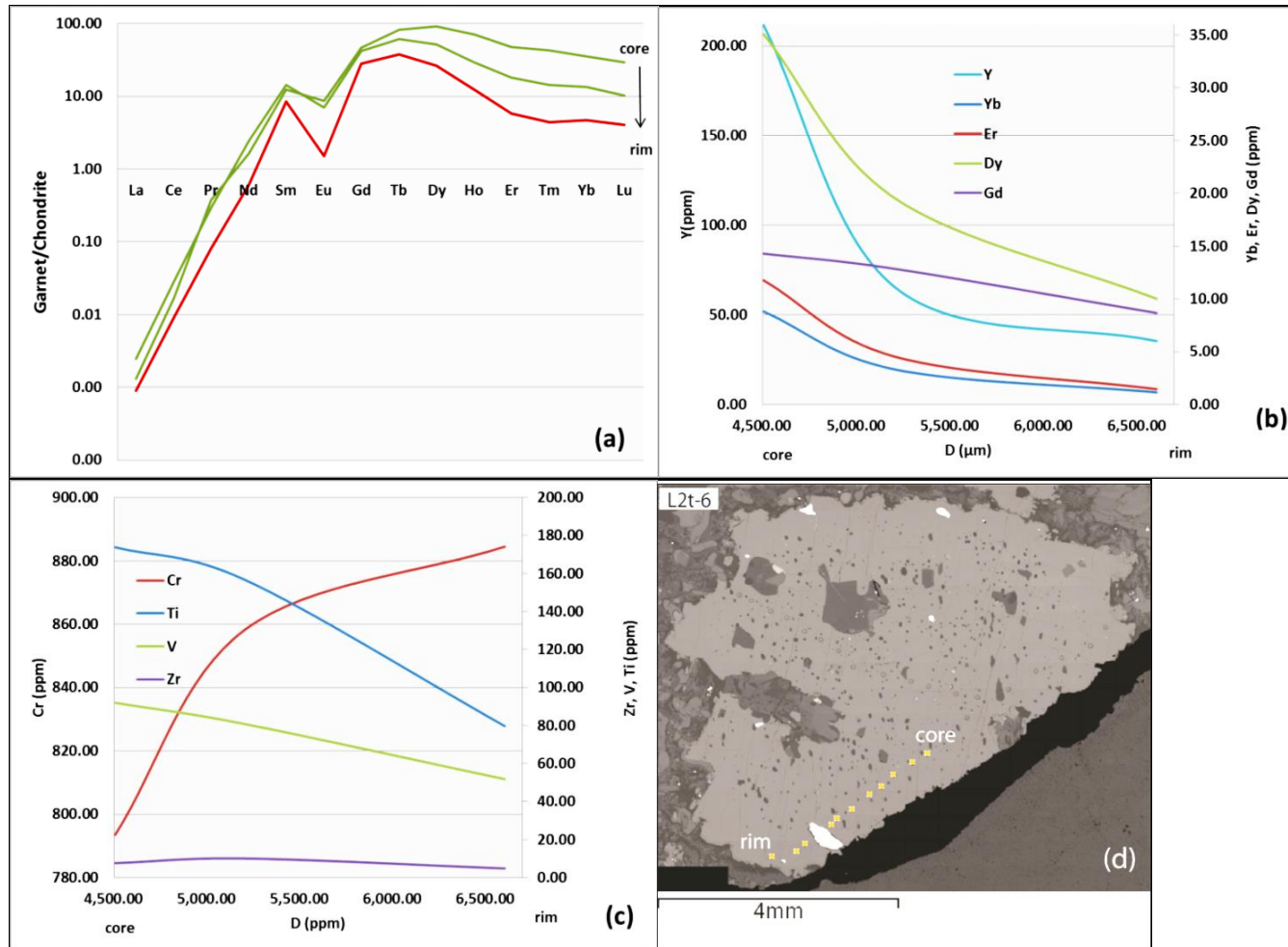


Figure 15: (a) Chondrite-normalized REE pattern of a garnet grain from sample L2t-6. This garnet is strongly zoned in terms of HREE, enriched in the HREE and has a negative pronounced Eu anomaly in the rims (b) Y, Yb, Er, Gd, Dy in ppm plotted as proxy for REE zonation from the same sample. The analysis is along the same traverse as in a. (c) Cr, Ti, V and Zr in ppm plotted as proxy for trace elements zonation in sample L2t-6. Analysis is along the same traverse as in a. (d) A core to rim analysis traverse illustrated by a yellow dotted line on the BSE image.

5.2.2. *Nebulitic leucosomes*

Garnet in sample L5GR-3 displays a relatively similar REE (+Y) zonation pattern to that in sample L2t-6 (Fig. 16a). This garnet shows a decrease in heavy REEs towards the rims. The cores are preferentially enriched in Yb, Er, Y and Dy compared to rims. Y abundance varies from (200-100ppm in cores), to (<50ppm in the rims). The heavy REEs follow spatial distribution pattern similar to Y, though at lower concentrations (20-10ppm in the cores, <5ppm in the rims, Fig. 16b). Dy follows a pattern similar to that of Y, and the heavy REEs, with slightly higher concentrations in the rims than the heavy REEs. Gd displays the similar zonation pattern to the HREEs although at lower abundances (<15 ppm). The inclusion free portion of this garnet is slightly enriched in REE (+Y) (Fig. 16a). Zr is commonly constant across garnet, whereas Ti and V decrease towards the rim. Cr shows variable distribution, with high values in the rims (Fig. 16c).

The garnet is characterized by a negative Eu/Eu* anomaly. The depth of the anomaly is more negative in the rims (Eu/Eu* = 0.008) than the cores (Eu/Eu* = 0.026). The Sm/Gd ratio does not show any defined pattern, but higher values are found in the rims (0.34-0.51). This garnet is characterized by somewhat flat to slightly positive chondrite-normalized slope ((Lu/Gd)_N = 1.02 – 2.99 in the cores, (Lu/Gd)_N = 0.78-0.215 in the rims).

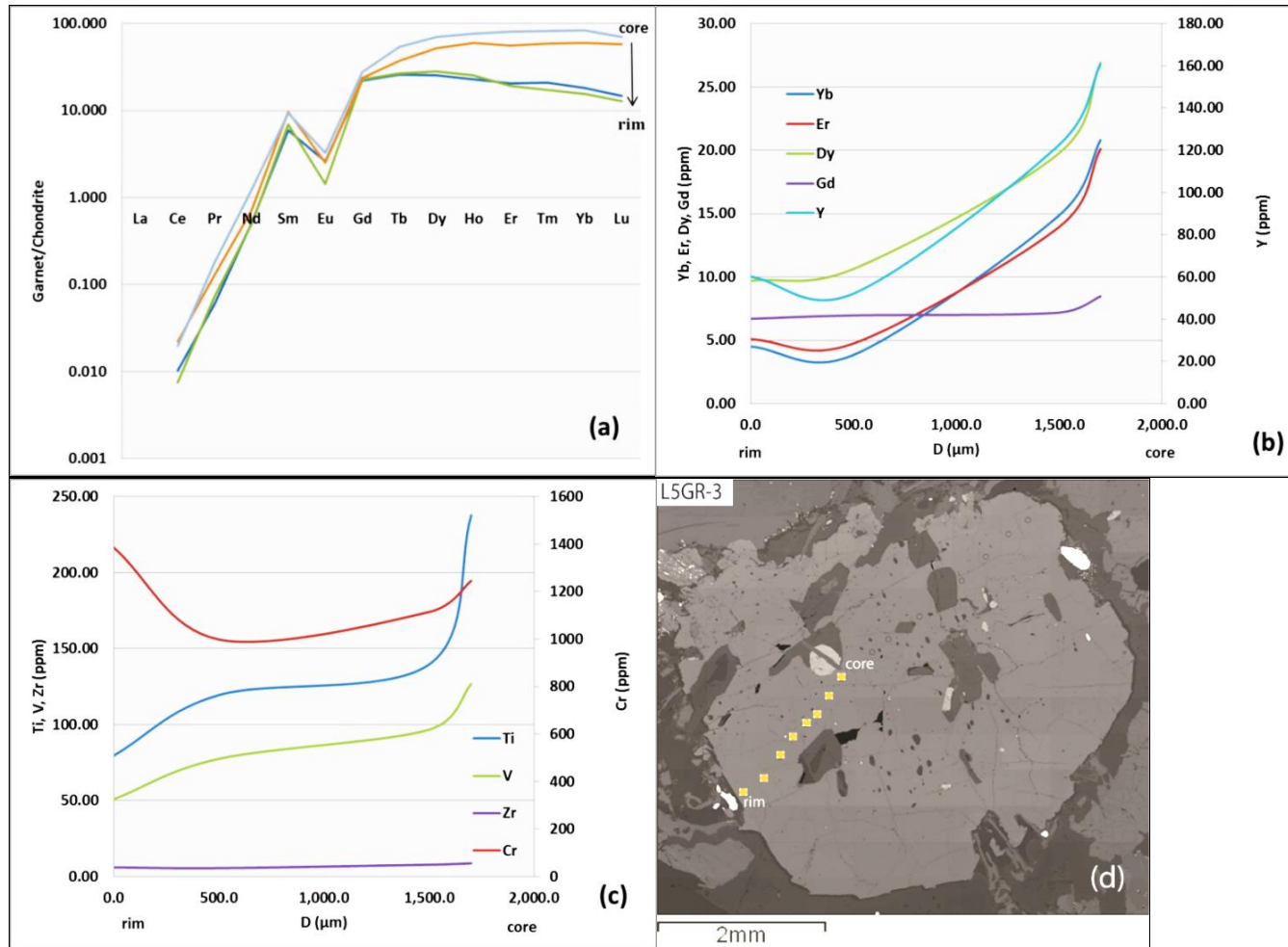


Figure 15: (a) Chondrite-normalized REE pattern of a garnet grain from sample L5GR-3. This garnet is strongly zoned in terms of HREE, enriched in the HREE and has a negative pronounced Eu anomaly in the rims. (b) Y, Yb, Er, Gd, Dy in ppm plotted as proxy for REE zonation from the same sample. The analysis is along the same traverse as in a. (c) Cr, Ti, V and Zr in ppm plotted as proxy for trace elements zonation in sample L5GR-3. The analysis is along the same traverse as in a. (e) A core to rim analysis traverse is illustrated by a yellow dotted line on the BSE image.

5.2.3. Residues

Garnet in sample CR1a displays a different REE (+Y) zonation pattern to those in sample L2t-6 and L5GR-3 (Fig. 17a). The rims are preferentially enriched in heavy REEs (+Y) and middle REEs than the cores. Y abundance varies (from 20ppm in cores, to ~100ppm in the rims). The heavy REEs follow spatial distribution patterns that are nearly identical to that of Y (Fig. 17b), although at lower concentrations (9-8ppm in the cores, 2-6ppm in the rims). The middle REEs (Dy) follows patterns similar to Y and the heavy REEs, with higher concentrations than those for heavy REEs (Fig. 17b). Gd and Zr show constant concentrations across garnet. Cr increases towards the rims, whereas Ti and V decrease in abundance towards the rims (Fig. 17c).

This garnet is characterized by negative Eu/Eu* anomaly, and the magnitude of the anomaly is quite variable across garnet, but low values are commonly found in the core (Eu/Eu* = 0.01). Sm/Gd displays a gradual decrease from the cores to the rims (0.79-0.26). This garnet has a flat to slightly negative chondrite-normalized slope ((Lu/Gd)_N = 1.82-0.36 in the cores, (Lu/Gd)_N = 0.39-0.52 in the rims).

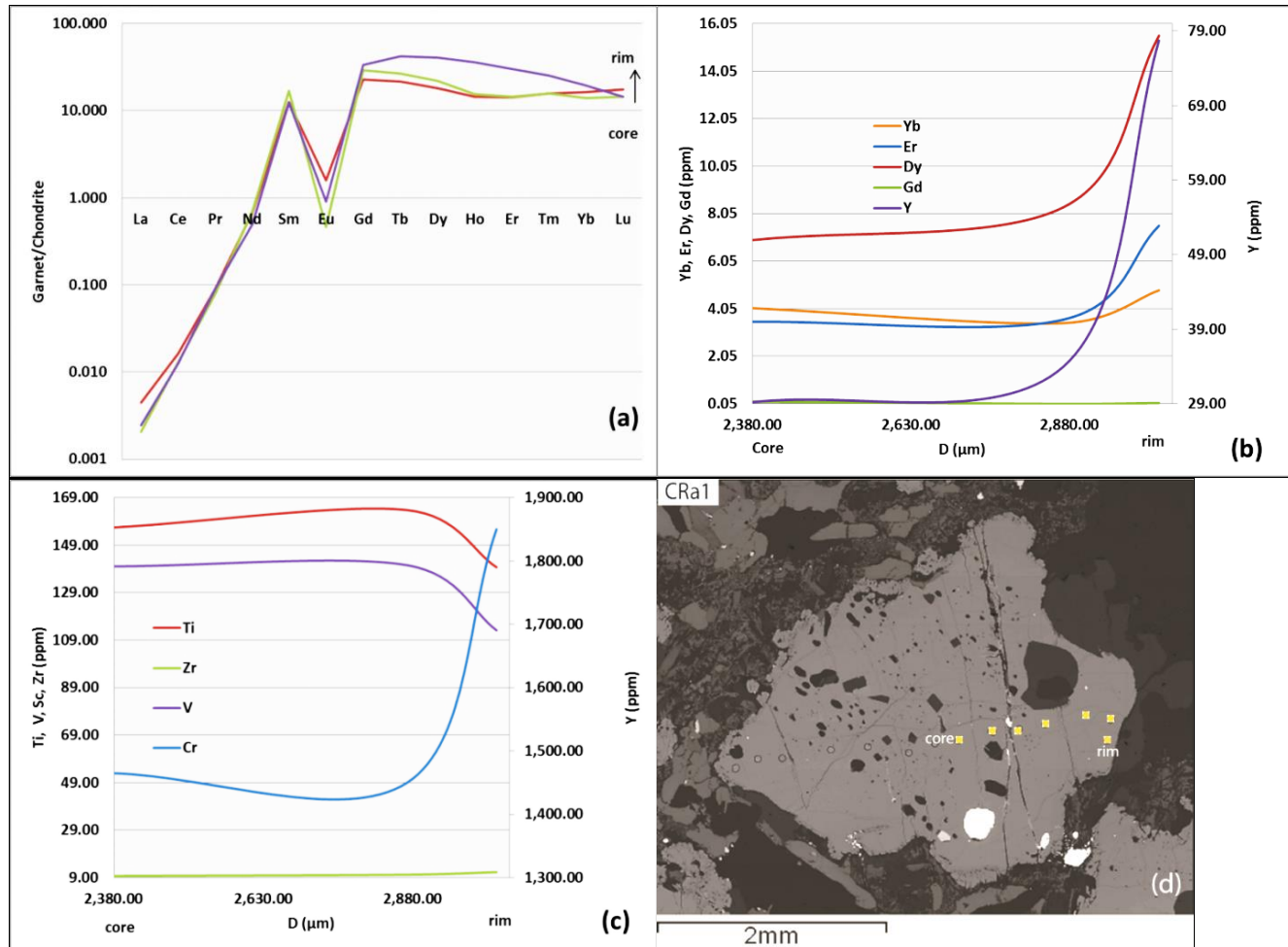


Figure 16: (a) Chondrite-normalized REE pattern of a garnet grain from sample CR1a. This garnet is strongly zoned in terms of HREE, enriched in the HREE and has a negative pronounced Eu anomaly in the rims. (b) Y, Yb, Er, Gd, Dy in ppm plotted as proxy for REE zonation from the same sample. The analysis is along the same traverse as in a. (c) Cr, Ti, V and Zr in ppm plotted as proxy for trace elements zonation in sample CR1a. The analysis is along the same traverse as in a. (d) A core to rim analytical traverse is illustrated by a yellow dotted line on the BSE image.

6. CHEMISTRY OF PLAGIOCLASE INCLUSIONS

Representative mineral chemistry of plagioclase inclusions taken from the rim through the core to the rim is presented in Table 4. The full data set is provided in the appendix E. Plagioclase inclusions within garnet as described above range in crystal shape from euhedral, anhedral to crystals that display negative garnet form. Euhedral crystals commonly occur as single crystals, clusters of crystals and polymineralic inclusions that consist of euhedral quartz, biotite orthopyroxene and rutile. The anhedral crystals commonly occur as single crystals and in some cases contain quartz inclusions. The crystals that display negative garnet form commonly contain rounded quartz inclusions.

Table 5: Representative electron beam analyses (EDS for major element and WDS for trace element) of plagioclase inclusions within garnet. L2t-6, L2t-7, L5GR-3 and CR1a are analysed in the same manner. Representative BSE images for quantitative spot analyses from rim to rim of Plag A-G are shown in the petrography section, the compositional data can be seen in Table 5.

Sample	L2t-6	L2t-6	L2t-6	L2t-6	L2t-6	L2t-6	L2t-6	L2t-6	L2t-6	L2t-6	L2t-6	L2t-6
Mineral	Plag(A)	Plag(A)	Plag(B)	Plag(B)	Plag(C)	Plag(C)	Plag(D)	Plag(D)	Plag(F)	Plag(F)	Plag(G)	Plag(G)
Generation	Rim	Core	Rim	Core	Rim	Core	Rim	Core	Rim	Core	Rim	Core
SiO ₂	49.80	55.03	53.66	54.23	47.37	47.71	60.72	60.57	48.90	53.20	47.71	48.36
Al ₂ O ₃	32.27	28.26	29.86	28.35	33.27	33.13	24.91	24.89	32.93	29.52	32.67	32.21
FeO	0.38	-	0.29	-	0.26	0.20	0.21	-	-	-	1.03	0.39
CaO	15.20	11.00	12.05	11.05	16.71	16.10	6.82	6.59	15.91	12.51	15.72	15.74
Na ₂ O	2.84	5.47	4.67	5.22	1.90	2.25	8.06	8.20	2.61	4.50	2.07	2.69
K ₂ O	-	0.23	0.14	0.23	-	0.10	-	-	-	0.16	0.11	-
Total	100.50	99.99	100.67	99.07	99.50	99.49	100.72	100.24	100.35	99.89	99.33	99.39
Number of anions on the basis of 8 oxygen atoms												
Si ⁴⁺	2.26	2.48	2.41	2.47	2.19	2.20	2.68	2.68	2.23	2.41	2.21	2.22
Al ³⁺	1.73	1.50	1.58	1.52	1.81	1.80	1.30	1.30	1.77	1.58	1.78	1.75
Fe ²⁺	0.01	-	0.01	-	0.01	0.01	0.01	-	-	-	0.04	0.02
Ca ²⁺	0.74	0.53	0.58	0.54	0.83	0.79	0.32	0.31	0.78	0.61	0.78	0.78
Na ⁺	0.25	0.48	0.41	0.46	0.17	0.20	0.69	0.70	0.23	0.40	0.19	0.24
K ⁺	-	0.01	0.01	0.01	-	0.01	-	-	0.00	0.01	0.01	-
Σ cat.	5.00	5.00	5.00	5.00	5.00	5.00	5.00	5.00	5.00	5.00	5.00	5.00
Anions	8.00	7.98	8.00	7.99	8.00	7.99	7.99	7.98	8.00	8.00	8.00	7.98
XAn	0.75	0.52	0.58	0.53	0.83	0.79	0.32	0.31	0.77	0.60	0.80	0.76
XAb	0.25	0.47	0.41	0.45	0.17	0.20	0.68	0.69	0.23	0.39	0.19	0.24
Sr (ppm)	152.29	-	136.48	178.14	-	-	271.85	389.91	145.69	-	-	187.49

Table 5 (continued)

Sample	L2t-7	L2t-7	L2t-7	L2t-7	L2t-7	L5GR-3	L5GR-3	L5GR-3	L5GR-3	L5GR-3	L5GR-3
Mineral	Plag-A	Plag-A	Plag-A	Plag-C	Plag-C	Plag-A	Plag-A	Plag-D	Plag-D	Plag-F	Plag-F
Generation	Rim	intermediate	Core	rim	core	Rim	Core	rim	Core	rim	core
SiO₂	55.29	50.27	51.85	60.15	60.69	49.16	53.76	50.04	54.81	57.10	57.33
Al₂O₃	28.86	30.85	30.68	25.38	24.84	31.82	28.92	31.06	27.98	27.15	26.54
FeO	0.19	-	-	0.31	-	0.40	0.17	0.22	-	0.19	-
CaO	11.46	14.42	13.61	7.30	6.86	15.13	11.67	14.38	10.45	9.48	8.73
Na₂O	5.13	3.27	4.12	7.57	7.82	2.76	5.01	3.42	5.57	6.25	6.61
K₂O	-	-	0.12	0.12	0.15	-	0.10	-	0.18	0.09	0.19
Total	100.92	98.81	100.37	100.83	100.37	99.26	99.63	99.11	98.99	100.26	99.40
Number of anions on the basis of 8 oxygen atoms											
Si⁴⁺	2.48	2.32	2.34	2.66	2.69	2.26	2.44	2.30	2.49	2.56	2.58
Al³⁺	1.52	1.68	1.63	1.32	1.30	1.73	1.54	1.68	1.50	1.43	1.41
Fe²⁺	0.01	-	-	0.01	-	0.02	0.01	0.01	-	0.01	-
Ca²⁺	0.55	0.71	0.66	0.35	0.33	0.75	0.57	0.71	0.51	0.46	0.42
Na⁺	0.45	0.29	0.36	0.65	0.67	0.25	0.44	0.30	0.49	0.54	0.58
K⁺	-	-	0.01	0.01	0.01	-	0.01	-	0.01	0.01	0.01
Σ cat.	5.00	5.00	5.00	5.00	5.00	5.00	5.00	5.00	5.00	5.00	5.00
Anions	8.01	8.01	7.97	8.00	8.00	8.00	7.99	7.99	7.99	8.00	7.99
XAn	0.55	0.71	0.64	0.35	0.32	0.75	0.56	0.70	0.50	0.45	0.42
XAb	0.45	0.29	0.35	0.65	0.67	0.25	0.43	0.30	0.49	0.54	0.57
Sr (ppm)	212.57	115.06	167.01	-	-	-	206.78	169.18	167.84	131.10	168.86

Table 5 (continued)

Sample	L2t-6	L2t-6	L2t-7	L2t-7	L5GR-3	L5GR-3
Mineral	Plag-matrix	Plag-matrix	Plag-matrix	Plag-matrix	Plag-matrix	Plag-matrix
Generation	Rim	Core	rim	core	Rim	Core
SiO₂	60.51	61.64	61.69	60.97	58.43	61.24
Al₂O₃	24.35	24.39	24.51	23.86	25.99	23.65
FeO	-	-	-	-	-	-
CaO	6.31	6.34	6.23	5.93	8.02	5.72
Na₂O	8.05	8.00	8.19	8.19	7.28	8.36
K₂O	0.14	0.18	0.11	0.24	-	0.09
Total	99.36	100.56	100.74	99.18	99.72	99.06
Number of anions on the basis of 8 oxygen atoms						
Si⁴⁺	2.71	2.73	2.72	2.73	2.61	2.75
Al³⁺	1.28	1.27	1.27	1.26	1.37	1.25
Fe²⁺	-	-	-	-	-	-
Ca²⁺	0.30	0.30	0.29	0.28	0.38	0.28
Na⁺	0.70	0.69	0.70	0.71	0.63	0.73
K⁺	0.01	0.01	0.01	0.01	-	0.01
Σ cat.	5.00	5.00	5.00	5.00	5.00	5.00
Anions	8.00	8.02	8.01	8.00	7.98	8.00
XAn	0.30	0.30	0.29	0.28	0.38	0.27
XAb	0.69	0.69	0.70	0.70	0.62	0.72
Sr (ppm)	220.11	232.48	208.01	232.48	268.08	-

XAn = Ca / (Ca + Na + K), XAb = Na / (Na + Ca + K)

6.1. Stromatitic leucosomes

6.1.1. L2t-6

Plagioclase inclusions in sample L2t-6 display considerable chemical heterogeneity (Fig. 18). Their compositions range from An₈₃ to An₃₂. Euhedral inclusions are considerably more anorthite-rich, with compositions that range from An₈₃ to An₅₂. However, the anhedral inclusions are less calcic (An₃₁ to An₃₃), displaying compositions similar to the matrix plagioclase around garnet (An₂₉ to An₃₃). Some of the euhedral inclusions are zoned, and the nature of the zoning is defined by low values in the core (An₅₃) to maximum values (An₇₅) in the rims. In some crystals, the zoning is observed on the BSE image (Fig. 12 A). However, other euhedral inclusions lack the zonation.

Sr concentration within single plagioclase crystals is variable. It ranges from below the detection limit to 389.91ppm, and there is no correlation between anorthite content and the Sr content (Fig. 18). Individual inclusions record a big range in Sr content within the zoned inclusions, but the anorthite range is less. Despite the large Sr concentration range in all populations and the fact that most of the inclusions are below the detection limit, the average of the euhedral groups is lower than the average of the anhedral inclusions or plagioclase around garnet (Fig. 18).

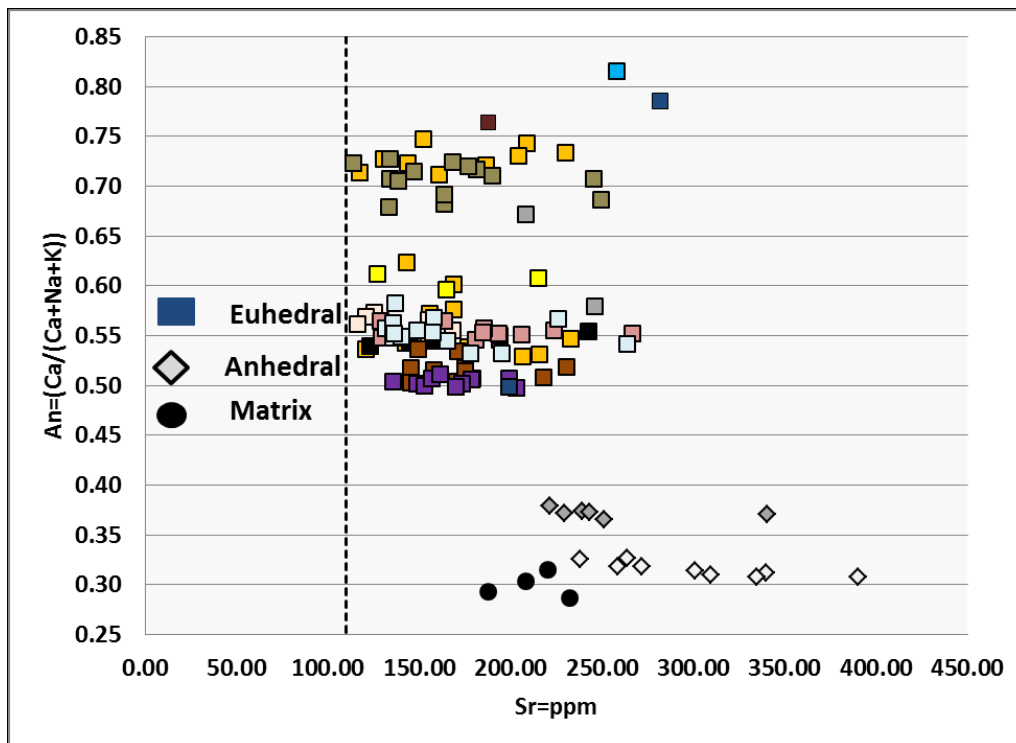


Figure 17: The diagram illustrates the relationship between the plagioclase anorthite content and Sr concentration in sample L2t-6. Each colour represents a traverse across an individual crystal. Euhedral and anhedral plagioclase inclusions as well as the plagioclase crystals from the matrix around garnet are illustrated by the different symbols as indicated in the legend. The vertical dotted line indicates the Sr detection limit. Sr content within individual plagioclase was highly variable. In some crystals all the points analysed had Sr above the detection limit. In others, only about 40 % of the points analysed had Sr above the detection limit. The points with Sr content below the detection limit are not plotted. The plagioclase anorthite range is kept constant from figure 18 to 21 to allow for direct comparison between the figures. The typical uncertainty for anorthite concentration is ~ 0.26 and that for Sr is 315.85ppm using the standard deviation values (Ca = 0.05, Na = 0.09 and K = 0.05).

6.1.2. L2t-7

Plagioclase inclusions in sample L2t-7 are compositionally similar to plagioclase inclusions in sample L2t-6, and are different in their zonation patterns. The euhedral inclusions in sample L2t-7 are also more Ca-rich with maximum values of (An₇₉) and minimum values of (An₅₅). However, matrix plagioclase around garnet ranges in composition from (An₂₈ to An₃₁). Plagioclase inclusions that displays negative garnet form are less calcic, their composition ranges from (An₃₀ to An₄₅). Some of the euhedral crystals are zoned, with a decrease in anorthite towards the rims. Others are complexly zoned. Their composition increases from core to intermediate (An₅₅ to ₇₁) and drops in the rims (An₆₁). This type of zoning is verified by the BSE image (Fig. 7A). However, the zonation is not systematic. Some inclusions lack the zonation.

The Sr concentration within individual plagioclase inclusions is variable; it ranges in concentration from below the detection limit to 493.76ppm. Moreover, there is no correlation between the Sr content and the anorthite content (Fig. 19). Individual inclusions record a big range in Sr content within the zoned inclusions, but the anorthite range is less. Despite the large Sr concentration range in all populations and the fact that most of the inclusions are below the detection limit, the average of the euhedral groups is lower than the average of the anhedral inclusions or matrix plagioclase around garnet.

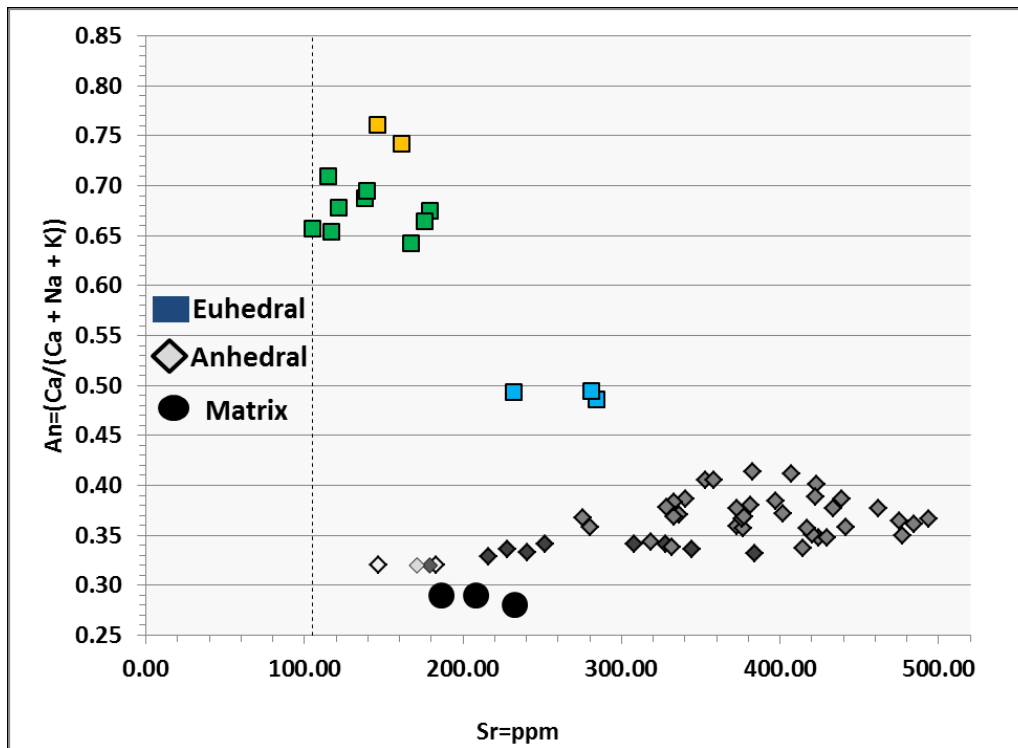


Figure 18: The diagram illustrates the relationship between the plagioclase anorthite content and Sr concentration in sample L2t-7. Each colour represents a traverse across an individual crystal. Euhedral and anhedral plagioclase inclusions as well as the plagioclase crystals from the matrix around garnet are illustrated by the different symbols as indicated in the legend. The vertical dotted line indicates the Sr detection limit. Sr content within individual plagioclase was highly variable. In some crystals all the points analysed had Sr above the detection limit. In others, only about 40 % of the points analysed had Sr above the detection limit. The points with Sr content below the detection limit are not plotted. The typical uncertainty for anorthite concentration is ~ 0.26 and that for Sr is 315.85ppm using the standard deviation values ($Ca = 0.05$, $Na = 0.09$ and $K = 0.05$). The plagioclase anorthite range is kept constant from figure 18 to 21 to allow for direct comparison between the figures.

6.2. *Nebulitic leucosomes*

Plagioclase inclusions in sample L5GR-3 are relatively large compared to inclusions in samples L2t-6 and L2t-7. The inclusions in sample L5GR-3 record a wide range of compositions, ranging from Ca-rich (An_{78}) to less calcic (An_{39}) compositions (Fig. 20). Euhedral inclusions are within the Ca-rich category and show an increase in anorthite towards the rims. Their composition ranges from (An_{78}) to (An_{51}). The nature of the zonation is not systematic. Some inclusions lack the zonation. In addition, some of the polymineralic inclusions which typically consist of orthopyroxene, rutile and biotite are also slightly zoned, whereas others lack the zonation. Their anorthite content ranges from (An_{70} to An_{51}) in some crystals and (An_{48} to An_{52}) in others. The anhedral plagioclase inclusions are within the Ca-poor group and show a little zonation. Their Ca content increases towards the rims from An_{39} to

An₄₂. Matrix plagioclase around garnet ranges in composition from An₄₀ to An₃₀ and are also slightly zoned.

Sr concentration is randomly distributed within individual plagioclase inclusions. It varies from below the detection limit to 303.56ppm. In addition, individual inclusions record a small range in Sr content within the zoned inclusions, but the anorthite range is large. Despite the large Sr concentration range in all populations and the fact that most of the inclusions are below the detection limit, the average of the euhedral groups is higher than the average range of the anhedral inclusions or plagioclase around garnet (Fig. 20).

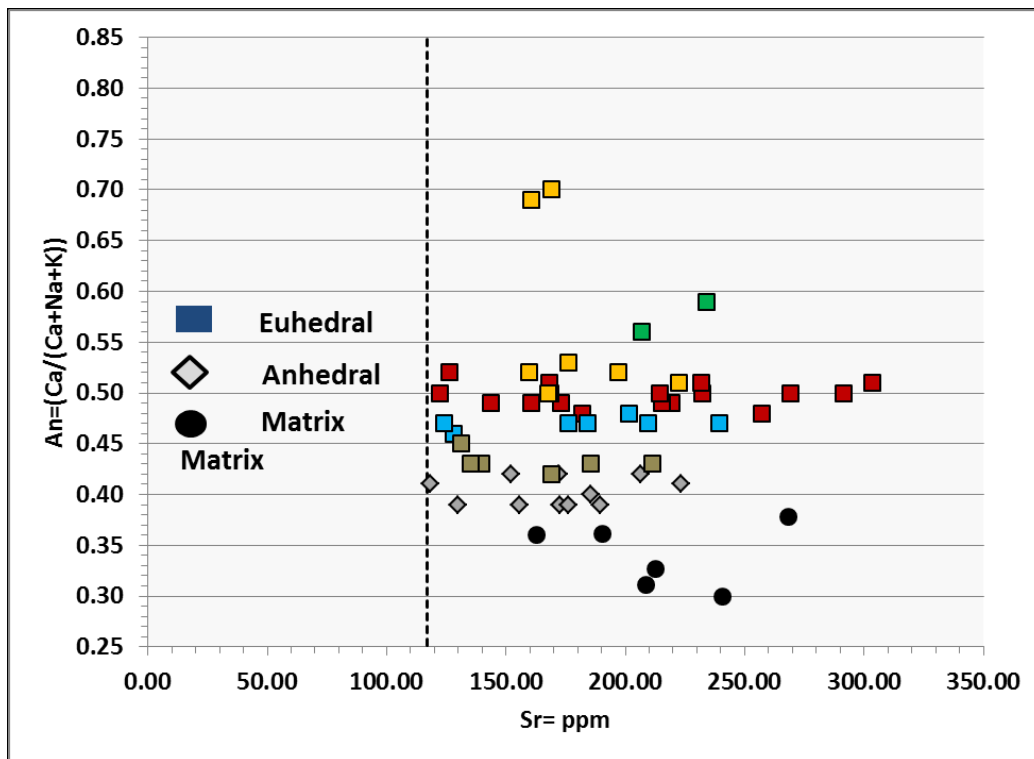


Figure 19: The diagram illustrates the relationship between the plagioclase anorthite content and Sr concentration in sample L5GR-3. Each colour represents a traverse across an individual crystal. Euhedral and anhedral plagioclase inclusions as well as the plagioclase crystals from the matrix around garnet are illustrated by the different symbols as indicated in the legend. The vertical dotted line indicates the Sr detection limit. Sr content within individual plagioclase was highly variable. In some crystals all the points analysed had Sr above the detection limit. In others, plagioclase crystals only about 40 % of the points analysed had Sr above the detection limit. The points with Sr content below the detection limit are not plotted. The typical uncertainty for anorthite concentration is ~ 0.26 and that for Sr is 315.85ppm using the standard deviation values ($Ca = 0.05$, $Na = 0.09$ and $K = 0.05$). The plagioclase anorthite range is kept constant from figure 18 to 21 to allow for direct comparison between the figures.

6.3. Residues

Plagioclase inclusions in sample CR1a display a smaller compositional range compared to those in the leucosomes (Fig. 21). Their composition ranges from An₃₀ to An₃₉. Some of the inclusions are zoned, and the nature of the zoning is defined by an increase in anorthite towards the rims. The composition of the euhedral and anhedral inclusions and the matrix plagioclase around garnet is within the same compositional range. This composition is similar to anhedral plagioclase crystals in the leucosomes. The euhedral and anhedral crystals, matrix plagioclase around garnet, range in compositions from (An₃₅ to An₃₀; An₃₈ to An₃₉ and from An₃₇ to An₃₀) respectively.

The Sr concentration within plagioclase inclusions vary from below the detection limit to 363.42ppm. In addition, Individual inclusions record a small range in Sr content within the zoned inclusions, but the anorthite range is large. Despite the small Sr concentration range in all populations and the fact that most of the inclusions are below the detection limit, the average of the euhedral groups is within the same range to the average of the anhedral inclusions or matrix plagioclase around garnet (Fig. 21).

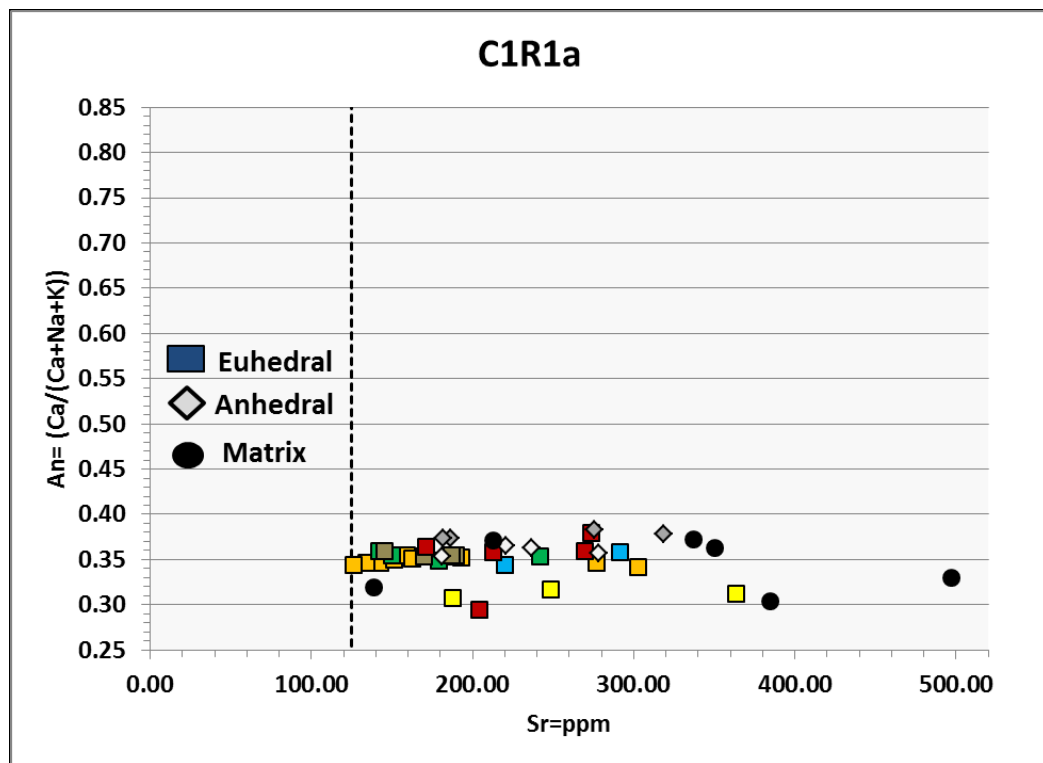


Figure 20: The diagram illustrates the relationship between the plagioclase anorthite content and Sr concentration in sample CR1a. Each colour represents a traverse across an individual crystal. Euhedral and anhedral plagioclase inclusions as well as the plagioclase crystals from the matrix around garnet are illustrated by the different symbols as indicated in the legend. The vertical dotted line indicates the Sr detection limit. Sr content within individual plagioclase was highly variable. In some crystals all the points analysed had Sr above the detection limit. In others, plagioclase crystals only about 40 % of the points analysed had Sr above the detection limit. The points with Sr content below the detection limit are not plotted. The typical uncertainty for anorthite concentration is ~ 0.26 and that for Sr is 315.85ppm using the standard deviation values (Ca = 0.05, Na = 0.09 and K = 0.05). The plagioclase anorthite range is kept constant from figure 18 to 21 to allow for direct comparison between the figures.

6.4. The relationship between plagioclase inclusion sizes and their anorthite content

Based on the 64 inclusions analysed in this study, it is seen that the composition of the inclusions show no real relationship to the size of the plagioclase crystal (Fig. 22) or the position within the garnet crystal (Fig. 23). However, the composition of the inclusions displays a clear relationship with the morphology of the plagioclase inclusions (Fig. 22).

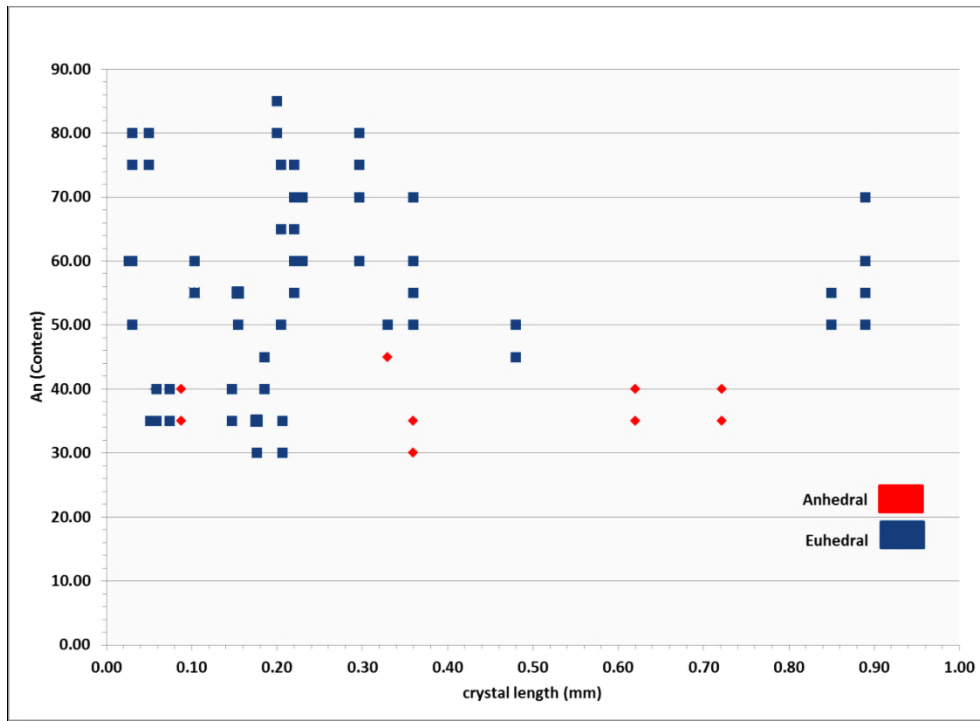


Figure 21: Plot showing the average composition of individual inclusions analysed in this study against their crystal size and morphology.

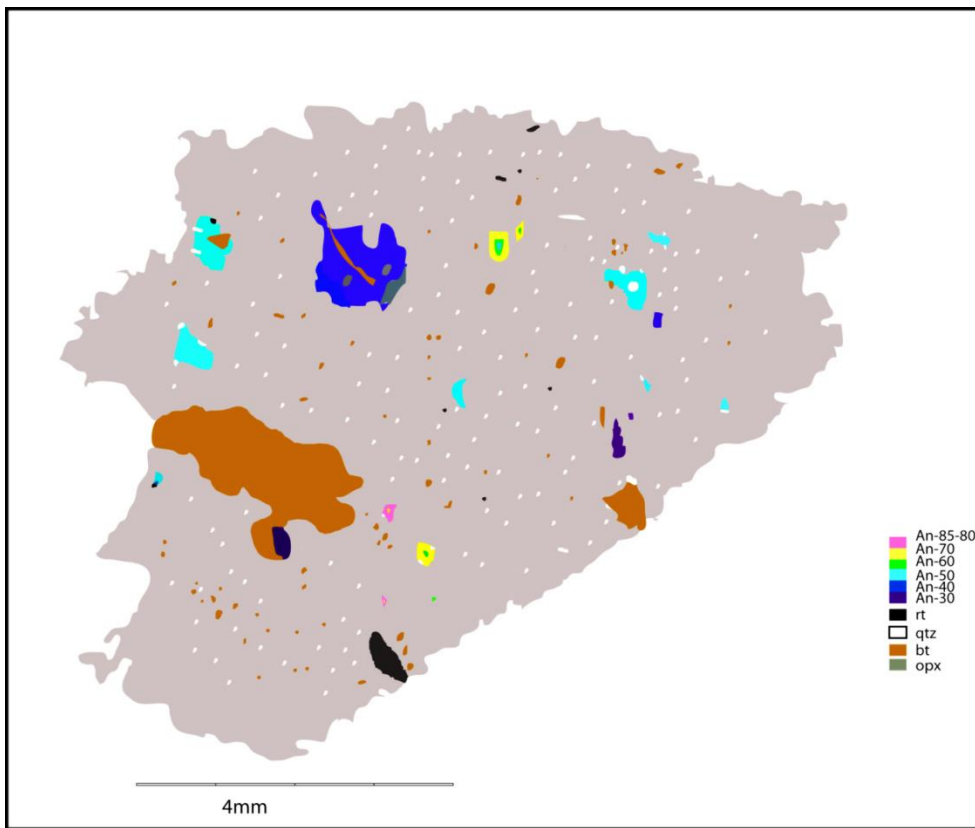


Figure 22: Schematic diagram illustrating the locality of the plagioclase crystals within garnet from sample L2t-6 against their composition.

7. DETAILS OF GARNET AND PLAGIOCLASE ZONATION IN THE VICINITY OF ZONED PLAGIOCLASE INCLUSIONS

Garnet crystals in the leucosomes are characterized by bell-shaped zonation patterns with respect to grossular. The grossular component in garnet drops across some of the plagioclase inclusions. This observation raised questions as to why these garnet crystals contain zoned plagioclase inclusions, in areas where grossular is high. Is there any relationship between the compositions of the inclusions to their garnet host? If so, is the Ca-rich nature of the inclusions a consequence of Ca-uptake from garnet?

To answer these questions, a detailed investigation of garnet zonation around plagioclase inclusions was examined, with short traverses taken from different directions. The traverses were taken around Ca-rich plagioclase inclusions and around less calcic plagioclase inclusions both displaying Ca- and Na-enriched rims. The results are presented in the figures below. The data is classified based on the Ca- and Na-rich rims of the plagioclase crystal even though some inclusions are not considerably zoned. However, no detailed investigation of zonation data was carried out for the residuum sample as the sample was lost.

7.1. Inclusions that increase in anorthite towards the rims

Most plagioclase inclusions investigated in this study display Ca-enriched rims. The detailed investigation of garnet zonation around plagioclase inclusions in both directions demonstrates that the Ca-rich nature of the plagioclase inclusions is not a consequence of Ca-uptake from garnet. This is because the Ca content of garnet around some of the small euhedral crystals (~0.1mm) that are more calcic (An₈₃) is constant in both directions (Fig. 25 B-C). In addition, the Ca content in garnet is also constant around some of the euhedral crystals that show a strong zonation (An₅₃ in the cores, An₇₅ in the rims) (Fig. 25A).

Similarly, plagioclase crystals in sample L5GR-3 are characterized by considerably larger crystal sizes (up to 0.9mm) compared to garnet crystals in samples L2t-6, and L2t-7. Garnet zoning around some of these inclusions also show that their Ca-rich nature is not a consequence of Ca-uptake from garnet. This is because the Ca content of garnet around these inclusions is constant in both directions (Fig. 27). However, Ca content of garnet decreases around some of the larger crystals in association with a crack. It must be noted that these inclusions occur in the core of the garnet where the

Ca content is typically high. Furthermore, plagioclase inclusions in samples L2t-6 and L2t-7 generally occur towards the rims, where Ca content of garnet is relatively low.

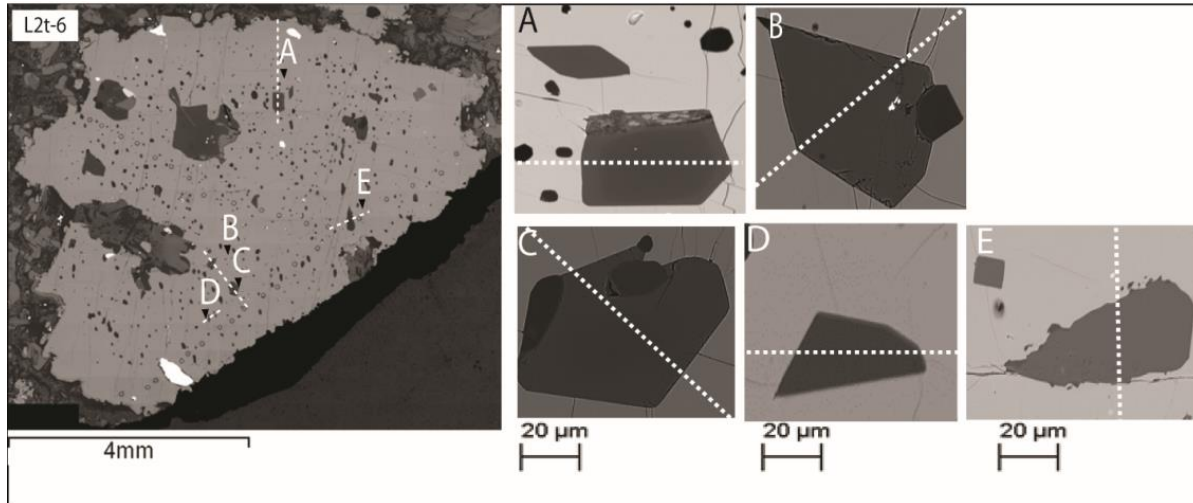


Figure 23: BSE images illustrating detailed electron microprobe analyses of cross-sections (dotted white lines) through the host garnet into the plagioclase inclusion in sample L2t-6. (A-E) Show magnified inclusions within garnet.

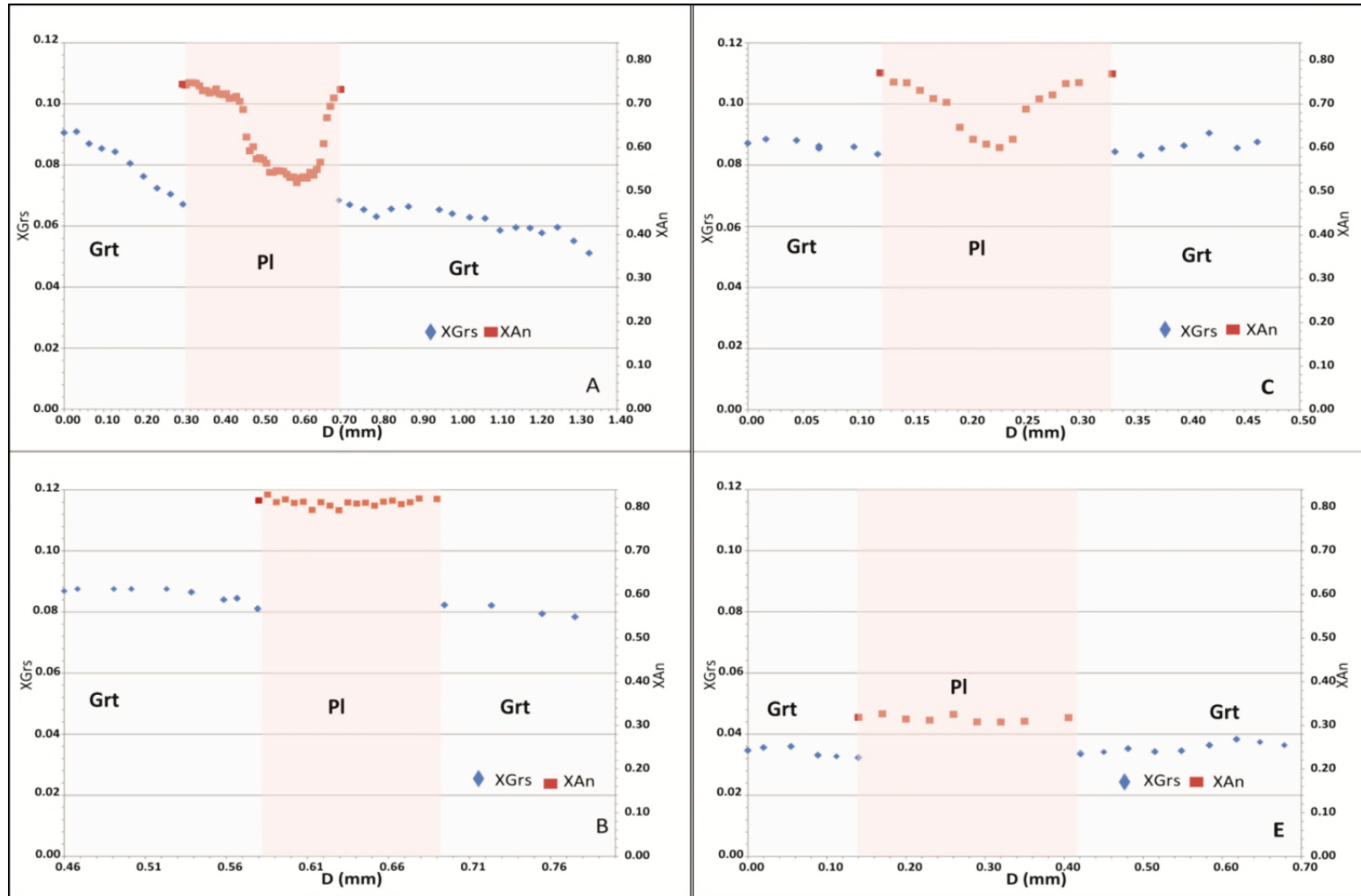


Figure 24: (A-E) Plots which highlight the detailed electron microprobe analyses of possible garnet zonation around the plagioclase inclusions. The orange shaded areas represent the position of the plagioclase crystals within garnet in sample L2t-6. The light grey shaded area represents garnet around the plagioclase inclusions. Traverses are indicated in the magnified images in Fig. 24.

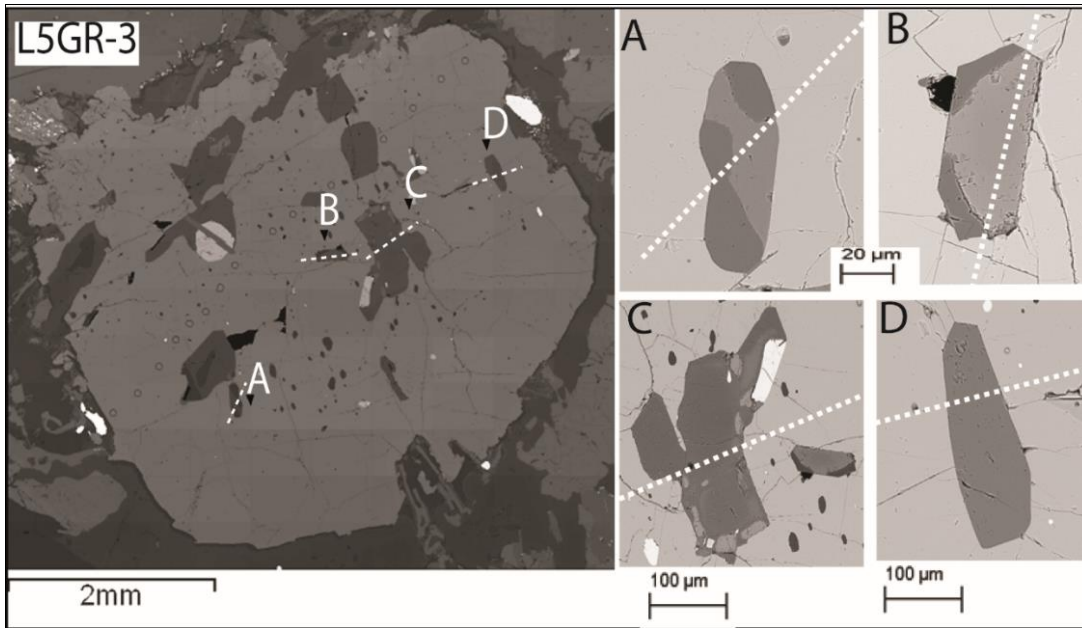


Figure 25: BSE images illustrating detailed electron microprobe analyses of cross-sections (dotted white lines) through the host garnet into the plagioclase inclusion in sample L5GR-3. (A-D) Show magnified inclusions within garnet.

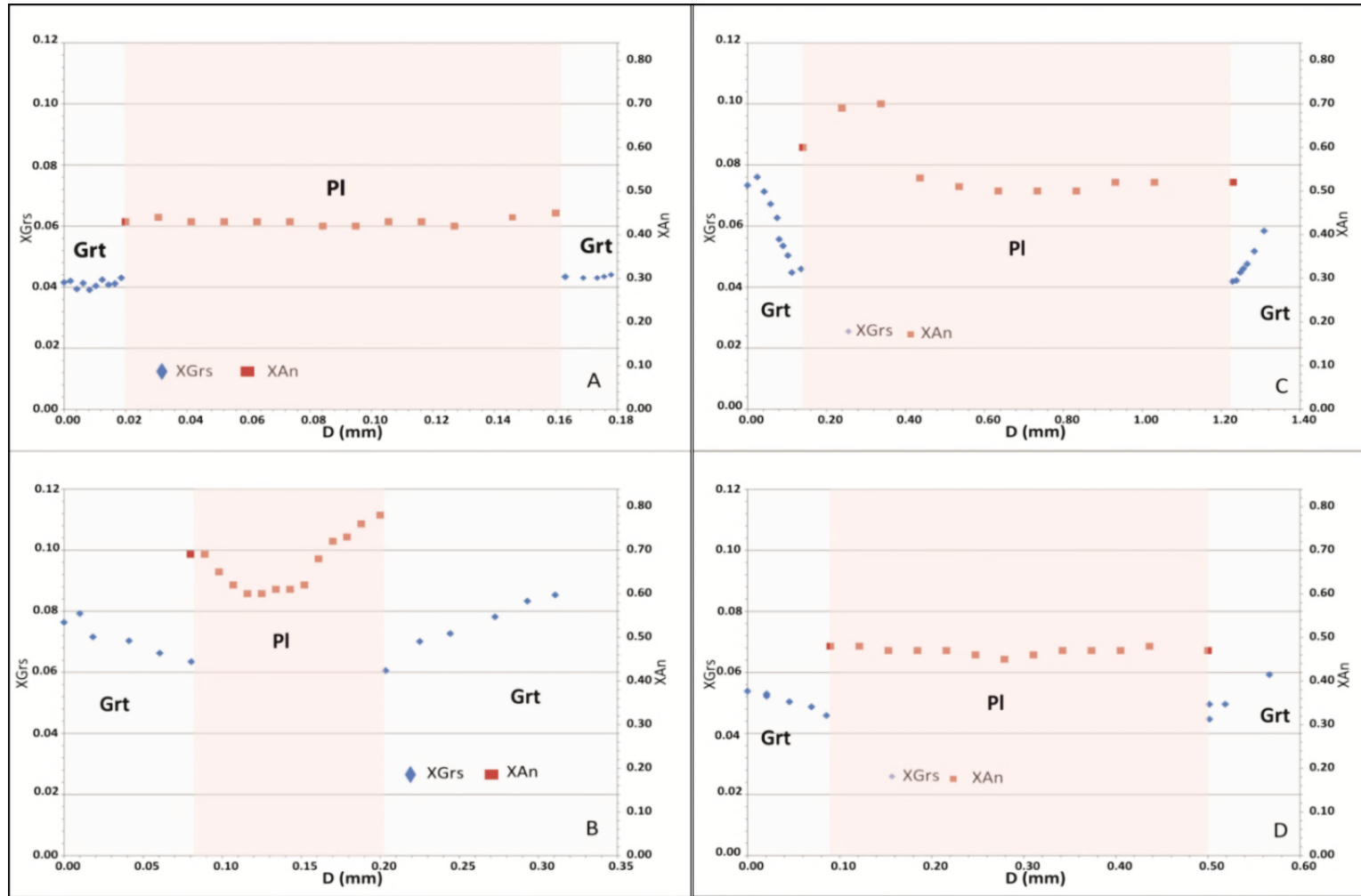


Figure 26: Plots which highlight the detailed electron microprobe analyses of possible garnet zonation around the plagioclase inclusions. The orange shaded areas represent the position of the plagioclase crystals within garnet in sample L5GR-3. The light grey shaded area represents garnet around the plagioclase inclusions. Traverses are indicated in the magnified images in Fig. 26.

7.2. Inclusions that decrease in anorthite towards the rims

A quantitative spot analysis across garnet and qualitative elemental maps demonstrate that garnet in sample L2t-7 possibly represents two amalgamated grains, with fused grain-boundaries (see Fig. 11). This garnet contains inclusions mostly in the rims of each amalgamated crystal. Plagioclase inclusions in this sample are characterized by Na-enriched rims compared to plagioclase inclusions in samples L2t-6 and L5GR-3. Garnet zoning around some of the small euhedral inclusions that occur as both single crystals or in contact with quartz is constant in both directions (Fig. 29A-B). However, a negligible rise in Ca content of garnet is observed around plagioclase crystals that display garnet symmetry, and around plagioclase crystals that display complex zoning. This increase does not interfere with the actual Ca content of the inclusions (Fig. 29).

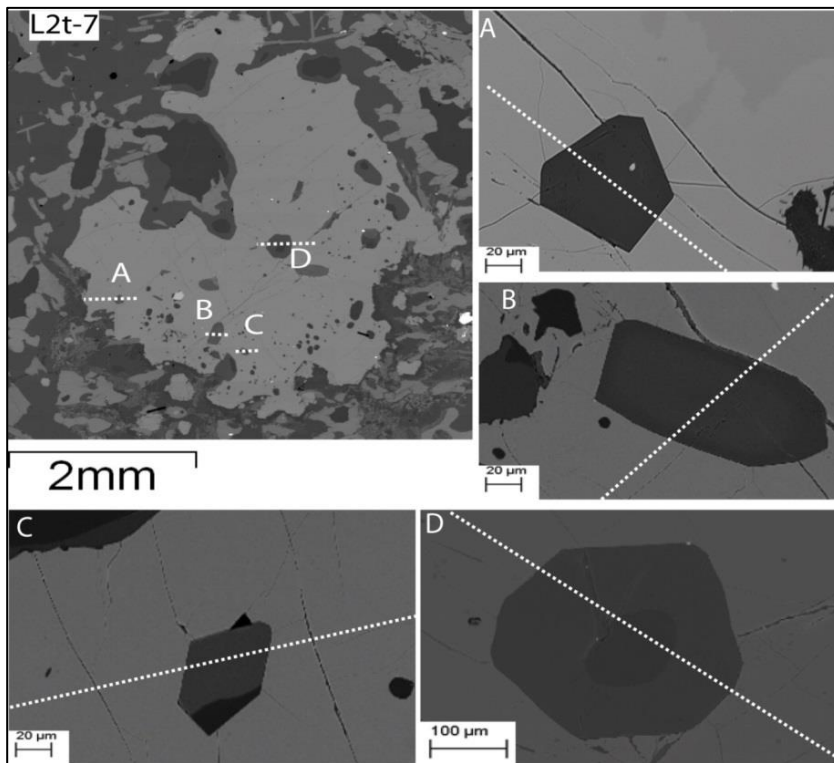


Figure 27: BSE images illustrating detailed electron microprobe analyses of cross-sections (dotted white lines) through the host garnet into the plagioclase inclusion in sample L2t-7. (A-D) Show magnified inclusions within garnet.

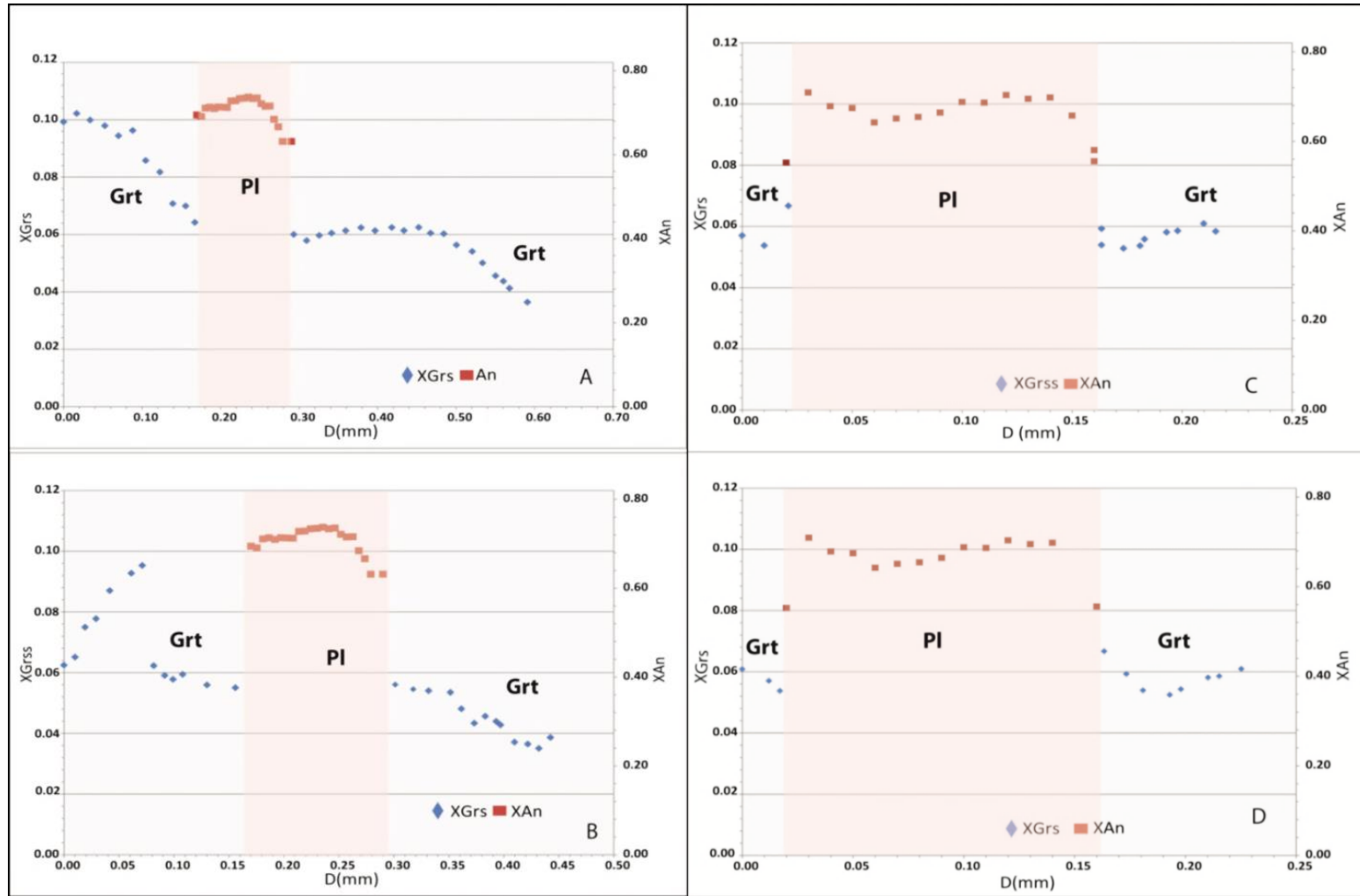


Figure 28: Plots which highlight the detailed electron microprobe analyses of possible garnet zonation around the plagioclase inclusions. The orange shaded areas represent the position of the plagioclase crystals within garnet in sample L2t-7. The light grey shaded area represents garnet around the plagioclase inclusions. Traverses are indicated in the magnified images in Fig. 28.

8. DISCUSSION

8.1. Origin of garnet

Within the BQ metapelites different garnet crystals are produced by various reactions that possibly include sub-solidus reactions as the rocks evolve along the prograde path. The larger garnet crystals occur in association with leucosomes, and are texturally different from the garnet within the matrix of the metapelites (Stevens and van Reenen, 1992). The garnet crystals within the leucosomes contain inclusions of biotite, plagioclase, quartz, and rutile and in rare cases sillimanite. Thus, the mineral inclusion relationships within garnet suggest that they are peritectic and formed by fluid-absent melting reaction (4) during the process that also produced the leucosomes.



Garnet textures, rimmed and partially replaced by cordierite and orthopyroxene, have resulted from continuous decompression controlled reactions at peak temperatures (Nicoli et al., 2014a; Taylor et al., 2014; Stevens and van Reenen, 1992a, b; Stevens, 1997). These garnet textures are heavily modified by decompression reactions in rocks of suitable bulk composition i.e. more Mg-rich rocks ($X_{Mg} > 0.6$) (Stevens and van Reenen, 1992). The minerals formed on the decompression path are later altered to fine-grained fibrous amphibolite-facies assemblages (biotite, kyanite and orthoamphibole) by subsequent hydration reactions (Stevens, 1997). As a consequence, this study examined unusual areas where larger garnet crystals (up to 20mm in diameter) within the leucosomes as well as in the residuum adjacent to the leucosomes survived the decompression history.

8.2. Major element zoning in garnet

As described above, garnet within the leucosomes are zoned with respect to almandine, pyrope and grossular (Figs. 10, 11, and 12). Grossular commonly shows two bell-shaped zonation profiles with a drop in grossular component through the central portion of the garnet. This is interpreted to either represent a plane along which two separate garnet crystals have been amalgamated (Taylor and Stevens, 2010), or as a consequence of cracks that have allowed the reequilibration of the grossular component in the central portion of the garnet to a composition similar to that of the rims. The grossular zoning is balanced by almandine and pyrope, with the spessartine component remaining relatively constant or rising slightly towards the rims. The general increase in pyrope with a decrease in

grossular from garnet core to garnet rim in greenschist-to amphibolite-facies conditions is generally accepted as a primary growth feature (Chernoff et al., 1997; Grover et al., 1992; Martin et al., 2011; Tracy et al., 1982; Tuccillo et al., 1990). A prominent change in texture and zonation is observed where the inclusion free rims start. This includes the lack of inclusions in the garnet rims (~140 to 50µm wide) and a sharp increase in grossular, almandine, trace and REE elements in this zone and in rare cases spessartine with a steep decrease in pyrope (Figs. 10 and 12). The lack of inclusions within the garnet rims is most likely a consequence of a dissolution-precipitation driven recrystallization processes (e.g. Villaros et al., 2009; Taylor and Stevens, 2010), or as a consequence of garnet recrystallization during the formation of symplectitic coronas in garnet. To decide which process produced this phenomenon would require further data.

Major element chemical zoning of the early stages of regional metamorphism are commonly preserved up to lower amphibolite-facies due to slow diffusion of the major cations (Fe, Mg, Mn and Ca) within garnet (Jung and Hellebrand, 2006). However, prograde chemical zonation is rare in higher-grade garnet of granulite-facies terranes (Martignole and Pouget, 1993), due to intra-crystalline diffusion at higher temperatures (Spear and Florence, 1992) and the dissolution-precipitation processes (Taylor and Stevens, 2010; Villaros et al., 2009). Typical garnet crystals previously investigated in the BQ are not zoned with respect to major elements (e.g. Stevens and van Reenen, 1992; Taylor et al., 2014). However, garnet crystals investigated in this study taken from the same locality preserve some remnant growth zoning in the cores, which is unusual for garnet in granulite-facies terranes. This preserved prograde chemical zoning raised questions as to why these garnet crystals survived intra-crystalline diffusion processes that usually re-equilibrate the garnet crystals in high-grade rocks. In addition, the crystals has also avoided the dissolution-precipitation processes proposed to occur in ganert bearing migmatite. Taylor et al. (2014) proposed that most of the leucosomes that host the garnet lost melt extremely rapidly on the prograde path. In addition, these garnet crystals commonly occur as large crystals. Therefore, the larger crystal size of the garnet combined with rapid melt loss is possibly why these garnet crystals survived the dissolution-precipitation mechanism and granulite-facies diffusional homogenization that usually re-equilibrate chemical zonation in the garnet in high-grade terranes (e.g. Taylor and Stevens, 2010; Villaros, 2009). The dissolution-precipitation process only affected the rims of the garnet as the process stopped when the leucosomes lost melt.

8.3.Trace element disequilibrium in garnet

Typical metapelitic garnet from the uppermost amphibolite-to granulite-facies are commonly characterized by heavy REE (Y) enrichment in the core and depleted rims. This records prograde zoning consistent with Rayleigh fractionation of REE and Y during garnet growth (Pyle and Spear, 1999; Otamendi et al., 2002). The enrichment of heavy REE in the rims is generally interpreted to record retrograde zoning and is consistent with either garnet resorption (Pyle and Spear, 1999) or recrystallization of garnet in the melt by a dissolution-precipitation mechanism (Taylor and Stevens, 2010; Villaros et al., 2009). It has been well documented that high concentrations of heavy REE in the peritectic garnet is controlled by the growth of peritectic garnet from a melt that has dissolved accessory phases enriched in these elements (Dorais and Tubrett, 2012; Pyle and Spear, 1999, 2000; Spear and Kohn, 1996).

Several studies have revealed that equilibrium conditions between accessory phases and anatectic melt must not be assumed (Bea, 1996; Bea and Montero, 1999). In disequilibrium melting, peritectic garnet are characterized by lower concentrations of elements that are contained in accessory phases and in garnet (e.g. heavy REE, Dorais and Tubrett, 2012). Peritectic garnet crystals in melanosomes of the MVS of Swaziland offer evidence for such disequilibrium melting (Taylor and Stevens, 2010). The abundance of heavy REE in the peritectic garnet are commonly lower, nearly an order on magnitude in chondrite-normalized REE patterns than the garnet crystals in the associated granitic sheet (Fig. 30). This is interpreted to suggest that accessory phases were not melting in their modal proportions, perhaps were isolated by minerals that were not melting. Therefore, producing low heavy REE concentrations to the anatectic melt (Dorais and Tubrett, 2012).

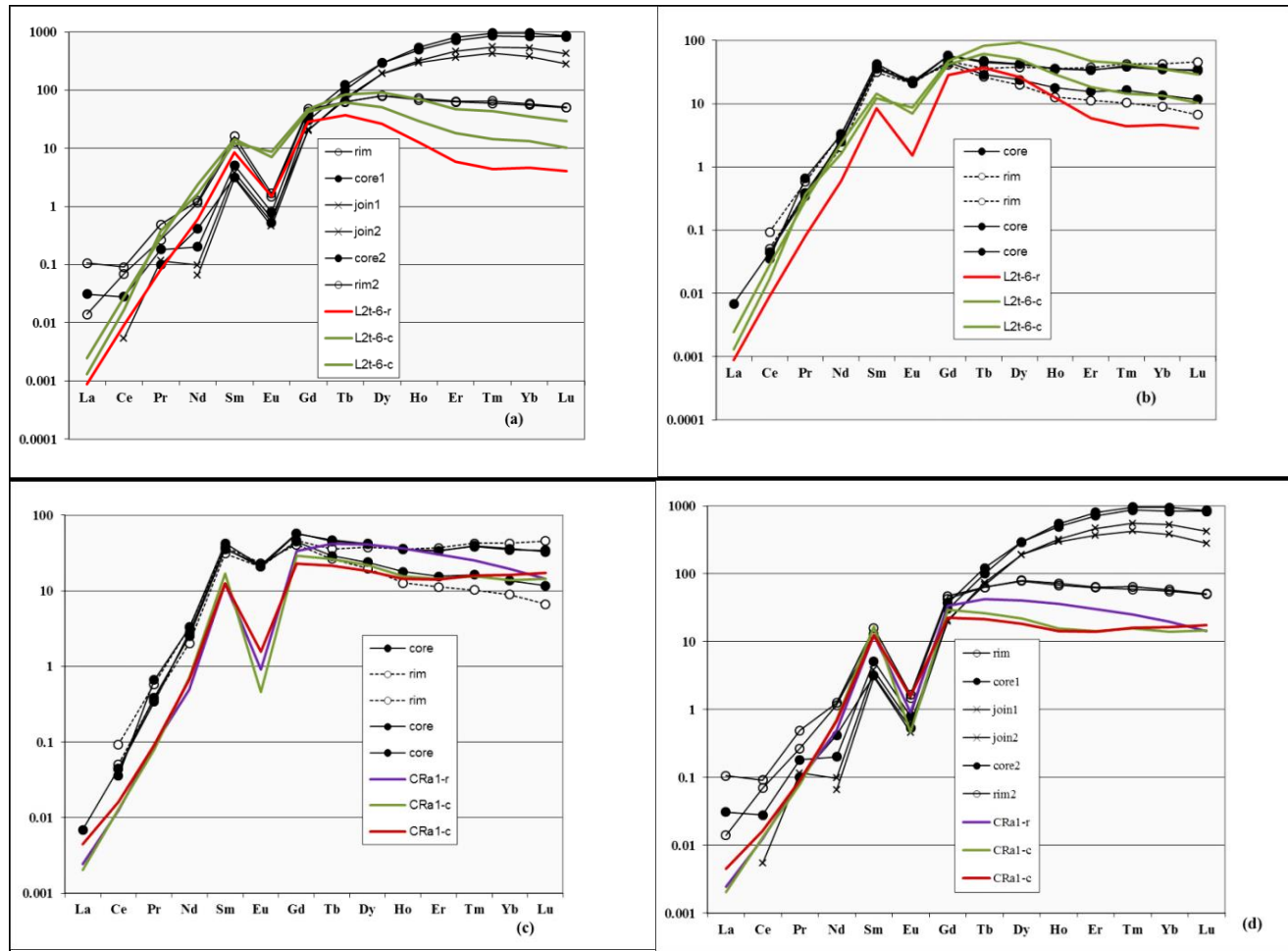


Figure 29: Comparison of chondrite-normalized REE zonation profiles within garnet crystals from: the metapelite residuum and the granitic sheet in melanosomes of the MVS of Swaziland (from Taylor and Stevens, 2010, Fig. 8) to chondrite-normalized REE zonation profiles within garnet crystals from: the stromatic leucosome (sample L2t-6) and the garnet-bearing residuum (sample CRA1). (a) Comparison of REE zonation profiles of garnet from the metapelites of the MVS to the garnet crystals from the stromatic leucosome. (b) Comparison of REE zonation profiles of garnet from the granitic sheet of the MVS to REE zonation patterns of garnet crystal from the stromatic leucosome. (c) Comparison of REE zonation profiles of garnet from the metapelites of the MVS to REE zonation profiles of garnet crystal from the residuum. (d) Comparison of REE zonation profiles of garnet crystal from granitic sheet to REE zonation patterns of garnet crystal in the residuum. r = rim and c = core. The red, green and purple profiles represent REE zonation patterns from this study. The black patterns represent REE zonation patterns from Taylor and Stevens (2010).

Peritectic garnet investigated in this study, particularly the garnet crystals in the leucosomes, are characterized by; absolute low Y and heavy REE concentrations, flat to slightly negative heavy REE slopes, small to strongly negative Eu anomalies, and bell-shaped zonation patterns with respect to trace elements. Compared to those contained in the granitic sheet in the MVMS reported by Taylor and Stevens, 2010. Garnet crystals in this study are also zoned in REEs, and these elements follow a spatial zonation pattern similar to the major elements (Fig. 30a). Heavy REEs are preferentially enriched in areas where garnet is also enriched in Ca. This suggests that the Ca zoning in the garnet crystals represents growth zoning rather than recrystallization of garnet. The outer most rims of these garnet crystals are inclusion free. This domain is characterized by a little increase in REE zonation profiles. The cores portray higher heavy REE concentrations and are associated with higher Ca contents. REE zonation patterns from garnet in the stromatic leucosomes overlap with those in the metapelitic residuum of the MVS (Fig. 30b).

Peritectic garnet in the leucosomes are marked by small negative Eu anomalies in the cores and strongly negative Eu in the rims compared to those in the granitic sheet of the MVS. Their anomaly is almost identical to those in the metapelitic residuum of the MVS. This is a typical feature for garnet in textural equilibrium with plagioclase in lower greenschist- to amphibolite-facies conditions (Buick et al., 2010). However, at granulite-grades the small negative Eu anomaly when the cores of the peritectic garnet grew in equilibrium with feldspar (either K-feldspar or plagioclase, Buick et al., 2010) is unusual. The co-formation with feldspar results in the more developed negative Eu anomalies. This has implications for the speed of melting reactions. It suggests that as melting initiates, peritectic garnet is out of equilibrium with plagioclase and only small volumes of plagioclase participate in the melting reaction (e.g. Taylor and Stevens, 2010). Furthermore, the more developed negative Eu anomaly towards the rims is consistent with the co-formation of these garnet crystals with peritectic plagioclase (Acosta-Vigil et al., 2010; Bea, 1996; Bea and Montero, 1999; Buick et al., 2010; Villaros et al., 2009). The increase in the negative Eu anomalies towards the rims is interpreted to indicate that the rims are in contact with a greater volume of plagioclase.

The low absolute abundances of REE (+Y) in these garnet crystals is consistent with the disequilibrium-influenced peritectic garnet of the MVMS (Fig. 30). It can be interpreted during the formations of the peritectic garnet by fluid-absent melting reactions that accessory phases were not melting in their modal proportions (e.g. Taylor and Stevens, 2010). Perhaps the melting reaction was

significantly faster than the rate at which heavy REE-rich accessory phases can dissolve in the melt. This is consistent with the findings of Villaros et al. (2009) who established that the rate of zircon dissolution in a peraluminous granitic melt is reasonably slow.

In summary, the low absolute REE (+Y) abundances of the peritectic garnet in the BQ suggest that these garnet crystals crystallized from a melt that was not buffered in heavy REE (+Y). This indicates that the melting reaction was fast enough for accessory phases to equilibrate. Moreover, the small negative Eu anomalies in the cores of the garnet in the leucosomes suggest that the melting reaction was too fast for feldspar to equilibrate. The larger developed Eu anomalies in the rims are consistent with co-formation of the garnet in the leucosomes with peritectic plagioclase.

8.4. Biotite inclusions within garnet

As stated above, one garnet crystal enclosed in sample L2t-6 within a stromatic leucosome contains different biotite crystals. The size of these crystals is grouped within two populations. The small crystal sizes (μm) and the large crystal (mm) sizes. The smaller biotite population have a rounded crystal habit, high Ti content and occur as individual crystals and as inclusions within plagioclase inclusions. The rounded crystal habit of the small biotite crystals represent remnant, reactant biotite from the partial melting process. The larger biotite population form polymineralic inclusions with plagioclase, quartz and rutile and are interpreted to represent crystallized magma inclusions. The lack of K-feldspar as part of magma inclusions suggests that the K_2O and water content in the melt are linked to the stoichiometry of biotite. Therefore, the ratio of K_2O and water in the magma is consistent with biotite formation. The entrainment of melt by garnet indicates that the reaction between melt and garnet to produce biotite is always able to run until the amount of K_2O and water in the melt are exhausted. Thus, explaining why these inclusions can never crystallize K-feldspar. In addition, the smaller biotite crystals (particularly in the upper part of the garnet crystal, Fig. 31a) show an optical continuity within garnet (Fig. 31). The optical continuity indicates that this garnet crystallized during biotite melting, and was mobilized by magma flow from the source into the leucosomes rather than being crystallized directly from the leucosomes.

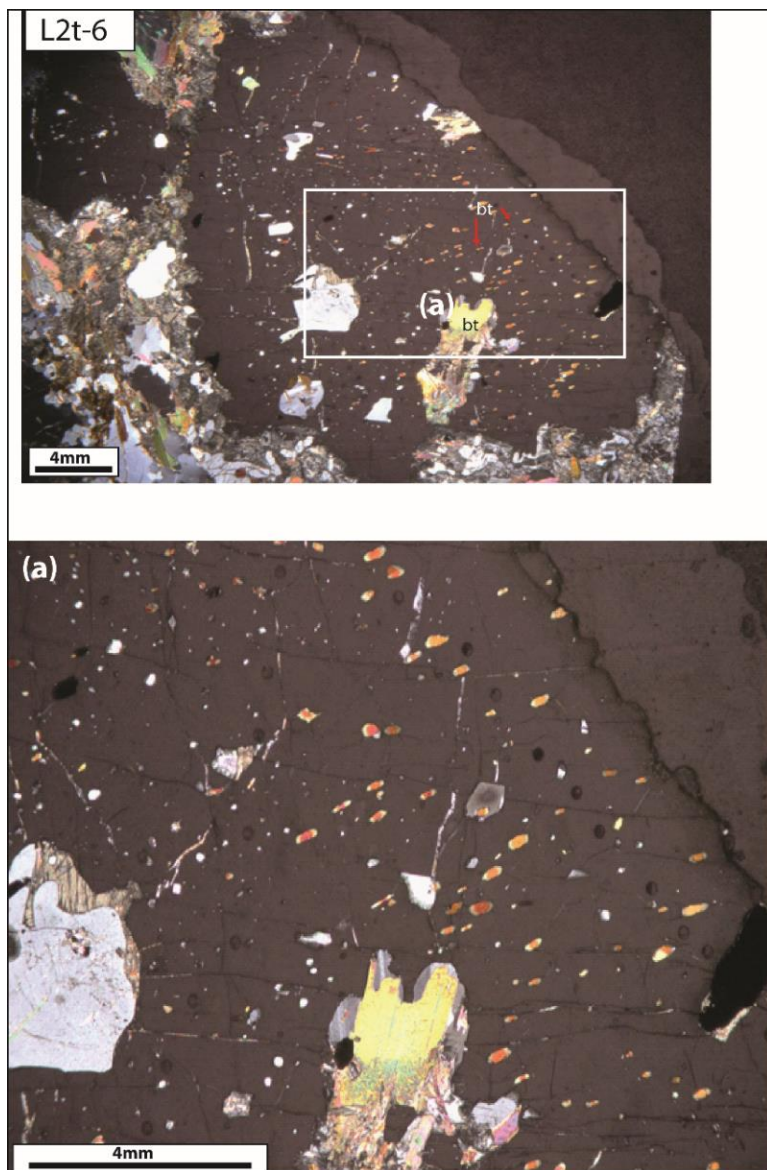


Figure 30: Thin section photomicrographs illustrating an optical continuity of biotite inclusions within garnet. (a) A magnified photograph illustrating optical continuity of biotite inclusions within garnet.

8.5. The origin of the plagioclase inclusions within garnet

A number of different samples were examined in this study. Certain samples provided the opportunity to see features that cannot be seen in every sample within the BQ. These targeted samples enclose peritectic garnet crystals, which contain small euhedral plagioclase inclusions. The euhedral crystal form of these plagioclase inclusions suggests crystallization from the melt. These small euhedral plagioclase inclusions existed in the melt that was produced by the biotite incongruent melting reactions that produced peritectic garnet. Clusters of orthopyroxene, rutile and euhedral plagioclase that

occur as inclusions in garnet represent the assemblage that existed with the melt at the time of peritectic garnet growth. Euhedral quartz crystals that display a hexagonal form also occur as inclusions within garnet. This suggests that plagioclase crystallization induced the co-precipitation of peritectic quartz. In rare cases plagioclase crystals display negative garnet form. These inclusions are interpreted to possibly represent trapped magma. Polyphase inclusions with low Ti biotite and anhedral plagioclase with or without quartz and rutile without K-feldspar probably represent magma inclusions that had a significant melt fraction. These are interpreted to represent micro-granites (Cesare et al., 2011).

8.6. Plagioclase petrogenesis and disequilibrium melting

Phase equilibrium modelling only considers phases that coexist in chemical equilibrium. However, natural features in rocks display chemical disequilibrium features (e.g. chemical zoning in plagioclase, Morse, 1984). In this study a number of features are observed in the rocks that are considered to represent disequilibrium processes. Such features include; plagioclase crystals within garnet having a strongly different composition to other inclusions within garnet and to matrix plagioclase around the garnet, the plagioclase crystals are considerably zoned yet their zonation is not systematic, and the Sr content in these crystals differs quite strongly even within individual crystals and the garnet crystals are zoned in both major and trace elements. All these features, particularly the strongly different major-element compositions of plagioclase inclusions within garnet are indicative of chemical disequilibrium. Consequently, in order to simulate this apparent disequilibrium process a phase equilibrium modelling technique (THERIAK DOMINO) was employed. In order to effectively model this disequilibrium process with THERIAK DOMINO, it is essential to understand how the disequilibrium process arises, i.e. due to slow cation diffusion in plagioclase (e.g. Morse, 1984). In essence, plagioclase can participate in the melting reaction more efficiently by dissolving than by diffusion (Best, 2003) with the dissolution rate of 10^{-7} cm/s at temperature in a range of 1220-1240°C (Agostini et al., 2013) and a maximum diffusion rate of 10^{-20} cm²/s at temperature in a range of 1250-1000°C (Morse, 1984). The presence of minerals that are extremely resistant to composition change by diffusion (e.g. plagioclase and garnet), indicate that in some cases dissolution-reprecipitation process exert an important influence on magma composition (Villaros et al., 2009). Moreover, the dissolution and re-precipitation process produces a new peritectic plagioclase component that is different in composition to the original plagioclase. Some of the original plagioclase does however remain unchanged (unreactive). This is where the disequilibrium arises. The domainal melting of residual

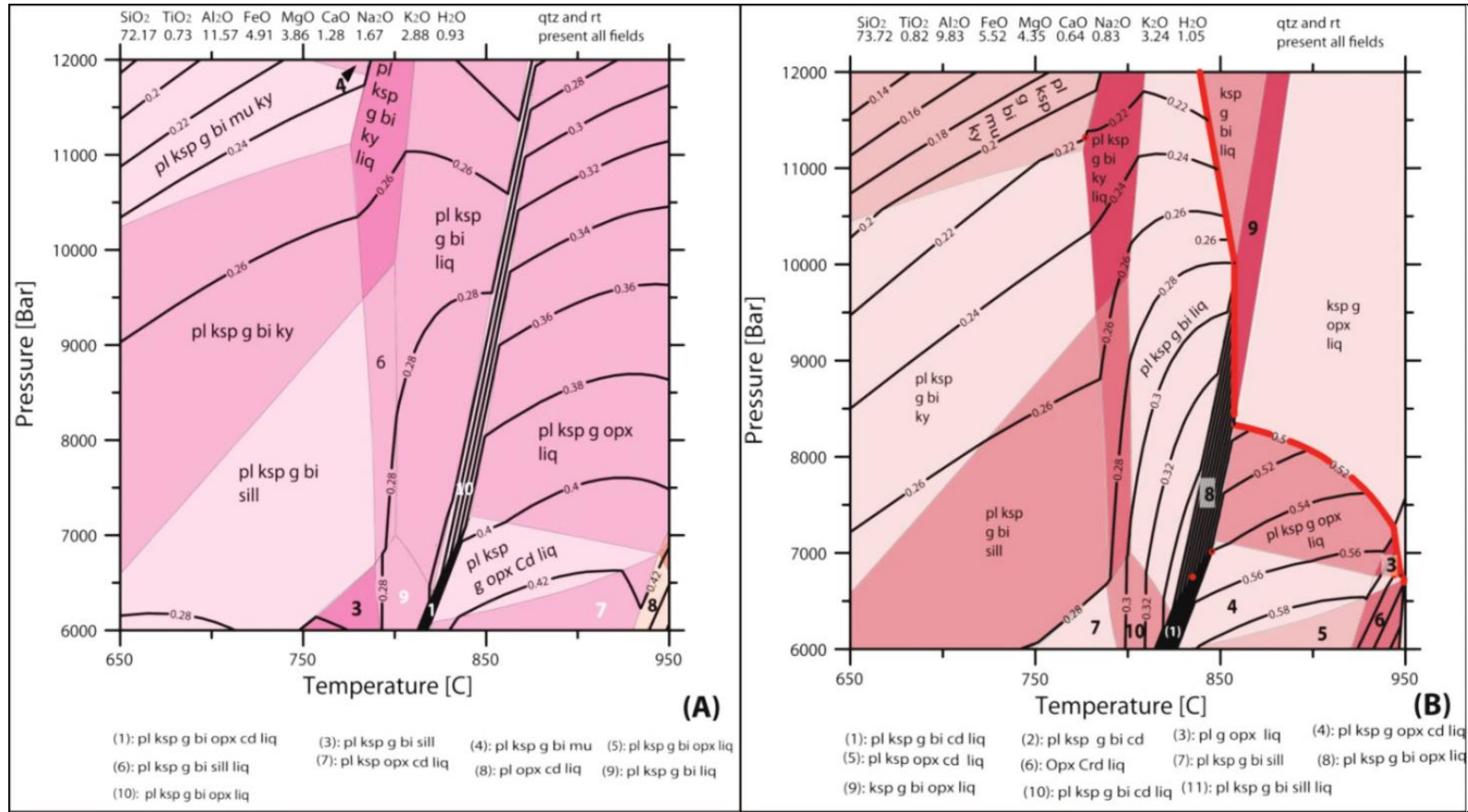
plagioclase gives rise to disequilibrium, with some domains in equilibrium and others out of equilibrium with bulk system. Hence, it was isolated from the melting reaction. This correlates well with observations of the experimental studies (e.g. Johannes, 1989), which show that only the outermost zones of plagioclase are available to participate in the melting reaction. Johannes (1989) also suggested that the process of dissolution-precipitation forms new calcic-rich peritectic plagioclase. In order to effectively model these rocks using the equilibrium modelling technique stated above, a synthetic bulk rock composition was designed where the amount of plagioclase available in the system was restricted. Thus, the effective bulk rock composition (presented in Table 2) is controlled within this study and the effects of this on the composition of the peritectic plagioclase and the volume of the peritectic plagioclase produced are examined.

The results are presented in Fig. 32, and show that two different processes control the behaviour of plagioclase during the melting processes. First, an increase in the amount of kinetically available plagioclase in the system results in an increase in the amount of peritectic plagioclase formed. Second, the composition of the peritectic plagioclase formed is controlled by the amount of plagioclase available in the system. When all of the residual plagioclase is available to participate in the melting reaction i.e. 20% of the bulk rock, the resultant peritectic plagioclase is less calcic (Fig. 32A). However, once the proportion of residual plagioclase in the melting reaction is restricted to 10%, the resultant peritectic plagioclase becomes more calcic (Fig. 32B). Similarly, as the amount of residual plagioclase is reduced to 5%, the peritectic plagioclase becomes even more calcic (Fig. 32C). The onset of the fields where biotite reacts out marks a very strong variation in plagioclase compositional isopleths over a narrow temperature band. This in turn marks a field where large proportions of peritectic garnet crystals are produced and where tight gradient in plagioclase composition is observed.

The modelling predicts that the composition of the peritectic plagioclase is strongly controlled by the chemical accessibility of pre-anatectic plagioclase during the melting reaction that is also controlled mainly by the crystal size of the sub-solidus plagioclase. So, this implies that the small plagioclase crystals are much more chemically accessible to the melting reaction because the movement of cations through the plagioclase structure travel short distances during melting. This is because the crystals have large surface areas that allow them to be more accessible to dissolution. As a result, the whole crystal is available in the melting reaction which results in more albitic peritectic plagioclase crystals. In contrast, the larger plagioclase crystals in the source rocks are chemically less available to the melting reaction because the kinetic obstacles are much higher. In the latter scenario

only the outermost zones of plagioclase participate in the melting reaction and more calcic peritectic crystals are produced. Another possibility affecting the availability of plagioclase in the melting reaction is deformation. This means that when the rocks are undergoing deformation at the same time with melting minerals undergo recrystallization. Therefore becoming more chemically accessible to the melting reaction than when the rocks are not undergoing deformation. In the BQ the rocks melted above the temperature of plagioclase recrystallization thus both the above processes are likely to occur.

The pseudosections illustrated in Fig. 32 demonstrate the effects of plagioclase availability on peritectic plagioclase compositions and provides an explanation for the origin of the calcic plagioclase inclusions. However, the modelling is a simplification of a more complex system in natural rocks. This is because the model only models the disequilibrium aspect of plagioclase and has not modelled the effects of removing garnet from equilibrating with plagioclase. For this reason, plagioclase is in complete equilibrium with garnet. In the diffusion limited system where only the outermost zones of the plagioclase participate in the melting system. The equilibration between plagioclase and garnet is unlikely to occur. In natural rocks garnet would also be affected by this disequilibrium process, which is confirmed in this study by its chemical zoning in both major and trace elements. These pseudosections are able to explain the evolution of plagioclase during the melting processes, the different euhedral crystals formed and their Ca-rich nature and link this strongly to the crystal size of the melting plagioclase. However, the modelling cannot explain the origin of chemical zoning within plagioclase inclusions. This is because the equilibrium modelling only predicts one composition of plagioclase at one P-T condition. Although the bulk composition was modified to mimic the disequilibrium melting, it is still an equilibrium modelling. Therefore, can only model phases that coexist in chemical equilibrium. The strong unsystematic (Ca- and Na-rich rims) zoning in plagioclase inclusions strongly suggests very local equilibrium with each plagioclase crystal seeing its own unique chemical environment. Thus, detailed investigation of garnet zoning around plagioclase inclusions was investigated to see if the zonation could be due to Ca-uptake from garnet or as a consequence of disequilibrium during anatexis.



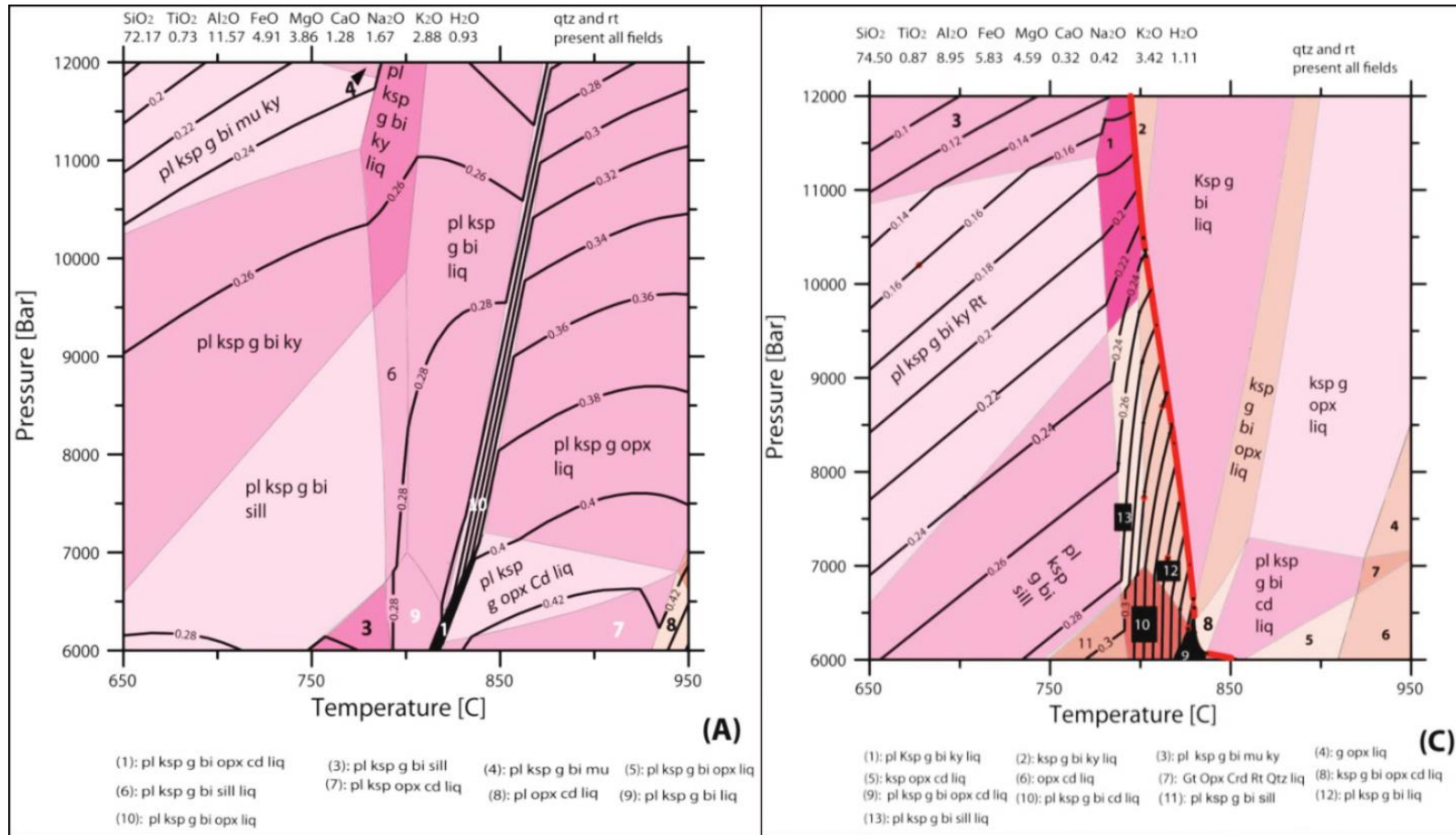
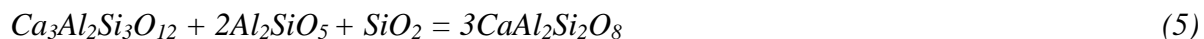


Figure 31: (A-C) Calculated P-T pseudosections investigating the consequences of changing effective bulk rock composition that is caused by slow diffusion in plagioclase. The composition of plagioclase within the different assemblage fields is illustrated by the plotted X_{An} isopleths. The modelling methodology is described in Table 2. Plagioclase out reaction is indicated by the red line. (A) A pseudosection where all of the plagioclase is available to participate in the melting reaction. Within this hypothetical rock that consists of quartz, plagioclase and biotite the plagioclase proportion is 20% of the rock. Plagioclase is stable everywhere in the diagram and the plagioclase anorthite content varies inversely with the amount of melt in the system. The onset of the fields where biotite reacts out marks a very strong variation over a narrow temperature band. (B) A pseudosection illustrating slow diffusion in plagioclase. Hypothetically restricting the amount of plagioclase in the rock to 10 % the formed peritectic plagioclase is more calcic. In this pseudosection the fields where biotite is reacting out marks a tighter variation in plagioclase composition, within this field plagioclase anorthite content is higher than in B. (C) A pseudosection illustrating only 5% proportion of plagioclase hypothetically present in a rock because of slow diffusion. In this pseudosection the plagioclase anorthite content is higher than in A-B, and plagioclase is not stable everywhere in the diagram.

8.7. *Are the compositions of the plagioclase inclusions affected by Ca exchange with garnet*

Different plagioclase inclusions within individual garnet crystals record a wide range of compositions. These plagioclase inclusions commonly occur in areas of garnet that preserve growth zoning and are also commonly randomly distributed within garnet. Some of the inclusions are strongly zoned and usually show an increase in anorthite towards the rims. The opposite zonation is also observed in some of the inclusions. Previous studies by (e.g. Tuccillo et al., 1990; Whitney, 1991) noted the increase of Ca towards the plagioclase rims within high-grade metapelites in sillimanite-bearing rocks from the Skagit Gneiss in the North Cascade Range of Washington (Whitney, 1991) and from the upper amphibolite-facies Britt domain, Ontario Grenville province (Tuccillo et al., 1990) to reflect reaction between plagioclase and garnet in the form of reaction (5). In these studies, plagioclase crystals contain relics of garnet and in some cases inclusions of sillimanite or kyanite. The presence of these inclusions in plagioclase acts as strong evidence for plagioclase attaining its composition through breakdown reactions that consume garnet to form Ca-rich plagioclase. Experimental studies explain the increase in anorthite towards the rims to arise when the outer portions (rims) of the sub-solidus plagioclase crystals participate in the melting reaction, where combined dissolution and precipitation produces new Ca-rich crystals (e.g. Acosta-Vigil et al., 2006; Grove et al., 1984; Johannes 1989), leaving a significant portion of the internal plagioclase inaccessible to the melting hence, unreacted (Fig. 33).



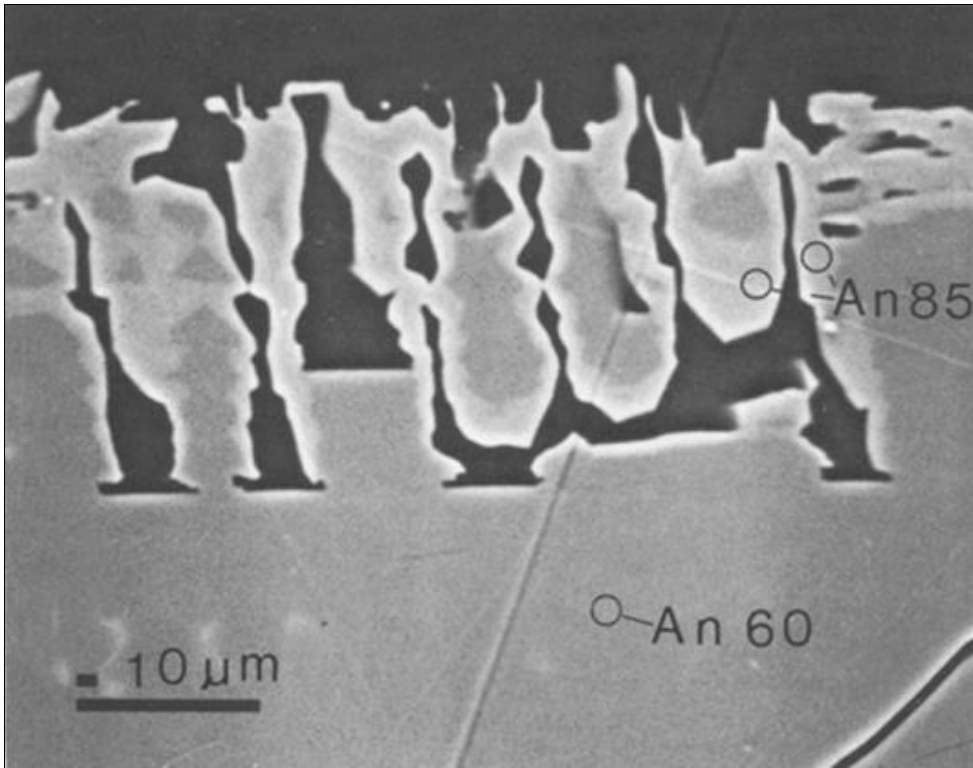


Figure 32: BSE image of the experimental results illustrating the lack of complete re-equilibration of plagioclase crystals during melting (from Johannes, 1989).

Two traverses in different directions through plagioclase-garnet interface were taken to investigate the detailed zonation between plagioclase and garnet. The traverses generally show a relatively constant composition in grossular around some of the euhedral plagioclase inclusions which in turn show an increase in anorthite towards the rims. Moreover, there appears to be a limited exchange between plagioclase and garnet around some of the plagioclase inclusions that show both decrease and an increase in anorthite towards the rims. This exchange is defined by a negligible increase and decrease in the grossular component around these plagioclase inclusions. This feature is interpreted to record the resetting of garnet due to the infiltration of fluids through cracks. This is consistent with the interpretation of Whitney (1991) who established that plagioclase inclusions within garnet can only change composition by a net transfer reaction if they are able to communicate with matrix phases (i.e. quartz and Al_2SiO_5) by fractures within garnet. Morse (1984) demonstrated that rate of diffusion within plagioclase crystals is very slow. Grove et al. (1984) established that anorthite and albite end members are linked by coupled substitutions $(\text{NaSi})^{5+} \rightarrow (\text{CaAl})^{5+}$. Thus, diffusion re-equilibration of anorthite requires the exchange of tetrahedral Al and Si, which is an extremely slow process. This is because it is difficult to break the strong bonds between Al-O-Si and Si-O-Si (Best, 2003).

In addition, Morse (1984) also added that a plagioclase crystal as small as 1mm in diameter would not be homogenized by internal diffusion at or above 1000°C in less than about 10^{10} years. As a result, complete re-equilibration of plagioclase crystals in the 1mm size range is very rare within the time available for typical melting events (e. g. Johannes, 1989; Morse, 1984). Consequently, anorthite zoning in plagioclase (Ca-enriched rims) commonly results from dissolution of old crystals in the melt with the reprecipitation of new grains or overgrowths (Grove et al., 1984; Johannes, 1989). In this study plagioclase crystal as small as 40µm are strongly zoned. It is uncertain as to what processes contributed to the zonation of these crystals, but it is clear that the plagioclase inclusions are not affected by Ca exchange with garnet. The origin of plagioclase zonation is explained in more detail below. It is important to note that there is no data for the detailed garnet zoning around the plagioclase inclusions for garnet within the residuum as this sample was lost.

In summary, reactions between garnet and plagioclase did not significantly alter the compositions of calcic plagioclase (An_{84}) inclusions and the intergrowths of plagioclase and quartz. Even though anorthite content decreases in some inclusions, their absolute anorthite content is still high. However, a small amount of resetting of grossular in garnet is observed around some of the inclusions. This resetting does not relate to plagioclase-garnet interaction, but is rather associated with the cracks. So, it can be assumed that the Ca- and Na-rich rims in euhedral plagioclase inclusions reflect growth zonation produced by the disequilibrium melting reaction. The details of how this zonation arises are explained below.

8.8. The composition of plagioclase inclusions

Plagioclase inclusions within garnet have a wide compositional range. Euhedral inclusions in the leucosomes range in composition from An_{45} to An_{84} . Their composition is different from the anhedral plagioclase inclusions and plagioclase in the matrix. In contrast, euhedral inclusions in the residuum are grouped within a less calcic category and do not record a wide range of composition (An_{30} to An_{35}). The compositions of these inclusions display no relationship to position within garnet. Phase equilibrium modelling was employed to investigate the origin of the Ca-rich nature of the plagioclase inclusions within the leucosomes and their chemical heterogeneity.

The modelling predicts that the composition of the peritectic plagioclase is controlled by the chemical accessibility of the source plagioclase and its crystal size. The strong chemical variability of

plagioclase inclusions trapped within garnet suggests a very local equilibrium with each plagioclase crystal seeing its own chemical environment. However, if the plagioclase crystals prior to entrainment by garnet are not in chemical equilibrium with the melt in terms of the Na/Ca ratio, plagioclase crystals can change their compositions to more calcic or less calcic rims by a combined dissolution and precipitation process (Johannes, 1989). Plagioclase crystals in this study show a perfect hexagonal crystal form and are not corroded. This suggests that their Ca-rich nature is not a consequence of a dissolution-precipitation mechanism, but is rather a primary feature attained in the source during crystal growth. As a result, the strong unsystematic zonation within the plagioclase crystals is assumed to indicate substantial disequilibrium during anatexis. Moreover, the large range in Sr content within the zoned inclusions and the fact that Sr differs quite strongly within the individual crystals, reflects the slow diffusion of plagioclase during partial melting.

9. GENERAL CONCLUSIONS

This study identified unusual, comparatively large poikiloblastic garnet crystals in two samples within the stromatic leucosomes, in one sample within nebulitic leucosome and within the residuum that hosts the leucosomes. These garnet crystals are uncommon because they contain unusual euhedral plagioclase inclusions and they are compositionally zoned in both major and trace elements. The inclusions are complex as they occur as various crystal forms; single crystals, clusters of crystals that contain euhedral quartz, orthopyroxene, biotite and rutile. The euhedral crystals have a wide compositional range from Ca-rich to less calcic compositions, with the exception of those in the residuum which record only less calcic compositions that are the same as the matrix plagioclase. There is no relationship between the composition of the inclusions to the position within the garnet crystal itself, nor with the size of the plagioclase crystal. Some of the plagioclase crystals are significantly zoned displaying both Na- and Ca-enriched rims. The detailed investigation of garnet zonation around the inclusions demonstrates that the Ca-rich nature of the inclusions is not a consequence of Ca-uptake from garnet. Zonation is rather a primary feature attained in the source. However, one garnet within the stromatic leucosome contains rounded biotite crystals that display optical continuity. This suggests that this garnet grew in the source and was later transported into the leucosomes. As it grew, the garnet trapped peritectic plagioclase crystals, quartz and remnant biotite crystals remaining from the melting reaction. This suggests that the conduit through which the magma moved was big enough to transport garnet crystals of a size fraction between 10 and 20mm.

Pseudosection modelling demonstrates that to form such Ca-rich peritectic plagioclase crystals, disequilibrium melting of plagioclase in the source is required. This is consistent with the findings by Taylor et al. (2014). Thus, it is implied that plagioclase melts incongruently to produce Ca-rich peritectic crystals with different compositions during incongruent breakdown of biotite, leaving a significant proportion of plagioclase inaccessible, due to diffusion constraints (Fig. 34). The peritectic plagioclase together with other peritectic phases produced by the melting reaction is entrained by the migrating magma and is transferred into leucosomes. The garnet transported into the leucosomes underwent dissolution-precipitation re-equilibration in the outer rims which removed the inclusions. This process stopped as the melt escapes from the leucosomes. All these different peritectic plagioclase, and quartz entrained into the ‘leucosomes with garnet’ re-crystallized due to decompression processes (Fig. 34). It can be concluded that the high Ca content seen in the leucosomes possibly relates to the amount of entrained peritectic plagioclase into the leucosomes. Thus, the

entrained peritectic plagioclase in the leucosomes shapes the chemistry of the leucosomes. In addition, the presence of these components in the granitic magma system is likely to have shaped the chemistry of granites. Therefore, it can be assumed that melt leaves the source rapidly with entrained peritectic plagioclase together with other ferromagnesian peritectic assemblages. Pseudosection calculations from this study confirm that the disequilibrium process is essential to attain the high Ca content seen in the leucosomes. This is in agreement with observations from experimental studies which confirm that diffusion rates within plagioclase are sufficiently slow to prevent diffusional equilibration within individual plagioclase crystals during anatexis (Morse, 1984; Johannes, 1989). Plagioclase is one of the minerals that are extremely resistant to compositional change through diffusion, suggesting that, in some cases, disequilibrium processes play a significant role in shaping the composition of granites (Farina and Stevens, 2011). The chemistry of the granitic magmas is controlled by the entrainment of the peritectic assemblages in the source and most importantly plagioclase. The current study aim to expand into other migmatite terranes to try to investigate if the preserved Ca-rich peritectic plagioclase crystals within the BQ is only a remnant evidence remaining within the SMZ of the Limpopo belt, or it can be also observed in other migmatitic environments.

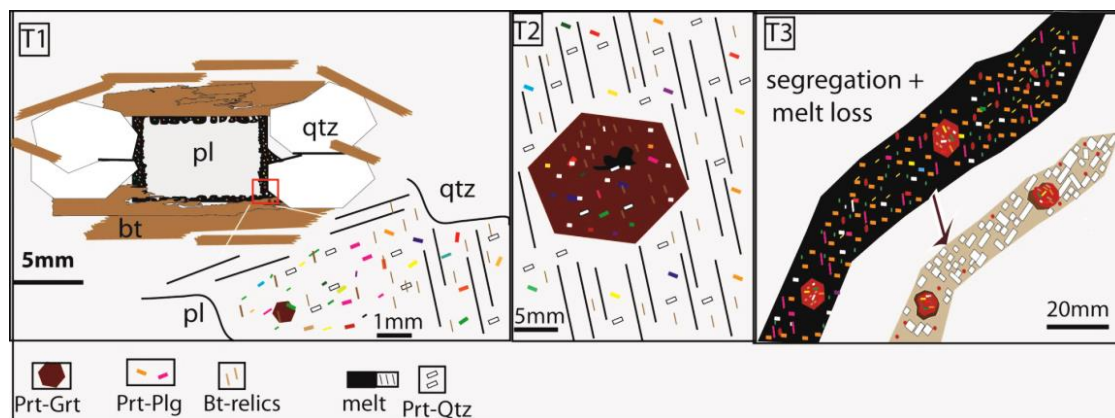


Figure 33: A model for the behaviour of plagioclase during biotite incongruent melting in the BQ migmatites that seem to encounter the requirement for the generation of peritectic plagioclase crystals with different compositions (indicated as different colours in the figure) during partial melting. Different peritectic plagioclase crystals results from the fact that the entire plagioclase crystal is not equilibrated with the melt. (T1) Peritectic more calcic plagioclase with different compositions is produced at the site of melting reaction in the source rock, due to the diffusion constrains in the source plagioclase. (T2) Garnet crystals trap peritectic minerals and remnant of biotite as they grow. The crystallisation of peritectic plagioclase induces co-precipitation of peritectic quartz. (T3) A proportion of this peritectic plagioclase together with peritectic garnet, quartz and remnant of biotite, is entrained to the magma and transported into the leucosomes. (T3) Melt (or less crystal-rich magma that segregated from the source) is lost from the structure producing K_2O depleted leucosomes. The remaining melt crystallizes quartz, plagioclase and K-feldspar and may also contribute in biotite producing retrograde reactions with ferromagnesian minerals in the source.

10. REFERENCES

- Acosta-vigil, A., Buick, I., Hermann, J., Cesare, B., Rubatto, D., London, D., Morgan, G.B., 2010. Mechanisms of Crustal Anatexis: a Geochemical Study of Partially Melted Metapelitic Enclaves and Host Dacite, SE Spain. *Journal of Petrology*, 51(4), 785-821.
- Acosta-vigil, A., Buick, I., Cesare, B., London, D., Morgan, G.B., 2012. The Extent of Equilibration between Melt and Residuum during Regional Anatexis and its implications for Differentiation of the Continental Crust: a Study of Partially Melted Metapelitic Enclaves. *Journal of Petrology*, 0, 1-38.
- Acosta-vigil, A., London, D., Morgan, G.B., 2006. Experiments on the kinetics of partial melting of a leucogranite at 200 MPa H₂O and 690-800 °C: compositional variability of melts during the onset of H₂O-saturated crustal anatexis. *Contributions to Mineralogy and Petrology*, 151, 539-557.
- Aulbach, S., 2012. Craton nucleation and formation of thick lithospheric roots. *Lithos*, 149, 16-30.
- Bartoli, O., Tajcmanov, L., Cesare, B., Acosta-vigil, A., 2013. Phase equilibria constraints on melting of stromatic migmatites from Ronda (S. Spain): insights on the formation of peritectic garnet. *Journal of Metamorphic Geology*, 31, 775-789.
- Bartoli, O., Cesare, B., Poli, S., Bodnar, R.J., Frezzotti, M.L., Vigi, A., Meli, S., 2011. Melting in the deep crust: Message from melt inclusions in peritectic garnet from migmatites. *Mineralogical Magazine*, www.minersoc.org.
- Bea, F., 1996. Residence of REE, Y, Th and U in Granites and Crustal Protoliths: Implications for the Chemistry of Crustal Melts. *Journal of Petrology*, 37(3), 521-552.
- Bea, F., Montero, P., 1999. Behavior of accessory phases and redistribution of Zr, REE, Y, Th and U during metamorphism and partial melting of metapelites in the lower crust. An example from the Kinzigite Formation of Ivrea-Verbano, NW Italy. *Geochimica et Cosmochimica Acta*, 63 (7/8), 1133-1153.
- Best, M.G., 2003. *Igneous and Metamorphic Petrology*, second ed. Blackwell Science Ltd.
- Blenkinsop, T.G., Kroner, A., Chiwara, V., 2004. Single stage, late Archean exhumation of granulites in the Northern Marginal Zone, Limpopo Belt, Zimbabwe, and relevance to gold mineralization. *South African Journal of Geology*, 107(3), 377-396.
- Buick, I.S., Hermann, J., Williams, I.S., Gibson, R.L. & Rubatto, D., 2006. A SHRIMP U-Pb and LA-ICP-MS trace element study of the petrogenesis of garnet-cordierite-orthoamphibole gneisses from the Central Zone of the Limpopo Belt, South Africa. *Lithos*, 88, 150-172.

- Buick, I.S., Clark, C., Rubatto, D., Hermann, J., Pandit, M., Hand, M., 2010. Constrains on the Proterozoic evolution of the Aravalli-Delhi Orogenic belt (NW India) from monazite geochronology and mineral trace element geochemistry. *Lithos*, 120, 511-528.
- Brien, P.J.O., 1999. Asymmetric zoning profiles in garnet from HP-HT granulite and implications for volume and grain-boundary diffusion. *Mineralogical Magazine*, 63(2), 227-238.
- Brown, M., 2007. Crustal melting and melt extraction, ascent and emplacement in orogens: mechanisms and consequences. *Journal of the Geological Society, London* 164, 709-730.
- Brown, M., Korhonen, F.J., 2009. Some remarks on melting and extreme metamorphism of crustal rocks. In: Gupta, A.K., Dasgupta, S., (eds) *Physics and Chemistry of the Earth's Interior*. Springer, India, New Delh, India, 67-87.
- Cesare, B., Acosta-vigil, A., Ferrero, S., Bartoli, O., 2011. Melt inclusions in migmatites and granulites. In: *The Science of Microstructure–Part II, Journal of the Virtual Explorer* (eds Forster, M.A. & Fitz Gerald, J.D.). The Virtual Explorer Pty Ltd, Canberra, Electronic Edition, ISSN 1441-8142. 38, paper 2.
- Chappell B.W., White, A.J.R., Wyborn, D., 1987. The importance of residual source material (restite) in granite petrogenesis. *Journal of Petrology*, 28, 1111-1138.
- Chappell B.W., White, A.J.R., 2001. Two contrasting granite types: 25 years later. *Journal of Petrology*, 28, 1111-1138. *Australian Journal of Earth Sciences*, 48, 489-499.
- Chappell, B.W., White, A.J.R., 1992. I- and S-type granites in the Lachlan Fold Belt. *Transactions of the Royal Society of Edinburgh: Earth Sciences*, 83, 1-26.
- Chappell, B.W., White, A.J.R., Williams, I.s., Wyborn, D., Wyborn, L.A.I., 2000. Lachlan Fold Belt granites revisited: high-and low-temperature granites and their implications. *Australian Journal of Earth Sciences*, 47, 123-138.
- Chappell, B.W., White, A.J.R., 1974. Two constrasting granite types. *Pacific geology*, 8(2), 173-174.
- Chernoff, C.B., Carlson, W.D., 1997. Disequilibrium for Ca during growth of pelitic garnet. *Journal of Metamorphic Geology*, 15, 421-438.
- Clemens, J.D., Helps, P.A., Stevens, G., 2009. Chemical structure in granitic magmas - a signal from the source? *Earth and Environmental Science Transactions of the Royal Society of Edinburgh*, 100, 159-172.
- Clemens, J.D., Stevens, G., Farina, F., 2011. The enigmatic sources of I-type granites: the peritectic connexion. *Lithos*, 126, 174-181.

- Clemens, J.D., 1990. The granulite-granite connexion. In: Veilzeuf, D., Vidal, P(Eds). *Granulites and Crustal Differentiation*. NATO ASI Series. Kluwer Academic Publishers, Dordrecht, p. 25-36.
- Clemens, J.D., Watkins, J.M., 2001. The fluid regime of high-temperature metamorphism during granitoid magma genesis. *Contributions to Mineralogy and Petrology*, 140, 600-606.
- Clemens, J.D., 2003. S-type granitic magma-petrogenetic issues, models and evidence. *Earth-Science Reviews*, 61, 1-18.
- Clemens, J.D., Mawer, C.K., 1992. Granitic magma transport by fracture propagation. *Tectonophysics*, 204, 339-360.
- Clemens, J.D., Vielzeuf, D., 1987. Constraints on melting and magma production in the crust. *Earth and Planetary Science Letters*, 86, 287-306.
- Coggon, R., Holland, T.J.B., 2002. Mixing properties of phengitic micas and revised garnet-phengite thermobarometers. *Journal of Metamorphic Geology*, 20, 683-696.
- Dorais, M.J., Tubrett, M., 2012. Detecting Peritectic Garnet in the Peraluminous Cardigan Pluton, New Hampshire. *Journal of Petrology*, 53, 299-324.
- De Paolo, D. J., 1981. Trace element and isotopic effects of combined wall rock assimilation and fractional crystallization. *Earth and planetary science letters*, 53(2), 189-202.
- de Wit, M.J., Roering, C., Hart, R.J., Armstrong, R.A., de Ronde, C.E.J., Green, R.W.E., Tredoux, M., Peberdy, E., Hart, R.A., 1992. Formation of an Archean continent. *Nature*, 357, 553– 562.
- Diener, J.F.A., Powell, R., 2012. Revised activity-composition models for clinopyroxene and amphibolite. *Journal of Metamorphic Geology*, 20, 131-141.
- Du Toit, M.C., Van Reenen, D.D. & Roering, C., 1983. Some aspects of the geology, structure and metamorphism of the Southern Marginal Zone of the Limpopo metamorphic complex. *Geological Society of South Africa, Special Publications*, 8, 121–142.
- Glazner, F.A., 2007. Thermal limitations on incorporation of wall rock into magma. *Geological Society of South Africa*, 35 (4), 319-322.
- Grove, L.T., Baker, B.M., Kinzler, J.R., 1984. Coupled CaAl-NaSi diffusion in plagioclase feldspar. Experiments and applications to cooling rate speedometry. *Geochimica et cosmochimica acta*, 48, 2113-2121.

- Grover, T.W., Rice, J.M., Carey, J.W., 1992. Petrology of aluminous schist in the Boehls Butte region of northern Idaho: Phase equilibria and P-T evolution. *American Journal*, 292, 494-507.
- Ferrero, S., Bartoli, O., Cesare, B., Salvioli-Mariani, E., Acosta-vigil, A., Cavallo, A., Groppo, C., Battiston, S., 2012. Microstructures of melt inclusions in anatexitic metasedimentary rocks. *Journal of Metamorphic Geology*, 30, 303-322.
- Holzer, L., Frei, R., Barton Jr., J.M., Kramers, J.D., 1998. Unravelling the record of successive high grade events in the Central Zone of the Limpopo belt using Pb single phase dating of metamorphic minerals. *Precambrian Research*, 87, 87-115.
- Holland, T.J.B., Powell, R., 1998. An internally consistent thermodynamic data set for phases of petrological interest. *Journal of Metamorphic Geology*, 16, 303-343.
- Holland, T., Powell, R., 2003. Activity-compositions relations for phases in petrological calculations: an asymmetric multicomponent formulation. *Contributions to Mineralogy and Petrology*, 145, 492-501.
- Johannes, W., 1989. Melting of plagioclase-quartz assemblages at 2 kbar water pressure. *Contributions to Mineralogy and Petrology*, 103, 270-276.
- Jung, S., Hellebrand, E., 2006. Trace element fractionation during high-grade metamorphism and crustal melting-constraints from ion microprobe data of metapelitic, migmatitic and igneous garnets and implications for Sm-Nd garnet chronology. *Lithos*, 87, 193-213.
- Kreissig, K., Nägler, T.F., Kramers, J.D., van Reenen, D.D., Smit, C.A., 2000. An isotopic and geochemical study of the northern Kaapvaal Craton and the Southern Marginal Zone of the Limpopo Belt: Are they juxtaposed terranes? *Lithos*, 50, 1-25.
- Retz, R., 1983. Symbols for rock-forming minerals. *American Mineralogist*, 68, 277-279.
- Laurent, O., Paquette, J.-L., Martin, H., Doucelance, R., Moyen, J.-F., 2013. LA-ICP-MS dating of zircons from Meso- and Neoproterozoic granitoids of the Pietersburg block (South Africa): crustal evolution at the northern margin of the Kaapvaal craton. *Precambrian Research*, 230, 209-226.
- McCourt, S., Vearncombe, J.R., 1987. Shear zones bounding the central zone of the Limpopo mobile belt, southern Africa. *Journal of Structural Geology*, 9, 127-137.
- McCourt, S., Vearncombe, J.R., 1992. Shear zones of the Limpopo Belt and adjacent granitoid-greenstone terranes: Implication for late Archaean collision tectonics in southern Africa. *Precambrian Research*, 55, 553-570.

- Mareschal, J.-C., Jaupart, C., 2013. Radiogenic heat production, thermal regime and evolution of continental crust. *Tectonophysics*, 609, 524-534.
- Martin, L.A.J., Ballèvre, M., Halpenny, A., Vanderhaeghe, S., Duchene, S., Deloule, E., 2011. Garnet re-equilibration by couple dissolution-precipitation: evidence from textural, major element and oxygen isotope zoning of cloudy garnet. *Journal of Metamorphic Geology*, 29, 213-231.
- Martignole, J., Pouhet, P., 1993. Contrasting zoning profiles in high-grade garnets: evidence for the allochthonous nature of a Grenville province terrane. *Earth and Planetary Science Letters*, 120, 177-185.
- Morse, S.A., 1984. Cation diffusion in plagioclase feldspar. *Science*, 225, 504-505.
- Nicoli, G., Stevens, G., Moyon, J-F., Frei, D., 2014. Rapid evolution from sediment to anatectic granulite in an Archean continental collision zone: The example of the Bandelierkop Formation metapelites, South Marginal Zone, Limpopo Belt, South Africa. *Journal of Metamorphic Geology*, doi:10.1111/jmg.12116.
- Otamendi, J.E., de la Rosa, J.D., Patiño Douce, A.E., Rayleigh fractionation of heavy rare earths and yttrium during metamorphic growth. *Geological Society of America*, 30, 159-162.
- Patiño Douce, A.E., Johnston, A.D., 1991. Phase equilibria and melt productivity in the pelitic system: implications for the origin of peraluminous granitoids and aluminous granulites. *Contributions to Mineralogy and Petrology*, 107, 202-218.
- Patiño Douce, A.E., 1999. What do experiments tell us about the relative contributions of crust and mantle to the origin of granitic magmas?, in : Castro, A., Fernandez, C., Vigneresse, J.L. (eds), *Understanding granites: integrating new and classical techniques*, Geological Society, London, Special Publications, 168, 55-75.
- Perugini, D., Poli, G., 2012. The mixing of magmas in plutonic and volcanic environments: Analogies and differences. *Lithos*, 153, 261-277.
- Poli, G., Tommasini, S., 1999. Geochemical modelling of acid–basic magma interaction in the Sardinia–Corsica Batholith: the case study of Sarrabus, southeastern Sardinia, Italy. *Lithos*, 46(3), 553-571.
- Pyle, J.M., Spear, F.S., 1999. Yttrium zoning in garnet: Coupling of major and accessory phases during metamorphic reactions. *Geological Materials Research*, 1, 1-49.
- Pyle, J.M., Spear, F.S., 2000. An empirical garnet (YAG) xenotime thermometer. *Contributions to Mineralogy and Petrology*, 138, 51-58.
- Roberts, M.P., Clemens, J.D., 1993. Origin of high-potassium, calc-alkaline, I-type granitoids. *Geology*, 21, 825-828.

- Roering, C., Van Reenen, D.D., de Wit, M., Smit, C.A., De Beer, J., Van Schalkwyk, J.F., 1992a. Structural, geological and metamorphic significance of the Kaapvaal craton, Limpopo belt contact. *Precambrian Research*, 55, 69-80.
- Roering, C., Van Reenen, D.D., Smit, C.A., Barton, J.M., Jr., de Beer, J.H., d Wit., Stettler, E.H., Van Schalkwyk, J.F., Stevens, G., Pretorius, S., 1992b. Tectonic model for the evolution of the Limpopo Belt. *Precambrian Research*, 55, 539–552.
- Schaller, M., Steiner, O., Studer, I., Holzer, L., Herwegh, M., Kramers, J.D., 1999. The Palala Shear Zone, Transvaal: Exhumation of the Limpopo Central Zone granulites and continent-scale transcurrent movement at 2.0 Ga. *Precambrian Research*, 96, 263–288.
- Spear, F.S., Florence, F.P., 1992. Thermobarometry in granulites: pitfalls and new approaches. *Precambrian Research*, 55, 209-241.
- Spear, F.S., Kohn, M.J., 1996. Trace element zoning in garnet as a monitor of crustal melting. *Geology*, 24, 1099-1102.
- Stevens, G., Clemens, J.D., Droop, G.T.R., 1997. Melt production during granulite-facies anatexis: experimental data from “primitive” metasedimentary protoliths. *Contributions to Mineralogy and Petrology*, 128, 352-370.
- Stevens, G., Clemens, J.D., 1993. Fluid absent melting and the roles of fluids in the lithosphere: a slanted summary? *Chemical Geology* 108, 1–17.
- Stevens, G., Van Reenen, D.D., 1992. Partial melting and the origin of metapelitic granulites in the Southern Marginal Zone of the Limpopo Belt, South Africa. *Precambrian Research*, 55, 303319.
- Stevens, G., Villaros, A., Moyen, J-F., 2007. Selective peritectic garnet entrainment as the origin of chemical diversity in S-type granites. *Geology*, 35, 9-12.
- Taylor, J., Nicoli, G., Stevens, G., Frei, D., Moyen, J-F., 2014. The processes that control leucosome compositions in metasedimentary granulites: perspectives from the Southern Marginal Zone migmatites, Limpopo Belt, South Africa. *Journal of Metamorphic Geology*, DOI: 10.1111/jmg.12087.
- Taylor, J., Stevens, G., 2010. Selective entrainment of peritectic garnet into S-type granitic magmas: evidence from Archaean mid-crustal anatexites. *Lithos*, 120, 277-292.
- Tracy, R.J., 1982. Compositional zoning and inclusions in metamorphic minerals, in: Ferry, M.J., (eds) *Characterization of metamorphism through mineral equilibria: Mineralogical Society of America Reviews in Mineralogy*, 10, 355-397.

- Tuccillo, M.E., Essene, E.J., van der Pluijm, B.A., 1990. Growth and retrograde zoning in garnets from high-grade metapelites: Implications for pressure-temperature paths. *Geology*, 18, 839-842.
- Van Reenen, D.D., 1986. Hydration of cordierite and hypersthene and a description of the retrograde orthoamphibole isograd in the Limpopo Belt, South Africa. *American Mineralogist*, 71, 900-915.
- Van Reenen, D.D., Barton, J.M., Roering, C., Smit, C.A., Van Schalkwyk, J.F., 1987. Deep crustal response to continental collision: the Limpopo belt of southern Africa. *Geology*, 15, 11-14.
- Van Reenen, D.D., Roering, C., Smit, C.A., Van Schalkwyk, J.F., Barton Jr., J.M., 1988. Evolution of the northern high-grade margin of the Kaapvaal Craton. *South African Journal of Geology* 96, 549-560.
- Van Reenen, D.D., Roering, C., Ashwal, L.D., de Wit, M.J., 1992. Regional geological setting of the Limpopo Belt. *Precambrian Research*, 55, 1-5.
- Van Reenen, D.D., Roering, C., Brandl, G., Smit, C.A., Barton, J.M., 1990. The granulite-facies rocks of the Limpopo belt, southern Africa. In: *Granulites and Crustal Evolution* (eds Vielzeuf, D., Vidal, P., 27-289. NATO ASI series C Mathematical and Physical Science, 311, Kluwer Academic Publishers., Dordrecht.
- Vance, J.A., 1962. Zoning in igneous plagioclase; normal and oscillatory zoning. *American Journal of Science*, 260, 746-760.
- Vennemann, T.W. & Smith, H.S., 1992. Stable isotope profile across the orthoamphibole isograd in the Southern Marginal Zone of the Limpopo Belt, South Africa. *Precambrian Research*, 55, 365-397
- Villaros, A., Stevens, G., Buick, I.S., 2009. Tracking S-type granite from source to emplacement: clues from garnet in the Cape Granite Suite. *Lithos*, 112, 217-235.
- White, A.J.R., Chappell, B.W., 1977. Ultrametamorphism and granite genesis. *Tectonophysics*, 43, 7-22.
- White, A.J.R., Chappell, B.W., Wyborn, D., 1999. Application of the restite model to the Deddick Granodiorite and its enclaves - a reinterpretation of the observations and data of Maas et al. (1997). *Journal of Petrology*, 40, 413-421.
- White, A.J.R., Allen, C.M., Beams, S.D., Carr, P.F., Champion, C.C., Chappell, B.W., Wyborn, D., Wyborn, L.A.I., 2001. Granite suites and supersuites of eastern Australia. *Australian Journal of Earth Sciences*, 48, 515-530.
- White, A.J.R., Powell, R., Haalpin, J.A., 2004. Spatially-focussed melt formation in aluminous metapelites from Brocken Hill, Australia, *Journal of Metamorphic Geology*, 22, 825-845.

- White, R.W., Pomroy, N.E., Powell, R., 2005. An in situ metatexite-diatexite transition in upper amphibolite facies rocks from Brocken Hill, Australia. *Journal of Metamorphic Geology*, 23, 579-602.
- White, R.W., Powell, R., Holland, T.J.B., 2007. Progress relating to calculation of partial melting equilibria for metapelites. *Journal of Metamorphic Geology*, 25, 511-527.
- White, R.W., Powell, R., Clarke, G.L., 2002. The interpretation of reaction textures in Fe-rich metapelite granulites of the Musgrave Block, central Australia: constraints from mineral equilibria calculations in the system $K_2O-FeO-MgO-Al_2O_3-SiO_2-H_2O-TiO_2-Fe_2O_3$. *Journal of metamorphic Geology*, 20, 41-55.
- Whitney, D.L., 1991. Calcium depletion halos and Fe-Mn-Mg zoning around faceted plagioclase inclusions in garnet from a high-grade pelitic gneiss. *American Mineralogy*, 76, 493-500.
- Yakymchuk, C., Brown, M., 2014. Consequences of open-system melting in tectonics. *Journal of the Geological Society, London*, 171, 2-40.
- Zeng, L., Saleeby, J.B., Asimow, P., 2005. Nd isotope disequilibrium during crustal anatexis: a record from the Goat Ranch migmatite complex, Southern Sierra Nevada batholith, California. *Geology*, 33(1), 53-56.
- Zeh, A., Gerdes, A., Barton, J. & Klemd, R., 2010. U-Th-Pb and Lu-Hf systematics of zircon from TTG's, leucosomes, meta-anorthosites and quartzites of the Limpopo Belt (South Africa): constraints for the formation, recycling and metamorphism of Palaeoarchean crust. *Precambrian Research*, 179, 50-68.
- Zhang, L., Lüttge, A., Theoretical approach to evaluating plagioclase dissolution mechanisms. *Geochemica et Cosmochimica Acta Journal*, 73, 2832-2849.

11. APPENDICES

APPENDIX A

Table A: Comparison of the mineral standard (wt. %) compositional variability.

Pyrope	Actual			Almandin e	Biotite			Chromite							
	Published	Measured (n=4)	STD		Actual	Measured (n=4)	Dev	Actual	Measured (n=4)	Dev					
SiO ₂	41.45	41.41	0.03	SiO ₂	39.19	39.19	0.00	SiO ₂	38.72	39.46	0.52	TiO ₂	0.12	0.11	0.01
TiO ₂	1.16	1.15	0.01	TiO ₂	0.00	0.00	0.00	TiO ₂	1.77	1.93	0.11	Al ₂ O ₃	9.92	9.91	0.01
Al ₂ O ₃	21.32	21.32	0.00	Al ₂ O ₃	22.05	22.01	0.03	Al ₂ O ₃	15.13	16.46	0.94	Cr ₂ O ₃	60.50	60.58	0.06
Cr ₂ O ₃	0.58	0.56	0.01	Cr ₂ O ₃	0.00	0.00	0.00	FeO	10.72	10.05	0.47	Fe ₂ O ₃	3.38	3.38	0.00
Fe ₂ O ₃	1.37	1.54	0.12	Fe ₂ O ₃	1.62	1.52	0.07	MnO	0.04	0.00	0.03	FeO	9.99	10.02	0.02
FeO	9.92	9.77	0.11	FeO	21.81	21.83	0.01	MgO	19.52	20.10	0.41	MnO	0.11	0.11	0.00
MnO	0.27	0.33	0.04	MnO	0.59	0.59	0.00	CaO	0.10	0.00	0.07	TiO ₂	15.20	15.21	0.01
MgO	19.33	19.34	0.01	MgO	10.70	10.69	0.01	K ₂ O	9.91	9.84	0.05	Na ₂ O	0.00	0.00	0.00
CaO	4.65	4.66	0.01	CaO	4.20	4.20	0.00	-	-	-	#DIV/0!	ZnO	0.14	0.12	0.01
Total	100.05	100.08	0.02	Total	100.16	100.03	0.09	Total	95.91	97.84	1.36	Total	99.36	99.36	0.00
Number of anions on the basis of XO⁻²															
Si ⁴⁺	2.98	2.98	0.00	Si ⁴⁺	2.97	2.97	0.00	Si ⁴⁺	2.81	2.79	0.01	Ti ³⁺	0.00	0.00	0.00
Ti ³⁺	0.06	0.06	0.00	Ti ³⁺	0.00	0.00	0.00	Ti ³⁺	0.10	0.10	0.00	Al ³⁺	0.38	0.38	0.00
Al ³⁺	1.81	1.81	0.00	Al ³⁺	1.97	1.97	0.00	Al ³⁺	1.30	1.37	0.05	Cr ³⁺	1.54	1.54	0.00
Cr ³⁺	0.03	0.03	0.00	Cr ³⁺	0.00	0.00	0.00	Fe ²⁺	0.65	0.59	0.04	Fe ³⁺	0.08	0.08	0.00
Fe ³⁺	0.07	0.08	0.01	Fe ³⁺	0.09	0.09	0.00	Mn ²⁺	0.00	0.00	0.00	Fe ²⁺	0.27	0.27	0.00
Fe ²⁺	0.60	0.59	0.01	Fe ²⁺	1.38	1.38	0.00	Mg ²⁺	2.11	2.12	0.01	Mn ²⁺	0.00	0.00	0.00
Mn ²⁺	0.02	0.02	0.00	Mn ²⁺	0.04	0.04	0.00	Ca ²⁺	0.01	0.00	0.01	Mg ²⁺	0.73	0.73	0.00
Mg ²⁺	2.07	2.07	0.00	Mg ²⁺	1.21	1.21	0.00	K ⁺	0.92	0.89	0.02	Zn ²⁺	0.00	0.00	0.00
Ca ²⁺	0.36	0.36	0.00	Ca ²⁺	0.34	0.34	0.00				#DIV/0!	ΣCat	3.00	3.00	0.00
ΣCat	8.00	8.00	0.00	ΣCat	8.00	8.00	0.00	ΣCat	7.90	7.87	0.02	Anions	4.00	4.00	0.00
Anions	12.00	12.00	0.00	Anions	12.00	12.00	0.00	Anions	11.00	11.00	0.00				

n = spot numbers

Table A: continued

Plag				Ilmenite				Rhodonite				Albite				Sanidine			
Actual		Measured		Actual		Measured		Actual		Measured		Actual		Measured		Actual		Measured	
		(n=4)	Dev			(n=4)	Dev			(n=4)	Dev			(n=4)	Dev			(n=4)	Dev
SiO ₂	53.00	52.66	0.24	TiO ₂	45.70	45.69	0.01	SiO ₂	45.97	45.98	0.00	SiO ₂	68.52	68.54	0.01	SiO ₂	64.67	64.67	0.00
Al ₂ O ₃	28.53	29.55	0.72	Fe ₂ O ₃	10.92	10.86	0.05	FeO	1.55	1.58	0.02	Al ₂ O ₃	19.54	19.53	0.01	TiO ₂	0.00	0.00	0.00
FeO	0.37	0.42	0.03	FeO	36.72	36.72	0.00	MnO	37.66	37.63	0.02	CaO	0.13	0.12	0.01	Al ₂ O ₃	18.76	18.78	0.02
MgO	0.13	0.03	0.07	MnO	4.77	4.77	0.00	MgO	0.89	0.90	0.00	Na ₂ O	11.59	11.56	0.02	FeO	0.18	0.20	0.01
CaO	11.80	11.87	0.05	MgO	0.31	0.31	0.00	CaO	6.40	6.37	0.02	K ₂ O	0.22	0.22	0.00	BaO	1.09	1.10	0.01
BaO	0.01	0.00	0.01	Na ₂ O	0.00	0.00	0.00	ZnO	7.51	7.57	0.05	-	-	-	-	Na ₂ O	3.01	3.01	0.00
Na ₂ O	4.35	4.47	0.09	Nb ₂ O ₅	0.92	0.93	0.00	V ₂ O ₅	0.00	0.00	0.00	-	-	-	-	K ₂ O	12.11	12.13	0.02
K ₂ O	0.41	0.34	0.05	-	-	-	-	-	-	-	-	-	-	-	-	-	-	-	-
SrO	0.08	0.04	0.03	-	-	-	-	-	-	-	-	-	-	-	-	-	-	-	-
Total	98.68	99.39	0.50	Total	99.34	99.27	0.05	Total	99.98	100.03	0.04	Total	99.96	100.00	0.03	Total	99.82	99.89	0.05
Number of anions on the basis of XO-2																			
Si ⁴⁺	2.44	2.40	0.03	Ti ³⁺	0.88	0.98	0.07	Si ⁴⁺	0.99	0.99	0.00	Si ⁴⁺	2.99	3.00	0.00	Si ⁴⁺	2.98	2.97	0.00
Al ³⁺	1.55	1.59	0.03	Fe ³⁺	0.21	0.00	0.15	Fe ³⁺	0.02	0.02	0.00	Al ³⁺	1.01	1.01	0.00	Al ³⁺	1.02	1.02	0.00
Fe ³⁺	0.00	0.00	0.00	Fe ²⁺	0.79	0.88	0.07	Fe ²⁺	0.01	0.01	0.00	Ca ²⁺	0.01	0.01	0.00	Fe ²⁺	0.01	0.01	0.00
Fe ²⁺	0.01	0.02	0.00	Mn ²⁺	0.10	0.12	0.01	Mn ²⁺	0.69	0.69	0.00	Na ⁺	0.98	0.98	0.00	Ca ²⁺	0.00	0.00	0.00
Mg ²⁺	0.01	0.00	0.00	Mg ²⁺	0.01	0.01	0.00	Mg ²⁺	0.03	0.03	0.00	K ⁺	0.01	0.01	0.00	Ba ²⁺	0.02	0.02	0.00
Ca ²⁺	0.58	0.58	0.00	Nb ⁵⁺	0.01	0.01	0.00	Ca ²⁺	0.15	0.15	0.00	-	-	-	-	Na ⁺	0.27	0.27	0.00
Ba ²⁺	0.00	0.00	0.00	-	-	-	-	Zn ²⁺	0.12	0.12	0.00	-	-	-	-	K ⁺	0.71	0.71	0.00
Na ⁺	0.39	0.40	0.01	-	-	-	-	-	-	-	-	-	-	-	-	-	-	-	-
K ⁺	0.02	0.02	0.00	-	-	-	-	-	-	-	-	-	-	-	-	-	-	-	-
ΣCations	5.00	5.00	0.00	ΣCations	2.00	2.00	0.00	ΣCations	2.00	2.00	0.00	ΣCations	5.00	5.00	0.00	ΣCations	5.00	5.00	0.00
Anions	8.00	7.99	0.01	Anions	3.00	3.00	0.00	Anions	3.00	3.00	0.00	Anions	8.00	8.00	0.00	Anions	8.00	7.99	0.00

APPENDIX B

Table B: Electron microprobe analysis of garnet (wt. %). The labels L2t-6, L2t-7, L5R-3 and CRa1 refer to the samples taken from stromatitic leucosomes, nebulitic leucosomes and residue respectively. The dashed lines represent values below the detection limit of the analytical routine.

Sample	L2t-6	L2t-6	L2t-6	L2t-6	L2t-6	L2t-6	L2t-6	L2t-6	L2t-6	L2t-6	L2t-6	L2t-6	L2t-6	L2t-6	L2t-6	L2t-6	L2t-6	L2t-6
Mineral	Garnet	Garnet	Garnet	Garnet	Garnet	Garnet	Garnet	Garnet	Garnet	Garnet	Garnet	Garnet	Garnet	Garnet	Garnet	Garnet	Garnet	Garnet
Generation	Rim	Rim	Rim	Core	Core	Core	Core	Core	Core	Core	Core	Core	Core	Core	Core	Core	Core	Core
SiO ₂	39.30	39.53	39.21	39.38	39.66	39.09	39.11	38.72	38.50	39.19	39.29	39.28	39.03	39.37	39.16	39.56	39.14	38.97
Al ₂ O ₃	22.54	22.13	22.53	22.40	22.25	22.25	22.36	22.38	22.17	22.24	22.35	22.56	22.34	22.20	22.63	22.53	22.39	22.18
Cr ₂ O ₃	0.17	-	0.25	-	0.19	0.19	0.31	-	-	-	-	-	-	0.16	0.19	-	-	-
Fe ₂ O ₃	0.00	0.00	0.08	0.31	0.00	0.11	0.00	0.40	0.68	0.00	0.00	0.00	0.34	0.19	0.21	0.00	0.31	0.00
FeO	25.58	25.30	25.36	25.84	25.55	25.34	25.46	24.62	24.70	25.21	25.22	24.92	25.28	25.16	25.21	25.12	24.68	24.77
MnO	0.71	0.76	0.75	0.70	0.71	0.66	0.71	0.59	0.55	0.60	0.61	0.61	0.62	0.63	0.56	0.76	0.70	0.62
MgO	9.92	10.04	9.97	9.80	9.81	9.64	9.54	9.68	9.55	9.45	9.40	9.50	9.48	9.69	9.48	9.58	9.54	9.47
CaO	2.32	2.39	2.34	2.40	2.43	2.78	2.80	2.98	2.93	3.03	3.02	3.01	3.02	3.12	3.23	3.30	3.43	3.36
Total	100.54	100.15	100.49	100.83	100.60	100.06	100.29	99.37	99.08	99.72	99.89	99.88	100.11	100.52	100.67	100.85	100.19	99.37
Number of anions on the basis of 12 oxygen atoms																		
Si ⁴⁺	2.99	3.01	2.98	2.99	3.01	2.99	2.99	2.98	2.97	3.01	3.01	3.00	2.98	2.99	2.97	3.00	2.98	3.00
Al ³⁺	2.02	1.99	2.02	2.00	1.99	2.00	2.01	2.03	2.02	2.01	2.02	2.03	2.01	1.99	2.03	2.01	2.01	2.01
Cr ³⁺	0.01	-	0.02	-	0.01	0.01	0.02	-	-	-	-	-	-	0.01	0.01	-	-	-
Fe ³⁺	-	-	-	0.02	-	0.01	-	0.02	0.04	-	-	-	0.02	0.01	0.01	-	0.02	-
Fe ²⁺	1.63	1.61	1.61	1.64	1.62	1.62	1.62	1.58	1.59	1.62	1.61	1.59	1.62	1.60	1.60	1.59	1.57	1.59
Mn ²⁺	0.05	0.05	0.05	0.04	0.05	0.04	0.05	0.04	0.04	0.04	0.04	0.04	0.04	0.04	0.04	0.05	0.05	0.04
Mg ²⁺	1.12	1.14	1.13	1.11	1.11	1.10	1.09	1.11	1.10	1.08	1.07	1.08	1.08	1.10	1.07	1.08	1.08	1.09
Ca ²⁺	0.19	0.19	0.19	0.19	0.20	0.23	0.23	0.25	0.24	0.25	0.25	0.25	0.25	0.25	0.26	0.27	0.28	0.28
Σcat	8.00	8.00	8.00	8.00	8.00	8.00	8.00	8.00	8.00	8.00	8.00	8.00	8.00	8.00	8.00	8.00	8.00	8.00
Anions	12.00	12.01	12.00	12.00	12.02	12.00	12.00	12.00	12.00	12.01	12.02	12.02	12.00	12.00	12.00	12.00	12.00	12.00
XAlm	0.54	0.54	0.54	0.55	0.55	0.54	0.54	0.53	0.54	0.54	0.54	0.54	0.54	0.53	0.54	0.53	0.53	0.53
XGrss	0.06	0.07	0.06	0.07	0.07	0.08	0.08	0.08	0.08	0.08	0.08	0.08	0.08	0.08	0.09	0.09	0.09	0.09
XSpss	0.02	0.02	0.02	0.01	0.02	0.01	0.02	0.01	0.01	0.01	0.01	0.01	0.01	0.01	0.01	0.02	0.02	0.01

XPyr	0.38	0.38	0.38	0.37	0.37	0.37	0.36	0.37	0.37	0.36	0.36	0.37	0.36	0.37	0.36	0.36	0.36	0.36
D	0.00	0.04	0.09	0.14	0.24	0.38	0.43	0.49	0.56	0.68	0.72	0.78	0.84	0.91	0.96	1.02	1.08	1.18

Table B: continued

Sample	L2t-6	L2t-6	L2t-6	L2t-6	L2t-6	L2t-6	L2t-6	L2t-6	L2t-6	L2t-6	L2t-6	L2t-6	L2t-6	L2t-6	L2t-6	L2t-6	L2t-6	L2t-6	L2t-6	L2t-6	L2t-6
Mineral	Grt	Grt	Grt	Grt	Grt	Grt	Grt	Grt	Grt	Grt	Grt	Grt	Grt	Grt	Grt	Grt	Grt	Grt	Grt	Grt	Grt
Generation	Core	Core	Core	Core	Core	Core	Core	Core	Core	Core	Core	Core	Core	Core	Core	Core	Core	Core	Core	Core	Core
SiO ₂	38.79	39.14	39.03	38.89	39.24	39.47	38.98	39.26	38.87	39.14	38.97	38.88	39.18	38.77	38.88	39.02	39.12	39.19	38.97	38.82	38.94
Al ₂ O ₃	22.49	22.38	22.27	22.20	22.34	22.42	22.60	22.23	22.01	22.56	22.25	22.56	22.32	22.44	22.23	22.40	22.14	22.55	21.86	22.40	22.40
Cr ₂ O ₃	0.26	-	0.16	0.16	0.20	-	0.16	-	-	-	-	-	-	0.16	0.18	0.19	-	-	-	0.18	-
Fe ₂ O ₃	0.33	0.00	0.36	0.16	0.20	0.00	0.00	0.04	0.00	0.64	0.42	0.00	0.16	0.02	0.00	0.00	0.15	0.87	0.42	0.07	0.91
FeO	24.59	24.95	24.76	25.18	25.17	25.12	25.22	24.92	24.75	24.87	24.85	24.83	24.91	24.92	24.64	24.88	25.12	24.92	25.07	25.42	24.88
MnO	0.68	0.53	0.76	0.65	0.68	0.59	0.56	0.65	0.67	0.68	0.73	0.73	0.74	0.60	0.68	0.58	0.63	0.64	0.63	0.61	0.67
MgO	9.50	9.46	9.57	9.46	9.74	9.84	9.49	9.75	9.48	9.62	9.40	9.28	9.56	9.39	9.38	9.54	9.67	10.05	9.98	9.92	10.41
CaO	3.25	3.24	3.19	2.96	2.90	2.92	2.98	3.11	3.24	3.19	3.33	3.21	3.25	3.19	3.14	3.09	2.95	2.63	2.42	2.11	1.90
Total	99.89	99.70	100.10	99.67	100.46	100.37	99.97	99.96	99.01	100.70	99.95	99.48	100.11	99.49	99.12	99.69	99.79	100.85	99.35	99.53	100.11
Number of anions on the basis of 12 oxygen atoms																					
Si ⁴⁺	2.97	3.00	2.98	2.99	2.99	3.00	2.98	3.00	3.00	2.97	2.98	2.99	2.99	2.98	3.00	2.99	3.00	2.97	3.00	2.98	2.97
Al ³⁺	2.03	2.02	2.01	2.01	2.00	2.01	2.04	2.00	2.00	2.02	2.01	2.04	2.01	2.03	2.02	2.02	2.00	2.01	1.98	2.03	2.01
Cr ³⁺	0.02	-	0.01	0.01	0.01	-	0.01	-	-	-	-	-	-	0.01	0.01	0.01	-	-	-	0.01	-
Fe ³⁺	0.02	-	0.02	0.01	0.01	-	-	-	-	0.04	0.02	-	0.01	-	-	-	0.01	0.05	0.02	-	0.05
Fe ²⁺	1.57	1.60	1.58	1.62	1.60	1.60	1.61	1.59	1.60	1.58	1.59	1.60	1.59	1.60	1.59	1.59	1.61	1.58	1.61	1.63	1.59
Mn ²⁺	0.04	0.03	0.05	0.04	0.04	0.04	0.04	0.04	0.04	0.04	0.05	0.05	0.05	0.04	0.04	0.04	0.04	0.04	0.04	0.04	0.04
Mg ²⁺	1.08	1.08	1.09	1.08	1.10	1.12	1.08	1.11	1.09	1.09	1.07	1.06	1.09	1.08	1.08	1.09	1.10	1.14	1.14	1.13	1.18
Ca ²⁺	0.27	0.27	0.26	0.24	0.24	0.24	0.24	0.25	0.27	0.26	0.27	0.26	0.27	0.26	0.26	0.25	0.24	0.21	0.20	0.17	0.16
Σcat	8.00	8.00	8.00	8.00	8.00	8.00	8.00	8.00	8.00	8.00	8.00	8.00	8.00	8.00	8.00	8.00	8.00	8.00	8.00	8.00	8.00
Anions	12.00	12.01	12.00	12.00	12.00	12.01	12.00	12.00	12.00	12.00	12.00	12.01	12.00	12.00	12.01	12.01	12.00	12.00	12.00	12.00	12.00
XAlm	0.53	0.54	0.53	0.54	0.54	0.53	0.54	0.53	0.53	0.53	0.53	0.54	0.53	0.54	0.53	0.54	0.54	0.53	0.54	0.55	0.53
XGrss	0.09	0.09	0.09	0.08	0.08	0.08	0.08	0.08	0.09	0.09	0.09	0.09	0.09	0.09	0.09	0.09	0.08	0.07	0.07	0.06	0.05
XSpss	0.01	0.01	0.02	0.01	0.01	0.01	0.01	0.01	0.01	0.01	0.02	0.02	0.02	0.01	0.01	0.01	0.01	0.01	0.01	0.01	0.01
XPyr	0.37	0.36	0.37	0.36	0.37	0.37	0.36	0.37	0.36	0.37	0.36	0.36	0.36	0.36	0.36	0.37	0.37	0.38	0.38	0.38	0.40
D	1.34	1.38	1.43	1.50	1.55	1.80	1.84	1.89	1.94	2.00	2.10	2.17	2.23	2.38	2.48	2.63	2.77	2.98	3.05	3.22	3.38

Table B: continued

Sample	L2t-6	L2t-6	L2t-6	L2t-6	L2t-6	L2t-6	L2t-6	L2t-7	L2t-7	L2t-7	L2t-7	L2t-7	L2t-7	L2t-7	L2t-7	L2t-7	L2t-7	L2t-7	L2t-7	L2t-7	L2t-7
Mineral	Grt	Grt	Grt	Grt	Grt	Grt	Grt	Grt	Grt	Grt	Grt	Grt	Grt	Grt	Grt	Grt	Grt	Grt	Grt	Grt	Grt
Generation	Core	Core	Core	Core	Rim	Rim	Rim	rim	rim	rim	core	core	core	core	core	core	core	core	core	core	core
SiO₂	39.24	38.83	39.22	39.28	39.10	38.92	39.29	39.34	38.72	39.25	39.21	39.40	39.36	39.38	39.51	39.48	39.31	39.23	39.19	39.49	39.49
Al₂O₃	22.64	22.29	22.57	22.07	22.06	22.41	22.47	22.19	22.16	21.98	21.95	22.52	22.28	22.21	22.38	22.41	22.27	22.17	22.02	22.19	22.17
Cr₂O₃	0.19	0.26	0.23	-	0.17	0.24	0.25	0.14	0.22	0.17	0.18	0.16	0.20	0.27	0.21	0.21	0.20	0.22	0.17	0.18	0.28
Fe₂O₃	-	0.66	0.17	-	-	0.27	0.37	-	0.49	0.07	-	0.38	-	-	-	0.02	-	0.19	-	-	-
FeO	25.60	25.37	25.81	25.65	25.26	25.25	25.03	25.86	25.09	24.97	25.01	24.69	24.85	24.49	24.54	24.71	24.39	24.86	24.55	24.79	24.94
MnO	0.56	0.64	0.62	0.75	0.75	0.75	0.66	0.98	0.79	0.85	0.74	0.88	0.63	0.61	0.79	0.84	0.91	0.70	0.79	0.84	0.69
MgO	10.35	10.19	10.08	9.95	9.84	10.13	10.92	9.94	9.64	9.68	9.46	9.57	9.48	9.41	9.50	9.59	9.67	9.60	9.54	9.58	9.92
CaO	1.71	1.75	1.95	1.98	2.18	1.94	1.42	1.77	2.51	3.00	3.35	3.49	3.60	3.55	3.51	3.56	3.46	3.29	3.10	3.02	3.05
Total	100.29	99.98	100.64	99.69	99.36	99.91	100.42	100.22	99.62	99.97	99.90	101.09	100.40	99.92	100.44	100.82	100.21	100.26	99.36	100.09	100.54
Number of anions on the basis of 12 oxygen atoms																					
Si⁴⁺	2.98	2.97	2.98	3.01	3.01	2.98	2.98	3.00	2.98	3.00	3.00	2.98	3.00	3.01	3.01	2.99	2.99	2.99	3.01	3.02	3.00
Al³⁺	2.03	2.01	2.02	1.99	2.00	2.02	2.01	2.00	2.01	1.98	1.98	2.01	2.00	2.00	2.01	2.00	2.00	1.99	2.00	2.00	1.98
Cr³⁺	0.01	0.02	0.01	-	0.01	0.01	0.01	0.01	0.01	0.01	0.01	0.01	0.01	0.02	0.01	0.01	0.01	0.01	0.01	0.01	0.02
Fe³⁺	-	0.04	0.01	-	-	0.02	0.02	-	-	-	-	0.02	-	-	-	-	-	0.01	-	-	-
Fe²⁺	1.63	1.62	1.64	1.64	1.62	1.61	1.59	1.65	1.61	1.60	1.60	1.56	1.58	1.57	1.56	1.57	1.55	1.59	1.58	1.58	1.58
Mn²⁺	0.04	0.04	0.04	0.05	0.05	0.05	0.04	0.06	0.05	0.06	0.05	0.06	0.04	0.04	0.05	0.05	0.06	0.05	0.05	0.05	0.04
Mg²⁺	1.17	1.16	1.14	1.14	1.13	1.15	1.23	1.13	1.10	1.10	1.08	1.08	1.08	1.07	1.08	1.08	1.10	1.09	1.09	1.09	1.12
Ca²⁺	0.14	0.14	0.16	0.16	0.18	0.16	0.12	0.14	0.21	0.25	0.27	0.28	0.29	0.29	0.29	0.29	0.28	0.27	0.26	0.25	0.25
Σcat	8.00	8.00	8.00	8.00	8.00	8.00	8.00	7.99	8.00	8.00	7.99	8.00	8.00	8.00	8.01	7.99	7.99	8.00	8.00	8.00	7.99
Anions	12.00	12.00	12.00	12.01	12.01	12.00	12.00	12.01	12.00	12.00	12.00	12.00	12.00	12.02	12.01	12.00	12.00	12.00	12.02	12.02	12.00
XAlm	0.55	0.55	0.55	0.55	0.54	0.54	0.53	0.05	0.07	0.08	0.09	0.09	0.10	0.10	0.10	0.10	0.09	0.09	0.09	0.08	0.08
XGrss	0.05	0.05	0.05	0.05	0.06	0.05	0.04	0.55	0.54	0.53	0.53	0.52	0.53	0.53	0.52	0.52	0.52	0.53	0.53	0.53	0.53
XSpss	0.01	0.01	0.01	0.02	0.02	0.02	0.01	0.38	0.37	0.37	0.36	0.36	0.36	0.36	0.36	0.36	0.37	0.36	0.37	0.37	0.37
XPyr	0.39	0.39	0.38	0.38	0.38	0.39	0.41	0.02	0.02	0.02	0.02	0.02	0.01	0.01	0.02	0.02	0.02	0.02	0.02	0.02	0.01
D	4.11	4.22	4.57	4.73	4.92	5.30	5.54	0.00	0.09	0.28	0.41	0.51	0.57	0.65	0.73	0.79	0.85	0.95	1.00	1.04	1.10

Table B: continued

Sample	L2t-7	L2t-7	L2t-7	L2t-7	L2t-7	L2t-7	L2t-7	L2t-7	L2t-7	L2t-7	L2t-7	L2t-7	L2t-7	L2t-7	L2t-7	L2t-7	L2t-7	L2t-7	L2t-7	L2t-7	L2t-7
Mineral	Grt	Grt	Grt	Grt	Grt	Grt	Grt	Grt	Grt	Grt	Grt	Grt	Grt	Grt	Grt	Grt	Grt	Grt	Grt	Grt	Grt
Generation	core	core	core	core	core	core	core	core	core	core	core	core	core	core	core	core	core	core	core	core	core
SiO ₂	39.10	39.17	39.16	39.16	39.35	39.47	39.49	39.43	39.42	39.18	39.00	39.37	39.28	38.78	39.43	39.11	39.54	39.31	39.40	38.94	38.78
Al ₂ O ₃	22.23	22.28	22.33	22.32	22.42	22.31	22.34	22.53	22.44	22.18	22.05	22.17	22.55	22.34	22.41	22.22	22.19	22.29	22.50	22.23	22.27
Cr ₂ O ₃	0.29	0.17	0.00	0.16	-	0.22	-	0.15	0.20	-	0.14	-	0.18	0.21	-	-	0.15	-	-	0.18	0.15
Fe ₂ O ₃	0.00	0.63	0.51	0.11	0.00	0.00	0.00	0.19	0.00	0.00	0.06	0.00	0.00	0.55	0.00	0.63	0.00	0.09	0.00	0.06	0.50
FeO	24.55	24.49	24.81	25.13	25.12	25.32	25.32	25.28	25.74	25.61	25.42	25.48	25.02	25.18	24.92	24.33	25.40	24.73	24.49	24.53	23.98
MnO	0.59	0.78	0.76	0.71	0.87	0.77	0.78	0.68	0.63	0.74	0.84	0.67	0.76	0.81	0.71	0.81	0.72	0.76	0.75	0.78	0.83
MgO	10.00	10.27	10.33	10.34	10.18	10.39	10.35	10.75	10.63	10.25	10.28	10.19	9.97	9.51	9.74	10.00	9.36	9.72	9.57	9.37	9.56
CaO	2.69	2.53	2.22	1.99	2.04	2.01	1.78	1.58	1.23	1.44	1.60	2.09	2.49	2.67	2.98	2.95	3.02	3.26	3.39	3.54	3.52
Total	99.45	100.32	100.12	99.92	99.98	100.49	100.06	100.59	100.29	99.40	99.39	99.97	100.25	100.05	100.19	100.05	100.38	100.16	100.10	99.63	99.59
Number of anions on the basis of 12 oxygen atoms																					
Si ⁴⁺	3.00	2.98	2.98	2.99	3.00	3.00	3.01	2.99	3.00	3.01	3.00	3.01	2.99	2.97	3.00	2.98	3.02	3.00	3.00	2.99	2.97
Al ³⁺	2.01	2.00	2.00	2.01	2.02	2.00	2.01	2.01	2.01	2.01	2.00	1.99	2.02	2.02	2.01	2.00	2.00	2.00	2.02	2.01	2.01
Cr ³⁺	0.02	0.01	-	0.01	-	0.01	-	0.01	0.01	-	0.01	-	0.01	0.01	-	-	0.01	-	-	0.01	0.01
Fe ³⁺	0.00	0.04	0.03	0.01	0.00	0.00	0.00	0.01	0.00	0.00	0.00	0.00	0.00	0.03	0.00	0.04	0.00	0.00	0.00	0.00	0.03
Fe ²⁺	1.57	1.56	1.58	1.60	1.60	1.61	1.61	1.60	1.64	1.64	1.63	1.63	1.59	1.61	1.59	1.55	1.62	1.58	1.56	1.57	1.54
Mn ²⁺	0.04	0.05	0.05	0.05	0.06	0.05	0.05	0.04	0.04	0.05	0.05	0.04	0.05	0.05	0.05	0.05	0.05	0.05	0.05	0.05	0.05
Mg ²⁺	1.14	1.16	1.17	1.18	1.16	1.18	1.18	1.21	1.20	1.17	1.18	1.16	1.13	1.09	1.11	1.14	1.06	1.10	1.09	1.07	1.09
Ca ²⁺	0.22	0.21	0.18	0.16	0.17	0.16	0.15	0.13	0.10	0.12	0.13	0.17	0.20	0.22	0.24	0.24	0.25	0.27	0.28	0.29	0.29
Σcat	8.00	8.01	7.99	8.01	8.01	8.01	8.01	8.00	8.00	8.00	8.00	8.00	7.99	8.00	8.00	8.00	8.01	8.00	8.00	7.99	7.99
Anions	12.01	12.00	12.00	12.00	12.01	12.00	12.01	12.00	12.01	12.01	12.00	12.00	12.01	12.00	12.01	12.00	12.02	12.00	12.01	12.00	12.00
XAlm	0.07	0.07	0.06	0.05	0.06	0.05	0.05	0.04	0.03	0.04	0.04	0.06	0.07	0.07	0.08	0.08	0.08	0.09	0.09	0.10	0.10
XGrss	0.53	0.52	0.53	0.54	0.54	0.54	0.54	0.54	0.55	0.55	0.54	0.54	0.54	0.54	0.53	0.52	0.54	0.53	0.52	0.53	0.52
XSpss	0.38	0.39	0.39	0.39	0.39	0.39	0.39	0.41	0.40	0.39	0.39	0.39	0.38	0.37	0.37	0.38	0.36	0.37	0.37	0.36	0.37
XPyrr	0.01	0.02	0.02	0.02	0.02	0.02	0.02	0.01	0.01	0.02	0.02	0.01	0.02	0.02	0.02	0.02	0.02	0.02	0.02	0.02	0.02
D	1.25	1.29	1.42	1.51	1.65	1.81	1.88	1.97	2.03	2.40	2.40	2.48	2.55	2.58	2.69	2.72	2.79	2.88	2.94	3.01	3.05

Table B: continued

Sample	L2t-7	L2t-7	L2t-7	L2t-7	L2t-7	L2t-7	L2t-7	L2t-7	L2t-7	L2t-7	L2t-7	L2t-7	L2t-7	L2t-7	L2t-7	L2t-7	L2t-7	L2t-7	L2t-7	L2t-7	L2t-7	
Mineral	Grt	Grt	Grt	Grt	Grt	Grt	Grt	Grt	Grt	Grt	Grt	Grt	Grt	Grt	Grt	Grt	Grt	Grt	Grt	Grt	Grt	
Generation	core	core	core	core	core	core	core	core	core	core	core	core	core	core	core	core	core	core	core	core	rim	rim
SiO ₂	39.26	39.00	38.89	38.82	38.93	39.09	39.10	39.30	39.21	39.43	39.22	39.32	38.97	38.87	39.44	39.25	38.99	39.37	39.10	39.41	39.78	
Al ₂ O ₃	22.14	22.32	22.15	21.81	22.21	22.39	22.49	22.45	22.15	22.34	22.36	22.16	22.33	22.16	22.09	22.13	22.25	22.48	22.37	22.50	22.35	
Cr ₂ O ₃	0.21	0.17	-	-	0.13	-	-	0.20	-	-	0.19	-	-	0.20	0.18	0.20	0.27	-	0.21	0.20	0.14	
Fe ₂ O ₃			0.06	0.66				0.12				0.23		0.53		0.02				0.08		
FeO	24.36	24.03	24.52	23.80	24.41	24.72	24.81	24.58	24.76	24.46	24.68	24.88	24.66	24.99	24.52	24.96	25.15	25.31	24.79	24.62	24.57	
MnO	0.88	0.72	0.73	0.76	0.78	0.79	0.67	0.70	0.83	0.87	0.83	0.76	0.81	0.76	0.71	0.79	0.82	0.74	0.80	0.77	0.81	
MgO	9.61	9.47	9.34	9.61	9.11	9.29	9.21	9.38	9.36	9.62	9.79	9.70	10.11	10.08	10.69	10.77	10.55	10.59	10.91	11.09	11.14	
CaO	3.55	3.50	3.59	3.68	3.61	3.64	3.66	3.42	3.35	3.12	3.06	2.67	2.42	2.11	1.93	1.54	1.39	1.66	1.34	1.20	1.22	
Total	100.01	99.21	99.28	99.14	99.18	100.04	99.94	100.03	99.66	99.84	100.36	99.49	99.83	99.17	99.56	99.66	99.42	100.15	99.60	99.79	100.01	
Number of anions on the basis of 12 oxygen atoms																						
Si ⁴⁺	3.00	3.00	2.99	2.99	3.00	2.99	2.99	3.00	3.01	3.01	2.98	3.02	2.98	2.99	3.01	3.00	2.99	2.99	2.98	3.00	3.02	
Al ³⁺	1.99	2.02	2.01	1.98	2.02	2.02	2.03	2.02	2.00	2.01	2.01	2.00	2.01	2.01	1.99	1.99	2.01	2.01	2.01	2.02	2.00	
Cr ³⁺	0.01	0.01	-	-	0.01	-	-	0.01	-	-	0.01	-	-	0.01	0.01	0.01	0.02	-	0.01	0.01	0.01	
Fe ³⁺	0.00	0.00	0.00	0.04	0.00	0.01	0.00	0.00	0.00	0.00	0.01	0.00	0.03	0.00	0.00	0.00	0.00	0.00	0.00	0.00	0.00	
Fe ²⁺	1.56	1.55	1.58	1.53	1.57	1.58	1.59	1.57	1.59	1.56	1.57	1.60	1.58	1.61	1.57	1.59	1.61	1.61	1.58	1.57	1.56	
Mn ²⁺	0.06	0.05	0.05	0.05	0.05	0.05	0.04	0.05	0.05	0.06	0.05	0.05	0.05	0.05	0.05	0.05	0.05	0.05	0.05	0.05	0.05	
Mg ²⁺	1.09	1.09	1.07	1.10	1.05	1.06	1.05	1.07	1.07	1.10	1.11	1.11	1.15	1.16	1.22	1.23	1.21	1.20	1.24	1.26	1.26	
Ca ²⁺	0.29	0.29	0.30	0.30	0.30	0.30	0.30	0.28	0.28	0.26	0.25	0.22	0.20	0.17	0.16	0.13	0.11	0.13	0.11	0.10	0.10	
Σcat	8.00	8.01	8.00	7.99	8.00	8.01	8.00	8.00	8.00	8.00	7.99	8.00	8.00	8.00	8.01	8.00	8.00	7.99	7.98	8.01	8.00	
Anions	12.00	12.02	12.00	12.00	12.02	12.00	12.00	12.02	12.01	12.02	12.00	12.02	12.00	12.00	12.01	12.00	12.00	12.00	12.00	12.01	12.02	
XAlm	0.10	0.10	0.10	0.10	0.10	0.10	0.10	0.09	0.09	0.09	0.08	0.07	0.07	0.06	0.05	0.04	0.04	0.05	0.04	0.03	0.03	
XGrss	0.52	0.52	0.53	0.51	0.53	0.53	0.53	0.53	0.53	0.53	0.53	0.54	0.53	0.54	0.52	0.53	0.54	0.54	0.53	0.53	0.52	
XSpss	0.36	0.37	0.36	0.37	0.35	0.35	0.35	0.36	0.36	0.37	0.37	0.37	0.39	0.39	0.41	0.41	0.40	0.40	0.42	0.42	0.42	
XPyr	0.02	0.02	0.02	0.02	0.02	0.02	0.01	0.02	0.02	0.02	0.02	0.02	0.02	0.02	0.02	0.02	0.02	0.02	0.02	0.02	0.02	
D	3.08	3.14	3.19	3.26	3.29	3.33	3.36	3.42	3.44	3.47	3.49	3.53	3.55	3.59	3.77	3.77	3.79	3.89	3.92	3.95	4.01	

Table B: continued

Sample	L2t-7	L2t-7	L2t-7	L2t-7	L2t-7	L2t-7	L2t-7	L2t-7	L2t-7	L2t-7	L2t-7	L2t-7	L2t-7	L2t-7	L2t-7	L2t-7	L2t-7	L2t-7	L2t-7	L2t-7	L2t-7	
Mineral	Grt	Grt	Grt	Grt	Grt	Grt	Grt	Grt	Grt	Grt	Grt	Grt	Grt	Grt	Grt	Grt	Grt	Grt	Grt	Grt	Grt	
Generation	core	core	core	core	core	core	core	core	core	core	core	core	core	core	core	core	core	core	core	core	rim	rim
SiO ₂	39.26	39.00	38.89	38.82	38.93	39.09	39.10	39.30	39.21	39.43	39.22	39.32	38.97	38.87	39.44	39.25	38.99	39.37	39.10	39.41	39.78	
Al ₂ O ₃	22.14	22.32	22.15	21.81	22.21	22.39	22.49	22.45	22.15	22.34	22.36	22.16	22.33	22.16	22.09	22.13	22.25	22.48	22.37	22.50	22.35	
Cr ₂ O ₃	0.21	0.17	-	-	0.13	-	-	0.20	-	-	0.19	-	-	0.20	0.18	0.20	0.27	-	0.21	0.20	0.14	
Fe ₂ O ₃			0.06	0.66							0.23		0.53			0.02				0.08		
FeO	24.36	24.03	24.52	23.80	24.41	24.72	24.81	24.58	24.76	24.46	24.68	24.88	24.66	24.99	24.52	24.96	25.15	25.31	24.79	24.62	24.57	
MnO	0.88	0.72	0.73	0.76	0.78	0.79	0.67	0.70	0.83	0.87	0.83	0.76	0.81	0.76	0.71	0.79	0.82	0.74	0.80	0.77	0.81	
MgO	9.61	9.47	9.34	9.61	9.11	9.29	9.21	9.38	9.36	9.62	9.79	9.70	10.11	10.08	10.69	10.77	10.55	10.59	10.91	11.09	11.14	
CaO	3.55	3.50	3.59	3.68	3.61	3.64	3.66	3.42	3.35	3.12	3.06	2.67	2.42	2.11	1.93	1.54	1.39	1.66	1.34	1.20	1.22	
Total	100.01	99.21	99.28	99.14	99.18	100.04	99.94	100.03	99.66	99.84	100.36	99.49	99.83	99.17	99.56	99.66	99.42	100.15	99.60	99.79	100.01	
Number of anions on the basis of 12 oxygen atoms																						
Si ⁴⁺	3.00	3.00	2.99	2.99	3.00	2.99	2.99	3.00	3.01	3.01	2.98	3.02	2.98	2.99	3.01	3.00	2.99	2.99	2.98	3.00	3.02	
Al ³⁺	1.99	2.02	2.01	1.98	2.02	2.02	2.03	2.02	2.00	2.01	2.01	2.00	2.01	2.01	1.99	1.99	2.01	2.01	2.01	2.02	2.00	
Cr ³⁺	0.01	0.01	-	-	0.01	-	-	0.01	-	-	0.01	-	-	0.01	0.01	0.01	0.02	-	0.01	0.01	0.01	
Fe ³⁺	0.00	0.00	0.00	0.04	0.00	0.01	0.00	0.00	0.00	0.00	0.01	0.00	0.03	0.00	0.00	0.00	0.00	0.00	0.00	0.00	0.00	
Fe ²⁺	1.56	1.55	1.58	1.53	1.57	1.58	1.59	1.57	1.59	1.56	1.57	1.60	1.58	1.61	1.57	1.59	1.61	1.61	1.58	1.57	1.56	
Mn ²⁺	0.06	0.05	0.05	0.05	0.05	0.05	0.04	0.05	0.05	0.06	0.05	0.05	0.05	0.05	0.05	0.05	0.05	0.05	0.05	0.05	0.05	
Mg ²⁺	1.09	1.09	1.07	1.10	1.05	1.06	1.05	1.07	1.07	1.10	1.11	1.11	1.15	1.16	1.22	1.23	1.21	1.20	1.24	1.26	1.26	
Ca ²⁺	0.29	0.29	0.30	0.30	0.30	0.30	0.30	0.28	0.28	0.26	0.25	0.22	0.20	0.17	0.16	0.13	0.11	0.13	0.11	0.10	0.10	
Σcat	8.00	8.01	8.00	7.99	8.00	8.01	8.00	8.00	8.00	8.00	7.99	8.00	8.00	8.00	8.01	8.00	8.00	7.99	7.98	8.01	8.00	
Anions	12.00	12.02	12.00	12.00	12.02	12.00	12.00	12.02	12.01	12.02	12.00	12.02	12.00	12.00	12.01	12.00	12.00	12.00	12.00	12.01	12.02	
XAlm	0.10	0.10	0.10	0.10	0.10	0.10	0.10	0.09	0.09	0.09	0.08	0.07	0.07	0.06	0.05	0.04	0.04	0.05	0.04	0.03	0.03	
XGrss	0.52	0.52	0.53	0.51	0.53	0.53	0.53	0.53	0.53	0.53	0.53	0.54	0.53	0.54	0.52	0.53	0.54	0.54	0.53	0.53	0.52	
XSpss	0.36	0.37	0.36	0.37	0.35	0.35	0.35	0.36	0.36	0.37	0.37	0.37	0.39	0.39	0.41	0.41	0.40	0.40	0.42	0.42	0.42	
XPyrr	0.02	0.02	0.02	0.02	0.02	0.02	0.01	0.02	0.02	0.02	0.02	0.02	0.02	0.02	0.02	0.02	0.02	0.02	0.02	0.02	0.02	
D	3.08	3.14	3.19	3.26	3.29	3.33	3.36	3.42	3.44	3.47	3.49	3.53	3.55	3.59	3.77	3.77	3.79	3.89	3.92	3.95	4.01	

Table B: continued

Sample	L2t-7	L2t-7	L2t-7	L2t-7	L2t-7	L2t-7	L2t-7	L2t-7	L2t-7	L2t-7	L2t-7	L2t-7	L2t-7	L2t-7	L2t-7	L2t-7	L2t-7	L2t-7	L2t-7	L2t-7	L2t-7	
Mineral	Grt	Grt	Grt	Grt	Grt	Grt	Grt	Grt	Grt	Grt	Grt	Grt	Grt	Grt	Grt	Grt	Grt	Grt	Grt	Grt	Grt	
Generation	core	core	core	core	core	core	core	core	core	core	core	core	core	core	core	core	core	core	core	core	rim	rim
SiO ₂	39.26	39.00	38.89	38.82	38.93	39.09	39.10	39.30	39.21	39.43	39.22	39.32	38.97	38.87	39.44	39.25	38.99	39.37	39.10	39.41	39.78	
Al ₂ O ₃	22.14	22.32	22.15	21.81	22.21	22.39	22.49	22.45	22.15	22.34	22.36	22.16	22.33	22.16	22.09	22.13	22.25	22.48	22.37	22.50	22.35	
Cr ₂ O ₃	0.21	0.17	-	-	0.13	-	-	0.20	-	-	0.19	-	-	0.20	0.18	0.20	0.27	-	0.21	0.20	0.14	
Fe ₂ O ₃			0.06	0.66							0.23		0.53			0.02				0.08		
FeO	24.36	24.03	24.52	23.80	24.41	24.72	24.81	24.58	24.76	24.46	24.68	24.88	24.66	24.99	24.52	24.96	25.15	25.31	24.79	24.62	24.57	
MnO	0.88	0.72	0.73	0.76	0.78	0.79	0.67	0.70	0.83	0.87	0.83	0.76	0.81	0.76	0.71	0.79	0.82	0.74	0.80	0.77	0.81	
MgO	9.61	9.47	9.34	9.61	9.11	9.29	9.21	9.38	9.36	9.62	9.79	9.70	10.11	10.08	10.69	10.77	10.55	10.59	10.91	11.09	11.14	
CaO	3.55	3.50	3.59	3.68	3.61	3.64	3.66	3.42	3.35	3.12	3.06	2.67	2.42	2.11	1.93	1.54	1.39	1.66	1.34	1.20	1.22	
Total	100.01	99.21	99.28	99.14	99.18	100.04	99.94	100.03	99.66	99.84	100.36	99.49	99.83	99.17	99.56	99.66	99.42	100.15	99.60	99.79	100.01	
Number of anions on the basis of 12 oxygen atoms																						
Si ⁴⁺	3.00	3.00	2.99	2.99	3.00	2.99	2.99	3.00	3.01	3.01	2.98	3.02	2.98	2.99	3.01	3.00	2.99	2.99	2.98	3.00	3.02	
Al ³⁺	1.99	2.02	2.01	1.98	2.02	2.02	2.03	2.02	2.00	2.01	2.01	2.00	2.01	2.01	1.99	1.99	2.01	2.01	2.01	2.02	2.00	
Cr ³⁺	0.01	0.01	-	-	0.01	-	-	0.01	-	-	0.01	-	-	0.01	0.01	0.01	0.02	-	0.01	0.01	0.01	
Fe ³⁺	0.00	0.00	0.00	0.04	0.00	0.01	0.00	0.00	0.00	0.00	0.01	0.00	0.03	0.00	0.00	0.00	0.00	0.00	0.00	0.00	0.00	
Fe ²⁺	1.56	1.55	1.58	1.53	1.57	1.58	1.59	1.57	1.59	1.56	1.57	1.60	1.58	1.61	1.57	1.59	1.61	1.61	1.58	1.57	1.56	
Mn ²⁺	0.06	0.05	0.05	0.05	0.05	0.05	0.04	0.05	0.05	0.06	0.05	0.05	0.05	0.05	0.05	0.05	0.05	0.05	0.05	0.05	0.05	
Mg ²⁺	1.09	1.09	1.07	1.10	1.05	1.06	1.05	1.07	1.07	1.10	1.11	1.11	1.15	1.16	1.22	1.23	1.21	1.20	1.24	1.26	1.26	
Ca ²⁺	0.29	0.29	0.30	0.30	0.30	0.30	0.30	0.28	0.28	0.26	0.25	0.22	0.20	0.17	0.16	0.13	0.11	0.13	0.11	0.10	0.10	
Σcat	8.00	8.01	8.00	7.99	8.00	8.01	8.00	8.00	8.00	8.00	7.99	8.00	8.00	8.00	8.01	8.00	8.00	7.99	7.98	8.01	8.00	
Anions	12.00	12.02	12.00	12.00	12.02	12.00	12.00	12.02	12.01	12.02	12.00	12.02	12.00	12.00	12.01	12.00	12.00	12.00	12.00	12.01	12.02	
XAlm	0.10	0.10	0.10	0.10	0.10	0.10	0.10	0.09	0.09	0.09	0.08	0.07	0.07	0.06	0.05	0.04	0.04	0.05	0.04	0.03	0.03	
XGrss	0.52	0.52	0.53	0.51	0.53	0.53	0.53	0.53	0.53	0.53	0.53	0.54	0.53	0.54	0.52	0.53	0.54	0.54	0.53	0.53	0.52	
XSpss	0.36	0.37	0.36	0.37	0.35	0.35	0.35	0.36	0.36	0.37	0.37	0.37	0.39	0.39	0.41	0.41	0.40	0.40	0.42	0.42	0.42	
XPyrr	0.02	0.02	0.02	0.02	0.02	0.02	0.01	0.02	0.02	0.02	0.02	0.02	0.02	0.02	0.02	0.02	0.02	0.02	0.02	0.02	0.02	
D	3.08	3.14	3.19	3.26	3.29	3.33	3.36	3.42	3.44	3.47	3.49	3.53	3.55	3.59	3.77	3.77	3.79	3.89	3.92	3.95	4.01	

Table B: continued

Sample	L2t-7	L5Gr-3	L5Gr-3	L5Gr-3	L5Gr-3	L5Gr-3	L5Gr-3	L5Gr-3	L5Gr-3	L5Gr-3	L5Gr-3	L5Gr-3	L5Gr-3	L5Gr-3	L5Gr-3	L5Gr-3	L5Gr-3	L5Gr-3
Mineral	Grt	Grt	Grt	Grt	Grt	Grt	Grt	Grt	Grt	Grt	Grt	Grt	Grt	Grt	Grt	Grt	Grt	Grt
Generation	rim	Rim	Rim	Rim	Core	Core	Core	Core	Core	Core	Core	Core	Core	Core	Core	Core	Core	Core
SiO ₂	39.41	39.24	39.23	39.58	39.49	39.76	39.12	39.68	39.40	39.45	39.46	39.83	39.55	39.21	39.51	39.60	39.74	40.18
Al ₂ O ₃	22.44	22.34	22.64	22.57	22.35	22.47	22.50	22.50	22.42	22.04	22.46	22.79	22.34	22.29	22.57	22.81	22.59	22.68
Cr ₂ O ₃	0.14	0.21	0.20	0.00	0.29	0.28	0.00	0.16	0.00	0.16	0.23	0.21	0.21	0.23	0.24	0.22	0.22	0.23
Fe ₂ O ₃	-	1.00	1.00	1.00	1.00	1.00	1.00	1.00	1.00	1.00	1.00	1.00	1.00	1.00	1.00	1.00	1.00	1.00
FeO	24.76	24.10	23.92	23.86	23.67	23.80	23.08	23.63	23.29	22.72	23.31	23.72	23.37	22.93	22.17	21.81	22.20	22.09
MnO	0.62	0.50	0.58	0.54	0.47	0.42	0.58	0.56	0.55	0.51	0.54	0.47	0.58	0.50	0.33	0.35	0.34	0.34
MgO	10.92	11.14	11.31	11.66	11.88	12.06	11.99	11.98	11.98	12.35	11.92	12.01	11.86	11.86	11.87	12.35	11.98	12.19
CaO	1.22	1.54	1.42	1.41	1.48	1.42	1.36	1.48	1.49	1.50	1.62	1.58	1.71	1.80	2.45	2.48	2.56	2.47
Total	99.50	100.07	100.30	100.62	100.63	101.21	99.63	100.99	100.13	99.73	100.54	101.61	100.62	99.82	100.14	100.62	100.63	101.18
Number of anions on the basis of 12 oxygen atoms																		
Si ⁴⁺	3.01	3.00	2.99	3.00	2.99	2.99	2.97	2.99	2.99	2.99	2.98	2.99	3.00	2.98	3.00	2.97	3.00	3.01
Al ³⁺	2.02	2.01	2.03	2.02	2.00	1.99	2.02	2.00	2.00	1.97	2.00	2.01	1.99	2.00	2.02	2.01	2.01	2.01
Cr ³⁺	0.01	0.01	0.01	0.00	0.02	0.02	0.00	0.01	0.00	0.01	0.01	0.01	0.01	0.01	0.01	0.01	0.01	0.01
Fe ³⁺	-	-	-	-	0.01	-	0.04	0.01	0.03	0.04	0.02	-	0.01	0.02	-	0.05	-	-
Fe ²⁺	1.58	1.54	1.53	1.51	1.50	1.50	1.47	1.49	1.48	1.44	1.47	1.49	1.48	1.46	1.41	1.37	1.40	1.39
Mn ²⁺	0.04	0.03	0.04	0.04	0.03	0.03	0.04	0.04	0.04	0.03	0.04	0.03	0.04	0.03	0.02	0.02	0.02	0.02
Mg ²⁺	1.24	1.27	1.29	1.32	1.34	1.35	1.36	1.35	1.35	1.40	1.34	1.34	1.34	1.35	1.34	1.38	1.35	1.36
Ca ²⁺	0.10	0.13	0.12	0.12	0.12	0.12	0.11	0.12	0.12	0.12	0.13	0.13	0.14	0.15	0.20	0.20	0.21	0.20
Σ cat	8.00	8.00	8.00	8.00	8.00	8.00	8.00	8.00	8.00	8.00	8.00	8.00	8.00	8.00	8.00	8.00	8.00	8.00
Anions	12.02	12.02	12.01	12.01	12.00	12.00	12.00	12.00	12.00	12.00	12.00	12.00	12.00	12.00	12.01	12.00	12.01	12.02
XAlm	0.53	0.52	0.51	0.51	0.50	0.50	0.49	0.50	0.49	0.48	0.49	0.50	0.49	0.49	0.47	0.46	0.47	0.47
XGrss	0.42	0.04	0.04	0.04	0.04	0.04	0.04	0.04	0.04	0.04	0.04	0.04	0.05	0.05	0.07	0.07	0.07	0.07
XPyrr	0.01	0.43	0.43	0.44	0.45	0.45	0.46	0.45	0.45	0.47	0.45	0.45	0.45	0.45	0.45	0.46	0.45	0.46
XSpss	4.06	0.01	0.01	0.01	0.01	0.01	0.01	0.01	0.01	0.01	0.01	0.01	0.01	0.01	0.01	0.01	0.01	0.01
D	0.00	0.00	0.06	0.09	0.13	0.18	0.24	0.32	0.41	0.44	0.53	0.59	0.73	0.86	1.80	1.86	1.99	2.09

Sample	L5Gr-3	L5Gr-3	L5Gr-3	L5Gr-3	L5Gr-3	L5Gr-3	L5Gr-3	L5Gr-3	L5Gr-3	L5Gr-3	L5Gr-3	L5Gr-3	L5Gr-3	L5Gr-3	L5Gr-3	
Mineral	Garnet	Garnet	Garnet	Garnet	Garnet	Garnet	Garnet	Garnet	Garnet	Garnet	Garnet	Garnet	Garnet	Garnet	Garnet	
Generation	Core	Core	Core	Core	Core	Core	Core	Core	Core	Core	Core	Core	Core	Rim	Rim	Rim
SiO ₂	39.71	39.99	39.94	39.66	39.89	39.95	40.03	39.9	39.67	39.48	39.5	39.78	39.67	39.85	39.25	
Al ₂ O ₃	22.89	22.58	22.57	22.78	22.83	22.55	22.96	22.8	22.49	22.38	22.66	22.68	22.72	22.67	22.71	
Cr ₂ O ₃	0.3	0	0	0.26	0.23	0.24	0.25	0.22	0	0.28	0.16	0.18	0.17	0.2	0.45	
Fe ₂ O ₃	1	1	1	1	1	1	0.04	0	0	0.1	0.49	0	0.25	0.33	0.28	
FeO	21.88	22.3	22.51	22.61	22.03	22.3	22.67	22.54	22.54	22.51	22.56	22.78	23.38	23.33	23.38	
MnO	0.26	0.45	0.46	0.27	0.41	0.4	0.32	0.48	0.48	0.4	0.4	0.43	0.53	0.41	0.56	
MgO	12.11	12.06	12.43	12.38	12.52	12.14	12.04	11.84	11.76	11.75	11.88	11.79	11.55	12.11	11.76	
CaO	2.93	2.67	1.95	1.93	2.29	2.67	2.67	2.71	2.52	2.61	2.41	2.54	2.28	1.82	1.58	
Total	101.08	101.05	100.86	100.89	101.2	101.25	100.97	100.5	99.47	99.51	100.05	100.18	100.55	100.72	99.98	
Number of anions on the basis of 12 oxygen atoms																
Si ⁴⁺	2.97	3.01	3	2.98	2.98	2.99	2.98	2.99	3	2.99	2.98	2.99	2.98	2.98	2.97	
Al ³⁺	2.02	2	2	2.02	2.01	1.99	2.02	2.01	2.01	2	2.01	2.01	2.01	2	2.02	
Cr ³⁺	0.02	0	0	0.02	0.01	0.01	0.01	0.01	0	0.02	0.01	0.01	0.01	0.01	0.03	
Fe ³⁺	0.02	0	0	0	0.02	0.01	0	0	0	0.01	0.03	0	0.01	0.02	0.02	
Fe ²⁺	1.37	1.4	1.42	1.42	1.38	1.4	1.41	1.41	1.43	1.43	1.42	1.43	1.47	1.46	1.48	
Mn ²⁺	0.02	0.03	0.03	0.02	0.03	0.03	0.02	0.03	0.03	0.03	0.03	0.03	0.03	0.03	0.04	
Mg ²⁺	1.35	1.35	1.39	1.39	1.39	1.36	1.34	1.32	1.33	1.33	1.33	1.32	1.29	1.35	1.33	
Ca ²⁺	0.24	0.22	0.16	0.16	0.18	0.21	0.21	0.22	0.2	0.21	0.19	0.2	0.18	0.15	0.13	
Σ cat	8	8	8	8	8	8	8	8	8	8	8	8	8	8	8	
Anions	12	12.01	12	12	12	12	12	12	12.01	12	12	12	12	12	12	
XAlm	0.46	0.47	0.47	0.48	0.46	0.47	0.47	0.47	0.48	0.48	0.48	0.48	0.49	0.49	0.5	
XGrss	0.08	0.07	0.05	0.05	0.06	0.07	0.07	0.07	0.07	0.07	0.07	0.07	0.06	0.05	0.04	
XPyrr	0.45	0.45	0.47	0.47	0.47	0.45	0.45	0.44	0.44	0.44	0.45	0.44	0.43	0.45	0.45	
XSpss	0.01	0.01	0.01	0.01	0.01	0.01	0.01	0.01	0.01	0.01	0.01	0.01	0.01	0.01	0.01	
D	2.53	2.62	2.7	2.83	2.88	2.96	3.26	3.37	3.43	3.52	3.66	3.92	4.15	4.69	4.84	

Table B: Continued

Sample	L2t-7	L2t-7	L2t-7	L2t-7	L2t-7	L2t-7	L2t-7	L2t-7	L2t-7	L2t-7	L2t-7	L2t-7	L2t-7
Mineral	Grt	Grt	Grt	Grt	Grt	Grt	Grt	Grt	Grt	Grt	Grt	Grt	Grt
Generation	C-2	C-2	C-2	C-2	C-2	C-2	C-2	C-2	C-2	C-2	C-2	C-2	C-2
SiO ₂	39.58	39.57	39.26	39.31	39.39	39.30	39.39	39.53	39.69	39.12	39.39	39.57	39.46
Al ₂ O ₃	22.29	22.44	22.26	22.43	22.60	22.36	22.38	22.64	22.48	22.30	22.34	22.46	22.54
Cr ₂ O ₃	0.13	-	0.17	0.20	-	0.17	-	0.14	-	0.19	0.19	-	0.19
Fe ₂ O ₃	-	-	0.64	-	-	0.26	-	-	-	-	-	-	-
FeO	24.98	25.21	24.77	24.94	25.22	25.13	25.19	25.31	25.61	25.20	25.33	25.25	25.40
MnO	0.79	0.81	0.81	0.78	0.80	0.87	0.84	0.79	0.96	0.83	0.82	0.96	0.79
MgO	10.27	10.23	10.41	9.96	10.23	10.31	10.28	10.05	10.25	10.21	10.37	10.33	10.50
CaO	2.28	2.24	2.17	2.17	2.09	2.04	2.10	2.01	1.97	1.84	1.71	1.77	1.65
Total	100.32	100.50	100.49	99.79	100.33	100.44	100.18	100.47	100.96	99.69	100.15	100.34	100.53
Number of anions on the basis of 12 oxygen atoms													
Si ⁴⁺	3.01	3.00	2.98	3.01	2.99	2.99	3.00	3.00	3.00	2.99	3.00	3.01	2.99
Al ³⁺	2.00	2.01	1.99	2.02	2.02	2.00	2.01	2.03	2.00	2.01	2.00	2.01	2.01
Cr ³⁺	0.01	-	0.01	0.01	-	0.01	-	0.01	-	0.01	0.01	-	0.01
Fe ³⁺	-	-	0.04	-	-	0.01	-	-	-	-	-	-	-
Fe ²⁺	1.59	1.60	1.57	1.60	1.60	1.60	1.60	1.61	1.62	1.61	1.61	1.60	1.61
Mn ²⁺	0.05	0.05	0.05	0.05	0.05	0.06	0.05	0.05	0.06	0.05	0.05	0.06	0.05
Mg ²⁺	1.16	1.16	1.18	1.14	1.16	1.17	1.17	1.14	1.16	1.16	1.18	1.17	1.19
Ca ²⁺	0.19	0.18	0.18	0.18	0.17	0.17	0.17	0.16	0.16	0.15	0.14	0.14	0.13
Σ cat	8.01	8.00	8.00	8.01	7.99	8.01	8.00	8.00	8.00	7.98	7.99	7.99	7.99
Anion	12.01	12.01	12.00	12.02	12.00	12.00	12.00	12.02	12.00	12.01	12.01	12.01	12.01
XGrss	0.06	0.06	0.06	0.06	0.06	0.06	0.06	0.06	0.05	0.05	0.05	0.05	0.04
XAlm	0.53	0.53	0.53	0.54	0.54	0.53	0.54	0.54	0.54	0.54	0.54	0.54	0.54
XPyr	0.39	0.39	0.40	0.38	0.39	0.39	0.39	0.38	0.39	0.39	0.39	0.39	0.40
XSpss	0.02	0.02	0.02	0.02	0.02	0.02	0.02	0.02	0.02	0.02	0.02	0.02	0.02
D	0.14	0.14	0.14	0.14	0.14	0.17	0.17	0.17	0.19	0.19	0.19	0.19	0.21

APPENDIX B-1

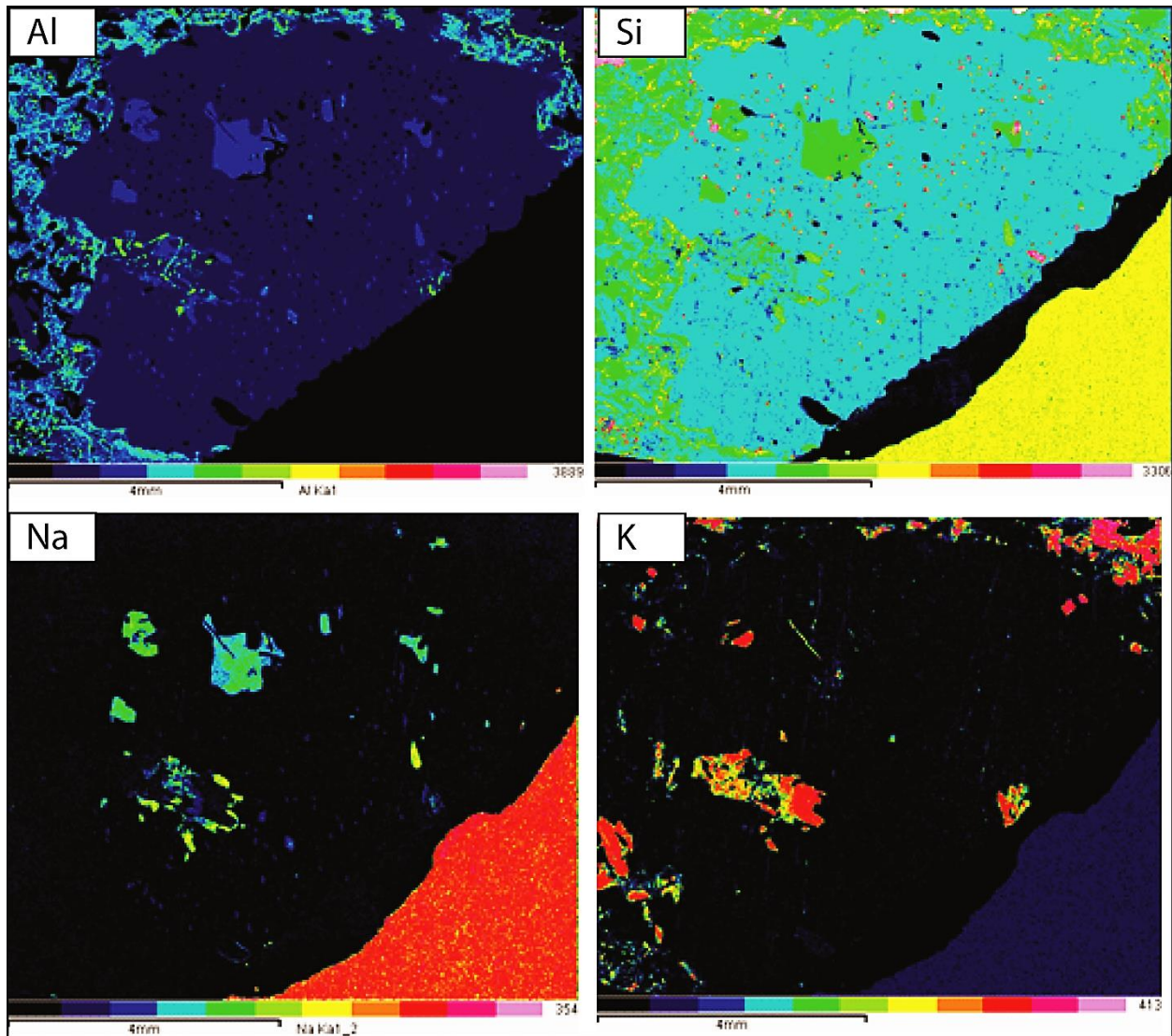


Figure 1: Elemental maps showing qualitative 2D X-ray mapping of a garnet from the stromatolitic leucosomes (L2t-6). The warm colour indicated on the colour bar show the highest concentration of an element

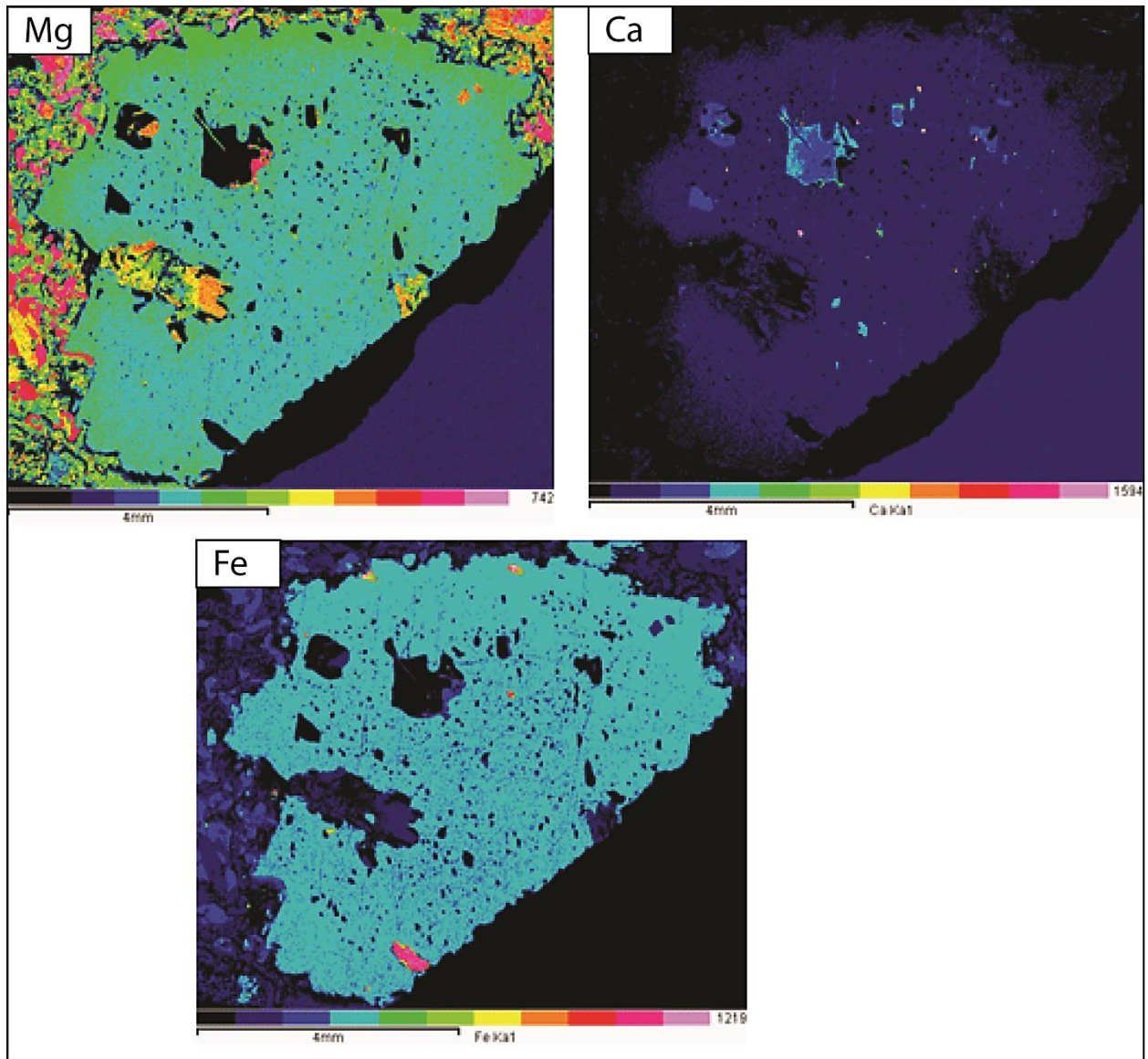


Figure 2: Elemental maps showing qualitative 2D X-ray mapping of a garnet from the stromatolitic leucosomes (L2t-6). The warm colour indicated on the colour bar show the highest concentration of an element

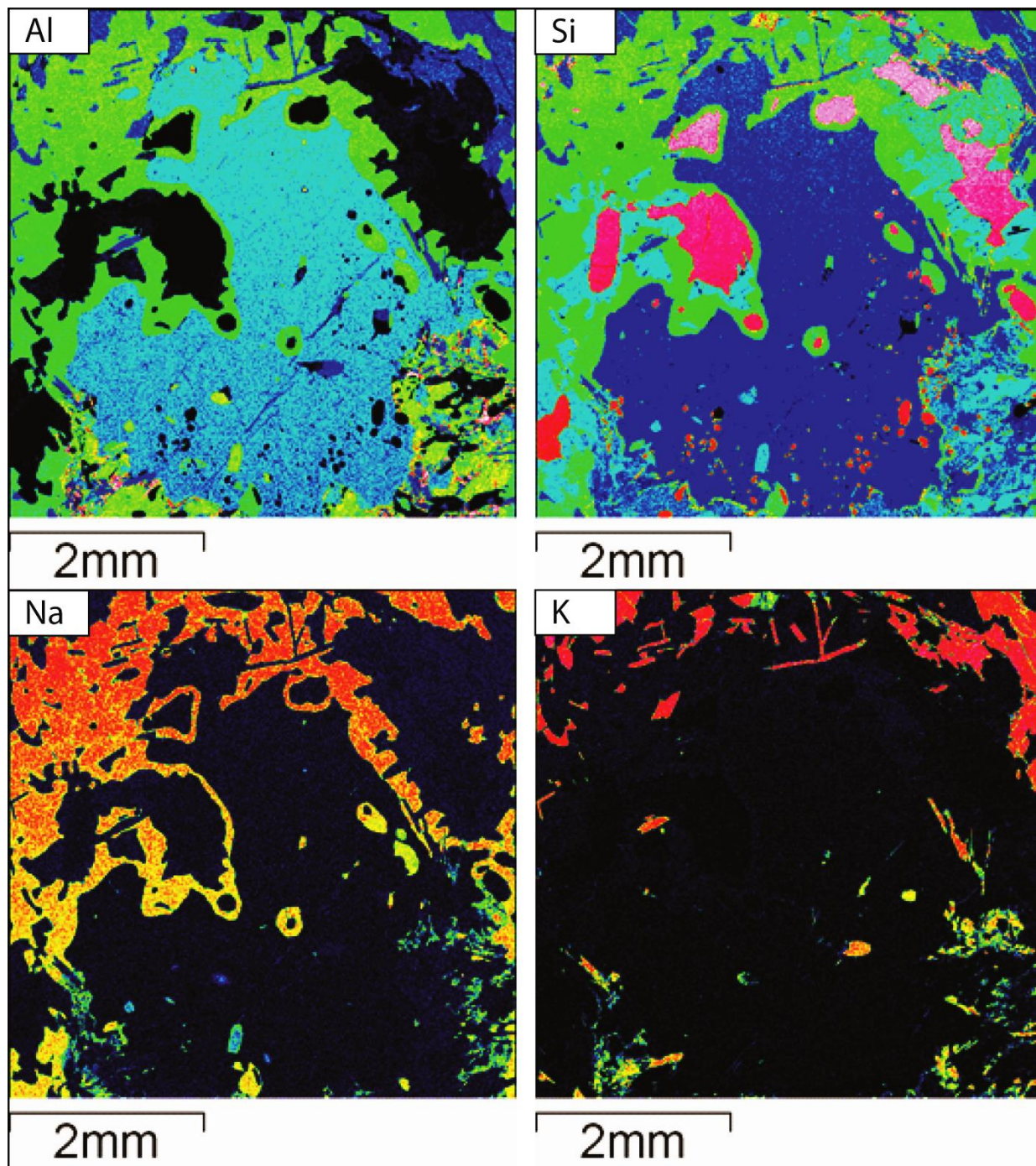


Figure 3: Elemental maps showing qualitative 2D X-ray mapping of a garnet from the stromatolitic leucosomes (L2-7). The warm colour indicated on the colour bar show the highest concentration of an element.

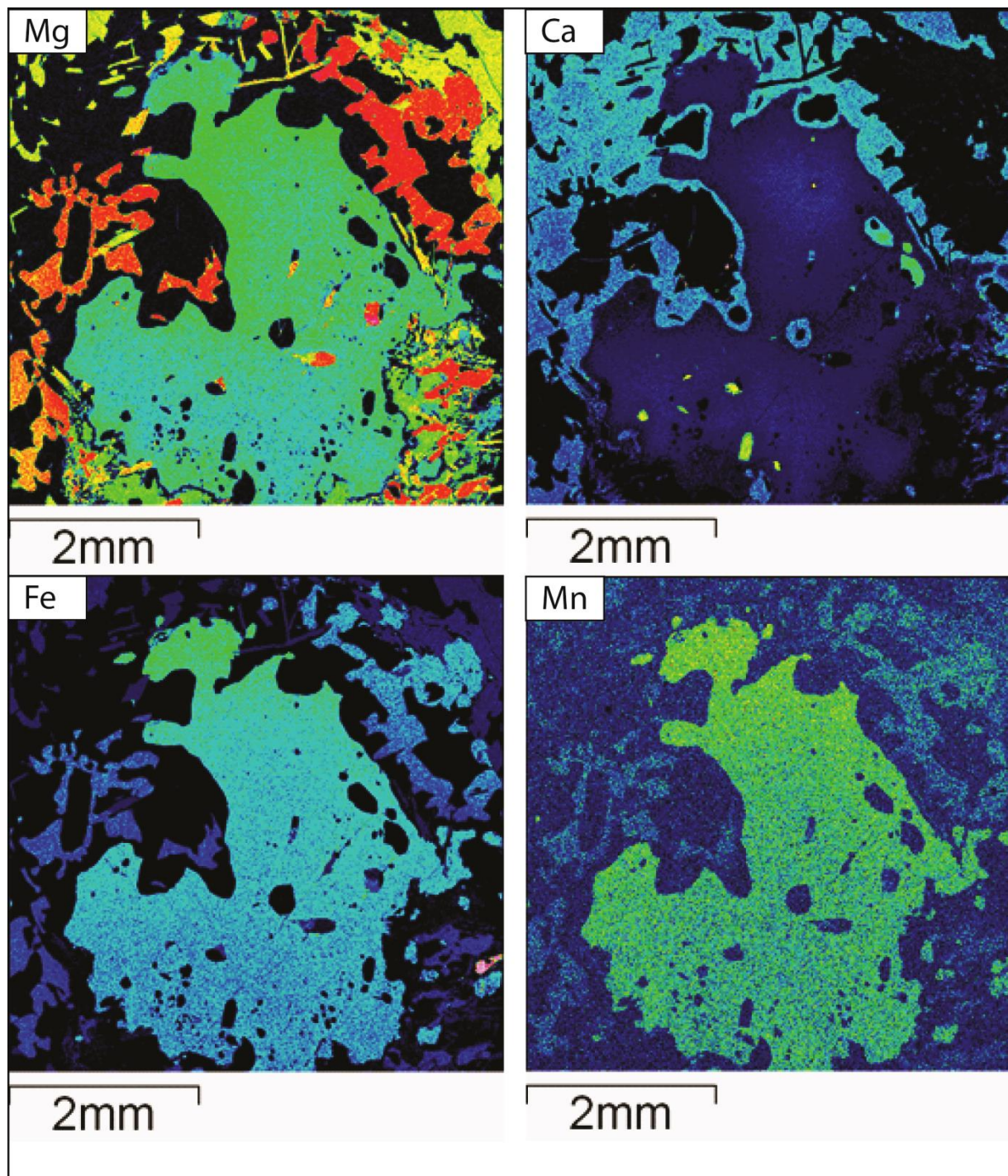


Figure 4: Elemental maps showing qualitative 2D X-ray mapping of a garnet from the stromatolitic leucosomes (L2-7). The warm colour indicated on the colour bar show the highest concentration of an element.

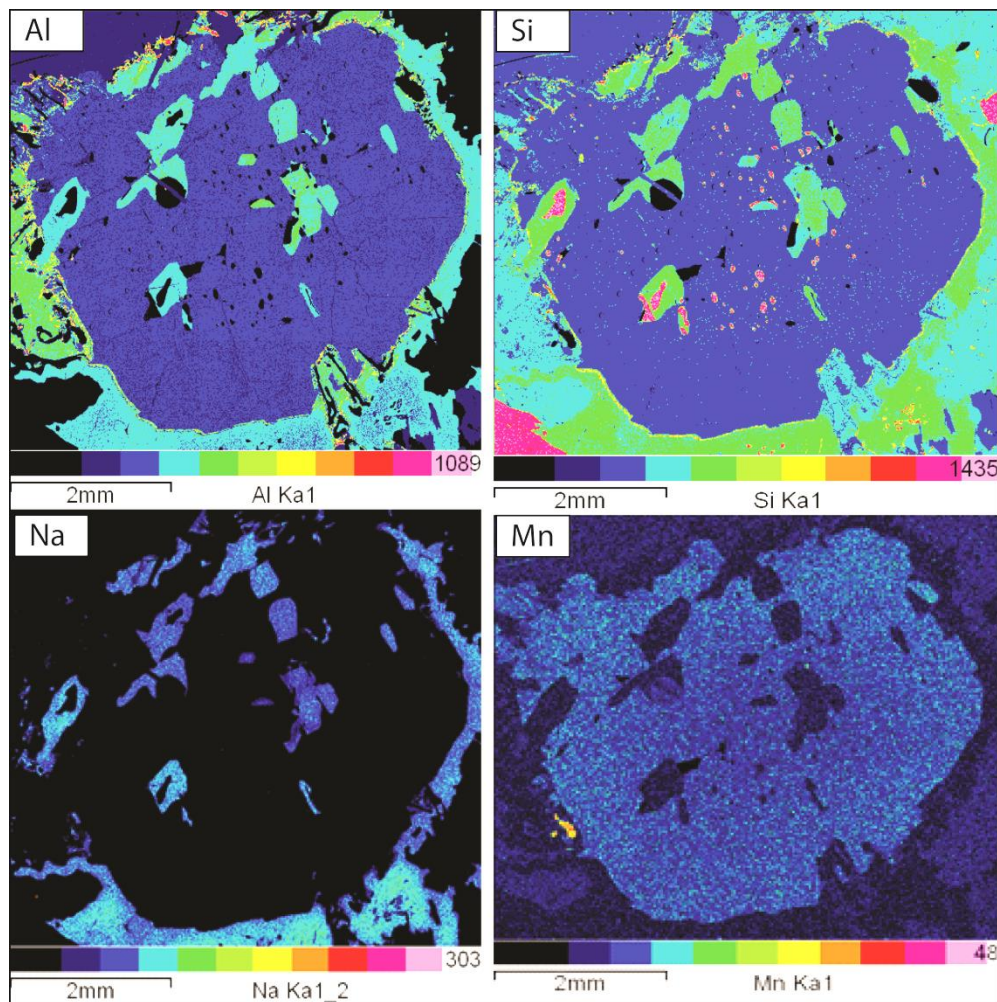


Figure 5: Elemental maps showing qualitative 2D X-ray mapping of a garnet from the stromatitic leucosomes (L5GR-3). The warm colour indicated on the colour bar show the highest concentration of an element.

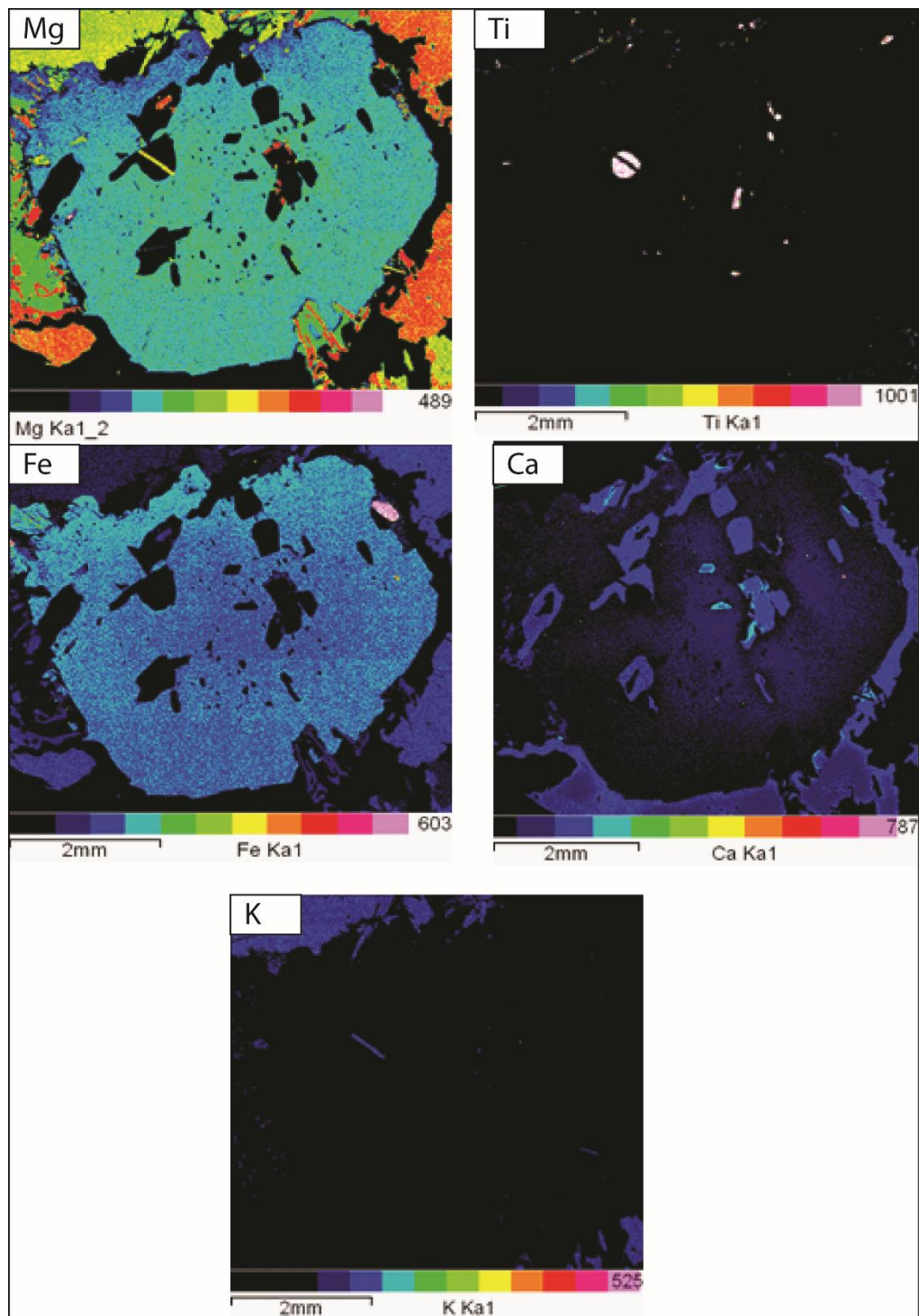


Figure 6: Elemental maps showing qualitative 2D X-ray mapping of a garnet from the stromatitic leucosomes (L5GR-3). The warm colour indicated on the colour bar show the highest concentration of an element.

APPENDIX C

Table C: LA ICP MS trace element compositions for garnet normalized to chondrite. L2t-6, L2t-7, L5R-3 and CRa1 refer to the samples taken from stromatitic leucosomes, nebilitic leucosomes and residue respectively. The dashed lines represent values below the detection limit of the analytical routine.

Sample	L2t-6	L2t-6	L2t-6	L2t-6	L2t-6	L2t-6	L2t-6	L2t-6	L2t-6	L2t-6	L2t-6	L2t-6	L2t-6	L2t-6	L2t-6	L2t-6	L2t-6	L2t-6
Element (ppm)	rim	rim	rim	core	core	core	core	core	core	core	core	core	core	core	core	rim	rim	rim
Li	-	20.55	-	-	14.16	12.45	20.41	-	-	-	-	-	14.19	-	-	14.71	-	-
P	0.098	0.057	0.061	0.047	0.0429	0.044	0.045	0.024	0.03	0.036	0.0184	0.028	0.031	0.033	0.046	0.065	0.11	0.098
Sc	25.33	25.1	23.39	25.61	27.77	25.3	28.66	24.39	24.74	25.19	26.03	27.1	27.36	28.38	31.09	28.74	27.31	27.67
Ti	0.1592	0.1761	0.21	0.249	0.1516	0.184	0.227	0.191	0.225	0.266	0.301	0.272	0.239	0.184	0.161	0.189	0.19	0.122
V	0.765	0.864	0.929	0.951	0.754	0.912	0.9	0.983	0.936	1.082	1.137	1.07	0.95	0.881	0.813	0.895	0.93	0.61
Cr	0.23	0.2092	0.214	0.205	0.2778	0.194	0.218	0.201	0.203	0.2	0.1988	0.196	0.216	0.217	0.219	0.186	0.177	0.223
Sr	0.0132	0.0014	8E-04	7E-04	0.00138	0.002	1.606	-	0.01	-	-	-	-	0.005	6E-04	0.002	-	0.013
Y	39.45	33.4	20.39	29.49	178.63	213	192.2	316.6	177.8	94.1	35.18	31.6	29.07	39.53	48.63	46.43	26.08	15.73
Zr	1.041	1.365	1.549	1.376	1.864	1.296	1.29	1.32	1.072	1.374	1.39	1.544	1.814	1.286	1.211	1.141	1.034	0.868
Nb	0.027	-	0.018	0.008	-	-	-	0.011	0.071	-	-	0.037	-	-	-	0.015	-	-
Cs	0.237	-	-	-	0.028	-	-	-	-	-	0.093	-	-	0.29	-	0.039	-	-
Ba	-	-	-	-	-	-	-	-	-	-	-	0.018	0.221	0.067	-	0.009	-	-
La	0.021	0.008	0.005	0.006	0.002	0.002	0.005	0.003	0.001	0.001	0.007	0.002	0.002	0.002	0.001	0.001	0.001	0.001
Ce	0.062	0.03	0.017	0.04	0.011	0.006	0.033	0.016	0.012	0.017	0.05	0.03	0.028	0.026	0.015	0.014	0.018	0.009
Pr	0.17	0.107	0.094	0.237	0.061	0.033	0.229	0.122	0.283	0.375	0.359	0.482	0.291	0.306	0.189	0.252	0.161	0.081
Nd	0.63	0.62	0.85	1.28	0.35	0.4	1.39	1.2	1.64	1.64	2.55	2.18	2.42	1.07	1.38	1.12	0.39	0.61
Sm	8.75	8.91	11.3	11.69	9.14	8.87	11.77	10.54	10.74	12.3	15.7	16.55	14.33	10.52	11.23	9.02	9.72	8.5
Eu	1.78	3.66	3.3	4.46	1.18	2.78	6.05	5.51	6.24	8.6	8.48	7.53	6.97	5.04	4.03	3.19	1.87	1.51
Gd	36.4	28.23	32.97	34.82	60.28	43.34	45.96	38.63	39.88	46.69	41.28	45.06	42	31.94	30.63	28.48	25.21	28.33
Tb	54.07	45.02	40.21	47.64	119.06	94.38	109.3	100.6	85.44	83	66.55	62.64	61.13	53.74	51.53	44.45	36.77	37.36
Dy	49.21	47.1	34.98	42.12	149.15	155.1	170.5	194.1	125.8	92.1	49.45	50.24	51.3	57.44	59.51	54.1	35.74	26.26
Ho	32.43	37.25	21.88	33.18	138.98	156	134.3	264	121.3	70.43	30.49	30.15	29.39	40.69	53.32	54.92	29.63	12.45
Er	22.27	29.83	15.34	24.34	106.73	121.7	87.23	285.8	100.8	47.21	18.57	17.06	18.19	27.61	45.51	47.42	20.08	5.82
Tm	18.02	27.49	14.87	20.88	99.66	102.4	68.82	288.7	95.72	43.01	14.7	14.28	14.44	23.48	46.64	47.04	15.67	4.37
Yb	16.55	26.47	15.67	22.96	96.74	91.8	57.47	265.4	91.02	35.51	14.35	12.25	13.37	24.2	41.23	45.76	16.79	4.65
Lu	14.08	31.95	16.94	23.5	70.74	62.23	41.05	195.5	57.05	29.3	14.22	14.08	10.32	20.63	45.21	57.38	13.09	4.05
Hf	1.02	1.16	0.59	0.87	0.7	0.99	1.39	1.19	0.66	0.54	1.44	0.81	1	0.91	0.62	0.66	0.45	-
Ta	0.4	-	-	-	0.47	0.8	0.36	-	-	0.69	0.3	-	-	-	0.43	-	-	-
Pb	-	-	-	-	0.0026	-	-	-	-	-	-	-	-	-	-	-	-	0.007
Th	-	0.1	-	0.11	-	0.1	-	-	-	-	-	-	-	-	-	-	-	-
U	1.63	-	-	-	-	-	1.12	-	1.81	-	1.43	1.06	1.61	-	1.65	1.89	-	-
Eu/Eu*	0.0002	0.0005	3E-04	3E-04	3.55E-05	2E-04	2E-04	5E-04	3E-04	3E-04	3.55E-05	2E-04	2E-04	4E-04	4E-04	3E-04	3E-04	2E-04

Table C. continued

Sample	CR1a	CR1a	CR1a	CR1a	CR1a	CR1a	CR1a	CR1a	CR1a	CR1a	CR1a	CR1a	CR1a	CR1a	CR1a
Element (ppm)	rim	rim	core	core	core	core	core	core	core	core	core	core	core	rim	rim
Li	8.58	11.67	-	35.87	25.47	-	-	-	-	49.09	-	-	47	-	6.3
P	0.0958	0.0782	0.0722	0.066	0.0609	-	-	-	0.0183	0.0278	0.028	0.0422	0.0252	0.0722	0.0855
Sc	27.48	21.35	17.51	20.28	17.75	19.74	25.35	23.37	22.45	23.74	23.19	19.97	27.24	26.6	27.28
Ti	0.1218	0.1591	0.1827	0.25	0.242	0.2134	0.364	0.135	0.1892	0.1985	0.731	0.1055	0.28	0.2054	0.191
V	0.599	0.85	0.912	1.166	1.107	1.137	1.492	1.051	1.334	1.898	1.572	1.199	1.261	1.078	0.92
Cr	0.349	0.303	0.2511	0.288	0.261	0.28	0.313	0.327	0.295	0.307	0.291	0.396	0.335	0.2404	0.255
Sr	0.00129	-	0.00065	0.0053	0.0014	0.0041	0.0034	0.0025	0.0022	0.00133	0.0122	-	-	-	-
Y	26.74	24.04	23.18	47.13	46.23	54.51	71.42	72.91	82.64	85.71	64.59	46.17	29.1	21.95	10.82
Zr	1.103	1.054	1.013	1.21	1.122	1.418	1.59	1.683	1.256	1.248	1.881	1.06	1.902	1.218	1.031
Nb	0.0076	0.0073	0.0077	-	-	-	1.08	-	0.131	0.016	0.904	-	-	0.016	-
Cs	-	-	-	0.16	-	-	-	-	-	-	-	-	-	0.041	-
Ba	-	-	-	-	-	-	0.174	0.0081	-	-	-	-	0.026	0.009	0.0079
La	0.002	0.002	0.001	0.007	0.011	0.005	0.002	0.003	0.006	0.003	0.007	0.005	0.003	0.004	0.001
Ce	0.01	0.014	0.007	0.03	0.034	0.022	0.019	0.017	0.022	0.024	0.032	0.02	0.014	0.024	0.006
Pr	0.06	0.135	0.074	0.151	0.135	0.129	0.182	0.12	0.069	0.176	0.173	0.071	0.093	0.145	0.057
Nd	0.52	0.54	0.5	0.7	0.68	0.72	1.24	0.38	0.69	0.97	0.78	0.4	0.51	0.56	0.39
Sm	5.87	8.41	6.95	11.57	7.75	9.6	9.34	10.84	9.68	10.9	11.01	10.76	15.6	12.58	8.76
Eu	2.61	2.25	1.43	2.02	1.74	2.52	3.27	1.43	2.3	1.73	1.96	1	2.9	3.05	1.46
Gd	21.88	27.38	22.74	30.57	20.64	23.47	27.69	30.61	28.45	29.94	36.35	50.04	57.77	24.81	19.02
Tb	25.64	30.36	26.84	53.22	33.91	37.54	53.42	52.02	47.09	53.21	52.97	62.33	70.41	26.66	17.78
Dy	25.44	27.33	27.94	50.76	44.23	51.91	70.64	66.77	71.95	76.86	67.2	56.75	51.31	27.66	14.83
Ho	22.76	21.05	25.12	48.02	49	59.96	76.93	75.97	89.39	91.94	68.33	48.57	25.6	25.17	10.34
Er	20.43	19.59	19.09	46.87	49.51	56.01	80.7	79.1	92.68	85.01	63.54	42.53	17.77	21.99	8.2
Tm	20.72	17.29	17.34	45.95	48.3	58.82	81.31	78.34	94.13	87.97	57.11	45.37	13.32	18.88	7.71
Yb	18.19	14.49	15.52	45.77	49.58	59.96	83.89	81.65	90.28	79.63	56.72	38.31	11.09	18.41	5.6
Lu	14.59	11.77	12.85	31.21	43.98	57.42	70.07	74.44	84.74	68.03	46.22	35.51	8.31	19.24	4.09
Hf	0.48	0.62	0.93	2.4	0.94	0.82	0.96	0.96	0.83	0.61	1.47	0.86	1.42	0.33	0.72
Ta	-	-	0.22	-	0.37	-	1.15	-	-	-	-	-	-	-	-
Pb	-	0.0047	-	0.061	-	-	-	-	-	-	-	-	-	-	-
Th	0.59	-	-	-	-	-	0.34	-	-	-	0.097	-	0.3	0.31	-
U	-	-	0.34	-	-	-	-	-	-	-	-	-	-	0.72	-
Eu/Eu*	0.00093	0.00036	0.0004	0.00019	0.00053	0.00048	0.00046	0.00014	0.00029	0.00018	0.00014	3.71E-05	5.57E-05	0.00039	0.00046

APPENDIX D

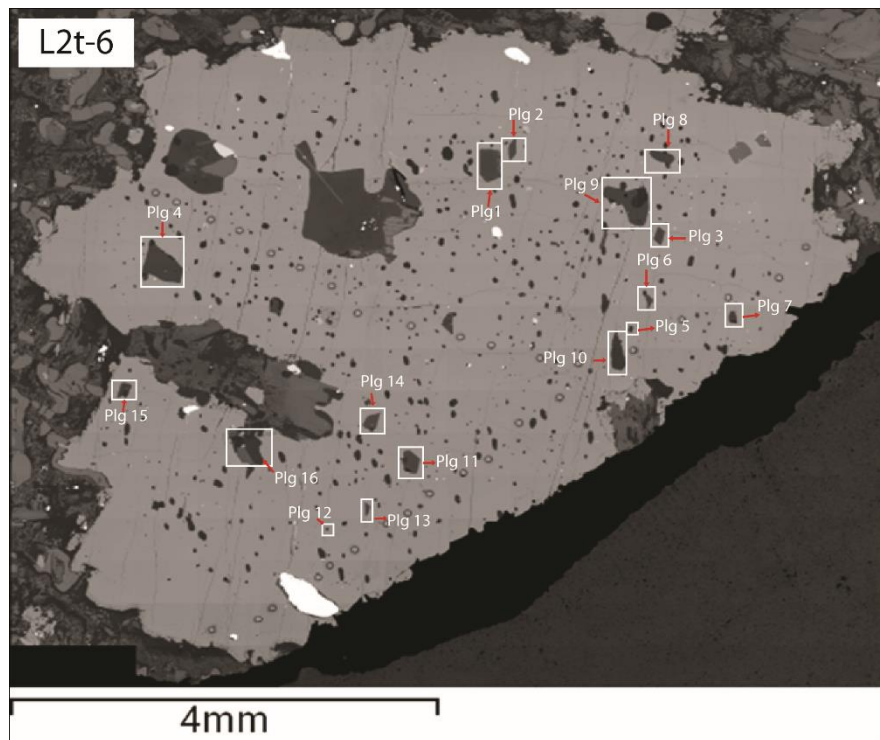


Figure 1: An overall BSE image showing the textural relationships between plagioclase inclusions and the surrounding garnet of sample L2t-6. Also shown is the location of the analyzed inclusions with respect to the garnet host. The full analyses of these plagioclase inclusions are presented in appendix E.

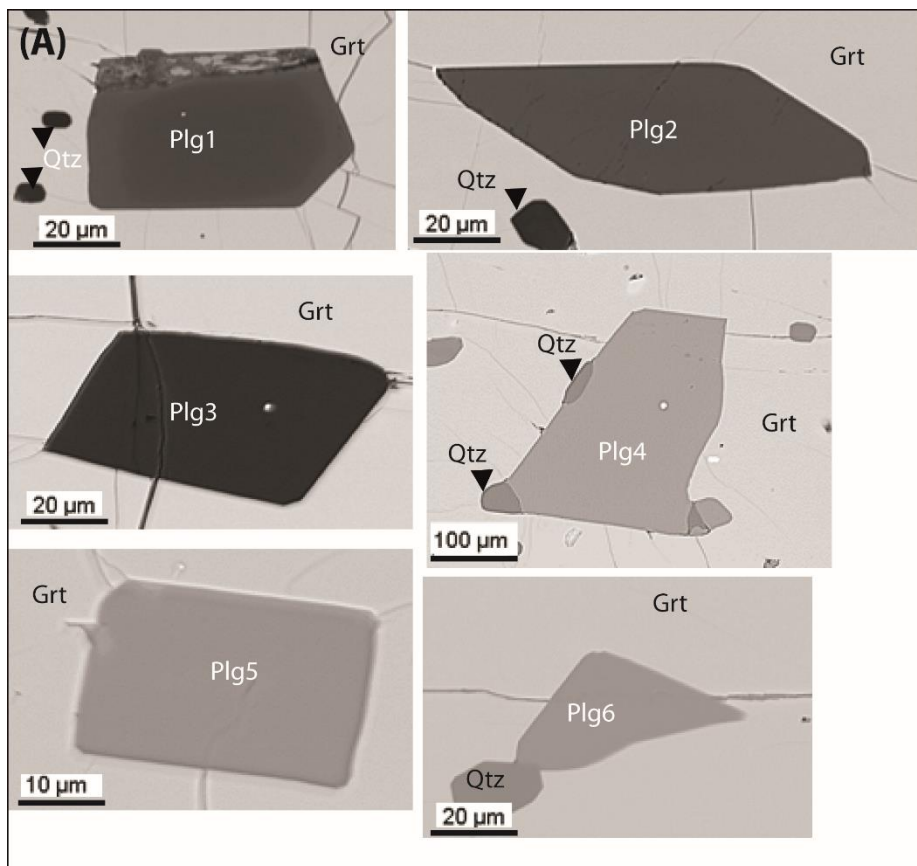


Figure 2: (A) Show magnified BSE images of the inclusions illustrated in Fig. 1.

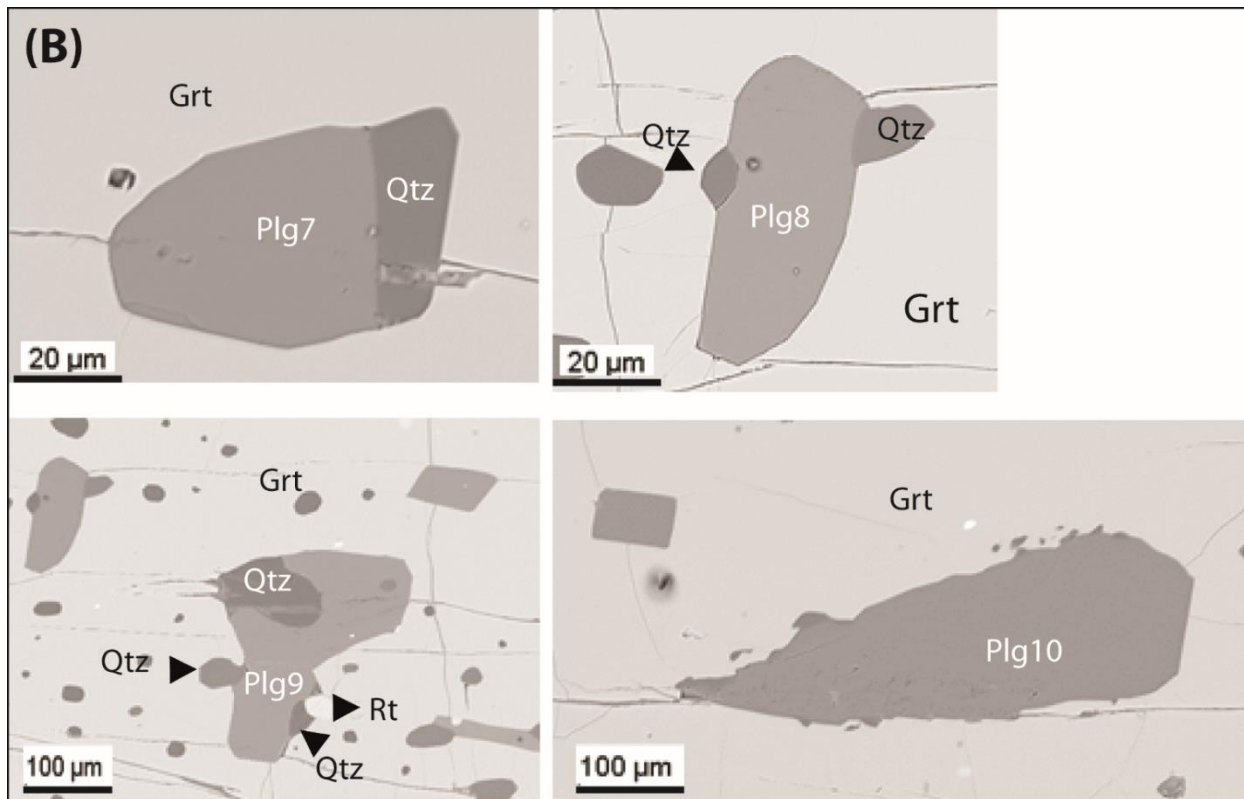
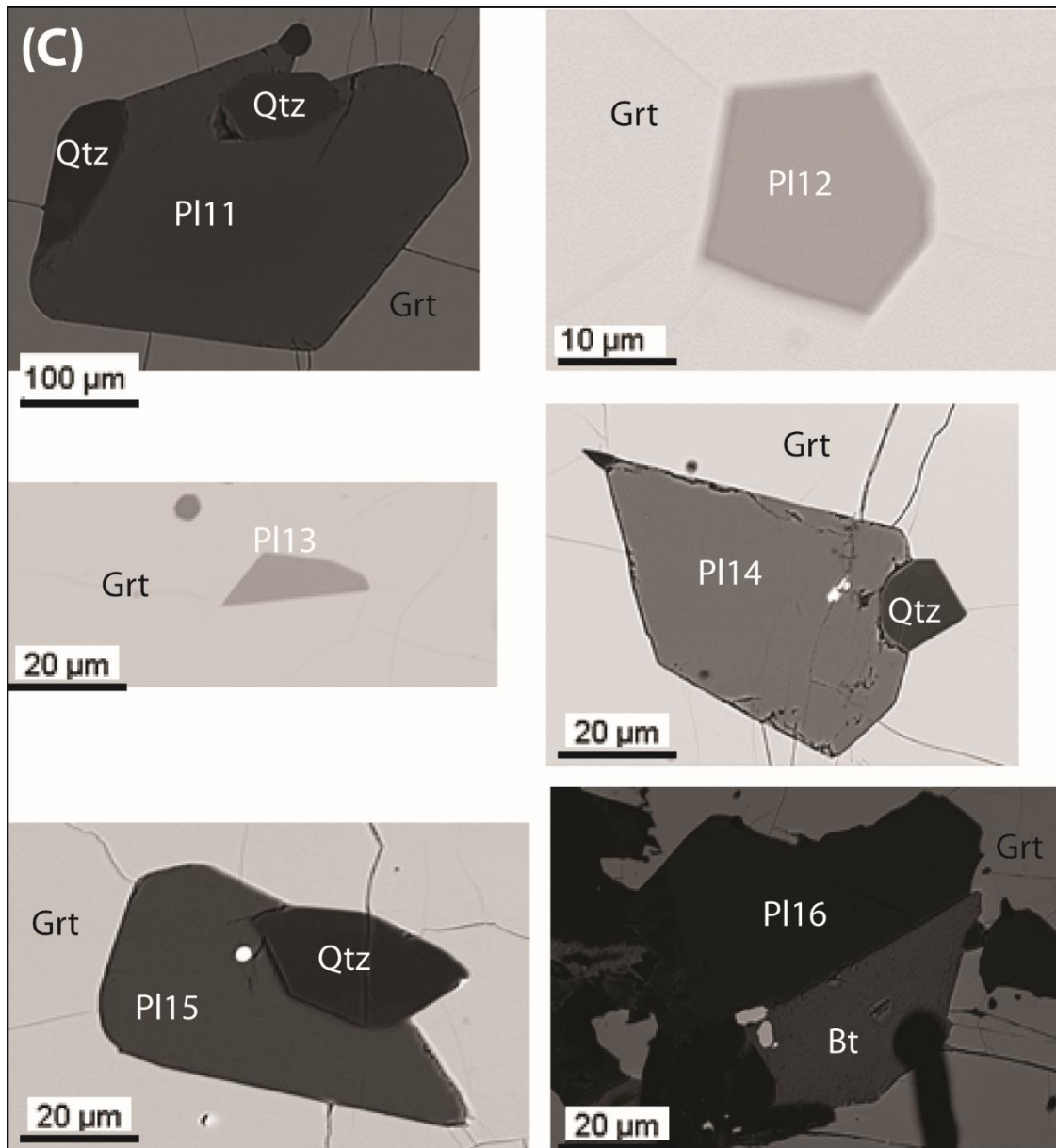


Figure 3: Show magnified BSE images of the inclusions shown in Fig. 1.



Show magnified BSE images of the inclusions illustrated in Fig. 1.

Figure 4:

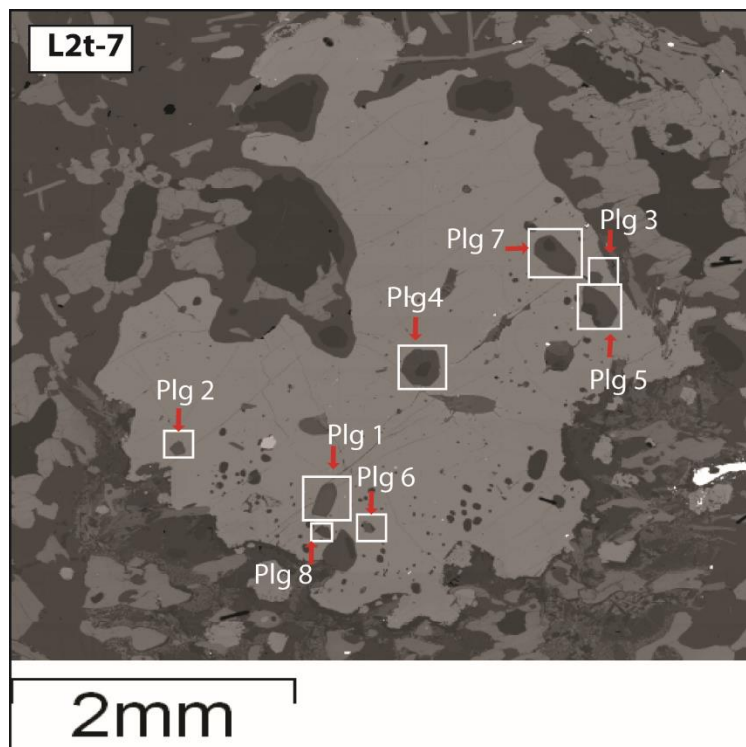


Figure 5: An overall BSE image showing the textural relationships between plagioclase inclusions and the surrounding garnet of sample L2t-6. Also shown is the location of the analyzed inclusions with respect to the garnet host. The full analyses of these plagioclase inclusions are presented in appendix E.

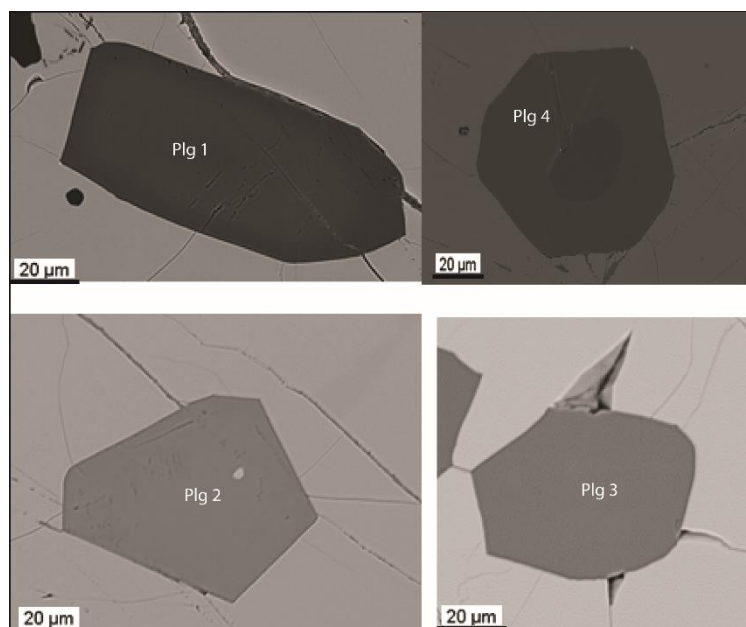


Figure 6: Show magnified BSE images of the inclusions in Fig. 5

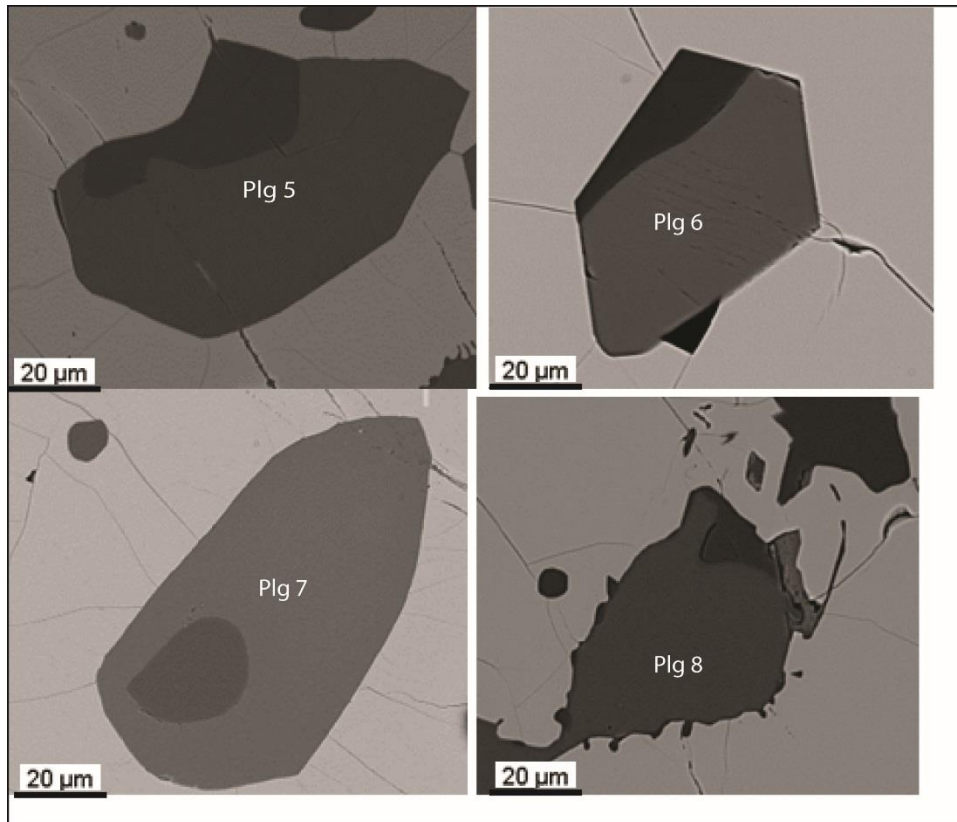


Figure 7: Show magnified BSE images of the inclusions illustrated in Fig 5.

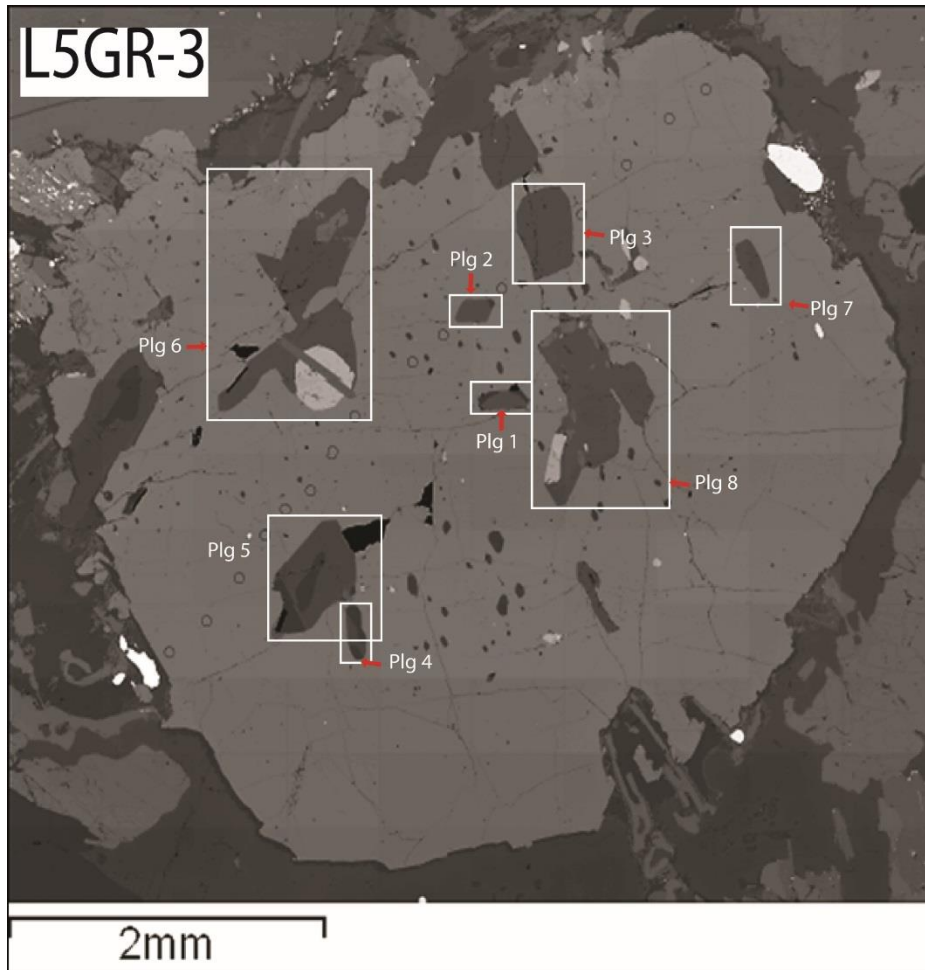


Figure 8: An overall BSE image showing the textural relationships between plagioclase inclusions and the surrounding garnet of sample L2t-6. Also shown is the location of the analyzed inclusions with respect to the garnet host. The full analyses of these plagioclase inclusions are presented in appendix E.

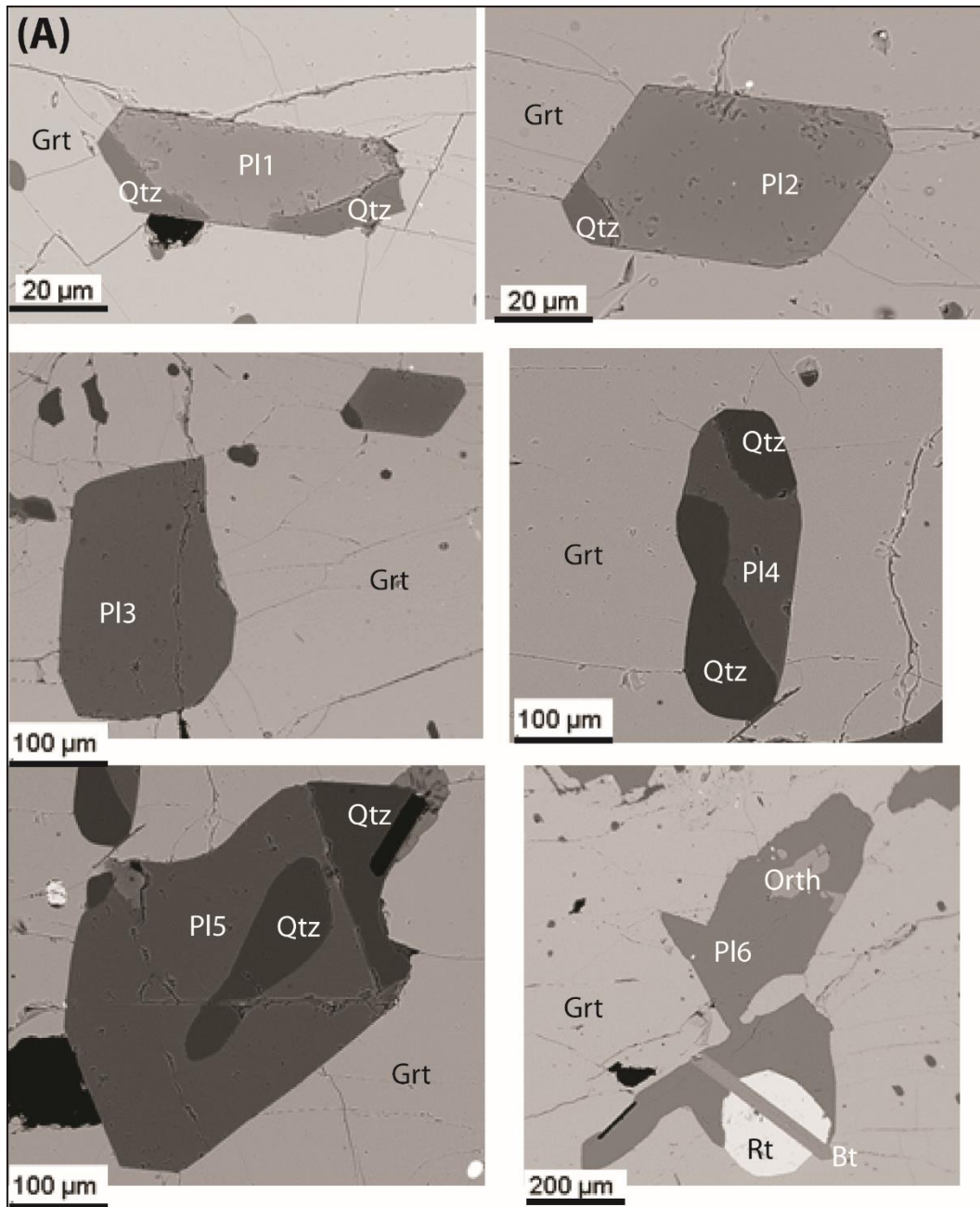


Figure 9: Show magnified BSE images of the inclusions in Fig. 8.

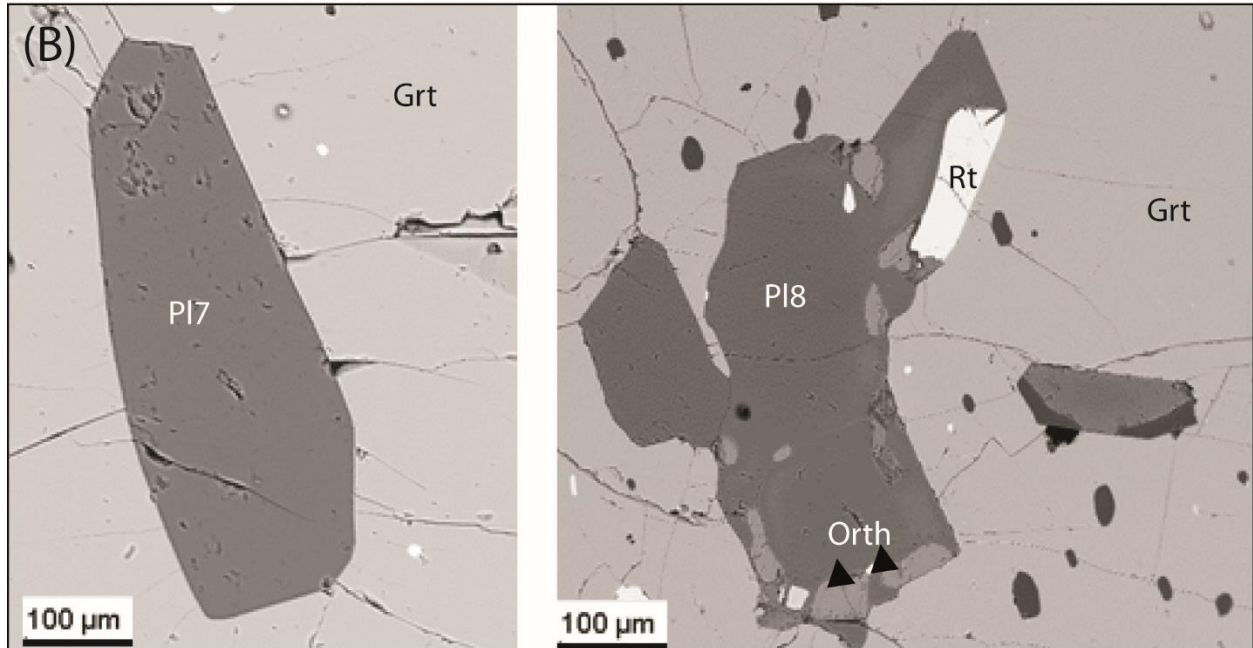


Figure 10: Show magnified BSE images of the inclusions in Fig. 9.

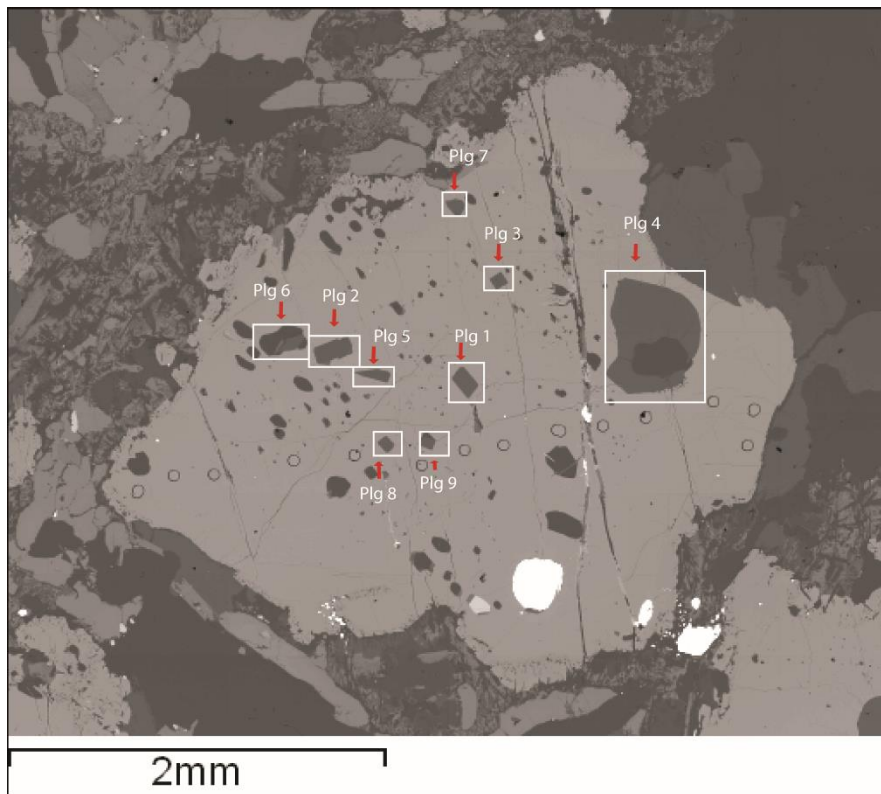


Figure 11: An overall BSE image showing the textural relationships between plagioclase inclusions and the surrounding garnet of sample L2t-6. Also shown is the location of the analyzed inclusions with respect to the garnet host. The full analyses of these plagioclase inclusions are presented in appendix E.

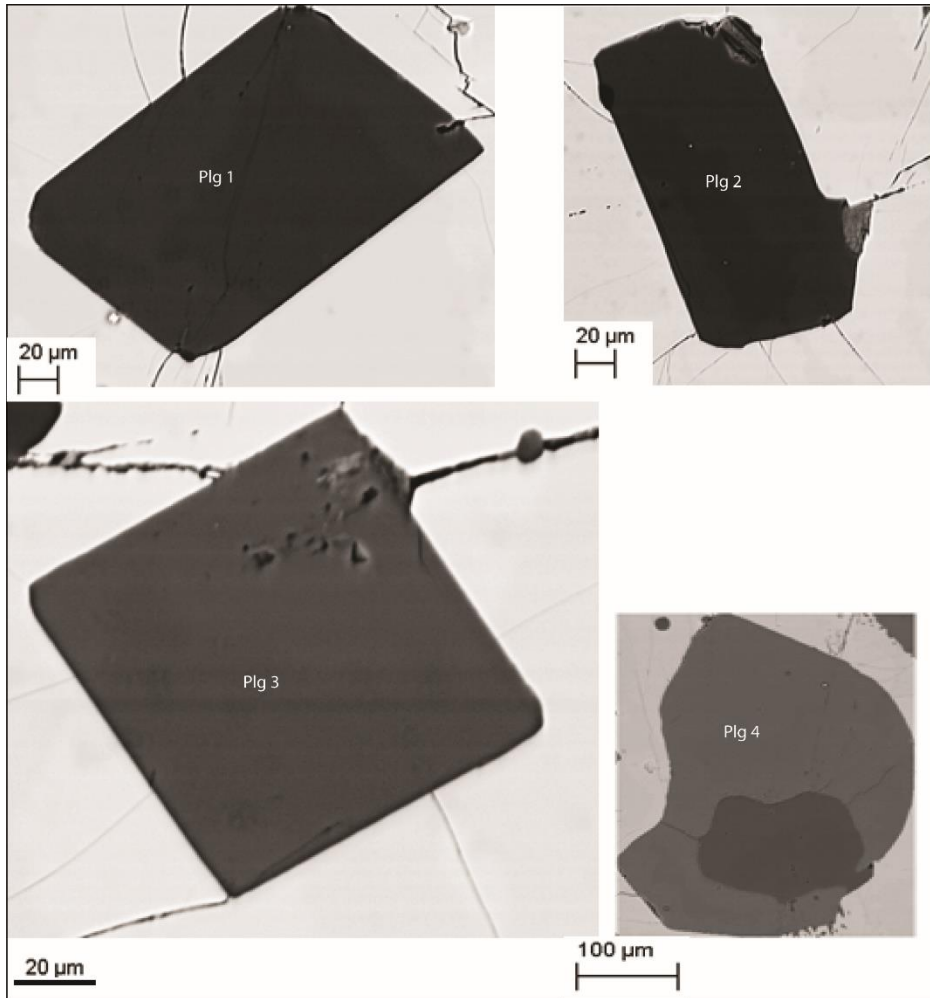


Figure 12: Show magnified BSE images of the inclusions in Fig.11.

APPENDIX E

Table E: Mineral chemistry of the individual plagioclase inclusions within peritectic garnet. Sr data is presented in ppm. L2t-6, L2t-7, L5R-3 and CRa1 refer to the samples taken from stromatitic leucosomes, nebulitic leucosomes and residue respectively. Dashed lines represent values that were below the detection limits of the analytical routine.

Sample	L2t-6	L2t-6	L2t-6	L2t-6	L2t-6	L2t-6	L2t-6	L2t-6	L2t-6	L2t-6	L2t-6	L2t-6	L2t-6	L2t-6	L2t-6	L2t-6	L2t-6	L2t-6	L2t-6	L2t-6	L2t-6
Mineral	Plag1	Plag1	Plag1	Plag1	Plag1	Plag1	Plag1	Plag1	Plag1	Plag1	Plag1	Plag1	Plag1	Plag1	Plag1	Plag1	Plag1	Plag1	Plag1	Plag1	Plag1
Generation	Rim	Rim	Rim	Rim	Rim	Core	Core	Core	Core	Core	Core	Core	Core	Core	Core	Core	Core	Core	Core	Core	Core
SiO ₂	49.43	49.58	49.90	50.16	49.80	49.45	49.91	49.99	49.80	50.02	50.11	50.25	50.39	49.70	50.44	50.56	50.88	50.78	51.32	53.25	53.13
Al ₂ O ₃	31.99	32.39	32.42	32.22	32.27	31.92	32.20	31.86	31.92	31.99	31.80	32.18	31.63	31.83	32.02	31.47	31.45	31.74	31.22	30.14	29.53
FeO	0.38	0.32	0.32	0.27	0.38	0.31	0.21	0.24	0.24	-	-	-	0.24	-	-	-	-	0.20	-	-	0.23
CaO	15.26	15.30	15.40	15.43	15.20	14.97	15.08	15.00	14.86	14.97	14.87	15.08	14.69	14.88	14.63	14.54	14.54	14.65	14.29	13.01	12.51
Na ₂ O	2.89	2.93	2.86	2.86	2.84	2.89	3.08	2.97	3.05	3.11	2.97	3.19	3.15	3.08	3.18	3.23	3.17	3.30	3.51	4.25	4.65
K ₂ O	-	-	-	-	-	-	-	0.12	0.11	-	-	-	-	0.10	0.13	-	-	0.12	0.13	0.13	0.16
Total	99.96	100.51	100.91	100.95	100.50	99.54	100.47	100.19	99.97	100.09	99.76	100.70	100.09	99.59	100.39	99.79	100.05	100.78	100.47	100.78	100.20
Number of anions on the basis of 8 oxygen atoms																					
Si ⁴⁺	2.26	2.25	2.26	2.27	2.26	2.27	2.27	2.28	2.27	2.28	2.29	2.27	2.30	2.27	2.29	2.31	2.32	2.30	2.32	2.40	2.40
Al ³⁺	1.72	1.73	1.73	1.72	1.73	1.73	1.72	1.71	1.72	1.72	1.71	1.72	1.70	1.72	1.71	1.69	1.69	1.69	1.67	1.60	1.57
Fe ²⁺	0.01	0.01	0.01	0.01	0.01	0.01	0.01	0.01	0.01	-	-	-	0.01	-	-	-	-	0.01	-	-	0.01
Ca ²⁺	0.75	0.74	0.75	0.75	0.74	0.74	0.73	0.73	0.73	0.73	0.73	0.73	0.72	0.73	0.71	0.71	0.71	0.71	0.69	0.63	0.61
Na ⁺	0.26	0.26	0.25	0.25	0.25	0.26	0.27	0.26	0.27	0.27	0.26	0.28	0.28	0.27	0.28	0.29	0.28	0.29	0.31	0.37	0.41
K ⁺	-	-	-	-	-	-	-	0.01	0.01	-	-	-	-	0.01	0.01	-	-	0.01	0.01	0.01	0.01
Σ cat.	5.00	5.00	5.00	5.00	5.00	5.00	5.00	5.00	5.00	5.00	5.00	5.00	5.00	5.00	5.00	5.00	5.00	5.00	5.00	5.00	5.00
Anions	7.99	7.99	8.00	8.00	8.00	8.00	7.99	8.00	7.99	8.00	8.02	7.99	8.01	7.99	8.00	8.01	8.02	7.99	8.00	8.01	7.98
XAn	0.74	0.74	0.75	0.75	0.75	0.74	0.73	0.73	0.72	0.73	0.73	0.72	0.72	0.72	0.71	0.71	0.72	0.71	0.69	0.62	0.59
XAb	0.26	0.26	0.25	0.25	0.25	0.26	0.27	0.26	0.27	0.27	0.27	0.28	0.28	0.27	0.28	0.29	0.28	0.29	0.31	0.37	0.40
SrO	-	209.04	-	-	152.29	-	-	204.08	-	130.36	230.01	-	186.59	143.38	160.70	117.04	-	-	-	-	143.07

Table E: continued

Sample	L2t-6	L2t-6	L2t-6	L2t-6	L2t-6	L2t-6	L2t-6	L2t-6	L2t-6	L2t-6	L2t-6	L2t-6	L2t-6	L2t-6	L2t-6	L2t-6	L2t-6	L2t-6	L2t-6	L2t-6	L2t-6
Mineral	Plag1	Plag1	Plag1	Plag1	Plag1	Plag1	Plag1	Plag1	Plag1	Plag1	Plag1	Plag1	Plag1	Plag1	Plag1	Plag1	Plag1	Plag1	Plag1	Plag1	Plag1
Generation	Core	Core	Core	Core	Core	Core	Core	Core	Core	Core	Core	Core	Core	Core	Core	Core	Core	Core	Core	Core	Core
SiO ₂	52.75	53.38	53.95	53.91	53.87	54.88	54.72	54.70	54.76	55.12	54.96	54.75	54.85	55.03	55.01	54.70	54.97	54.99	54.98	54.88	54.00
Al ₂ O ₃	29.93	29.32	29.38	29.30	28.78	29.00	28.91	28.83	29.10	29.07	28.84	28.72	28.40	28.26	28.51	28.44	28.37	28.79	28.94	29.09	29.34
FeO	-	-	-	-	-	-	0.25	-	-	-	-	-	-	-	0.24	-	-	0.21	-	-	0.22
CaO	12.44	12.03	11.96	11.89	11.57	11.47	11.25	11.38	11.45	11.35	11.30	11.28	11.02	11.00	10.87	10.96	11.16	11.13	11.27	11.54	11.82
Na ₂ O	4.46	4.82	4.73	4.84	4.84	5.23	5.13	5.09	5.13	5.12	5.20	5.35	5.23	5.47	5.20	5.15	5.33	5.02	5.28	5.08	4.90
K ₂ O	0.15	0.18	0.19	0.12	0.17	0.15	0.16	0.18	0.20	0.16	0.23	0.23	0.18	0.23	0.20	0.25	0.22	0.24	0.16	0.22	0.17
Total	99.73	99.73	100.21	100.07	99.22	100.74	100.41	100.18	100.63	100.83	100.53	100.33	99.67	99.99	100.03	99.50	100.06	100.38	100.62	100.81	100.45
Number of anions on the basis of 8 oxygen atoms																					
Si ⁴⁺	2.39	2.42	2.43	2.43	2.45	2.46	2.46	2.46	2.46	2.47	2.47	2.46	2.48	2.48	2.48	2.48	2.48	2.48	2.46	2.46	2.43
Al ³⁺	1.60	1.56	1.56	1.56	1.54	1.53	1.53	1.53	1.54	1.53	1.53	1.52	1.51	1.50	1.52	1.52	1.51	1.53	1.53	1.54	1.56
Fe ²⁺	-	-	-	-	-	-	0.01	-	-	-	-	-	-	-	0.01	-	-	0.01	-	-	0.01
Ca ²⁺	0.60	0.58	0.58	0.58	0.56	0.55	0.54	0.55	0.55	0.54	0.54	0.54	0.53	0.53	0.53	0.53	0.54	0.54	0.54	0.55	0.57
Na ⁺	0.39	0.42	0.41	0.42	0.43	0.45	0.45	0.44	0.45	0.44	0.45	0.47	0.46	0.48	0.45	0.45	0.47	0.44	0.46	0.44	0.43
K ⁺	0.01	0.01	0.01	0.01	0.01	0.01	0.01	0.01	0.01	0.01	0.01	0.01	0.01	0.01	0.01	0.01	0.01	0.01	0.01	0.01	0.01
Σ cat.	5.00	5.00	5.00	5.00	5.00	5.00	5.00	5.00	5.00	5.00	5.00	5.00	5.00	5.00	5.00	5.00	5.00	5.00	5.00	5.00	5.00
Anions	7.99	7.98	8.00	8.00	8.01	7.99	8.00	8.00	8.00	8.01	8.00	7.98	8.00	7.98	8.01	8.01	7.99	8.01	7.99	8.00	7.99
XAn	0.60	0.57	0.58	0.57	0.56	0.54	0.54	0.55	0.55	0.55	0.54	0.53	0.53	0.52	0.53	0.53	0.53	0.54	0.54	0.55	0.57
XAb	0.39	0.42	0.41	0.42	0.43	0.45	0.45	0.44	0.44	0.45	0.45	0.46	0.46	0.47	0.46	0.45	0.46	0.44	0.45	0.44	0.42
SrO	168.67	-	168.63	155.47	-	-	-	232.69	146.66	193.97	176.65	215.51	-	-	-	-	206.51	142.16	120.73	193.99	-

Table E: continued

Sample	L2t-6	L2t-6	L2t-6	L2t-6	L2t-6	L2t-6	L2t-6	L2t-6	L2t-6	L2t-6	L2t-6	L2t-6	L2t-6	L2t-6	L2t-6	L2t-6	L2t-6	L2t-6	L2t-6	L2t-6	L2t-6
Mineral	Plag1	Plag1	Plag1	Plag1	Plag1	Plag2	Plag2	Plag2	Plag2	Plag2	Plag2	Plag2	Plag2	Plag2	Plag2	Plag2	Plag2	Plag2	Plag2	Plag2	Plag2
Generation	Rim	Rim	Rim	Rim	Rim	Rim	Rim	Rim	Rim	Core	Core	Core	Core	Core	Core	Core	Core	Core	Core	Core	Core
SiO ₂	53.06	51.68	51.06	50.17	50.25	50.06	50.17	50.58	50.05	50.19	50.39	50.42	50.61	50.10	50.52	50.57	50.60	50.77	50.63	50.87	50.72
Al ₂ O ₃	30.02	31.05	31.62	31.93	32.46	31.98	32.10	31.65	31.36	31.88	31.65	31.34	31.92	31.65	31.53	31.40	31.39	31.18	30.82	31.17	31.21
FeO	-	0.24	0.20	0.34	0.18	-	0.37	0.40	0.27	0.19	0.18	-	0.30	0.28	0.30	-	0.30	-	-	0.22	0.32
CaO	12.59	13.72	14.53	14.66	14.96	14.80	15.02	14.71	14.30	14.74	14.48	14.67	14.71	14.55	14.61	14.29	14.19	14.04	14.07	13.87	13.82
Na ₂ O	4.33	3.77	3.53	3.18	3.01	2.92	3.10	3.21	3.15	3.16	3.17	3.09	3.24	3.25	3.31	3.32	3.38	3.47	3.39	3.56	3.54
K ₂ O	0.21	-	-	0.12	-	-	0.13	0.10	0.10	0.15	-	-	-	0.10	0.10	0.11	0.10	0.11	0.14	-	0.11
Total	100.21	100.46	100.94	100.39	100.86	99.75	100.88	100.64	99.22	100.31	99.87	99.51	100.77	99.94	100.37	99.68	99.96	99.57	99.04	99.69	99.72
Number of anions on the basis of 8 oxygen atoms																					
Si ⁴⁺	2.40	2.34	2.30	2.28	2.27	2.29	2.27	2.29	2.30	2.28	2.30	2.31	2.29	2.28	2.29	2.31	2.31	2.32	2.33	2.32	2.31
Al ³⁺	1.60	1.66	1.68	1.71	1.73	1.72	1.71	1.69	1.70	1.71	1.70	1.69	1.70	1.70	1.69	1.69	1.69	1.68	1.67	1.68	1.68
Fe ²⁺	-	0.01	0.01	0.01	0.01	-	0.01	0.02	0.01	0.01	0.01	-	0.01	0.01	0.01	-	0.01	-	-	0.01	0.01
Ca ²⁺	0.61	0.67	0.7	0.71	0.73	0.73	0.73	0.71	0.70	0.72	0.71	0.72	0.71	0.71	0.71	0.70	0.69	0.69	0.69	0.68	0.68
Na ⁺	0.38	0.33	0.31	0.28	0.26	0.26	0.27	0.28	0.28	0.28	0.28	0.27	0.28	0.29	0.29	0.29	0.30	0.31	0.30	0.32	0.31
K ⁺	0.01	-	-	0.01	-	-	0.01	0.01	0.01	0.01	-	-	-	0.01	0.01	0.01	0.01	0.01	0.01	-	0.01
Σ cat.	5.00	5.00	5.00	5.00	5.00	5.00	5.00	5.00	5.00	5.00	5.00	5.00	5.00	5.00	5.00	5.00	5.00	5.00	5.00	5.00	5.00
Anions	8.00	8.00	7.99	7.99	8.01	8.02	7.98	7.99	8.01	7.99	8.01	8.02	8.00	7.99	7.99	8.01	8.00	8.00	8.01	8.00	7.99
XAn	0.61	0.67	0.69	0.71	0.73	0.74	0.72	0.71	0.71	0.71	0.72	0.72	0.72	0.71	0.70	0.70	0.69	0.69	0.69	0.68	0.68
XAb	0.38	0.33	0.31	0.28	0.27	0.26	0.27	0.28	0.28	0.28	0.28	0.28	0.28	0.29	0.29	0.29	0.30	0.31	0.30	0.32	0.31
SrO	-	-	-	-	-	-	113.62	-	190.00	-	181.37	168.04	146.92	133.97	138.11	-	-	249.32	-	163.51	133.45

Table E: continued

Sample	L2t-6	L2t-6	L2t-6	L2t-6	L2t-6	L2t-6	L2t-6	L2t-6	L2t-6	L2t-6	L2t-6	L2t-6	L2t-6	L2t-6	L2t-6	L2t-6	L2t-6	L2t-6	L2t-6	L2t-6	L2t-6	L2t-6
Mineral	Plag2	Plag2	Plag2	Plag2	Plag2	Plag2	Plag2	Plag3	Plag3	Plag3	Plag3	Plag3	Plag3	Plag3	Plag3	Plag3	Plag3	Plag3	Plag4	Plag4	Plag4	Plag4
Generation	Core	Core	Core	Rim	Rim	Rim	Rim	Rim	Rim	Core	Core	Core	Core	Core	Core	Core	Rim	Rim	Rim	Rim	Rim	Core
SiO ₂	50.49	50.62	50.39	50.12	49.85	49.96	50.24	54.03	54.21	54.44	54.30	54.72	54.30	54.71	54.23	54.15	54.15	54.70	54.95	54.39	54.60	54.20
Al ₂ O ₃	31.01	31.49	31.63	31.63	31.60	31.90	31.69	28.91	28.79	28.67	28.81	28.75	28.44	28.57	29.00	28.91	29.44	28.29	29.12	28.75	28.48	28.43
FeO	0.24	0.31	0.33	0.42	0.32	0.51	0.74	0.26	0.19	0.19	-	0.19	0.30	-	-	0.22	0.41	-	-	-	-	-
CaO	14.10	14.42	14.62	14.43	14.71	15.11	14.88	11.56	11.36	11.02	11.28	11.24	10.95	11.09	11.45	11.36	11.46	10.74	11.62	11.14	11.16	11.12
Na ₂ O	3.47	3.29	3.14	3.30	3.24	3.09	3.08	4.98	5.15	5.08	5.23	5.24	5.16	5.29	5.08	5.09	5.02	5.49	5.19	5.18	5.28	5.19
K ₂ O	-	-	-	0.15	0.12	-	-	0.10	0.21	0.24	0.25	0.22	0.19	0.23	0.11	0.14	-	0.30	-	0.22	0.20	0.25
Total	99.32	100.13	100.11	100.05	99.84	100.57	100.63	99.84	99.92	99.63	99.87	100.37	99.34	99.88	99.87	99.86	100.47	99.51	100.89	99.67	99.73	99.19
Number of anions on the basis of 8 oxygen atoms																						
Si ⁴⁺	2.31	2.30	2.30	2.28	2.28	2.27	2.28	2.44	2.45	2.47	2.45	2.46	2.47	2.47	2.45	2.45	2.44	2.47	2.46	2.46	2.47	2.46
Al ³⁺	1.68	1.69	1.70	1.70	1.70	1.71	1.70	1.54	1.53	1.53	1.53	1.52	1.52	1.52	1.54	1.54	1.56	1.51	1.54	1.53	1.52	1.52
Fe ²⁺	0.01	0.01	0.01	0.02	0.01	0.02	0.03	0.01	0.01	0.01	-	0.01	0.01	-	-	0.01	0.02	-	-	-	-	-
Ca ²⁺	0.69	0.70	0.71	0.70	0.72	0.73	0.72	0.56	0.55	0.53	0.55	0.54	0.53	0.54	0.55	0.55	0.55	0.52	0.56	0.54	0.54	0.54
Na ⁺	0.31	0.29	0.28	0.29	0.29	0.27	0.27	0.44	0.45	0.45	0.46	0.46	0.46	0.46	0.45	0.45	0.44	0.48	0.45	0.45	0.46	0.46
K ⁺	-	0.00	0.00	0.01	0.01	-	-	0.01	0.01	0.01	0.01	0.01	0.01	0.01	0.01	0.01		0.02	0.00	0.01	0.01	0.01
Σcat.	5.00	5.00	5.00	5.00	5.00	5.00	5.00	5.00	5.00	5.00	5.00	5.00	5.00	5.00	5.00	5.00	5.00	5.00	5.00	5.00	5.00	5.00
Anions	8.00	8.00	8.01	7.98	7.98	7.98	7.99	7.99	7.98	8.00	7.98	7.99	8.00	7.99	8.00	7.99	8.00	7.98	8.00	7.99	7.99	7.99
XAn	0.69	0.71	0.72	0.70	0.71	0.73	0.73	0.55	0.54	0.54	0.54	0.53	0.53	0.53	0.54	0.54	0.56	0.51	0.55	0.54	0.53	0.53
XAb	0.31	0.29	0.28	0.29	0.28	0.27	0.27	0.44	0.45	0.45	0.45	0.46	0.46	0.46	0.45	0.45	0.44	0.47	0.45	0.45	0.46	0.45
SrO	163.45	245.37	176.58	-	-	-	133.63	242.33	144.48	-	123.12	-	-	-	-	157.34	-	-	-	-	-	171.01

Table E: continued

Sample	L2t-6	L2t-6	L2t-6	L2t-6	L2t-6	L2t-6	L2t-6	L2t-6	L2t-6	L2t-6	L2t-6	L2t-6	L2t-6	L2t-6	L2t-6	L2t-6	L2t-6	L2t-6	L2t-6	L2t-6	L2t-6	
Mineral	Plag4	Plag4	Plag4	Plag4	Plag4	Plag4	Plag4	Plag4	Plag4	Plag4	Plag4	Plag4	Plag4	Plag4	Plag4	Plag5	Plag5	Plag5	Plag5	Plag5	Plag5	
Generation	Core	Core	Core	Core	Core	Core	Core	Core	Core	Core	Core	Core	Core	Rim	Rim	Rim	Rim	Core	Core	Core	Core	Rim
SiO ₂	54.65	55.10	55.32	54.96	55.44	55.36	55.59	55.33	55.70	55.56	55.61	55.70	55.53	55.37	55.25	59.13	57.83	58.96	59.24	59.40	59.14	
Al ₂ O ₃	28.51	28.41	28.22	27.97	28.29	28.09	28.38	28.27	28.27	28.26	28.45	28.45	28.64	28.71	28.67	25.95	25.27	25.93	25.94	25.71	25.78	
FeO	-	-	-	-	0.19	-	-	-	-	-	-	-	-	-	-	0.50	0.41	0.62	0.33	0.49	0.28	
CaO	10.88	10.74	10.83	10.60	10.67	10.49	10.78	10.62	10.61	10.58	10.71	10.63	10.98	10.91	11.20	7.86	7.80	7.87	7.66	7.88	7.88	
Na ₂ O	5.48	5.41	5.58	5.37	5.68	5.53	5.64	5.54	5.61	5.59	5.43	5.72	5.45	5.43	5.23	7.17	6.92	7.16	7.23	7.23	7.33	
K ₂ O	0.17	0.19	0.18	0.20	0.22	0.17	0.19	0.24	0.24	0.24	0.24	0.25	0.20	0.24	0.20	0.19	0.18	0.22	0.17	0.18	0.09	
Total	99.69	99.84	100.13	99.11	100.48	99.64	100.58	100.01	100.43	100.22	100.45	100.76	100.80	100.66	100.54	100.80	98.41	100.75	100.58	100.91	100.50	
Number of anions on the basis of 8 oxygen atoms																						
Si ⁴⁻	2.47	2.49	2.49	2.50	2.48	2.50	2.49	2.49	2.50	2.50	2.49	2.49	2.48	2.48	2.48	2.62	2.63	2.62	2.63	2.63	2.63	
Al ³⁻	1.52	1.51	1.50	1.50	1.49	1.50	1.50	1.50	1.49	1.50	1.50	1.50	1.51	1.51	1.52	1.36	1.35	1.36	1.36	1.34	1.35	
Fe ²⁺	-	-	-	-	0.01	-	-	-	-	-	-	-	-	-	-	0.02	0.02	0.02	0.01	0.02	0.01	
Ca ²⁺	0.53	0.52	0.52	0.52	0.51	0.51	0.52	0.51	0.51	0.51	0.51	0.51	0.53	0.52	0.54	0.37	0.38	0.37	0.36	0.37	0.37	
Na ⁺	0.48	0.47	0.49	0.47	0.49	0.48	0.49	0.48	0.49	0.49	0.47	0.49	0.47	0.47	0.45	0.62	0.61	0.62	0.62	0.62	0.63	
K ⁺	0.01	0.01	0.01	0.01	0.01	0.01	0.01	0.01	0.01	0.01	0.01	0.01	0.01	0.01	0.01	0.01	0.01	0.01	0.01	0.01	0.01	
Σcat.	5.00	5.00	5.00	5.00	5.00	5.00	5.00	5.00	5.00	5.00	5.00	5.00	5.00	5.00	5.00	5.00	5.00	5.00	5.00	5.00	5.00	
Anions	7.98	8.00	7.99	8.01	7.98	8.00	7.99	7.99	7.99	7.99	8.00	7.98	7.99	7.99	8.00	7.99	8.00	7.98	8.00	7.99	7.98	
XAn	0.52	0.52	0.51	0.52	0.50	0.51	0.51	0.51	0.50	0.50	0.51	0.50	0.52	0.52	0.54	0.37	0.38	0.37	0.37	0.37	0.37	
XAb	0.47	0.47	0.48	0.47	0.48	0.48	0.48	0.48	0.48	0.48	0.47	0.49	0.47	0.47	0.45	0.62	0.61	0.61	0.62	0.62	0.62	
SrO	145.47	175.14	-	157.81	145.24	179.20	217.73	-	170.66	-	174.97	-	-	230.77	149.46	238.88	221.57	243.25	250.97	229.41	340.14	

Table E: continued

Sample	L2t-6	L2t-6	L2t-6	L2t-6	L2t-6	L2t-6	L2t-6	L2t-6	L2t-6	L2t-6	L2t-6	L2t-6	L2t-6	L2t-6	L2t-6	L2t-6	L2t-6	L2t-6	L2t-6	L2t-6	L2t-6
Mineral	Plag6	Plag6	Plag6	Plag6	Plag6	Plag6	Plag6	Plag6	Plag6	Plag6	Plag6	Plag7	Plag7	Plag7	Plag7	Plag7	Plag7	Plag7	Plag7	Plag7	Plag7
Generation	Rim	Rim	Core	Core	Core	Core	Core	Core	Core	Rim	Rim	Rim	Rim	Core	Core	Core	Core	Core	Core	Core	Core
SiO ₂	53.77	53.62	53.83	53.49	53.51	53.66	53.42	53.44	53.56	53.71	53.91	53.71	53.65	53.55	53.62	53.72	53.87	53.77	53.53	54.20	53.62
Al ₂ O ₃	29.73	29.41	29.03	28.96	29.55	29.01	29.19	28.86	28.86	28.99	28.94	28.93	28.81	28.83	28.65	28.79	28.67	28.58	29.13	29.08	28.81
FeO	0.51	0.52	0.68	0.50	0.43	0.58	0.57	0.47	0.70	0.66	0.82	0.27	0.24	0.19	0.20	0.25	0.35	0.20	0.00	0.00	0.35
CaO	11.76	11.93	11.74	11.75	11.51	11.49	11.60	11.66	11.62	11.27	11.45	11.49	11.35	11.30	11.38	11.42	11.34	11.55	11.46	11.45	11.39
Na ₂ O	5.02	4.91	4.91	4.98	4.98	5.08	4.84	5.02	5.02	4.92	4.85	4.89	5.11	5.15	5.24	5.05	5.08	5.20	5.08	4.88	5.19
K ₂ O	-	-	-	-	0.13	-	-	-	-	-	-	0.00	0.00	0.00	0.00	0.09	0.00	0.00	0.00	0.00	0.00
Total	100.79	100.40	100.19	99.69	100.12	99.83	99.61	99.45	99.77	99.54	99.96	99.28	99.16	99.02	99.09	99.32	99.31	99.31	99.20	99.61	99.36
Number of anions on the basis of 8 oxygen atoms																					
Si ⁴⁺	2.41	2.41	2.43	2.42	2.41	2.43	2.43	2.43	2.43	2.44	2.44	2.45	2.44	2.44	2.44	2.44	2.45	2.44	2.43	2.46	2.43
Al ³⁺	1.57	1.56	1.55	1.55	1.57	1.55	1.56	1.55	1.54	1.55	1.55	1.55	1.55	1.55	1.54	1.54	1.54	1.53	1.56	1.56	1.54
Fe ²⁺	0.02	0.02	0.03	0.02	0.02	0.02	0.02	0.02	0.03	0.02	0.03	0.01	0.01	0.01	0.01	0.01	0.01	0.01	0.00	0.00	0.01
Ca ²⁺	0.56	0.58	0.57	0.57	0.56	0.56	0.56	0.57	0.56	0.55	0.56	0.56	0.55	0.55	0.55	0.56	0.55	0.56	0.56	0.56	0.55
Na ⁺	0.44	0.43	0.43	0.44	0.44	0.45	0.43	0.44	0.44	0.43	0.43	0.43	0.45	0.46	0.46	0.45	0.45	0.46	0.45	0.43	0.46
K ⁺	-	-	-	-	0.01	-	-	-	-	-	-	0.00	0.00	0.00	0.00	0.01	0.00	0.00	0.00	0.00	0.00
Σcat.	5.00	5.00	5.00	5.00	5.00	5.00	5.00	5.00	5.00	5.00	5.00	5.00	5.00	5.00	5.00	5.00	5.00	5.00	5.00	5.00	5.00
Anions	7.98	7.98	7.99	7.98	7.98	7.98	7.99	7.98	7.98	8.00	8.00	8.01	7.99	7.98	7.98	7.99	7.99	7.98	7.99	8.02	7.98
XAn	0.56	0.57	0.57	0.57	0.56	0.56	0.57	0.56	0.56	0.56	0.57	0.56	0.55	0.55	0.55	0.55	0.55	0.55	0.55	0.55	0.56
XAb	0.44	0.43	0.43	0.43	0.44	0.44	0.43	0.44	0.44	0.44	0.43	0.44	0.45	0.45	0.45	0.44	0.45	0.45	0.45	0.44	0.45
SrO	-	125.29	120.79	-	-	167.96	-	-	116.22	-	154.89	163.38	-	129.09	180.58	193.41	266.40	206.17	223.84	128.85	-

Table E: continued

Sample	L2t-6	L2t-6	L2t-6	L2t-6	L2t-6	L2t-6	L2t-6	L2t-6	L2t-6	L2t-6	L2t-6	L2t-6	L2t-6	L2t-6	L2t-6	L2t-6	L2t-6	L2t-6	L2t-6	L2t-6	L2t-6
Mineral	Plag9	Plag9	Plag9	Plag9	Plag9	Plag9	Plag9	Plag9	Plag9	Plag9	Plag9	Plag9	Plag9	Plag10	Plag10	Plag10	Plag10	Plag10	Plag10	Plag10	Plag10
Generation	Core	Core	Core	Core	Core	Core	Core	Core	Core	Core	Core	Rim	Rim	Rim	Core	Core	Core	Core	Core	Core	Core
SiO ₂	54.80	54.70	54.23	54.20	54.21	54.02	53.92	53.88	54.03	53.71	53.95	54.27	53.52	60.72	60.84	60.68	60.44	60.76	61.01	60.57	60.60
Al ₂ O ₃	28.97	29.07	28.35	28.61	28.33	28.35	28.60	28.79	28.66	28.63	28.88	28.65	29.17	24.91	25.32	24.65	24.94	25.32	25.09	24.89	25.06
FeO	-	-	-	-	-	-	0.17	0.18	-	-	-	0.21	0.18	0.21	0.00	0.00	0.00	0.00	0.00	0.00	0.00
CaO	11.52	11.54	11.05	11.18	11.31	11.21	11.24	11.12	11.38	11.26	11.37	11.47	11.80	6.82	6.86	6.71	6.70	6.82	6.54	6.59	6.62
Na ₂ O	5.17	4.96	5.22	5.02	5.08	5.33	5.05	5.05	5.04	5.06	5.07	5.03	4.91	8.06	7.82	8.09	8.10	7.81	8.12	8.20	8.16
K ₂ O	0.24	0.22	0.23	0.22	0.12	0.15	0.12	0.22	0.19	0.16	-	0.17	0.11	0.00	0.00	0.00	0.10	0.00	0.00	0.00	0.00
Total	100.70	100.49	99.07	99.49	99.05	99.07	99.11	99.23	99.30	98.82	99.27	99.80	99.69	100.72	100.85	100.13	100.28	100.71	100.77	100.24	100.44
Number of anions on the basis of 8 oxygen atoms																					
Si ⁴⁺	2.45	2.46	2.47	2.46	2.47	2.46	2.46	2.45	2.46	2.45	2.45	2.46	2.42	2.68	2.69	2.69	2.68	2.69	2.69	2.68	2.68
Al ³⁺	1.53	1.54	1.52	1.53	1.52	1.52	1.54	1.54	1.54	1.54	1.55	1.53	1.56	1.30	1.32	1.29	1.30	1.32	1.30	1.30	1.31
Fe ²⁺	0.00	0.00	0.00	0.00	0.00	0.00	0.01	0.01	0.00	0.00	0.00	0.01	0.01	0.01	0.00	0.00	0.00	0.00	0.00	0.00	0.00
Ca ²⁺	0.55	0.56	0.54	0.54	0.55	0.55	0.55	0.54	0.55	0.55	0.55	0.56	0.57	0.32	0.32	0.32	0.32	0.32	0.31	0.31	0.31
Na ⁺	0.45	0.43	0.46	0.44	0.45	0.47	0.45	0.44	0.44	0.45	0.45	0.44	0.43	0.69	0.67	0.70	0.70	0.67	0.69	0.70	0.70
K ⁺	0.01	0.01	0.01	0.01	0.01	0.01	0.01	0.01	0.01	0.01	-	0.01	0.01	0.00	0.00	0.00	0.01	0.00	0.00	0.00	0.00
Σ cat.	5.00	5.00	5.00	5.00	5.00	5.00	5.00	5.00	5.00	5.00	5.00	5.00	5.00	5.00	5.00	5.00	5.00	5.00	5.00	5.00	5.00
Anions	7.99	8.01	7.99	8.01	8.00	7.98	8.00	7.99	8.00	7.99	8.00	7.99	7.98	7.99	8.01	7.99	7.98	8.01	8.00	7.98	7.98
XAn	0.54	0.56	0.53	0.54	0.55	0.53	0.55	0.54	0.55	0.55	0.55	0.55	0.57	0.32	0.33	0.31	0.31	0.33	0.31	0.31	0.31
XAb	0.44	0.43	0.45	0.44	0.45	0.46	0.45	0.45	0.44	0.44	0.45	0.44	0.43	0.68	0.67	0.69	0.68	0.67	0.69	0.69	0.69
SrO	-	148.54	178.14	165.45	135.65	195.25	-	263.60	140.09	-	157.33	135.82	225.65	271.85	263.43	301.17	339.91	238.00	334.76	389.91	309.58

Table E: continued

Sample	L2t-6	L2t-6	L2t-6	L2t-6	L2t-6	L2t-6	L2t-6	L2t-6	L2t-6	L2t-6	L2t-6	L2t-6	L2t-6	L2t-6	L2t-6	L2t-6	L2t-6	L2t-6	L2t-6	L2t-6	L2t-6	
Mineral	Plag10	Plag11	Plag11	Plag11	Plag11	Plag11	Plag11	Plag11	Plag11	Plag11	Plag11	Plag11	Plag11	Plag11	Plag11	Plag11	Plag11	Plag11	Plag12	Plag12	Plag12	
Generation	Rim	Rim	Rim	Core	Core	Core	Core	Core	Core	Core	Core	Core	Core	Core	Core	Core	Core	Rim	Rim	Rim	Core	Core
SiO ₂	60.53	48.90	48.98	49.79	49.66	50.80	50.72	51.72	52.66	53.20	53.20	52.71	50.95	50.55	50.57	49.57	49.01	49.22	52.39	52.83	53.30	
Al ₂ O ₃	25.02	32.93	32.53	32.02	32.28	32.00	31.65	30.79	30.45	29.89	29.52	30.67	30.97	32.00	31.73	32.78	32.08	32.79	29.74	29.73	29.93	
FeO	0.00	-	-	0.26	-	-	-	-	-	-	-	-	-	0.17	0.20	-	0.39	0.20	0.44	0.25	0.27	
CaO	6.69	15.91	15.46	15.15	15.07	14.80	14.47	13.38	12.93	12.97	12.51	12.93	14.15	14.66	14.77	15.44	15.35	15.80	12.61	12.58	12.68	
Na ₂ O	7.94	2.61	2.78	2.81	3.06	3.30	3.36	3.89	4.28	4.51	4.50	4.33	3.54	3.28	3.16	2.90	2.77	2.62	4.42	4.41	4.46	
K ₂ O	0.00	0.00	0.10	0.00	0.00	0.00	0.00	0.23	0.17	0.17	0.16	0.10	0.00	0.00	0.00	0.00	0.11	0.00	-	-	0.09	
Total	100.19	100.35	99.84	100.03	100.08	100.89	100.20	100.01	100.48	100.73	99.89	100.73	99.61	100.66	100.43	100.69	99.70	100.63	99.60	99.80	100.74	
Number of anions on the basis of 8 oxygen atoms																						
Si ⁴⁺	2.69	2.23	2.24	2.28	2.26	2.29	2.30	2.35	2.37	2.39	2.41	2.37	2.33	2.29	2.30	2.25	2.25	2.24	2.38	2.40	2.40	
Al ³⁺	1.31	1.77	1.75	1.72	1.73	1.70	1.69	1.65	1.62	1.58	1.58	1.62	1.67	1.71	1.70	1.75	1.73	1.76	1.60	1.59	1.59	
Fe ²⁺	0.00	-	-	0.01	-	-	-	-	-	-	-	-	-	0.01	0.01	-	0.01	0.01	0.02	0.01	0.01	
Ca ²⁺	0.32	0.78	0.76	0.74	0.74	0.72	0.70	0.65	0.62	0.62	0.61	0.62	0.69	0.71	0.72	0.75	0.75	0.77	0.61	0.61	0.61	
Na ⁺	0.68	0.23	0.25	0.25	0.27	0.29	0.30	0.34	0.37	0.39	0.40	0.38	0.31	0.29	0.28	0.25	0.25	0.23	0.39	0.39	0.39	
K ⁺	0.00	-	0.01	-	-	-	-	0.01	0.01	0.01	0.01	0.01	0.01	-	-	-	-	0.01	-	-	0.01	
Σcat.	5.00	5.00	5.00	5.00	5.00	5.00	5.00	5.00	5.00	5.00	5.00	5.00	5.00	5.00	5.00	5.00	5.00	5.00	5.00	5.00	5.00	
Anions	8.00	8.00	7.99	8.01	7.99	8.00	8.00	7.99	7.99	7.98	8.00	7.99	8.00	8.00	8.01	7.99	7.99	8.00	7.99	8.00	7.99	
XAn	0.32	0.77	0.75	0.75	0.73	0.71	0.70	0.65	0.62	0.61	0.60	0.62	0.69	0.71	0.72	0.75	0.75	0.77	0.61	0.61	0.61	
XAb	0.68	0.23	0.24	0.25	0.27	0.29	0.30	0.34	0.37	0.38	0.39	0.38	0.31	0.29	0.28	0.25	0.24	0.23	0.39	0.39	0.39	
SrO	258.47	145.69	137.00	-	-	153.54	-	144.45	279.93	169.15	-	-	207.84	161.84	-	153.76	196.23	-	-	126.71	-	

Table E: continued

Sample	L2t-6	L2t-6	L2t-6	L2t-6	L2t-6	L2t-6	L2t-6	L2t-6	L2t-6	L2t-6	L2t-6	L2t-6	L2t-6	L2t-6	L2t-6	L2t-6	L2t-6	L2t-6	L2t-6	L2t-6	L2t-6
Mineral	Plag12	Plag12	Plag12	Plag12	Plag12	Plag12	Plag12	Plag13	Plag13	Plag13	Plag13	Plag13	Plag13	Plag13	Plag13	Plag14	Plag14	Pla14	Plag14	Plag14	Plag14
Generation	Core	Core	Core	Core	Core	Core	Rim	Rim	Core	Core	Core	Core	Core	Core	Rim	Rim	Rim	Rim	Core	Core	Core
SiO ₂	53.32	53.42	53.43	52.82	52.48	52.73	52.45	48.19	48.98	48.90	48.36	47.82	47.83	48.02	47.71	46.86	47.37	47.78	47.72	47.70	48.04
Al ₂ O ₃	29.95	29.78	29.65	29.40	29.36	29.74	29.76	32.69	32.88	32.51	32.21	32.63	32.61	32.87	32.67	33.42	33.27	33.27	32.95	33.02	33.39
FeO	0.29	0.31	0.34	0.26	0.38	0.35	0.61	0.76	0.47	0.45	0.39	0.55	0.63	0.61	1.03	0.23	0.26	0.22	0.23	0.00	0.18
CaO	12.59	12.63	12.39	12.27	12.50	12.38	12.44	15.62	15.76	15.64	15.74	15.93	15.76	15.84	15.72	16.70	16.71	16.57	16.28	16.44	16.54
Na ₂ O	4.63	4.53	4.54	4.56	4.43	4.52	4.43	2.38	2.48	2.59	2.69	2.40	2.21	2.42	2.07	2.08	1.90	2.12	2.00	2.13	2.11
K ₂ O	0.13	-	0.13	0.11	-	0.14	-	-	-	-	-	-	-	-	0.11	-	-	-	-	-	-
Total	100.91	100.67	100.47	99.41	99.14	99.87	99.69	99.65	100.58	100.09	99.39	99.34	99.04	99.75	99.33	99.29	99.50	99.96	99.18	99.29	100.26
Number of anions on the basis of 8 oxygen atoms																					
Si ⁴⁺	2.39	2.40	2.41	2.41	2.40	2.39	2.39	2.22	2.23	2.24	2.22	2.20	2.22	2.20	2.21	2.16	2.19	2.19	2.21	2.20	2.20
Al ³⁺	1.58	1.58	1.58	1.58	1.58	1.59	1.59	1.77	1.76	1.75	1.75	1.77	1.78	1.78	1.78	1.82	1.81	1.80	1.80	1.80	1.80
Fe ²⁺	0.01	0.01	0.01	0.01	0.01	0.01	0.02	0.03	0.02	0.02	0.02	0.02	0.02	0.02	0.04	0.01	0.01	0.01	0.01		0.01
Ca ²⁺	0.60	0.61	0.60	0.60	0.61	0.60	0.61	0.77	0.77	0.77	0.78	0.79	0.78	0.78	0.78	0.83	0.83	0.81	0.81	0.81	0.81
Na ⁺	0.40	0.40	0.40	0.40	0.39	0.40	0.39	0.21	0.22	0.23	0.24	0.21	0.20	0.22	0.19	0.19	0.17	0.19	0.18	0.19	0.19
K ⁺	0.01	-	0.01	0.01	-	0.01	-	-	-	-	-	-	-	-	0.01	-	-	-	-	-	-
Σ cat.	5.00	5.00	5.00	5.00	5.00	5.00	5.00	5.00	5.00	5.00	5.00	5.00	5.00	5.00	5.00	5.00	5.00	5.00	5.00	5.00	5.00
Anions	7.98	8.00	7.99	7.99	7.99	7.98	7.99	8.00	8.00	8.00	7.98	7.98	8.01	7.99	8.00	7.98	8.00	8.00	8.02	8.00	8.00
XAn	0.60	0.61	0.60	0.59	0.61	0.60	0.61	0.78	0.78	0.77	0.76	0.79	0.80	0.78	0.80	0.82	0.83	0.81	0.82	0.81	0.81
XAb	0.40	0.39	0.40	0.40	0.39	0.39	0.39	0.22	0.22	0.23	0.24	0.21	0.20	0.22	0.19	0.18	0.17	0.19	0.18	0.19	0.19
SrO	-	-	164.53	-	-	-	215.28	-	-	-	187.49	281.87	-	-	-	-	-	-	-	-	-

Table E: continued

Sample	L2t-6	L2t-6	L2t-6	L2t-6	L2t-6	L2t-6	L2t-6	L2t-6	L2t-6	L2t-6	L2t-6	L2t-6	L2t-6	L2t-6	L2t-6	L2t-6	L2t-6	L2t-6	L2t-6	L2t-6	L2t-6
Mineral	Plag14	Plag14	Pla14	Plag14	Plag14	Pla14	Plag14	Plag14	Pla14	Plag14	Plag14	Pla14	Plag14	Plag14	Plag15	Plag15	Plag15	Plag15	Plag15	Plag15	Plag15
Generation	Core	Core	Core	Core	Core	Core	Core	Core	Core	Core	Core	Rim	Rim	Rim	Rim	Core	Core	Core	Core	Core	Core
SiO ₂	47.69	48.03	48.12	47.71	47.93	48.00	47.91	47.82	47.92	47.90	47.88	48.20	47.71	47.51	55.46	55.44	55.61	55.63	55.70	55.29	55.57
Al ₂ O ₃	32.87	33.25	33.25	33.13	33.00	33.70	33.17	33.13	33.30	33.45	33.53	33.42	33.64	33.88	28.01	28.01	28.41	28.33	27.80	28.30	28.07
FeO	0.23	0.00	0.19	0.20	0.00	0.00	0.00	0.00	0.00	0.21	0.24	0.29	0.35	0.27	0.26	0.25	0.27	0.31	0.26	0.23	0.21
CaO	16.42	16.36	16.29	16.10	16.35	16.59	16.66	16.42	16.33	16.47	16.70	16.42	16.77	16.68	10.39	10.54	10.58	10.52	10.31	10.38	10.46
Na ₂ O	2.28	2.10	2.20	2.25	2.11	2.17	2.15	2.21	2.08	2.06	2.20	2.11	2.03	2.03	5.62	5.72	5.64	5.64	5.63	5.75	5.60
K ₂ O	0.11	-	-	0.10	-	-	-	-	-	-	-	-	-	-	0.25	0.23	0.28	0.21	0.30	0.17	0.24
Total	99.60	99.73	100.05	99.49	99.38	100.46	99.89	99.58	99.63	100.10	100.55	100.43	100.51	100.37	99.97	100.19	100.80	100.63	100.33	100.12	100.15
Number of anions on the basis of 8 oxygen atoms																					
Si ⁴⁺	2.19	2.21	2.20	2.20	2.21	2.19	2.20	2.20	2.20	2.19	2.18	2.20	2.18	2.17	2.50	2.49	2.48	2.49	2.50	2.48	2.50
Al ³⁺	1.78	1.80	1.79	1.80	1.79	1.81	1.79	1.80	1.81	1.81	1.80	1.80	1.81	1.82	1.49	1.48	1.50	1.49	1.47	1.50	1.49
Fe ²⁺	0.01		0.01	0.01						0.01	0.01	0.01	0.01	0.01	0.01	0.01	0.01	0.01	0.01	0.01	0.01
Ca ²⁺	0.81	0.81	0.80	0.79	0.81	0.81	0.82	0.81	0.80	0.81	0.81	0.80	0.82	0.82	0.50	0.51	0.51	0.50	0.50	0.50	0.50
Na ⁺	0.20	0.19	0.20	0.20	0.19	0.19	0.19	0.20	0.19	0.18	0.19	0.19	0.18	0.18	0.49	0.50	0.49	0.49	0.49	0.50	0.49
K ⁺	0.01	-	-	0.01	-	-	-	-	-	-	-	-	-	-	0.01	0.01	0.02	0.01	0.02	0.01	0.01
Σcat.	5.00	5.00	5.00	5.00	5.00	5.00	5.00	5.00	5.00	5.00	5.00	5.00	5.00	5.00	5.00	5.00	5.00	5.00	5.00	5.00	5.00
Anions	7.98	8.01	8.00	7.99	8.01	8.00	8.00	8.00	8.01	8.01	7.98	8.01	7.99	7.99	7.99	7.98	7.98	7.99	8.00	7.98	7.99
XAn	0.79	0.81	0.80	0.79	0.81	0.81	0.81	0.80	0.81	0.82	0.81	0.81	0.82	0.82	0.50	0.50	0.50	0.50	0.49	0.49	0.50
XAb	0.20	0.19	0.20	0.20	0.19	0.19	0.19	0.20	0.19	0.18	0.19	0.19	0.18	0.18	0.49	0.49	0.48	0.49	0.49	0.50	0.49
SrO	-	-	-	-	-	-	-	-	-	257.94	-	-	-	-	-	-	-	199.31	-	-	-

Table E: continued

Sample	L2t-6	L2t-6	L2t-6	L2t-6	L2t-6	L2t-6	L2t-6	L2t-6	L2t-6	L2t-6	L2t-6	L2t-6	L2t-6	L2t-6	L2t-6	L2t-6	L2t-6	L2t-6	L2t-6	L2t-6	L2t-6	
Mineral	Plag15	Plag15	Plag15	Plag16	Plag16	Plag16	Plag16	Plag16	Plag16	Plag16	Plag16	Plag16	Plag16	Plag16	Plag17	Plag17	Plag17	Plag17	Plag17	Plag17	Plag17	
Generation	Core	Core	Rim	Rim	Core	Core	Core	Core	Core	Core	Core	Core	Core	Core	Rim	Rim	Rim	Rim	Core	Core	Core	Core
SiO ₂	55.45	55.80	55.10	60.59	60.25	60.64	60.58	60.83	60.80	60.54	60.31	60.80	60.24	60.36	55.32	55.82	55.81	55.45	55.46	56.36	55.98	
Al ₂ O ₃	27.99	28.01	28.01	25.06	25.09	25.07	25.07	25.07	25.07	25.01	24.96	24.91	24.99	25.44	28.23	28.29	27.89	27.81	27.72	28.07	27.66	
FeO	-	0.23	0.23	-	-	-	-	-	-	-	-	-	-	-	0.22	0.23	-	-	-	-	-	
CaO	10.25	10.10	10.06	6.88	6.81	6.93	6.69	6.67	6.71	6.73	6.71	6.93	6.81	6.98	11.00	10.47	10.50	10.52	10.44	10.56	10.34	
Na ₂ O	5.70	5.71	5.75	7.91	7.88	8.09	8.03	7.96	8.06	7.93	7.89	7.89	7.86	7.90	5.51	5.62	5.72	5.70	5.70	5.74	5.79	
K ₂ O	0.35	0.31	0.20	0.00	0.00	0.00	0.10	0.00	0.00	0.09	0.00	0.13	0.00	0.09	-	-	-	0.09	0.11	0.14	-	
Total	99.74	100.17	99.35	100.45	100.03	100.73	100.48	100.53	100.64	100.31	99.87	100.66	99.90	100.78	100.28	100.43	99.91	99.58	99.42	100.86	99.77	
Number of anions on the basis of 8 oxygen atoms																						
Si ⁴⁺	2.50	2.51	2.49	2.68	2.68	2.68	2.68	2.69	2.69	2.69	2.69	2.69	2.68	2.66	2.49	2.50	2.51	2.51	2.51	2.51	2.52	
Al ³⁺	1.49	1.48	1.49	1.31	1.32	1.30	1.31	1.31	1.31	1.31	1.31	1.30	1.31	1.32	1.50	1.50	1.48	1.48	1.48	1.48	1.47	
Fe ²⁺	-	0.01	0.01	-	-	-	-	-	-	-	-	-	-	-	0.01	0.01	-	-	-	-	-	
Ca ²⁺	0.49	0.49	0.49	0.33	0.32	0.33	0.32	0.32	0.32	0.32	0.32	0.33	0.33	0.33	0.53	0.50	0.51	0.51	0.51	0.50	0.50	
Na ⁺	0.50	0.50	0.50	0.68	0.68	0.69	0.69	0.68	0.69	0.68	0.68	0.68	0.68	0.68	0.48	0.49	0.50	0.50	0.50	0.50	0.51	
K ⁺	0.02	0.02	0.01	-	-	-	0.01	-	-	0.01	-	0.01	-	0.01	-	-	-	0.01	0.01	0.01	-	
Σ cat.	5.00	5.00	5.00	5.00	5.00	5.00	5.00	5.00	5.00	5.00	5.00	5.00	5.00	5.00	5.00	5.00	5.00	5.00	5.00	5.00	5.00	
Anions	7.98	7.99	7.98	8.00	8.00	7.98	7.99	8.00	7.99	8.00	8.00	8.00	8.00	7.99	7.99	8.01	8.00	7.99	8.00	8.00	8.01	
XAn	0.49	0.49	0.49	0.32	0.32	0.32	0.31	0.32	0.31	0.32	0.32	0.32	0.32	0.33	0.52	0.51	0.50	0.50	0.50	0.50	0.50	
XAb	0.49	0.50	0.50	0.68	0.68	0.68	0.68	0.68	0.69	0.68	0.68	0.67	0.68	0.67	0.48	0.49	0.50	0.49	0.49	0.49	0.50	
SrO	-	-	-	-	-	-	-	-	-	-	-	-	-	-	-	-	-	-	-	-	-	

Table E: continued

Sample	L2t-6	L2t-6	L2t-6	L2t-6	L2t-6	L2t-6	L2t-6	L2t-6	L2t-6	L2t-6	L2t-6	L2t-6	L2t-6	L2t-6	L2t-6	L2t-6	L2t-6	L2t-6	L2t-6	L2t-6	L2t-6
Mineral	Plag17	Plag17	Plag17	Plag17	Plag17	Plag17	Plag17	Plag17	Plag17	Plag17	Plag18	Plag18	Plag18	Plag18	Plag18	Plag18	Plag18	Plag18	Plag18	Plag18	Plag18
Generation	Core	Core	Core	Core	Core	Core	Core	Rim	Rim	Rim	Rim	Rim	Rim	Core	Core	Core	Core	Core	Core	Core	Core
SiO ₂	56.36	56.93	56.82	57.09	56.46	56.62	56.60	56.44	56.22	55.67	50.87	53.31	54.53	54.12	53.25	53.20	52.98	53.05	54.39	54.61	54.39
Al ₂ O ₃	27.40	27.24	27.14	27.52	27.22	27.67	28.11	27.99	28.13	28.43	30.92	29.56	29.31	29.06	29.30	29.38	29.45	29.74	28.75	28.72	28.68
FeO	-	-	-	-	-	-	-	-	0.31	0.32	0.29	0.00	0.00	0.00	0.00	0.00	0.00	0.00	0.00	0.00	0.00
CaO	10.11	9.49	9.52	9.74	10.05	10.17	10.21	10.38	10.46	10.87	14.00	11.93	11.65	12.09	11.96	12.32	12.62	12.85	11.66	11.47	11.29
Na ₂ O	6.06	6.22	6.32	6.29	6.02	5.99	5.95	5.91	5.75	5.60	3.59	4.79	5.05	5.01	4.83	4.55	4.64	4.57	5.32	5.20	5.19
K ₂ O	0.14	0.09	-	0.12	0.09	-	-	-	-	0.09	0.30	-	-	0.14	-	-	-	-	-	-	-
Total	100.07	99.97	99.81	100.76	99.83	100.45	100.87	100.71	100.87	100.98	99.97	99.58	100.54	100.43	99.34	99.45	99.69	100.21	100.13	100.00	99.55
Number of anions on the basis of 8 oxygen atoms																					
Si ⁴⁺	2.53	2.56	2.55	2.54	2.54	2.53	2.52	2.52	2.51	2.48	2.31	2.42	2.45	2.43	2.42	2.42	2.40	2.40	2.45	2.46	2.46
Al ³⁺	1.45	1.44	1.44	1.44	1.44	1.46	1.48	1.47	1.48	1.49	1.66	1.58	1.55	1.54	1.57	1.58	1.57	1.58	1.53	1.53	1.53
Fe ²⁺	-	-	-	-	-	-	-	-	0.01	0.01	0.01	0.00	0.00	0.00	0.00	0.00	0.00	0.00	0.00	0.00	0.00
Ca ²⁺	0.49	0.46	0.46	0.46	0.48	0.49	0.49	0.50	0.50	0.52	0.68	0.58	0.56	0.58	0.58	0.60	0.61	0.62	0.56	0.55	0.55
Na ⁺	0.53	0.54	0.55	0.54	0.53	0.52	0.51	0.51	0.50	0.48	0.32	0.42	0.44	0.44	0.43	0.40	0.41	0.40	0.46	0.45	0.46
K ⁺	0.01	0.01	-	0.01	-	-	-	-	-	0.01	0.02	-	-	0.01	-	-	-	-	-	-	-
Σ cat.	5.00	5.00	5.00	5.00	5.00	5.00	5.00	5.00	5.00	5.00	5.00	5.00	5.00	5.00	5.00	5.00	5.00	5.00	5.00	5.00	5.00
Anions	7.99	8.00	8.00	7.99	8.00	8.00	8.00	8.00	8.00	7.99	7.98	8.00	8.00	7.98	7.99	8.01	7.99	7.99	7.98	8.00	8.00
XAn	0.48	0.45	0.45	0.46	0.48	0.48	0.49	0.49	0.50	0.52	0.67	0.58	0.56	0.57	0.58	0.60	0.60	0.61	0.55	0.55	0.55
XAb	0.52	0.54	0.55	0.53	0.52	0.52	0.51	0.51	0.50	0.48	0.31	0.42	0.44	0.43	0.42	0.40	0.40	0.39	0.45	0.45	0.45
SrO	-	-	-	-	-	-	-	-	-	-	208.34	246.21	-	-	-	-	-	-	-	-	-

Table E: continued

Sample	L2t-6	L2t-6	L2t-6	L2t-6	L2t-6	L2t-6	L2t-6	L2t-6	L2t-6	L2t-6	L2t-6	L2t-6	L2t-6	L2t-6	L2t-6	L2t-6	L2t-6	L2t-6	L2t-6	L2t-6	L2t-6
Mineral	Plag18	Plag18	Plag18	Plag18	Plag18	Plag18	Plag18	Plag18	Plag18	Plag18	Plag18	Plag18	Plag18	Matrix	Matrix	Matrix	Matrix	Matrix	Matrix	Matrix	Matrix
Generation	Core	Core	Core	Core	Core	Core	Core	Core	Core	Core	Rim	Rim	Rim	Rim	Rim	Core	Core	Core	Core	Core	Core
SiO ₂	54.39	54.57	54.57	54.64	54.77	55.16	55.28	55.16	54.74	55.03	55.04	55.03	54.50	60.53	60.85	61.05	61.01	61.28	60.95	61.18	61.33
Al ₂ O ₃	28.68	28.81	28.50	28.39	28.54	28.48	28.86	28.58	28.30	28.27	28.06	28.24	28.41	24.36	24.29	24.41	24.15	24.59	24.29	24.43	24.39
FeO	0.00	0.00	0.00	0.00	0.00	0.00	0.00	0.00	0.00	0.00	0.00	0.00	0.00	-	-	-	-	-	-	0.17	-
CaO	11.29	11.50	11.23	11.22	11.17	11.04	10.99	11.22	10.87	10.67	10.98	10.85	11.49	6.32	6.27	6.25	6.12	6.20	6.22	6.19	6.11
Na ₂ O	5.19	5.27	5.09	5.37	5.33	5.41	5.48	5.63	5.25	5.47	5.49	5.46	5.31	8.00	8.07	8.21	8.32	8.34	8.10	8.15	8.20
K ₂ O	-	-	-	-	-	-	-	-	-	-	-	-	-	-	0.10	0.17	0.12	0.13	0.12	0.13	-
Total	99.55	100.15	99.39	99.64	99.82	100.09	100.61	100.59	99.16	99.44	99.58	99.58	99.70	99.20	99.58	100.09	99.73	100.54	99.67	100.25	100.03
Number of anions on the basis of 8 oxygen atoms																					
Si ⁴⁺	2.46	2.46	2.48	2.47	2.47	2.48	2.47	2.47	2.49	2.49	2.49	2.49	2.46	2.71	2.72	2.71	2.72	2.71	2.72	2.71	2.73
Al ³⁺	1.53	1.53	1.53	1.51	1.52	1.51	1.52	1.51	1.52	1.51	1.50	1.51	1.51	1.29	1.28	1.28	1.27	1.28	1.28	1.28	1.28
Fe ²⁺	0.00	0.00	0.00	0.00	0.00	0.00	0.00	0.00	0.00	0.00	0.00	0.00	0.00	-	-	-	-	-	-	0.01	-
Ca ²⁺	0.55	0.55	0.55	0.54	0.54	0.53	0.53	0.54	0.53	0.52	0.53	0.53	0.56	0.30	0.30	0.30	0.29	0.29	0.30	0.29	0.29
Na ⁺	0.46	0.46	0.45	0.47	0.47	0.47	0.48	0.49	0.46	0.48	0.48	0.48	0.47	0.70	0.70	0.71	0.72	0.71	0.70	0.70	0.71
K ⁺	-	-	-	-	-	-	-	-	-	-	-	-	-	-	0.01	0.01	0.01	0.01	0.01	0.01	-
Σ cat.	5.00	5.00	5.00	5.00	5.00	5.00	5.00	5.00	5.00	5.00	5.00	5.00	5.00	5.00	5.00	5.00	5.00	5.00	5.00	5.00	5.00
Anions	8.00	7.99	8.02	7.99	8.00	8.00	8.00	7.98	8.02	8.01	8.00	8.00	7.99	8.01	8.00	7.99	7.99	7.99	8.00	8.00	8.01
XAn	0.55	0.55	0.55	0.54	0.54	0.53	0.53	0.52	0.53	0.52	0.52	0.52	0.54	0.30	0.30	0.29	0.29	0.29	0.30	0.29	0.29
XAb	0.45	0.45	0.45	0.46	0.46	0.47	0.47	0.48	0.47	0.48	0.48	0.48	0.46	0.70	0.70	0.70	0.71	0.70	0.70	0.70	0.71
SrO	-	-	-	-	-	-	-	-	-	-	-	-	-	-	-	208.01	-	187.38	-	-	-

Table E: continued

Sample	L2t-6	L2t-6	L2t-6	L2t-6	L2t-6	L2t-6	L2t-6	L2t-6	L2t-6	L2t-7	L2t-7	L2t-7	L2t-7	L2t-7	L2t-7	L2t-7	L2t-7	L2t-7	L2t-7	L2t-7	L2t-7
Mineral	Matrix	Matrix	Matrix	Matrix	Matrix	Matrix	Matrix	Matrix	Matrix	Plag	Plag	Plag	Plag	Plag	Plag	Plag	Plag	Plag	Plag	Plag	Plag
Generation	Core	Core	Core	Core	Core	Core	Core	Rim	Rim	rim	rim	rim	core	core	core	core	core	core	core	core	core
SiO ₂	61.42	61.31	61.77	61.64	60.82	59.80	60.58	60.51	60.61	60.15	59.58	60.07	60.55	60.33	60.42	60.49	60.72	60.48	60.69	60.38	60.72
Al ₂ O ₃	24.57	24.39	24.44	24.39	24.73	24.77	24.55	24.35	24.71	25.38	24.90	25.23	25.06	25.32	25.16	24.83	25.14	25.00	24.84	25.03	24.92
FeO	-	-	-	-	-	-	-	-	-	0.31	0.24	0.19	0.34	0.22	0.20	-	0.16	0.15	-	0.17	0.15
CaO	6.14	6.15	6.05	6.34	6.87	6.60	6.42	6.31	6.65	7.30	6.94	6.95	6.94	7.08	7.07	6.98	6.94	6.73	6.86	6.74	6.89
Na ₂ O	8.31	8.34	8.24	8.00	7.80	7.81	8.10	8.05	7.83	7.57	7.67	7.66	7.66	7.76	7.72	7.57	7.83	7.79	7.82	7.71	7.97
K ₂ O	0.16	0.15	0.18	0.18	0.10	0.14	0.10	0.14	-	0.12	0.14	0.13	0.16	0.17	0.11	0.12	0.13	0.15	0.15	0.12	-
Total	100.59	100.34	100.68	100.56	100.32	99.13	99.75	99.36	99.80	100.83	99.47	100.36	100.70	100.87	100.68	99.98	100.91	100.29	100.37	100.16	100.66
Number of anions on the basis of 8 oxygen atoms																					
Si ⁴⁺	2.71	2.71	2.73	2.73	2.70	2.68	2.70	2.71	2.70	2.66	2.67	2.67	2.68	2.66	2.68	2.70	2.68	2.69	2.69	2.69	2.69
Al ³⁺	1.28	1.27	1.27	1.27	1.29	1.31	1.29	1.28	1.30	1.32	1.31	1.32	1.31	1.32	1.31	1.31	1.31	1.31	1.30	1.31	1.30
Fe ²⁺	-	-	-	-	-	-	-	-	-	0.01	0.01	0.01	0.01	0.01	0.01	-	0.01	0.01	-	0.01	0.01
Ca ²⁺	0.29	0.29	0.29	0.30	0.33	0.32	0.31	0.30	0.32	0.35	0.33	0.33	0.33	0.33	0.34	0.33	0.33	0.32	0.33	0.32	0.33
Na ⁺	0.71	0.72	0.71	0.69	0.67	0.68	0.70	0.70	0.68	0.65	0.67	0.66	0.66	0.66	0.66	0.65	0.67	0.67	0.67	0.67	0.68
K ⁺	0.01	0.01	0.01	0.01	0.01	0.01	0.01	0.01	-	0.01	0.01	0.01	0.01	0.01	0.01	0.01	0.01	0.01	0.01	0.01	-
Σ cat.	5.00	5.00	5.00	5.00	5.00	5.00	5.00	5.00	5.00	5.00	5.00	5.00	5.00	5.00	5.00	5.00	5.00	5.00	5.00	5.00	5.00
Anions	7.99	7.99	8.00	8.02	8.01	8.00	7.99	8.00	8.02	8.00	7.99	8.00	8.00	7.99	8.00	8.02	8.00	8.00	8.00	8.01	7.99
XAn	0.29	0.29	0.29	0.30	0.33	0.32	0.30	0.30	0.32	0.35	0.33	0.33	0.33	0.33	0.33	0.34	0.33	0.32	0.32	0.32	0.32
XAb	0.70	0.70	0.70	0.69	0.67	0.68	0.69	0.69	0.68	0.19	0.20	0.21	0.22	0.23	0.24	0.24	0.25	0.26	0.27	0.28	0.29
SrO	-	-	-	232.48	-	-	-	220.11	-	-	-	-	-	-	-	-	-	-	-	-	-

Table E: continued

Sample	L2t-7	L2t-7	L2t-7	L2t-7	L2t-7	L2t-7	L2t-7	L2t-7	L2t-7	L2t-7	L2t-7	L2t-7	L2t-7	L2t-7	L2t-7	L2t-7	L2t-7	L2t-7	L2t-7	L2t-7	L2t-7
Mineral	Plag	Plag	Plag	Plag	Plag	Plag	Plag	Plag	Plag	Plag	Plag	Plag	Plag	Plag	Plag	Plag	Plag	Plag	Plag	Plag	Plag
Generation	core	core	core	core	core	core	core	core	core	core	core	core	core	core	core	core	core	core	core	core	core
SiO ₂	60.55	60.93	60.33	60.40	60.42	60.29	60.94	60.54	60.64	60.83	60.36	60.59	61.16	60.80	60.94	60.61	60.61	60.76	60.59	60.64	60.41
Al ₂ O ₃	25.02	24.90	24.90	24.58	24.75	24.60	24.95	24.77	24.92	24.60	24.74	24.94	24.97	24.90	25.05	24.76	24.76	24.83	24.93	25.22	25.08
FeO	-	-	-	-	-	-	-	-	-	-	-	-	-	-	0.16	0.14	0.14	-	-	-	0.22
CaO	6.84	6.85	6.70	6.66	6.82	6.68	6.67	6.74	6.71	6.74	6.75	6.72	6.67	6.89	6.85	7.00	7.00	6.93	6.93	7.05	7.08
Na ₂ O	7.77	7.92	7.63	7.85	7.64	7.83	7.79	7.71	7.79	7.79	7.68	7.73	8.01	7.88	7.83	7.73	7.73	7.75	7.69	7.69	7.67
K ₂ O	0.18	0.10	0.10	0.13	0.19	0.14	0.16	0.13	0.15	0.13	0.09	0.12	0.12	0.11	0.11	0.14	0.14	0.12	0.14	0.12	0.10
Total	100.37	100.85	99.85	99.62	99.82	99.54	100.51	99.90	100.20	100.28	99.62	100.10	100.94	100.58	100.94	100.39	100.39	100.40	100.28	100.72	100.55
Number of anions on the basis of 8 oxygen atoms																					
Si ⁴⁺	2.69	2.69	2.70	2.70	2.70	2.70	2.70	2.70	2.70	2.70	2.70	2.70	2.70	2.69	2.69	2.69	2.69	2.70	2.69	2.68	2.68
Al ³⁺	1.31	1.30	1.31	1.29	1.30	1.30	1.30	1.30	1.31	1.29	1.30	1.31	1.30	1.30	1.30	1.30	1.30	1.30	1.31	1.32	1.31
Fe ²⁺	-	-	0.01	-	-	-	-	-	-	0.01	-	-	-	-	0.01	0.01	0.01	-	-	-	0.01
Ca ²⁺	0.33	0.32	0.32	0.32	0.33	0.32	0.32	0.32	0.32	0.32	0.32	0.32	0.32	0.33	0.32	0.33	0.33	0.33	0.33	0.33	0.34
Na ⁺	0.67	0.68	0.66	0.68	0.66	0.68	0.67	0.67	0.67	0.67	0.67	0.67	0.67	0.68	0.68	0.67	0.67	0.67	0.67	0.66	0.66
K ⁺	0.01	0.01	0.01	0.01	0.01	0.01	0.01	0.01	0.01	0.01	0.01	0.01	0.01	0.01	0.01	0.01	0.01	0.01	0.01	0.01	0.01
Σcat	5.00	5.00	5.00	5.00	5.00	5.00	5.00	5.00	5.00	5.00	5.00	5.00	5.00	5.00	5.00	5.00	5.00	5.00	5.00	5.00	5.00
Anions	8.00	8.00	8.02	8.00	8.01	8.00	8.01	8.01	8.01	8.01	8.02	8.01	8.00	8.00	8.00	8.00	8.00	8.01	8.01	8.01	8.00
XAn	0.32	0.32	0.32	0.32	0.33	0.32	0.32	0.32	0.32	0.32	0.33	0.32	0.31	0.32	0.32	0.33	0.33	0.33	0.33	0.33	0.34
XAb	0.30	0.31	0.32	0.33	0.34	0.34	0.35	0.36	0.37	0.38	0.39	0.40	0.41	0.42	0.43	0.44	0.45	0.45	0.46	0.47	0.48
SrO	-	-	-	-	-	-	-	-	-	-	-	-	-	-	-	-	-	-	-	-	-

Table E: continued

Sample	L2t-7	L2t-7	L2t-7	L2t-7	L2t-7	L2t-7	L2t-7	L2t-7	L2t-7	L2t-7	L2t-7	L2t-7	L2t-7	L2t-7	L2t-7	L2t-7	L2t-7	L2t-7	L2t-7	L2t-7	L2t-7
Mineral	Plag	Plag	Plag	Plag	Plag	Plag	Plag	Plag	Plag	Plag	Plag	Plag	Plag	Plag	Plag	Plag	Plag	Plag	Plag	Plag	Plag
Generation	core	rim	rim	core	core	core	core	core	core	core	core	core	core	core	core	core	core	core	core	core	core
SiO ₂	60.34	51.03	50.81	50.46	50.23	50.29	50.51	50.80	50.26	50.35	50.42	49.93	49.36	49.89	49.49	49.89	50.02	49.99	50.30	51.14	50.94
Al ₂ O ₃	25.61	31.31	31.12	31.60	31.59	31.49	31.64	31.57	31.76	31.57	32.15	32.06	31.61	31.33	31.59	31.80	31.69	31.57	31.65	30.93	30.08
FeO	0.21	0.28	0.23	0.31	0.24	0.22	0.20	0.17	0.19	0.15	0.20	0.21	0.21	-	0.19	0.18	0.23	-	0.21	0.18	0.96
CaO	7.37	14.24	14.17	14.69	14.68	14.93	14.79	14.64	14.69	14.87	15.07	14.95	15.18	14.95	14.81	14.71	14.99	14.74	14.47	13.91	13.27
Na ₂ O	7.44	3.46	3.44	3.30	3.20	3.32	3.28	3.26	3.20	3.07	3.10	3.00	2.98	2.94	2.97	2.93	3.20	3.19	3.17	3.54	3.61
K ₂ O	-	-	0.09	-	0.09	0.09	-	-	0.12	-	-	-	0.08	-	-	-	-	0.08	-	-	0.10
Total	100.97	100.32	99.87	100.35	100.03	100.33	100.42	100.43	100.22	100.02	100.94	100.15	99.42	99.11	99.05	99.51	100.13	99.56	99.82	99.70	99.45
Number of anions on the basis of 8 oxygen atoms																					
Si ⁴⁺	2.67	2.32	2.32	2.29	2.29	2.28	2.29	2.31	2.29	2.30	2.28	2.28	2.27	2.30	2.28	2.29	2.28	2.29	2.30	2.33	2.33
Al ³⁺	1.34	1.68	1.67	1.69	1.70	1.69	1.69	1.69	1.70	1.70	1.71	1.72	1.71	1.70	1.72	1.72	1.70	1.70	1.70	1.66	1.62
Fe ²⁺	0.01	0.01	0.01	0.01	0.01	0.01	0.01	0.01	0.01	0.01	0.01	0.01	0.01	-	0.01	0.01	0.01	-	0.01	0.01	0.04
Ca ²⁺	0.35	0.69	0.69	0.71	0.72	0.73	0.72	0.71	0.72	0.73	0.73	0.73	0.75	0.74	0.73	0.72	0.73	0.72	0.71	0.68	0.65
Na ⁺	0.64	0.30	0.30	0.29	0.28	0.29	0.29	0.29	0.28	0.27	0.27	0.27	0.27	0.26	0.27	0.26	0.28	0.28	0.28	0.31	0.32
K ⁺	-	-	0.01	-	-	-	-	-	0.01	-	-	-	-	-	-	-	-	-	-	-	0.01
Σcat	5.00	5.00	5.00	5.00	5.00	5.00	5.00	5.00	5.00	5.00	5.00	5.00	5.00	5.00	5.00	5.00	5.00	5.00	5.00	5.00	5.00
Anions	8.02	8.00	8.00	7.99	7.99	7.98	7.99	8.01	7.99	8.01	8.00	8.00	7.99	8.02	8.01	8.02	7.99	7.99	8.01	8.01	7.98
XAn	0.35	0.69	0.69	0.71	0.71	0.71	0.71	0.71	0.71	0.73	0.73	0.73	0.73	0.74	0.73	0.74	0.72	0.72	0.72	0.68	0.67
XAb	0.50	0.31	0.30	0.29	0.28	0.29	0.29	0.29	0.28	0.27	0.27	0.27	0.26	0.26	0.27	0.26	0.28	0.28	0.28	0.32	0.33
SrO	-	-	-	-	-	-	-	-	-	-	-	-	-	-	-	-	-	-	-	-	-

Table E: continued

Sample	L2t-7	L2t-7	L2t-7	L2t-7	L2t-7	L2t-7	L2t-7	L2t-7	L2t-7	L2t-7	L2t-7	L2t-7	L2t-7	L2t-7	L2t-7	L2t-7	L2t-7	L2t-7	L2t-7	L2t-7	L2t-7
Mineral	Plag	Plag	Plag1	Plag1	Plag1	Plag1	Plag1	Plag1	Plag1	Plag1	Plag1	Plag2	Plag2	Plag2	Plag2	Plag2	Plag2	Plag2	Plag2	Plag2	Plag2
Generation	rim	rim	Rim	Core	Core	Core	Core	Core	Core	Core	Rim	Rim	Core	Core	Core	Core	Core	Core	Core	Core	Core
SiO ₂	53.00	52.44	50.06	49.59	49.48	49.81	49.11	49.10	48.63	49.44	49.10	55.29	50.27	51.06	51.82	51.85	51.91	52.14	51.49	50.92	50.79
Al ₂ O ₃	30.58	30.15	32.16	31.87	32.06	32.15	32.11	32.40	32.37	32.52	32.83	28.86	30.85	31.24	30.94	30.68	30.17	30.28	30.59	30.97	30.59
FeO	0.26	0.31	0.28	0.34	0.42	0.43	0.57	0.27	0.20	0.28	0.23	0.19	-	-	-	-	-	-	0.27	-	-
CaO	13.05	12.84	15.18	15.08	14.93	15.09	15.29	15.64	15.64	15.74	15.66	11.46	14.42	14.08	14.00	13.61	13.17	13.61	13.59	14.16	14.09
Na ₂ O	4.15	4.14	3.00	2.85	2.81	2.73	2.73	2.45	2.32	2.71	2.71	5.13	3.27	3.69	3.65	4.12	3.91	3.98	3.80	3.55	3.55
K ₂ O	0.09	-	-	-	0.09	0.14	0.15	-	-	-	-	-	-	-	0.13	0.12	-	-	-	-	-
Total	101.13	99.87	100.69	99.72	99.79	100.34	99.96	99.86	99.15	100.69	100.53	100.92	98.81	100.07	100.53	100.37	99.16	100.00	99.74	99.59	99.02
Number of anions on the basis of 8 oxygen atoms																					
Si ⁴⁺	2.38	2.38	2.27	2.27	2.27	2.27	2.25	2.25	2.25	2.25	2.23	2.48	2.32	2.32	2.34	2.34	2.38	2.37	2.35	2.33	2.33
Al ³⁺	1.62	1.62	1.72	1.72	1.73	1.73	1.73	1.75	1.76	1.74	1.76	1.52	1.68	1.67	1.65	1.63	1.63	1.62	1.64	1.67	1.66
Fe ²⁺	0.01	0.01	0.01	0.01	0.02	0.02	0.02	0.01	0.01	0.01	0.01	0.01	-	-	-	-	-	-	0.01	-	-
Ca ²⁺	0.63	0.63	0.74	0.74	0.73	0.74	0.75	0.77	0.77	0.77	0.76	0.55	0.71	0.68	0.68	0.66	0.65	0.66	0.66	0.69	0.69
Na ⁺	0.36	0.36	0.26	0.25	0.25	0.24	0.24	0.22	0.21	0.24	0.24	0.45	0.29	0.32	0.32	0.36	0.35	0.35	0.34	0.31	0.32
K ⁺	0.01	-	0.00	0.00	0.01	0.01	0.01	0.00	0.00	0.00	0.00	-	-	-	0.01	0.01	-	-	-	-	-
Σcat.	5.00	5.00	5.00	5.00	5.00	5.00	5.00	5.00	5.00	5.00	5.00	5.00	5.00	5.00	5.00	5.00	5.00	5.00	5.00	5.00	5.00
Anions	8.00	8.01	8.00	8.01	8.00	8.01	7.99	8.02	8.02	8.00	7.99	8.01	8.01	7.99	8.01	7.97	8.02	8.00	8.00	8.00	8.00
XAn	0.63	0.63	0.74	0.75	0.74	0.75	0.75	0.78	0.79	0.76	0.76	0.55	0.71	0.68	0.67	0.64	0.65	0.65	0.66	0.69	0.69
XAb	0.36	0.37	0.26	0.25	0.25	0.24	0.24	0.22	0.21	0.24	0.24	0.45	0.29	0.32	0.32	0.35	0.35	0.35	0.34	0.31	0.31
SrO	-	-	0.00	0.00	161.55	0.00	0.00	0.00	0.00	0.00	146.07	-	115.06	121.40	179.41	167.01	-	116.64	175.45	137.96	-

Table E: continued

Sample	L2t-7	L2t-7	L2t-7	L2t-7	L2t-7	L2t-7	L2t-7	L2t-7	L2t-7	L2t-7	L2t-7	L2t-7	L2t-7	L2t-7	L2t-7	L2t-7	L2t-7	L2t-7	L2t-7	L2t-7	L2t-7
Mineral	Plag2	Plag2	Plag2	Plag2	Plag2	Plag2	Plag3	Plag3	Plag3	Plag3	Plag3	Plag3	Plag3	Plag3	Plag3	Plag3	Plag3	Plag3	Plag3	Plag3	Plag3
Generation	Core	Core	Core	Core	Core	Rim	Rim	Rim	Rim	Core	Core	Core	Core	Core	Core	Core	Core	Core	Core	Core	Core
SiO ₂	51.07	50.88	50.84	52.39	53.62	55	59.37	59.64	59.35	60.12	59.73	60.16	59.28	59.73	59.39	59.08	59.13	59.28	58.71	58.84	58.66
Al ₂ O ₃	31.21	31.25	31.05	30.52	29.55	28.56	24.91	24.89	25.09	25.47	25.82	25.55	25.56	25.25	25.53	25.46	25.37	25.28	25.64	26.06	25.27
FeO	-	-	-	-	0.27	0.27	0.40	-	-	-	-	-	-	-	-	-	-	-	-	-	-
CaO	14.42	14.41	14.22	13.54	12.08	11.41	7.00	7.18	7.23	7.39	7.51	7.33	7.50	7.53	7.65	7.78	7.50	7.68	7.78	7.72	7.88
Na ₂ O	3.36	3.50	3.40	3.90	4.82	5.04	7.48	7.39	7.4	7.51	7.33	7.44	7.29	7.27	7.46	7.28	7.38	7.24	7.17	7.23	7.40
K ₂ O	-	-	-	-	-	-	0.13	0.30	0.14	0.16	0.10	0.12	0.23	0.16	0.20	0.23	0.13	0.12	0.19	0.15	0.13
Total	100.07	100.04	99.52	100.35	100.35	100.3	99.3	99.41	99.2	100.64	100.5	100.59	99.86	99.94	100.23	99.83	99.51	99.61	99.48	99.99	99.33
Number of anions on the basis of 8 oxygen atoms																					
Si ⁴⁺	2.33	2.31	2.33	2.37	2.42	2.48	2.67	2.68	2.67	2.66	2.65	2.67	2.65	2.67	2.64	2.64	2.65	2.66	2.64	2.63	2.63
Al ³⁺	1.67	1.67	1.67	1.63	1.57	1.52	1.32	1.32	1.33	1.33	1.35	1.34	1.35	1.33	1.34	1.34	1.34	1.34	1.36	1.37	1.34
Fe ²⁺	-	-	-	-	0.01	0.01	0.01	-	-	-	-	-	-	-	-	-	-	-	-	-	-
Ca ²⁺	0.70	0.70	0.70	0.66	0.58	0.55	0.34	0.35	0.35	0.35	0.36	0.35	0.36	0.36	0.36	0.37	0.36	0.37	0.37	0.37	0.38
Na ⁺	0.30	0.31	0.30	0.34	0.42	0.44	0.65	0.64	0.64	0.64	0.63	0.64	0.63	0.63	0.64	0.63	0.64	0.63	0.62	0.63	0.64
K ⁺	-	-	-	-	-	-	0.01	0.02	0.01	0.01	0.01	0.01	0.01	0.01	0.01	0.01	0.01	0.01	0.01	0.01	0.01
Σ cat.	5.00	5.00	5.00	5.00	5.00	5.00	5.00	5.00	5.00	5.00	5.00	5.00	5.00	5.00	5.00	5.00	5.00	5.00	5.00	5.00	5.00
Anions	8.01	8.00	8.01	8.02	7.99	8.02	8.00	8.01	8.01	8.00	8.01	8.01	8.00	8.01	7.98	7.99	8.00	8.01	8.00	7.99	7.98
XAn	0.70	0.69	0.70	0.66	0.58	0.56	0.34	0.34	0.35	0.35	0.36	0.35	0.36	0.36	0.36	0.37	0.36	0.37	0.37	0.37	0.37
XAb	0.30	0.31	0.30	0.34	0.42	0.44	0.65	0.64	0.64	0.64	0.63	0.64	0.63	0.63	0.63	0.62	0.64	0.63	0.62	0.62	0.63
SrO	-	139.12	-	104.96	-	-	331.79	318.86	424.53	477.16	372.73	420.66	441.34	484.79	376.58	493.76	417.04	376.03	336.38	332.95	275.39

Table E: continued

Sample	L2t-7	L2t-7	L2t-7	L2t-7	L2t-7	L2t-7	L2t-7	L2t-7	L2t-7	L2t-7	L2t-7	L2t-7	L2t-7	L2t-7	L2t-7	L2t-7	L2t-7	L2t-7	L2t-7	L2t-7	L2t-7	
Mineral	Plag3	Plag3	Plag3	Plag3	Plag3	Plag3	Plag3	Plag3	Plag3	Plag3	Plag3	Plag3	Plag3	Plag3	Plag3	Plag3	Plag3	Plag3	Plag3	Plag3	Plag3	
Generation	Core	Core	Core	Core	Core	Core	Core	Core	Core	Core	Core	Core	Core	Core	Core	Core	Core	Core	Core	Rim	Rim	Rim
SiO ₂	58.52	58.51	58.52	58.46	58.26	58.16	58.16	57.93	58.64	58.03	58.30	58.11	58.24	58.71	58.77	58.82	58.49	59.35	59.12	59.28	59.20	
Al ₂ O ₃	25.64	25.69	25.59	25.55	25.55	25.86	25.78	25.71	26.28	26.18	26.48	26.35	26.03	26.05	25.94	25.50	25.34	25.57	25.46	24.71	25.13	
FeO	-	-	-	-	-	-	-	-	-	-	-	-	-	-	-	-	-	0.25	0.23	0.28	0.21	
CaO	7.81	7.80	7.92	7.90	8.06	7.94	8.01	8.09	8.60	8.38	8.67	8.67	8.44	8.13	8.15	7.90	7.84	7.62	7.53	7.28	7.10	
Na ₂ O	7.26	7.04	7.11	7.13	6.98	7.05	7.00	7.10	6.90	6.69	6.67	6.76	6.88	7.05	7.01	7.08	7.22	7.25	7.39	7.47	7.64	
K ₂ O	0.20	0.13	0.21	0.15	0.14	0.16	0.14	0.17	0.14	0.17	0.16	0.15	0.13	0.15	0.14	0.14	0.15	0.15	0.09	0.12	0.15	
Total	99.43	99.17	99.35	99.18	99.00	99.17	99.09	99.00	100.56	99.46	100.28	100.03	99.72	100.09	100.02	99.43	99.04	100.19	99.83	99.13	99.43	
Number of anions on the basis of 8 oxygen atoms																						
Si ⁴⁺	2.63	2.64	2.63	2.63	2.63	2.62	2.62	2.61	2.61	2.61	2.60	2.60	2.61	2.62	2.63	2.64	2.64	2.65	2.64	2.67	2.65	
Al ³⁺	1.36	1.36	1.36	1.36	1.36	1.37	1.37	1.37	1.38	1.39	1.39	1.39	1.38	1.37	1.37	1.35	1.35	1.34	1.34	1.31	1.33	
Fe ²⁺	-	-	-	-	-	-	-	-	-	-	-	-	-	-	-	-	-	0.01	0.01	0.01	0.01	
Ca ²⁺	0.38	0.38	0.38	0.38	0.39	0.38	0.39	0.39	0.41	0.40	0.41	0.42	0.41	0.39	0.39	0.38	0.38	0.36	0.36	0.35	0.34	
Na ⁺	0.63	0.62	0.62	0.62	0.61	0.62	0.61	0.62	0.59	0.58	0.58	0.59	0.60	0.61	0.61	0.62	0.63	0.63	0.64	0.65	0.66	
K ⁺	0.01	0.01	0.01	0.01	0.01	0.01	0.01	0.01	0.01	0.01	0.01	0.01	0.01	0.01	0.01	0.01	0.01	0.01	0.01	0.01	0.01	
Σ cat.	5.00	5.00	5.00	5.00	5.00	5.00	5.00	5.00	5.00	5.00	5.00	5.00	5.00	5.00	5.00	5.00	5.00	5.00	5.00	5.00	5.00	
Anions	7.98	8.01	7.99	8.00	8.00	7.99	8.00	7.98	8.00	8.01	8.01	8.00	8.00	8.00	8.00	8.01	7.99	8.00	7.99	7.99	7.98	
XAn	0.37	0.38	0.38	0.38	0.39	0.38	0.38	0.38	0.40	0.40	0.41	0.41	0.40	0.39	0.39	0.38	0.37	0.36	0.36	0.35	0.34	
XAb	0.62	0.62	0.61	0.61	0.61	0.61	0.61	0.61	0.59	0.59	0.58	0.58	0.59	0.61	0.60	0.61	0.62	0.63	0.64	0.65	0.66	
SrO	377.16	433.79	461.90	372.84	340.33	381.58	397.59	332.82	353.03	358.16	382.69	407.15	423.02	439.15	422.67	328.73	401.95	475.08	280.38	429.42	414.24	

Table E: continued

Sample	L2t-7	L2t-7	L2t-7	L2t-7	L2t-7	L2t-7	L2t-7	L2t-7	L2t-7	L2t-7	L2t-7	L2t-7	L2t-7	L2t-7	L2t-7	L2t-7	L2t-7	L2t-7	L2t-7	L2t-7	L2t-7
Mineral	Plag4	Plag4	Plag4	Plag4	Plag4	Plag4	Plag4	Plag4	Plag4	Plag4	Plag4	Plag4	Plag4	Plag4	Plag4	Plag4	Plag4	Plag5	Plag5	Plag5	Plag5
Generation	rim	rim	core	core	core	core	core	core	core	core	core	core	core	core	core	rim	rim	rim	rim	core	core
SiO ₂	55.84	55.88	55.46	55.35	55.93	55.91	55.88	55.77	56.03	55.92	55.71	55.7	55.86	55.9	56.67	55.98	56.47	59.92	60.6	60.19	60.31
Al ₂ O ₃	27.13	27.54	27.41	27.35	27.26	27.75	27.86	28.01	28.00	27.69	27.52	27.48	27.81	28.02	27.68	27.83	27.54	24.65	24.92	24.77	24.8
FeO	0.19	0.19	0.20	0.18	0.23	0.18	-	-	-	-	-	-	-	0.22	-	0.19	0.43	0.32	0.18	-	0.17
CaO	9.95	10.07	10.11	10.15	10.17	10.36	10.33	10.57	10.58	10.54	10.42	10.26	10.60	10.49	10.35	10.28	9.86	6.79	7.08	7.03	7.02
Na ₂ O	5.71	5.93	5.83	5.80	5.88	5.65	5.80	5.80	5.74	5.68	5.6	5.71	5.69	5.81	5.73	5.72	5.93	7.47	7.64	7.65	7.57
K ₂ O	0.16	0.13	0.19	0.18	0.18	0.10	0.14	0.16	-	0.20	0.14	0.18	-	0.24	0.16	0.14	0.25	0.15	0.15	0.21	0.15
Total	98.98	99.74	99.19	99.00	99.64	99.94	100.01	100.31	100.35	100.03	99.38	99.34	99.97	100.67	100.6	100.13	100.46	99.29	100.57	99.84	100.03
Number of anions on the basis of 8 oxygen atoms																					
Si ⁴⁺	2.54	2.52	2.51	2.51	2.52	2.52	2.51	2.50	2.51	2.52	2.52	2.52	2.52	2.50	2.54	2.52	2.53	2.70	2.69	2.69	2.69
Al ³⁺	1.45	1.46	1.46	1.46	1.45	1.47	1.48	1.48	1.48	1.47	1.47	1.47	1.48	1.48	1.46	1.47	1.45	1.31	1.30	1.30	1.30
Fe ²⁺	0.01	0.01	0.01	0.01	0.01	0.01	-	-	-	-	-	-	-	0.01	-	0.01	0.02	0.01	0.01	-	0.01
Ca ²⁺	0.49	0.49	0.49	0.49	0.49	0.50	0.50	0.51	0.51	0.51	0.51	0.50	0.51	0.50	0.50	0.50	0.47	0.33	0.34	0.34	0.34
Na ⁺	0.50	0.52	0.51	0.51	0.51	0.49	0.51	0.50	0.5	0.50	0.49	0.50	0.50	0.50	0.50	0.50	0.51	0.65	0.66	0.66	0.65
K ⁺	0.01	0.01	0.01	0.01	0.01	0.01	0.01	0.01		0.01	0.01	0.01		0.01	0.01	0.01	0.01	0.01	0.01	0.01	0.01
Σ cat.	5.00	5.00	5.00	5.00	5.00	5.00	5.00	5.00	5.00	5.00	5.00	5.00	5.00	5.00	5.00	5.00	5.00	5.00	5.00	5.00	5.00
Anions	8.01	7.99	7.98	7.99	7.99	8.01	7.99	7.98	8.00	8.00	8.01	8.00	8.00	7.98	8.01	8.00	7.99	8.02	8.01	8.00	8.01
XAn	0.49	0.48	0.48	0.49	0.48	0.5	0.49	0.5	0.50	0.50	0.50	0.49	0.51	0.49	0.50	0.49	0.47	0.33	0.34	0.33	0.34
XAb	0.50	0.51	0.51	0.50	0.51	0.49	0.5	0.49	0.50	0.49	0.49	0.50	0.49	0.49	0.50	0.50	0.51	0.66	0.66	0.66	0.66
SrO	284.01	-	-	-	-	-	-	-	-	-	-	-	-	232.01	-	280.63	-	-	-	240.26	344.41

Table E: continued

Sample	L2t-7	L2t-7	L2t-7	L2t-7	L2t-7	L2t-7	L2t-7	L2t-7	L2t-7	L2t-7	L2t-7	L2t-7	L2t-7	L2t-7	L2t-7	L2t-7	L2t-7	L2t-7	L2t-7	L2t-7	L2t-7
Mineral	Plag5	Plag5	Plag5	Plag5	Plag5	Plag5	Plag5	Plag5	Plag6	Plag6	Plag6	Plag6	Plag6	Plag6	Plag6	Plag6	Plag7	Plag7	Plag7	Plag7	Plag7
Generation	core	core	core	core	core	core	rim	rim	Rim	Core	Core	Core	Core	Core	Core	Rim	Rim	Core	Core	Core	Core
SiO ₂	60.42	60.38	60.39	60.22	59.62	60.00	59.79	59.98	52.45	53.37	52.63	52.91	52.71	52.93	52.45	52.26	60.37	60.08	59.73	59.79	60.47
Al ₂ O ₃	24.82	24.86	24.68	24.83	24.95	24.64	24.58	24.51	28.95	29.94	29.83	29.62	29.43	29.42	29.41	29.44	24.64	24.76	24.49	24.69	25.20
FeO	-	0.23	-	-	-	-	-	-	0.85	0.29	0.54	0.30	0.34	0.19	0.29	0.49	0.44	0.21	0.27	-	0.19
CaO	7.08	6.99	7.13	7.08	7.10	7.13	6.94	6.84	12.27	12.46	12.39	12.37	12.44	12.62	12.63	12.69	6.69	6.69	6.66	6.98	6.88
Na ₂ O	7.50	7.72	7.47	7.66	7.57	7.47	7.51	7.54	4.14	4.40	4.26	4.33	4.40	4.41	4.36	4.39	7.94	7.75	7.69	7.74	7.77
K ₂ O	0.10	0.26	0.22	0.130	0.13	0.20	0.13	0.10	0.16	0.16	0.18	0.16	0.13	0.13	0.12	-	0.21	0.14	0.23	0.12	-
Total	99.92	100.45	99.9	99.92	99.37	99.45	98.95	98.97	99.11	100.64	99.83	99.7	99.45	99.70	99.26	99.26	100.29	99.63	99.07	99.33	100.51
Number of anions on the basis of 8 oxygen atoms																					
Si ⁴⁺	2.70	2.68	2.70	2.69	2.67	2.69	2.70	2.70	2.40	2.40	2.39	2.41	2.40	2.41	2.40	2.39	2.68	2.69	2.69	2.68	2.68
Al ³⁺	1.31	1.30	1.30	1.31	1.32	1.30	1.31	1.30	1.56	1.59	1.60	1.59	1.58	1.58	1.58	1.58	1.29	1.31	1.30	1.30	1.32
Fe ²⁺	-	0.01	-	-	-	-	-	-	0.03	0.01	0.02	0.01	0.01	0.01	0.01	0.02	0.02	0.01	0.01	-	0.01
Ca ²⁺	0.34	0.33	0.34	0.34	0.34	0.34	0.34	0.33	0.60	0.60	0.60	0.60	0.61	0.61	0.62	0.62	0.32	0.32	0.32	0.34	0.33
Na ⁺	0.65	0.66	0.65	0.66	0.66	0.65	0.66	0.66	0.37	0.38	0.38	0.38	0.39	0.39	0.39	0.39	0.68	0.67	0.67	0.67	0.67
K ⁺	0.01	0.01	0.01	0.01	0.01	0.01	0.01	0.01	0.01	0.01	0.01	0.01	0.01	0.01	0.01	-	0.01	0.01	0.01	0.01	-
Σ cat.	5.00	5.00	5.00	5.00	5.00	5.00	5.00	5.00	5.00	5.00	5.00	5.00	5.00	5.00	5.00	5.00	5.00	5.00	5.00	5.00	5.00
Anions	8.02	7.99	8.02	8.00	8.00	8.01	8.02	8.02	8.00	8.00	8.00	8.00	7.99	8.00	7.99	7.98	7.98	8.00	7.99	7.99	8.01
XAn	0.34	0.33	0.34	0.34	0.34	0.34	0.34	0.33	0.62	0.60	0.61	0.61	0.61	0.61	0.61	0.61	0.31	0.32	0.32	0.33	0.33
XAb	0.65	0.66	0.65	0.66	0.65	0.65	0.66	0.66	0.38	0.39	0.38	0.38	0.39	0.38	0.38	0.39	0.67	0.67	0.67	0.66	0.67
SrO	252.11	216.38	307.84	-	-	328	228.18	384.13	-	-	-	-	-	-	-	-	-	-	-	-	-

Table E: continued

Sample	L2t-7	L2t-7	L2t-7	L2t-7	L2t-7	L2t-7	L2t-7	L2t-7	L2t-7	L2t-7	L2t-7	L2t-7	L2t-7	L2t-7	L2t-7	L2t-7	L2t-7	L2t-7	L2t-7	L2t-7	L2t-7
Mineral	Plag7	Plag7	Plag7	Plag7	Plag7	Plag7	Plag7	Plag7	Plag7	Plag7	Plag7	Plag8	Plag8	Plag8	Plag8	Plag8	Plag8	Plag8	Plag8	Plag8	Plag8
Generation	Core	Core	Core	Core	Core	Core	Core	Core	Core	Core	Rim	Rim	Core	Core	Core	Core	Core	Core	Core	Core	Core
SiO ₂	60.18	60.48	60.93	60.23	60.00	60.46	60.21	60.25	59.88	61.07	60.04	54.41	54.44	54.21	54.41	54.20	53.73	53.91	54.29	53.84	53.55
Al ₂ O ₃	24.80	24.99	24.86	24.71	24.45	25.06	24.77	24.66	24.35	24.87	24.57	28.89	29.18	28.76	28.75	29.10	28.91	29.02	28.66	28.79	29.01
FeO	-	-	-	-	0.18	-	-	-	-	-	-	0.21	0.26	-	0.28	0.22	0.22	-	-	0.30	0.23
CaO	6.82	6.74	6.85	6.85	6.66	6.74	6.91	6.68	6.64	6.85	6.55	11.49	11.72	11.66	11.47	11.69	11.69	11.80	11.78	11.63	11.50
Na ₂ O	7.87	7.87	7.89	7.92	7.79	7.87	7.63	7.82	7.81	7.87	7.78	4.90	4.99	4.79	4.89	4.97	4.98	5.00	4.96	5.01	4.91
K ₂ O	0.25	0.20	0.11	0.16	0.14	0.16	0.17	0.11	0.18	0.15	0.19	0.20	0.17	0.23	0.19	0.14	0.16	0.17	0.16	0.17	0.21
Total	99.93	100.28	100.65	99.86	99.21	100.29	99.70	99.53	99.09	100.80	99.13	100.09	100.75	99.65	100.00	100.32	99.70	99.90	99.85	99.75	99.40
Number of anions on the basis of 8 oxygen atoms																					
Si ⁴⁺	2.68	2.68	2.70	2.68	2.69	2.68	2.69	2.70	2.69	2.70	2.70	2.46	2.44	2.46	2.46	2.44	2.43	2.44	2.46	2.44	2.43
Al ³⁺	1.30	1.31	1.30	1.30	1.29	1.31	1.31	1.30	1.29	1.30	1.30	1.54	1.54	1.54	1.53	1.54	1.54	1.55	1.53	1.54	1.55
Fe ²⁺	-	-	-	-	0.01	-	-	-	-	-	-	0.01	0.01	-	0.01	0.01	0.01	-	-	0.01	0.01
Ca ²⁺	0.33	0.32	0.32	0.33	0.32	0.32	0.33	0.32	0.32	0.32	0.32	0.56	0.56	0.57	0.56	0.56	0.57	0.57	0.57	0.56	0.56
Na ⁺	0.68	0.68	0.68	0.68	0.68	0.68	0.66	0.68	0.68	0.67	0.68	0.43	0.43	0.42	0.43	0.43	0.44	0.44	0.44	0.44	0.43
K ⁺	0.01	0.01	0.01	0.01	0.01	0.01	0.01	0.01	0.01	0.01	0.01	0.01	0.01	0.01	0.01	0.01	0.01	0.01	0.01	0.01	0.01
Σ cat.	5.00	5.00	5.00	5.00	5.00	5.00	5.00	5.00	5.00	5.00	5.00	5.00	5.00	5.00	5.00	5.00	5.00	5.00	5.00	5.00	5.00
Anions	7.98	7.99	8.00	7.98	8.00	8.00	8.01	8.00	7.99	8.00	8.00	8.01	7.99	8.01	8.01	7.99	7.98	7.98	8.00	7.98	7.99
XAn	0.32	0.32	0.32	0.32	0.32	0.32	0.33	0.32	0.32	0.32	0.31	0.56	0.56	0.57	0.56	0.56	0.56	0.56	0.56	0.56	0.56
XAb	0.67	0.67	0.67	0.67	0.67	0.67	0.66	0.67	0.67	0.67	0.68	0.43	0.43	0.42	0.43	0.43	0.43	0.43	0.43	0.43	0.43
SrO	-	-	-	-	-	-	-	-	-	-	-	-	-	-	-	-	-	-	-	-	-

Table E: continued

Sample	L2t-7	L2t-7	L2t-7	L2t-7	L2t-7	L2t-7	L2t-7	L2t-7	L2t-7	L2t-7	L2t-7	L2t-7	L2t-7	L2t-7	L2t-7	L2t-7	L2t-7	L2t-7	L2t-7	L2t-7	L2t-7
Mineral	Plag9	Plag9	Plag9	Plag9	Plag9	Plag9	Plag9	Plag9	Plag9	Plag9	Plag8	Plag8	Plag8	Plag8	Plag10	Plag10	Plag10	Plag10	Plag10	Plag10	Plag10
Generation	Rim	Core	Core	Core	Core	Core	Core	core	Core	rim	Core	Core	Core	rim	Rim	Core	Core	Core	Core	Core	Core
SiO ₂	60.00	59.97	59.45	59.65	60.03	60.38	60.37	60.37	60.49	60.21	53.36	54.24	54.46	54.15	59.61	60.35	60.17	60.22	60.24	60.14	60.20
Al ₂ O ₃	25.08	24.76	24.92	24.34	24.76	24.69	24.68	24.65	24.49	24.57	28.77	28.88	28.98	28.79	24.55	24.86	24.88	24.95	24.82	24.72	24.93
FeO	0.45	0.38	0.29	0.27	0.25	0.25	0.33	-	0.35	0.61	0.18	0.26	0.27	0.56	0.34	0.27	0.21	0.19	0.21	-	0.22
CaO	6.85	6.91	6.90	6.86	6.92	6.89	6.61	6.74	6.60	6.58	11.61	11.74	11.77	11.28	6.68	7.08	6.63	6.80	6.74	6.81	6.61
Na ₂ O	7.83	7.55	7.55	7.75	7.61	7.97	7.81	7.96	7.86	7.82	5.01	4.93	4.97	5.15	7.72	7.67	7.59	7.76	7.81	7.91	7.67
K ₂ O	-	0.12	0.16	0.13	0.12	0.17	0.16	0.15	0.17	0.15	0.15	0.20	0.16	0.14	0.20	0.25	0.17	0.18	0.19	0.15	0.20
Total	100.22	99.69	99.27	99.00	99.70	100.36	99.97	99.87	99.96	99.94	99.08	100.25	100.61	100.07	99.11	100.48	99.65	100.10	100.02	99.74	99.84
Number of anions on the basis of 8 oxygen atoms																					
Si ⁴⁺	2.67	2.69	2.67	2.68	2.69	2.68	2.69	2.69	2.70	2.69	2.43	2.45	2.45	2.44	2.68	2.68	2.69	2.68	2.68	2.68	2.69
Al ³⁺	1.31	1.31	1.32	1.29	1.31	1.29	1.30	1.29	1.29	1.29	1.54	1.53	1.53	1.53	1.30	1.30	1.31	1.31	1.30	1.30	1.31
Fe ²⁺	0.02	0.01	0.01	0.01	0.01	0.01	0.01	-	0.01	0.02	0.01	0.01	0.01	0.02	0.01	0.01	0.01	0.01	0.01	-	0.01
Ca ²⁺	0.33	0.33	0.33	0.33	0.33	0.33	0.32	0.32	0.32	0.31	0.57	0.57	0.57	0.55	0.32	0.34	0.32	0.32	0.32	0.33	0.32
Na ⁺	0.68	0.66	0.66	0.68	0.66	0.69	0.67	0.69	0.68	0.68	0.44	0.43	0.43	0.45	0.67	0.66	0.66	0.67	0.67	0.68	0.66
K ⁺	-	0.01	0.01	0.01	0.01	0.01	0.01	0.01	0.01	0.01	0.01	0.01	0.01	0.01	0.01	0.01	0.01	0.01	0.01	0.01	0.01
Σ_{cat}	5.00	5.00	5.00	5.00	5.00	5.00	5.00	5.00	5.00	5.00	5.00	5.00	5.00	5.00	5.00	5.00	5.00	5.00	5.00	5.00	5.00
Anions	7.99	8.01	8.00	7.99	8.01	7.98	8.00	7.99	7.99	7.99	7.98	7.99	7.99	7.98	7.99	7.99	8.01	7.99	7.99	7.99	8.01
XAn	0.33	0.33	0.33	0.33	0.33	0.32	0.32	0.32	0.31	0.31	0.56	0.56	0.56	0.54	0.32	0.33	0.32	0.32	0.32	0.32	0.32
XAb	0.67	0.66	0.66	0.67	0.66	0.67	0.68	0.68	0.68	0.68	0.43	0.43	0.43	0.45	0.67	0.65	0.67	0.67	0.67	0.67	0.67
SrO	-	-	-	178.95	-	170.90	-	-	-	-	-	-	-	-	-	-	-	-	-	183.18	-

Table E: continued

Sample	L2t-7	L2t-7	L2t-7	L2t-7	L2t-7	L2t-7	L2t-7	L2t-7	L2t-7	L2t-7	L2t-7	L2t-7	L2t-7	L2t-7	L2t-7	L2t-7	L2t-7	L2t-7	L2t-7	L2t-7	L2t-7
Mineral	Plag10	Plag10	Plag10	Plag10	Plag10	Plag10	Plag10	Plag10	Plag10	Plag10	Plag10	Plag11	Plag11	Plag11	Plag11	Plag11	Plag11	Plag11	Plag11	Plag11	Plag11
Generation	Rim	Core	Core	Core	Core	Core	Core	core	Core	core	rim	rim	rim	core	core	core	core	core	core	core	core
SiO ₂	59.61	60.35	60.17	60.22	60.24	60.14	60.20	60.28	60.18	60.21	59.90	60.36	61.36	61.23	61.11	61.43	61.14	60.97	61.28	61.30	61.88
Al ₂ O ₃	24.55	24.86	24.88	24.95	24.82	24.72	24.93	24.97	24.70	24.93	24.39	24.40	24.07	24.78	24.32	23.95	24.05	23.86	23.82	24.01	24.14
FeO	0.34	0.27	0.21	0.19	0.21	-	0.22	0.22	0.24	0.20	0.35	0.00	0.00	0.00	0.00	0.00	0.00	0.00	0.00	0.00	0.00
CaO	6.68	7.08	6.63	6.80	6.74	6.81	6.61	6.66	6.75	6.82	6.65	6.49	6.09	6.07	6.42	6.10	5.91	5.93	5.91	5.90	5.92
Na ₂ O	7.72	7.67	7.59	7.76	7.81	7.91	7.67	7.96	7.65	7.81	7.77	7.94	8.10	8.35	8.21	8.33	7.98	8.19	8.06	8.30	8.40
K ₂ O	0.20	0.25	0.17	0.18	0.19	0.15	0.20	0.15	0.17	0.14	0.13	0.22	0.26	0.23	0.23	0.27	0.22	0.24	0.22	0.27	0.27
Total	99.11	100.48	99.65	100.10	100.02	99.74	99.84	100.25	99.68	100.10	99.19	99.42	99.89	100.66	100.29	100.07	99.30	99.18	99.29	99.79	100.61
Number of anions on the basis of 8 oxygen atoms																					
Si ⁴⁺	2.68	2.68	2.69	2.68	2.68	2.68	2.69	2.68	2.69	2.68	2.69	2.70	2.73	2.70	2.71	2.73	2.74	2.73	2.75	2.73	2.73
Al ³⁺	1.30	1.30	1.31	1.31	1.30	1.30	1.31	1.31	1.30	1.31	1.29	1.29	1.26	1.29	1.27	1.25	1.27	1.26	1.26	1.26	1.26
Fe ²⁺	0.01	0.01	0.01	0.01	0.01	-	0.01	0.01	0.01	0.01	0.01	0.00	0.00	0.00	0.00	0.00	0.00	0.00	0.00	0.00	0.00
Ca ²⁺	0.32	0.34	0.32	0.32	0.32	0.33	0.32	0.32	0.32	0.32	0.32	0.31	0.29	0.29	0.30	0.29	0.28	0.28	0.28	0.28	0.28
Na ⁺	0.67	0.66	0.66	0.67	0.67	0.68	0.66	0.69	0.66	0.67	0.68	0.69	0.70	0.71	0.71	0.72	0.69	0.71	0.70	0.72	0.72
K ⁺	0.01	0.01	0.01	0.01	0.01	0.01	0.01	0.01	0.01	0.01	0.01	0.01	0.01	0.01	0.01	0.02	0.01	0.01	0.01	0.02	0.02
Σ cat.	5.00	5.00	5.00	5.00	5.00	5.00	5.00	5.00	5.00	5.00	5.00	5.00	5.00	5.00	5.00	5.00	5.00	5.00	5.00	5.00	5.00
Anions	7.99	7.99	8.01	7.99	7.99	7.99	8.01	7.98	8.01	7.99	7.99	7.99	8.01	7.98	7.98	7.99	8.02	8.00	8.02	7.99	7.99
XAn	0.32	0.33	0.32	0.32	0.32	0.32	0.32	0.31	0.32	0.32	0.32	0.31	0.29	0.28	0.30	0.28	0.29	0.28	0.28	0.28	0.28
XAb	0.67	0.65	0.67	0.67	0.67	0.67	0.67	0.68	0.67	0.67	0.67	0.68	0.70	0.70	0.69	0.70	0.70	0.70	0.70	0.71	0.71
SrO	-	-	-	-	183.18	-	-	-	146.42	-	-	-	-	-	-	-	400.00	400.00	-	-	-

Table E: continued

Sample	L2t-7	L2t-7	L2t-7	L2t-7	L2t-7	L5GR-3	L5GR-3	L5GR-3	L5GR-3	L5GR-3	L5GR-3	L5GR-3	L5GR-3	L5GR-3	L5GR-3	L5GR-3	L5GR-3	L5GR-3	L5GR-3	L5GR-3	L5GR-3
Mineral	Plag11	Plag11	Plag11	Plag11	Plag11	Plag1	Plag1	Plag1	Plag1	Plag1	Plag1	Plag1	Plag1	Plag1	Plag1	Plag1	Plag1	Plag1	Plag1	plag3	plag3
Generation	core	core	core	rim	rim	Rim	Rim	Core	Core	Core	Core	Core	Core	Core	Core	Core	Core	Rim	Rim	Rim	Core
SiO ₂	60.95	61.66	61.27	61.69	61.27	51.02	51.05	51.66	52.47	53.18	53.26	53.06	52.76	52.88	51.77	50.44	50.36	49.04	48.84	55.24	54.75
Al ₂ O ₃	23.78	24.52	24.07	24.51	24.32	31.31	31.19	30.58	30.10	29.88	29.80	29.84	30.19	30.39	31.20	31.58	31.92	32.31	32.92	28.34	28.30
FeO	0.00	0.00	0.00	0.00	0.00	-	-	0.20	-	0.19	-	0.20	0.19	0.19	0.19	-	0.21	-	0.20	0.25	0.22
CaO	5.82	6.16	6.14	6.23	6.06	14.16	14.07	13.41	12.83	12.49	12.60	12.49	12.63	12.81	14.15	14.63	14.90	15.33	15.99	10.86	10.67
Na ₂ O	8.24	8.24	8.08	8.19	8.15	3.51	3.47	3.94	4.34	4.64	4.63	4.48	4.54	4.38	3.65	3.14	3.11	2.60	2.45	5.50	5.42
K ₂ O	0.28	0.23	0.26	0.11	0.17	-	-	-	0.10	-	-	-	-	-	-	-	-	-	-	0.11	0.15
Total	99.08	100.81	99.82	100.74	99.97	100.00	99.78	99.80	99.85	100.37	100.29	100.08	100.30	100.65	100.95	99.79	100.50	99.29	100.39	100.29	99.51
Number of anions on the basis of 8 oxygen atoms																					
Si ⁴⁺	2.73	2.72	2.73	2.72	2.72	2.32	2.33	2.35	2.38	2.40	2.40	2.40	2.38	2.38	2.33	2.30	2.29	2.26	2.23	2.48	2.48
Al ³⁺	1.26	1.27	1.26	1.27	1.27	1.68	1.68	1.64	1.61	1.59	1.58	1.59	1.61	1.61	1.66	1.70	1.71	1.75	1.77	1.50	1.51
Fe ²⁺	0.00	0.00	0.00	0.00	0.00	-	-	0.01	-	0.01	-	0.01	0.01	0.01	0.01	-	0.01	-	0.01	0.01	0.01
Ca ²⁺	0.28	0.29	0.29	0.29	0.29	0.69	0.69	0.65	0.62	0.60	0.61	0.61	0.61	0.62	0.68	0.72	0.72	0.76	0.78	0.52	0.52
Na ⁺	0.72	0.70	0.70	0.70	0.70	0.31	0.31	0.35	0.38	0.41	0.40	0.39	0.40	0.38	0.32	0.28	0.27	0.23	0.22	0.48	0.48
K ⁺	0.02	0.01	0.01	0.01	0.01	-	-	-	0.01	-	-	-	-	-	-	-	-	-	-	0.01	0.01
Σcat.	5.00	5.00	5.00	5.00	5.00	5.00	5.00	5.00	5.00	5.00	5.00	5.00	5.00	5.00	5.00	5.00	5.00	5.00	5.00	5.00	5.00
Anions	7.99	8.00	8.01	8.01	8.01	8.01	8.01	8.00	7.99	7.99	7.99	8.00	7.98	8.00	8.00	8.02	8.00	8.02	8.00	7.99	7.99
XAn	0.28	0.29	0.29	0.29	0.29	0.69	0.69	0.65	0.62	0.60	0.60	0.61	0.61	0.62	0.68	0.72	0.73	0.76	0.78	0.52	0.52
XAb	0.71	0.70	0.69	0.70	0.70	0.31	0.31	0.35	0.38	0.40	0.40	0.39	0.39	0.38	0.32	0.28	0.27	0.24	0.22	0.48	0.48
SrO				400.00		-	-	-	-	-	-	-	-	-	-	-	-	-	-	-	-

Table E: continued

Sample	L5GR-3	L5GR-3	L5GR-3	L5GR-3	L5GR-3	L5GR-3	L5GR-3	L5GR-3	L5GR-3	L5GR-3	L5GR-3	L5GR-3	L5GR-3	L5GR-3	L5GR-3	L5GR-3	L5GR-3	L5GR-3	L5GR-3	L5GR-3	L5GR-3
Mineral	plag3	plag3	plag3	plag3	plag3	plag3	plag3	plag3	plag3	plag3	Plag2	Plag2	Plag2	Plag2	Plag2	Plag2	Plag2	Plag2	Plag2	Plag2	Plag2
Generation	Core	Core	Core	Core	Core	Core	Core	Core	Core	Rim	Rim	Rim	Core	Core	Core	Core	Core	Core	Core	Core	Core
SiO ₂	55.32	55.59	56.15	56.18	56.39	56.04	56.14	56.45	55.88	55.85	49.73	49.16	51.69	53.55	53.62	53.84	54.20	54.17	53.96	54.61	53.76
Al ₂ O ₃	28.22	28.25	27.46	27.65	27.88	27.92	27.46	27.88	28.02	28.36	32.18	31.82	30.27	29.54	29.48	29.26	28.92	29.08	29.06	29.08	28.92
FeO	0.22	-	-	-	-	-	-	-	-	-	0.25	0.40	0.27	-	0.20	-	-	-	-	0.25	0.17
CaO	10.58	10.44	10.41	10.35	10.21	10.24	10.11	10.23	10.55	10.47	15.13	15.13	13.10	12.29	12.04	11.66	11.53	11.76	11.64	11.84	11.67
Na ₂ O	5.53	5.81	5.77	5.78	5.78	6.01	5.95	5.93	5.68	5.73	2.98	2.76	4.10	4.70	4.85	4.92	5.02	4.97	4.91	5.03	5.01
K ₂ O	0.16	0.23	0.14	0.22	0.13	0.17	0.17	0.10	0.13	0.17	-	-	-	-	-	0.10	-	0.14	-	-	0.10
Total	100.03	100.32	99.93	100.18	100.39	100.37	99.83	100.60	100.26	100.59	100.27	99.26	99.43	100.08	100.20	99.79	99.66	100.13	99.58	100.80	99.63
Number of anions on the basis of 8 oxygen atoms																					
Si ⁴⁺	2.49	2.49	2.53	2.52	2.53	2.51	2.53	2.52	2.51	2.50	2.26	2.26	2.36	2.42	2.42	2.44	2.46	2.44	2.45	2.45	2.44
Al ³⁺	1.50	1.49	1.46	1.46	1.47	1.47	1.46	1.47	1.48	1.49	1.73	1.73	1.63	1.57	1.57	1.56	1.54	1.55	1.55	1.54	1.54
Fe ²⁺	0.01	-	-	-	-	-	-	-	-	-	0.01	0.02	0.01	-	0.01	-	-	-	-	0.01	0.01
Ca ²⁺	0.51	0.50	0.50	0.50	0.49	0.49	0.49	0.49	0.51	0.50	0.74	0.75	0.64	0.59	0.58	0.57	0.56	0.57	0.57	0.57	0.57
Na ⁺	0.48	0.50	0.50	0.50	0.50	0.52	0.52	0.51	0.49	0.50	0.26	0.25	0.36	0.41	0.42	0.43	0.44	0.43	0.43	0.44	0.44
K ⁺	0.01	0.01	0.01	0.01	0.01	0.01	0.01	0.01	0.01	0.01	-	-	-	-	-	0.01	-	0.01	-	-	0.01
Σ cat.	5.00	5.00	5.00	5.00	5.00	5.00	5.00	5.00	5.00	5.00	5.00	5.00	5.00	5.00	5.00	5.00	5.00	5.00	5.00	5.00	5.00
Anions	7.99	7.98	8.00	8.00	8.01	7.98	7.99	8.00	8.00	7.99	8.00	8.00	7.99	8.00	7.99	8.00	8.01	7.99	8.01	8.00	7.99
XAn	0.51	0.49	0.50	0.49	0.49	0.48	0.48	0.49	0.50	0.50	0.74	0.75	0.64	0.59	0.58	0.56	0.56	0.56	0.57	0.57	0.56
XAb	0.48	0.50	0.50	0.50	0.50	0.51	0.51	0.51	0.49	0.49	0.26	0.25	0.36	0.41	0.42	0.43	0.44	0.43	0.43	0.43	0.43
SrO	-	-	-	-	-	-	-	-	-	-	-	-	-	-	-	-	-	-	-	-	206.78

Table E: continued

Sample	L5GR-3	L5GR-3	L5GR-3	L5GR-3	L5GR-3	L5GR-3	L5GR-3	L5GR-3	L5GR-3	L5GR-3	L5GR-3	L5GR-3	L5GR-3	L5GR-3	L5GR-3	L5GR-3	L5GR-3	L5GR-3	L5GR-3	L5GR-3	L5GR-3
Mineral	Plag2	Plag2	Plag2	Plag2	Plag4	Plag4	Plag4	Plag4	Plag4	Plag4	Plag4	Plag4	Plag4	Plag4	Plag4	Plag4	Plag5	Plag5	Plag5	Plag5	Plag5
Generation	Core	Core	Rim	Rim	rim	core	core	core	core	core	core	core	core	core	core	rim	Rim	Rim	Core	Core	Core
SiO ₂	53.75	53.41	51.5	51.34	58.04	57.3	56.74	56.91	56.71	56.51	57.54	57.33	57.6	57.34	57.7	57.1	57.2	57.83	58.21	58.59	58.05
Al ₂ O ₃	29.6	29.98	30.76	31.26	27.24	26.6	26.59	26.58	26.85	26.22	26.58	26.54	26.74	26.79	26.78	27.15	26.86	26.83	26.53	26.61	26.39
FeO	0.26	-	0.3	0.44	0.21	0.39	0.32	0.3	0.23	0.19	0.21	-	0.26	0.19	0.3	0.19	-	-	-	-	-
CaO	11.96	12.16	13.44	14.04	9.08	9	9.01	8.79	8.8	8.72	8.9	8.73	8.98	8.79	8.87	9.48	8.77	8.84	8.5	8.65	8.71
Na ₂ O	4.71	4.57	3.81	3.55	6.68	6.25	6.48	6.53	6.58	6.28	6.62	6.61	6.5	6.48	6.62	6.25	6.71	6.7	6.89	6.86	6.61
K ₂ O	0.13	0.11	-	-	0.1	0.13	-	-	-	0.13	0.12	0.19	0.13	-	0.15	0.09	-	-	0.14	-	-
Total	100.4	100.23	99.82	100.63	101.35	99.67	99.14	99.11	99.17	98.05	99.97	99.4	100.21	99.59	100.42	100.26	99.54	100.19	100.27	100.71	99.77
Number of anions on the basis of 8 oxygen atoms																					
Si ⁴⁺	2.42	2.41	2.34	2.32	2.57	2.58	2.57	2.57	2.56	2.59	2.58	2.58	2.58	2.58	2.58	2.56	2.57	2.58	2.6	2.6	2.61
Al ³⁺	1.57	1.59	1.65	1.67	1.42	1.41	1.42	1.42	1.43	1.41	1.4	1.41	1.41	1.42	1.41	1.43	1.42	1.41	1.39	1.39	1.4
Fe ²⁺	0.01	-	0.01	0.02	0.01	0.02	0.01	0.01	0.01	0.01	0.01	-	0.01	0.01	0.01	0.01	0	0	0	0	0
Ca ²⁺	0.58	0.59	0.66	0.68	0.43	0.44	0.44	0.43	0.43	0.43	0.43	0.42	0.43	0.42	0.42	0.46	0.42	0.42	0.41	0.41	0.42
Na ⁺	0.41	0.4	0.34	0.31	0.57	0.55	0.57	0.57	0.58	0.56	0.58	0.58	0.56	0.57	0.57	0.54	0.58	0.58	0.6	0.59	0.58
K ⁺	0.01	0.01	-	-	0.01	0.01	-	-	-	0.01	0.01	0.01	0.01	-	0.01	0.01	-	-	0.01	-	-
Σcat.	5	5	5	5	5	5	5	5	5	5	5	5	5	5	5	5	5	5	5	5	5
Anions	8	8	8	8	7.99	8.01	7.99	8	7.99	8.01	7.99	7.99	8	8.01	7.99	8	7.99	8	7.99	8.01	8.02
XAn	0.58	0.59	0.66	0.69	0.43	0.44	0.43	0.43	0.43	0.43	0.42	0.42	0.43	0.43	0.42	0.45	0.42	0.42	0.4	0.41	0.42
XAb	0.41	0.4	0.34	0.31	0.57	0.55	0.57	0.57	0.57	0.56	0.57	0.57	0.56	0.57	0.57	0.54	0.58	0.58	0.59	0.59	0.58
SrO	-	233.85	-	-	-	-	-	139.58	-	185.73	-	168.86	135.14	211.37	-	131.1	-	152.07	185.6	223.46	206.47

Table E: continued

Sample	L5GR-3	L5GR-3	L5GR-3	L5GR-3	L5GR-3	L5GR-3	L5GR-3	L5GR-3	L5GR-3	L5GR-3	L5GR-3	L5GR-3	L5GR-3	L5GR-3	L5GR-3	L5GR-3	L5GR-3	L5GR-3	L5GR-3	L5GR-3	L5GR-3
Mineral	Plag5	Plag5	Plag5	Plag5	Plag5	Plag5	Plag5	Plag5	Plag5	Plag5	Plag6	Plag6	Plag6	Plag6	Plag6	Plag6	Plag6	Plag6	Plag6	Plag6	Plag6
Generation	Core	Core	Core	Core	Core	Core	Core	Core	Rim	Rim	Rim	Rim	Core	Core	Core	Core	Core	Core	Core	Core	Core
SiO ₂	57.71	57.74	58.51	58.68	58.41	58.96	58.58	58.93	58.09	58.24	55.78	55.76	55.82	56.11	55.61	56.32	55.79	56.05	56.24	56.18	56.22
Al ₂ O ₃	26.66	26.05	25.98	25.92	26.24	26.24	26.18	26.20	26.91	26.63	27.99	28.03	27.85	27.92	27.86	27.93	28.25	27.99	27.95	28.33	28.01
FeO	-	-	-	-	-	-	-	-	-	0.38	0.19	0.20	-	-	-	-	-	-	-	-	-
CaO	8.62	8.49	8.32	8.32	8.34	8.34	8.42	8.37	8.71	8.83	10.58	10.58	10.38	10.43	10.22	10.23	10.40	10.33	10.30	10.22	10.52
Na ₂ O	6.82	6.96	7.06	7.01	7.01	7.21	7.10	7.00	6.90	6.74	5.82	5.78	5.77	5.93	5.79	5.94	6.01	5.87	5.96	6.00	5.67
K ₂ O	0.09	-	0.10	0.12	0.09	0.14	0.16	0.13	0.16	-	0.13	-	-	-	-	0.11	-	0.11	0.10	-	-
Total	99.90	99.24	99.97	100.05	100.08	100.89	100.45	100.63	100.77	100.83	100.49	100.35	99.82	100.40	99.50	100.52	100.45	100.34	100.55	100.74	100.42
Number of anions on the basis of 8 oxygen atoms																					
Si ⁴⁺	2.58	2.60	2.62	2.62	2.61	2.61	2.61	2.62	2.58	2.59	2.50	2.50	2.52	2.51	2.51	2.52	2.49	2.51	2.51	2.50	2.52
Al ³⁺	1.41	1.38	1.37	1.36	1.38	1.37	1.37	1.37	1.41	1.40	1.48	1.48	1.48	1.47	1.48	1.47	1.49	1.48	1.47	1.49	1.48
Fe ²⁺	0.00	0.00	0.00	0.00	0.00	0.00	0.00	0.00	0.00	0.01	0.01	0.01	-	-	-	-	-	-	-	-	-
Ca ²⁺	0.41	0.41	0.40	0.40	0.40	0.40	0.40	0.40	0.41	0.42	0.51	0.51	0.50	0.50	0.50	0.49	0.50	0.50	0.49	0.49	0.51
Na ⁺	0.59	0.61	0.61	0.61	0.61	0.62	0.61	0.60	0.59	0.58	0.51	0.50	0.50	0.51	0.51	0.51	0.52	0.51	0.52	0.52	0.49
K ⁺	0.01	-	0.01	0.01	0.01	0.01	0.01	0.01	0.01	-	0.01	0.00	-	-	-	0.01	-	0.01	0.01	-	-
Σcat.	5.00	5.00	5.00	5.00	5.00	5.00	5.00	5.00	5.00	5.00	5.00	5.00	5.00	5.00	5.00	5.00	5.00	5.00	5.00	5.00	5.00
Anions	7.99	7.99	7.99	8.00	7.99	7.98	7.98	8.00	7.98	8.00	7.98	7.99	8.00	7.99	8.00	7.99	7.98	7.99	7.99	7.99	8.01
XAn	0.41	0.40	0.39	0.39	0.39	0.39	0.39	0.39	0.41	0.42	0.50	0.50	0.50	0.49	0.49	0.48	0.49	0.49	0.49	0.48	0.51
XAb	0.59	0.60	0.60	0.60	0.60	0.61	0.60	0.60	0.58	0.58	0.50	0.50	0.50	0.51	0.51	0.51	0.51	0.50	0.51	0.52	0.49
SrO	118.27	-	189.39	155.59	-	172.65	175.97	129.77	-	172.17	291.32	232.32	122.36	219.41	215.34	257.28	160.72	143.49	172.98	181.82	303.56

Table E: continued

Sample	L5GR-3	L5GR-3	L5GR-3	L5GR-3	L5GR-3	L5GR-3	L5GR-3	L5GR-3	L5GR-3	L5GR-3	L5GR-3	L5GR-3	L5GR-3	L5GR-3	L5GR-3	L5GR-3	L5GR-3	L5GR-3	L5GR-3	L5GR-3	
Mineral	Plag6	Plag6	Plag6	Plag6	Plag6	Plag6	Plag6	Plag7	Plag7	Plag7	Plag7	Plag7	Plag7	Plag7	Plag7	Plag7	Plag7	Plag7	Plag7	Plag7	
Generation	Core	Core	Core	Core	Core	Rim	Rim	Rim	Core	Core	Core	Core	Core	Core	Core	Core	Core	Core	Core	Rim	Rim
SiO ₂	55.37	55.58	55.45	55.34	55.65	55.42	55.22	56.67	55.93	56.35	56.02	56.14	56.07	56.13	56.31	56.20	56.32	56.00	56.30	56.30	52.93
Al ₂ O ₃	27.78	28.15	28.50	28.16	28.35	28.39	28.30	27.52	27.41	27.62	27.46	27.22	27.59	27.34	27.31	27.73	27.37	28.06	27.85	27.52	29.75
FeO	-	-	-	-	0.20	0.31	0.34	0.25	0.23		0.21		0.22	0.00		0.21	0.26	0.26	0.37	0.40	-
CaO	10.53	10.50	10.55	10.51	10.81	10.94	10.83	10.09	10.04	9.99	9.75	9.63	9.65	9.59	9.59	9.79	9.77	9.71	9.89	9.71	12.34
Na ₂ O	5.76	5.87	5.67	5.78	5.55	5.71	5.50	6.16	6.00	6.09	6.15	6.12	6.19	6.38	6.16	6.16	6.19	6.13	6.00	6.12	4.64
K ₂ O	-	-	0.11	0.14	0.12	-	-	-	0.09	0.10	-	-	-	-	-	-	-	-	-	-	-
Total	99.43	100.10	100.28	99.93	100.67	100.78	100.20	100.69	99.71	100.16	99.59	99.11	99.73	99.44	99.36	100.09	99.91	100.15	100.41	100.05	99.66
Number of anions on the basis of 8 oxygen atoms																					
Si ⁴⁺	2.50	2.50	2.49	2.49	2.49	2.48	2.48	2.53	2.52	2.53	2.53	2.54	2.52	2.53	2.54	2.52	2.53	2.51	2.52	2.53	2.40
Al ³⁺	1.48	1.49	1.51	1.49	1.50	1.49	1.50	1.45	1.46	1.46	1.46	1.45	1.46	1.45	1.45	1.47	1.45	1.48	1.47	1.46	1.59
Fe ²⁺	-	-	-	-	0.01	0.01	0.01	0.01	0.01	-	0.01	-	0.01	-	-	0.01	0.01	0.01	0.01	0.02	-
Ca ²⁺	0.51	0.50	0.51	0.51	0.52	0.52	0.52	0.48	0.48	0.48	0.47	0.47	0.47	0.46	0.46	0.47	0.47	0.47	0.47	0.47	0.60
Na ⁺	0.51	0.51	0.49	0.50	0.48	0.49	0.48	0.53	0.52	0.53	0.54	0.54	0.54	0.56	0.54	0.54	0.54	0.53	0.52	0.53	0.41
K ⁺	-	-	0.01	0.01	0.01	-	-	-	0.01	0.01	-	-	-	-	-	-	-	-	-	-	-
Σcat.	5.00	5.00	5.00	5.00	5.00	5.00	5.00	5.00	5.00	5.00	5.00	5.00	5.00	5.00	5.00	5.00	5.00	5.00	5.00	5.00	5.00
Anions	7.99	7.98	7.99	7.98	7.99	7.98	7.99	7.99	7.98	7.99	7.99	8.00	7.98	7.98	8.00	7.99	7.99	7.98	7.99	7.99	7.99
XAn	0.50	0.50	0.50	0.50	0.51	0.51	0.52	0.48	0.48	0.47	0.47	0.47	0.46	0.45	0.46	0.47	0.47	0.47	0.48	0.47	0.60
XAb	0.50	0.50	0.49	0.50	0.48	0.49	0.48	0.52	0.52	0.52	0.53	0.53	0.54	0.55	0.54	0.53	0.53	0.53	0.52	0.53	0.40
SrO	-	269.30	168.46	214.60	168.24	231.67	126.33	-	201.46	176.23	209.51	-	-	-	128.08	-	123.89	184.35	-	239.44	-

Table E: continued

Sample	L5GR-3	L5GR-3	L5GR-3	L5GR-3	L5GR-3	L5GR-3	L5GR-3	L5GR-3	L5GR-3	L5GR-3	L5GR-3	L5GR-3	L5GR-3	L5GR-3	L5GR-3	L5GR-3	L5GR-3	L5GR-3	L5GR-3	L5GR-3	L5GR-3
Mineral	plag8	plag8	plag8	plag8	plag8	plag8	plag8	plag8	plag8	plag8	Matrix	Matrix	Matrix	Matrix	Matrix	Matrix	Matrix	Matrix	Matrix	Matrix	Matrix
Generation	Core	Core	Core	Core	Core	Core	Core	Core	Core	Rim	Rim	Core	Core	Core	Core	Core	Core	Core	Core	Core	Core
SiO ₂	50.43	50.04	54.73	55.05	55.1	54.76	54.81	54.66	54.94	54.4	58.26	59.21	58.97	59.35	59.49	60.58	60.98	61.24	61.12	60.72	60.3
Al ₂ O ₃	31.11	31.06	28.17	27.83	27.74	28.01	27.98	28.23	28.27	28.45	26.43	26.13	25.23	25.22	24.53	24.51	24.65	23.65	24.51	25.05	25.2
FeO	-	0.22	-	-	-	-	-	-	-	-	0.21	-	-	-	-	-	-	-	-	-	-
CaO	14.1	14.38	10.84	10.51	10.53	10.42	10.45	10.65	10.78	11.02	8.45	8.29	7.43	6.98	6.6	6.45	6.42	5.72	6.68	6.79	7
Na ₂ O	3.50	3.42	5.39	5.61	5.75	5.76	5.57	5.42	5.46	5.51	6.89	7.05	7.47	7.61	8	8.06	8.29	8.36	8.09	8.22	7.97
K ₂ O	-	-	-	-	0.10	-	0.18	-	0.09	-	0.12	-	0.11	0.17	0.13	0.09	-	0.09	-	-	-
Total	99.14	99.11	99.13	99	99.22	98.96	98.99	98.97	99.54	99.38	100.36	100.68	99.21	99.33	98.98	99.69	100.34	99.06	100.4	100.78	100.47
Number of anions on the basis of 8 oxygen atoms																					
Si ⁴⁺	2.31	2.30	2.49	2.50	2.50	2.49	2.49	2.49	2.49	2.46	2.6	2.63	2.65	2.66	2.67	2.70	2.70	2.75	2.71	2.68	2.67
Al ³⁺	1.68	1.68	1.51	1.49	1.48	1.5	1.50	1.51	1.51	1.52	1.39	1.37	1.34	1.33	1.30	1.29	1.29	1.25	1.28	1.30	1.32
Fe ²⁺	-	0.01	-	-	-	-	-	-	-	-	0.01	-	-	-	-	-	-	-	-	-	-
Ca ²⁺	0.69	0.71	0.53	0.51	0.51	0.51	0.51	0.52	0.52	0.53	0.40	0.40	0.36	0.34	0.32	0.31	0.30	0.28	0.32	0.32	0.33
Na ⁺	0.31	0.30	0.48	0.49	0.50	0.51	0.49	0.48	0.48	0.48	0.60	0.61	0.65	0.66	0.70	0.70	0.71	0.73	0.70	0.70	0.68
K ⁺	-	-	-	-	0.01	-	0.01	-	0.01	-	0.01	-	0.01	0.01	0.01	0.01	-	0.01	-	-	-
Σcat.	5.00	5.00	5.00	5.00	5.00	5.00	5.00	5.00	5.00	5.00	5.00	5.00	5.00	5.00	5.00	5.00	5.00	5.00	5.00	5.00	5.00
Anions	8.00	7.99	8.00	8.00	7.98	7.98	7.99	8.01	8.00	7.98	7.99	8.01	7.99	7.99	7.98	8.00	7.99	8.00	8.00	7.98	7.99
XAn	0.69	0.70	0.53	0.51	0.50	0.50	0.50	0.52	0.52	0.52	0.40	0.39	0.35	0.33	0.31	0.30	0.30	0.27	0.31	0.31	0.33
XAb	0.31	0.30	0.47	0.49	0.49	0.50	0.49	0.48	0.48	0.48	0.59	0.61	0.64	0.66	0.68	0.69	0.700	0.72	0.69	0.69	0.67
SrO	160.42	169.18	176.3	222.24	-	-	167.84	159.63	197.29	-	-	-	-	-	208.54	-	240.7	-	-	-	212.49

Table E: continued

Sample	L5GR-3	L5GR-3	L5GR-3	L5GR-3	CR1a	CRa1	CR1a	CRa2	CR1a	CRa3	CR1a	CRa4	CR1a	CRa5	CR1a	CRa6	CR1a	CRa7	CR1a	CR1a	CRa1	
Mineral	Matrix	Matrix	Matrix	Matrix	Plag1	Plag1	Plag1	Plag1	Plag1	Plag1	Plag1	Plag1	Plag1	Plag1	Plag1	Plag1	Plag1	Plag1	Plag1	Plag1	Plag2	Plag2
Generation	Core	Rim	rim	Rim	rim	rim	core	core	core	core	core	core	core	core	core	core	core	rim	rim	rim	rim	core
SiO ₂	60.53	59.11	59.32	58.43	59.43	59.49	59.72	59.66	59.33	59.79	59.77	60.13	59.89	59.97	59.83	59.72	59.62	59.60	59.56	59.40	59.70	
Al ₂ O ₃	25.20	25.78	25.61	25.99	25.26	25.36	25.19	25.25	25.38	25.35	25.37	25.65	25.34	25.61	25.85	25.05	25.28	25.50	25.67	25.73	25.51	
FeO	-	-	-	-	-	-	-	0.15	-	-	-	-	-	-	-	-	-	-	-	-	-	
CaO	7.27	7.59	7.42	8.02	7.33	7.17	7.50	7.33	7.34	7.19	7.51	7.50	7.32	7.60	7.53	7.35	7.53	7.40	7.28	7.52	7.53	
Na ₂ O	7.81	7.45	7.25	7.28	7.41	7.39	7.42	7.31	7.31	7.29	7.35	7.35	7.47	7.43	7.29	7.64	7.36	7.33	7.54	7.53	7.42	
K ₂ O	0.09	-	-	-	0.34	0.31	0.27	0.26	0.32	0.32	0.28	0.27	0.34	0.33	0.29	0.32	0.36	0.31	0.32	0.11	-	
Total	100.90	99.93	99.60	99.72	99.77	99.73	100.08	99.96	99.68	99.94	100.27	100.90	100.37	100.95	100.79	100.07	100.16	100.13	100.37	100.29	100.16	
Number of anions on the basis of 8 oxygen atoms																						
Si ⁴⁺	2.67	2.64	2.66	2.61	2.66	2.66	2.66	2.67	2.66	2.67	2.66	2.66	2.66	2.65	2.65	2.66	2.66	2.66	2.64	2.64	2.66	
Al ³⁺	1.31	1.36	1.35	1.37	1.33	1.34	1.32	1.33	1.34	1.33	1.33	1.34	1.33	1.33	1.35	1.31	1.33	1.34	1.34	1.35	1.34	
Fe ²⁺	-	-	-	-	-	-	-	0.01	-	-	-	-	-	-	-	-	-	-	-	-	-	
Ca ²⁺	0.34	0.36	0.36	0.38	0.35	0.34	0.36	0.35	0.35	0.34	0.36	0.36	0.35	0.36	0.36	0.35	0.36	0.35	0.35	0.36	0.36	
Na ⁺	0.67	0.64	0.63	0.63	0.64	0.64	0.64	0.63	0.63	0.63	0.63	0.63	0.64	0.64	0.63	0.66	0.64	0.63	0.65	0.65	0.64	
K ⁺	0.01	-	-	-	0.02	0.02	0.02	0.01	0.02	0.02	0.02	0.02	0.02	0.02	0.02	0.02	0.02	0.02	0.02	0.01	-	
Σcat.	5.00	5.00	5.00	5.00	5.00	5.00	5.00	5.00	5.00	5.00	5.00	5.00	5.00	5.00	5.00	5.00	5.00	5.00	5.00	5.00	5.00	
Anions	7.99	7.99	8.02	7.98	7.99	8.00	8.00	8.01	8.00	8.01	8.00	8.01	7.99	7.99	8.00	7.98	7.99	8.00	7.98	7.99	8.01	
XAn	0.34	0.36	0.36	0.38	0.35	0.34	0.35	0.35	0.35	0.35	0.36	0.35	0.34	0.35	0.36	0.34	0.35	0.35	0.34	0.35	0.36	
XAb	0.66	0.64	0.64	0.62	0.63	0.64	0.63	0.63	0.63	0.64	0.63	0.63	0.64	0.63	0.63	0.64	0.63	0.63	0.64	0.64	0.64	
SrO	-	162.96	190.50	268.08	360.60	763.90	487.37	434.60	381.98	339.20	402.78	731.70	318.05	315.94	600.86	389.25	473.44	410.82	-	379.23	304.90	

Table E: continued

Sample	CR1a	CRA2	CR1a	CRA3	CR1a	CR1a	CR1a	CR1a	CR1a	CR1a	CR1a	CR1a	CR1a	CR1a	CR1a	CR1a	CR1a	CR1a	CR1a	CR1a	CR1a
Mineral	Plag2	Plag2	Plag2	Plag2	Plag2	Plag3	Plag3	Plag3	Plag3	Plag3	Plag3	Plag3	Plag3	Plag3	Plag3	Plag3	Plag4	Plag4	Plag4	Plag4	Plag4
Generation	core	core	core	core	rim	rim	core	core	core	core	core	core	core	core	core	rim	rim	core	core	core	core
SiO ₂	59.57	59.06	59.12	59.19	58.77	59.08	59.81	60.16	60.27	59.52	59.41	59.65	59.53	60.47	60.37	59.92	59.36	59.47	59.66	59.28	59.73
Al ₂ O ₃	25.77	25.60	25.30	25.40	25.63	25.09	25.48	25.29	25.56	25.45	25.38	25.73	25.17	25.42	25.48	25.57	25.35	25.47	25.26	25.47	25.44
FeO	-	-	-	-	-	0.01	-	-	-	-	-	-	-	-	-	-	0.25	0.46	0.27	0.36	0.26
CaO	7.49	7.52	7.37	7.41	7.61	7.44	7.37	7.50	7.42	7.45	7.34	7.31	7.24	7.43	7.28	7.22	7.33	7.16	7.49	7.34	7.19
Na ₂ O	7.35	7.59	7.57	7.46	7.54	7.33	7.66	7.71	7.60	7.51	7.62	7.64	7.33	7.50	7.66	7.45	7.42	7.43	7.43	7.32	7.29
K ₂ O	-	-	-	-	-	0.10	0.13	0.11	-	-	-	0.09	0.09	-	0.10	0.14	0.34	0.31	0.27	0.32	0.31
Total	100.17	99.77	99.35	99.46	99.55	99.04	100.45	100.77	100.85	99.93	99.74	100.42	99.36	100.82	100.89	100.31	100.05	100.30	100.38	100.09	100.22
Number of anions on the basis of 8 oxygen atoms																					
Si ⁴⁺	2.65	2.64	2.65	2.65	2.63	2.66	2.65	2.66	2.67	2.66	2.65	2.65	2.67	2.68	2.67	2.66	2.65	2.65	2.65	2.64	2.66
Al ³⁺	1.35	1.35	1.34	1.34	1.35	1.33	1.33	1.32	1.33	1.34	1.34	1.34	1.33	1.33	1.33	1.34	1.33	1.34	1.32	1.34	1.34
Fe ²⁺	-	-	-	-	-	-	-	-	-	-	-	-	-	-	-	-	0.01	0.02	0.01	0.01	0.01
Ca ²⁺	0.36	0.36	0.35	0.36	0.36	0.36	0.35	0.36	0.35	0.36	0.35	0.35	0.35	0.35	0.34	0.34	0.35	0.34	0.36	0.35	0.34
Na ⁺	0.64	0.66	0.66	0.65	0.65	0.64	0.66	0.66	0.65	0.65	0.66	0.66	0.64	0.64	0.66	0.64	0.64	0.64	0.64	0.63	0.63
K ⁺	-	-	-	-	-	0.01	0.01	0.01	-	-	-	0.01	0.01	-	0.01	0.01	0.02	0.02	0.02	0.02	0.02
Σcat.	5.00	5.00	5.00	5.00	5.00	5.00	5.00	5.00	5.00	5.00	5.00	5.00	5.00	5.00	5.00	5.00	5.00	5.00	5.00	5.00	5.00
Anions	8.01	7.98	7.99	8.00	7.98	8.01	7.99	7.99	8.01	8.00	7.99	7.99	8.02	8.02	8.00	8.01	7.98	7.99	7.99	7.99	8.01
XAn	0.36	0.35	0.35	0.35	0.36	0.36	0.34	0.35	0.35	0.35	0.35	0.34	0.35	0.35	0.34	0.35	0.35	0.34	0.35	0.35	0.35
XAb	0.64	0.65	0.65	0.65	0.64	0.64	0.65	0.65	0.65	0.65	0.65	0.65	0.64	0.65	0.65	0.65	0.63	0.64	0.63	0.63	0.64
SrO	357.90	568.98	452.48	610.25	432.25	382.20	-	646.77	498.82	366.27	471.09	0.00	438.72	375.91	407.63	-	142.80	302.74	193.01	151.32	134.33

Table E: continued

Sample	CR1a	CR1a	CR1a	CR1a	CR1a	CR1a	CR1a	CR1a	CR1a	CR1a	CR1a	CR1a	CR1a	CR1a	CR1a	CR1a	CR1a	CR1a	CR1a	CR1a	CR1a
Mineral	Plag4	Plag4	Plag4	Plag4	Plag4	Plag4	Plag4	Plag4	Plag4	Plag4	Plag5	Plag5	Plag5	Plag5	Plag5	Plag5	Plag5	Plag6	Plag6	Plag6	Plag6
Generation	rim	core	core	core	core	core	core	core	core	rim	rim	core	core	core	core	rim	rim	core	core	core	core
SiO ₂	59.36	59.47	59.66	59.28	59.73	59.73	59.82	60.30	59.56	59.56	59.36	59.63	59.53	60.02	59.09	59.18	58.63	59.17	59.46	59.39	59.58
Al ₂ O ₃	25.35	25.47	25.26	25.47	25.44	25.46	25.43	25.50	25.37	25.60	25.84	25.59	25.87	25.91	25.42	25.53	25.20	25.07	25.53	25.50	25.82
FeO	0.25	0.46	0.27	0.36	0.26	0.34	0.20	0.25	0.26	0.41	0.43	0.21	0.44	0.38	0.48	0.54	0.41	0.45	0.30	0.50	0.32
CaO	7.33	7.16	7.49	7.34	7.19	7.50	7.31	7.46	7.53	7.39	7.52	7.52	7.48	7.55	7.37	7.40	7.15	7.18	7.45	7.33	7.31
Na ₂ O	7.42	7.43	7.43	7.32	7.29	7.37	7.48	7.56	7.36	7.35	7.56	7.43	7.38	7.59	7.60	7.50	7.47	7.53	7.53	7.66	7.66
K ₂ O	0.34	0.31	0.27	0.32	0.31	0.28	0.34	0.31	0.36	0.30	-	-	-	-	-	-	0.14	0.10	-	-	0.09
Total	100.05	100.30	100.38	100.09	100.22	100.68	100.58	101.38	100.44	100.61	100.71	100.38	100.70	101.45	99.96	100.15	99.00	99.50	100.27	100.38	100.78
Number of anions on the basis of 8 oxygen atoms																					
Si ₄₊	2.65	2.65	2.65	2.64	2.66	2.65	2.65	2.65	2.65	2.64	2.63	2.65	2.64	2.64	2.64	2.64	2.64	2.65	2.65	2.64	2.63
Al ₃₊	1.33	1.34	1.32	1.34	1.34	1.33	1.33	1.32	1.33	1.34	1.35	1.34	1.35	1.34	1.34	1.34	1.34	1.32	1.34	1.33	1.35
Fe ₂₊	0.01	0.02	0.01	0.01	0.01	0.01	0.01	0.01	0.01	0.02	0.02	0.01	0.02	0.01	0.02	0.02	0.02	0.02	0.01	0.02	0.01
Ca ₂₊	0.35	0.34	0.36	0.35	0.34	0.36	0.35	0.35	0.36	0.35	0.36	0.36	0.36	0.36	0.35	0.35	0.35	0.34	0.36	0.35	0.35
Na ₊	0.64	0.64	0.64	0.63	0.63	0.63	0.64	0.65	0.63	0.63	0.65	0.64	0.63	0.65	0.66	0.65	0.65	0.65	0.65	0.66	0.66
K ₊	0.02	0.02	0.02	0.02	0.02	0.02	0.02	0.02	0.02	0.02	-	-	-	-	-	-	0.01	0.01	-	-	0.01
Σ cat.	5.00	5.00	5.00	5.00	5.00	5.00	5.00	5.00	5.00	5.00	5.00	5.00	5.00	5.00	5.00	5.00	5.00	5.00	5.00	5.00	5.00
Anions	7.98	7.99	7.99	7.99	8.01	7.99	7.99	7.98	7.98	7.99	7.98	8.00	8.00	7.99	7.98	7.98	7.98	7.99	7.99	7.98	7.98
XAn	0.35	0.34	0.35	0.35	0.35	0.35	0.34	0.35	0.35	0.35	0.35	0.36	0.36	0.35	0.35	0.35	0.34	0.34	0.35	0.35	0.34
XAb	0.63	0.64	0.63	0.63	0.64	0.63	0.64	0.64	0.63	0.63	0.65	0.64	0.64	0.65	0.65	0.65	0.65	0.65	0.65	0.65	0.65
SrO	142.80	302.74	193.01	151.32	134.33	159.55	125.94	276.93	187.50	162.76	150.26	-	141.81	170.93	179.32	241.90	189.41	-	145.07	186.71	-

Table E: continued

Sample	CR1a	CR1a	CR1a	CR1a	CR1a	CR1a	CR1a	CR1a	CR1a	CR1a	CR1a	CR1a	CR1a	CR1a	CR1a	CR1a	CR1a	CR1a	CR1a	CR1a	CR1a
Mineral	Plag6	Plag6	Plag6	Plag7	Plag7	Plag7	Plag7	Plag7	Plag7	Plag7	Plag7	Plag7	Plag7	Plag7	Plag7	Plag7	Plag8	Plag8	Plag8	Plag8	Plag8
Generation	core	core	rim	rim	rim	core	core	core	core	core	core	core	core	core	rim	rim	rim	core	core	core	core
SiO ₂	59.31	59.48	58.86	59.68	60.21	60.65	61.38	60.18	59.94	60.92	60.40	60.48	60.44	59.87	61.17	60.21	60.67	60.82	60.64	61.10	60.77
Al ₂ O ₃	25.02	25.24	24.93	24.77	24.40	24.41	24.69	24.31	24.39	24.54	24.58	24.95	25.07	24.51	24.55	24.68	24.81	24.43	24.53	24.71	24.22
FeO	0.45	0.30	0.43	0.64	0.62	0.54	0.64	0.66	0.54	0.63	0.47	0.75	0.71	0.57	0.68	0.84	0.46	0.30	0.33		0.24
CaO	7.19	7.24	7.28	6.71	6.38	6.43	6.25	6.22	6.09	6.38	6.48	6.76	6.72	6.63	6.65	6.82	6.52	6.40	6.37	6.57	6.47
Na ₂ O	7.51	7.34	7.56	7.56	8.00	8.02	7.92	8.01	7.94	7.91	8.02	7.81	7.89	7.59	7.62	7.49	8.04	8.05	8.02	7.98	8.02
K ₂ O	-	0.09	0.09	-	-	0.11	-	-	0.11	-	0.11	0.12	-	0.10	0.13	0.14	0.16	-	0.17	0.10	-
Total	99.48	99.69	99.15	99.36	99.61	100.17	100.89	99.38	99.01	100.38	100.05	100.86	100.83	99.28	100.81	100.18	100.66	100.00	100.07	100.47	99.72
Number of anions on the basis of 8 oxygen atoms																					
Si ⁴⁺	2.66	2.67	2.65	2.68	2.69	2.70	2.71	2.70	2.70	2.71	2.69	2.68	2.67	2.69	2.71	2.69	2.68	2.71	2.70	2.71	2.71
Al ³⁺	1.32	1.33	1.32	1.31	1.29	1.28	1.29	1.28	1.29	1.28	1.29	1.30	1.31	1.30	1.28	1.30	1.29	1.28	1.29	1.29	1.27
Fe ²⁺	0.02	0.01	0.02	0.02	0.02	0.02	0.02	0.02	0.02	0.02	0.02	0.03	0.03	0.02	0.03	0.03	0.02	0.01	0.01	-	0.01
Ca ²⁺	0.35	0.35	0.35	0.32	0.31	0.31	0.30	0.30	0.29	0.30	0.31	0.32	0.32	0.32	0.32	0.33	0.31	0.31	0.30	0.31	0.31
Na ⁺	0.65	0.64	0.66	0.66	0.69	0.69	0.68	0.70	0.69	0.68	0.69	0.67	0.68	0.66	0.66	0.65	0.69	0.69	0.69	0.69	0.69
K ⁺	-	0.01	0.01	-	-	0.01	-	-	0.01	-	0.01	0.01	-	0.01	0.01	0.01	0.01	-	0.01	0.01	0.00
Σ cat.	5.00	5.00	5.00	5.00	5.00	5.00	5.00	5.00	5.00	5.00	5.00	5.00	5.00	5.00	5.00	5.00	5.00	5.00	5.00	5.00	5.00
Anions	8.00	8.01	7.98	8.01	7.99	7.99	8.02	7.99	7.99	8.01	7.98	7.99	7.99	8.01	8.02	8.01	7.98	8.00	7.99	8.01	8.00
XAn	0.35	0.35	0.35	0.33	0.31	0.30	0.30	0.30	0.30	0.31	0.31	0.32	0.32	0.32	0.32	0.33	0.31	0.31	0.30	0.31	0.31
XAb	0.65	0.64	0.65	0.67	0.69	0.69	0.70	0.70	0.70	0.69	0.69	0.67	0.68	0.67	0.67	0.66	0.68	0.69	0.69	0.68	0.69
SrO	169.71	173.76	236.01	-	-	-	-	-	-	-	-	219.81	-	291.76	-	-	-	-	-	-	-

Table E: continued

Sample	CR1a	CR1a	CR1a	CR1a	CR1a	CR1a	CR1a	CR1a	CR1a	CR1a	CR1a	CR1a	CR1a	CR1a	CR1a	CR1a	CR1a	CR1a	CR1a	CR1a	CR1a
Mineral	Plag8	Plag8	Plag8	Plag8	Plag8	Plag8	Plag8	Plag8	Plag8	Plag8	Plag9	Plag9	Plag9	Plag9	Plag9	Plag9	Plag9	Plag9	Plag9	Plag9	Plag9
Generation	core	core	core	core	core	core	core	core	core	rim	rim	rim	core	core	core	core	core	core	core	core	rim
SiO ₂	60.82	60.64	61.1	60.77	60.71	61.02	61.27	60.85	61.14	59.76	60.79	60.74	60.95	60.83	60.56	60.49	60.07	60.82	60.39	60.61	60.50
Al ₂ O ₃	24.43	24.53	24.71	24.22	24.59	24.32	24.63	24.41	24.61	24.45	24.72	24.22	24.59	24.11	24.38	24.54	24.42	24.83	24.22	24.20	24.65
FeO	0.30	0.33		0.24	0.18	0.35	0.25	0.21	0.47	0.62	0.25	0.37	0.25	0.19		0.25	0.19	0.26	0.29	0.38	0.39
CaO	6.40	6.37	6.57	6.47	6.61	6.66	6.33	6.35	6.27	6.68	6.42	6.59	6.54	6.41	6.65	6.6	6.41	6.51	6.39	6.44	6.57
Na ₂ O	8.05	8.02	7.98	8.02	7.82	7.85	8.02	8.11	7.98	7.72	7.75	7.85	8.17	8.16	7.77	7.94	7.98	7.94	7.96	7.91	7.94
K ₂ O	-	0.17	0.10	-	0.12	-	0.09	0.13	0.10	0.12	0.09	-	-	0.09	0.13	0.09	0.15	0.11	-	0.12	0.09
Total	100	100.07	100.47	99.72	100.03	100.2	100.6	100.06	100.59	99.35	100.02	99.78	100.5	99.79	99.49	99.91	99.22	100.47	99.26	99.66	100.14
Number of anions on the basis of 8 oxygen atoms																					
Si ⁴⁺	2.71	2.70	2.71	2.71	2.70	2.72	2.71	2.70	2.71	2.68	2.71	2.71	2.70	2.71	2.71	2.7	2.69	2.70	2.71	2.71	2.69
Al ³⁺	1.28	1.29	1.29	1.27	1.29	1.28	1.28	1.28	1.28	1.29	1.30	1.28	1.28	1.27	1.29	1.29	1.29	1.30	1.28	1.28	1.29
Fe ²⁺	0.01	0.01	-	0.01	0.01	0.01	0.01	0.01	0.02	0.02	0.01	0.01	0.01	0.01		0.01	0.01	0.01	0.01	0.01	0.01
Ca ²⁺	0.31	0.30	0.31	0.31	0.32	0.32	0.30	0.30	0.30	0.32	0.31	0.32	0.31	0.31	0.32	0.31	0.31	0.31	0.31	0.31	0.31
Na ⁺	0.69	0.69	0.69	0.69	0.68	0.68	0.69	0.70	0.69	0.67	0.67	0.68	0.70	0.71	0.67	0.69	0.69	0.68	0.69	0.69	0.68
K ⁺	-	0.01	0.01	0	0.01	-	0.01	0.01	0.01	0.01	0.01	-	-	0.01	0.01	0.01	0.01	0.01	-	0.01	0.01
Σcat.	5.00	5.00	5.00	5.00	5.00	5.00	5.00	5.00	5.00	5.00	5.00	5.00	5.00	5.00	5.00	5.00	5.00	5.00	5.00	5.00	5.00
Anions	8.00	7.99	8.01	8.00	8.01	8.02	8.01	7.99	8.00	7.99	8.02	8.01	7.99	7.99	8.01	7.99	7.99	8.00	8.00	8.00	7.99
XAn	0.31	0.30	0.31	0.31	0.32	0.32	0.30	0.30	0.30	0.32	0.31	0.32	0.31	0.30	0.32	0.31	0.30	0.31	0.31	0.31	0.31
XAb	0.69	0.69	0.68	0.69	0.68	0.68	0.69	0.69	0.69	0.67	0.68	0.68	0.69	0.69	0.67	0.68	0.69	0.68	0.69	0.68	0.68
SrO	-	-	-	-	-	-	-	-	-	-	363.42	248.27	-	-	-	-	-	-	187.45	-	-

Table E: continued

Sample	CR1a	CR1a	CR1a	CR1a	CR1a	CR1a	CR1a	CR1a	CR1a	CR1a	CR1a	CR1a	CR1a	CR1a	CR1a	CR1a	CR1a	CR1a	CR1a	CR1a	CR1a
Mineral	Plag9	Plag10	Plag10	Plag10	Plag10	Plag10	Plag10	Plag10	Plag11	Plag11	Plag11	Plag11	Plag11	Plag11	Plag11	Plag11	Plag11	Plag11	Plag11	Plag12	Plag12
Generation	rim	rim	core	core	core	core	core	rim	rim	core	core	core	core	core	core	core	core	core	rim	rim	rim
SiO ₂	59.58	57.78	58.54	59.37	58.83	58.82	60.00	58.34	58.42	58.54	59.11	58.78	58.84	58.51	58.64	58.81	57.89	58.48	58.65	58.57	59.12
Al ₂ O ₃	24.58	25.91	25.84	25.88	25.24	25.38	25.63	26.24	25.78	25.54	25.86	25.83	25.86	26.08	25.76	26.21	25.91	25.48	25.89	25.39	25.67
FeO	0.38	0.86	0.44	0.37	0.40	0.25	0.21	-	0.47	0.32	0.39	0.27	0.32	0.36	0.37	0.27	0.34	0.26	0.27	0.39	0.21
CaO	6.70	7.99	7.87	7.52	7.56	7.52	6.13	8.02	8.00	8.06	7.99	7.94	7.83	7.81	8.03	7.96	7.76	8.02	7.87	7.13	7.67
Na ₂ O	7.80	6.72	6.94	7.27	7.12	7.24	7.40	7.16	7.11	7.17	7.39	7.19	7.36	7.26	7.19	7.30	7.21	7.30	7.28	7.27	7.28
K ₂ O	0.10	0.21	0.27	0.28	0.25	0.26	1.07	0.16	-	-	-	-	-	-	-	-	-	-	-	0.31	0.12
Total	99.14	99.47	99.91	100.69	99.41	99.47	100.45	99.92	99.78	99.63	100.74	100.01	100.21	100.02	99.99	100.55	99.11	99.54	99.96	99.07	100.07
Number of anions on the basis of 8 oxygen atoms																					
Si ⁴⁺	2.68	2.60	2.62	2.63	2.65	2.64	2.66	2.61	2.62	2.63	2.62	2.63	2.62	2.61	2.62	2.61	2.61	2.62	2.62	2.64	2.64
Al ³⁺	1.30	1.38	1.36	1.35	1.34	1.34	1.34	1.38	1.36	1.35	1.35	1.36	1.36	1.37	1.36	1.37	1.38	1.35	1.36	1.35	1.35
Fe ²⁺	0.01	0.03	0.02	0.01	0.01	0.01	0.01	-	0.02	0.01	0.01	0.01	0.01	0.01	0.01	0.01	0.01	0.01	0.01	0.01	0.01
Ca ²⁺	0.32	0.39	0.38	0.36	0.36	0.36	0.29	0.38	0.38	0.39	0.38	0.38	0.37	0.37	0.38	0.38	0.37	0.39	0.38	0.34	0.37
Na ⁺	0.68	0.59	0.60	0.63	0.62	0.63	0.64	0.62	0.62	0.62	0.64	0.62	0.64	0.63	0.62	0.63	0.63	0.63	0.63	0.64	0.63
K ⁺	0.01	0.01	0.02	0.02	0.01	0.01	0.06	0.01	-	-	-	-	-	-	-	-	-	-	-	0.02	0.01
Σ cat.	5.00	5.00	5.00	5.00	5.00	5.00	5.00	5.00	5.00	5.00	5.00	5.00	5.00	5.00	5.00	5.00	5.00	5.00	5.00	5.00	5.00
Anions	7.98	7.99	8.00	7.99	8.00	7.99	7.98	7.98	7.99	7.99	7.98	7.99	7.98	7.98	7.99	7.98	7.98	7.98	7.99	7.99	8.00
XAn	0.32	0.39	0.38	0.36	0.36	0.36	0.29	0.38	0.38	0.38	0.37	0.38	0.37	0.37	0.38	0.38	0.37	0.38	0.37	0.35	0.37
XAb	0.67	0.60	0.61	0.63	0.62	0.63	0.64	0.61	0.62	0.62	0.63	0.62	0.63	0.63	0.62	0.62	0.63	0.62	0.63	0.64	0.63
SrO	-	-	273.94	212.54	171.32	269.41	203.87	-	275.54	-	-	-	-	-	-	-	186.31	318.87	181.92	-	-

Table E: continued

Sample	CR1a	CR1a	CR1a	CR1a	CR1a	CR1a	CR1a	CR1a	CR1a	CR1a	CR1a	CR1a	CR1a	CR1a	CR1a	CR1a	CR1a	CR1a	CR1a	CR1a	CR1a
Mineral	Plag12	Plag12	Plag12	Plag12	Plag12	Plag12	Plag12	Plag12	Plag12	Plag12	Plag12	Plag12	Plag12	Matrix	Matrix	Matrix	Matrix	Matrix	Matrix	Matrix	Matrix
Generation	core	core	core	core	core	core	core	core	core	core	core	core	rim	rim	rim	core	core	core	core	core	core
SiO ₂	59.33	59.45	59.69	59.24	59.50	59.38	59.52	59.18	59.47	59.06	59.34	59.08	58.77	59.46	60.89	60.97	60.52	60.53	58.72	58.89	59.25
Al ₂ O ₃	25.51	25.33	25.64	25.19	24.93	25.27	24.91	25.13	25.28	25.23	25.23	25.42	25.67	25.50	24.84	25.02	24.94	25.33	25.37	25.66	25.71
FeO	0.17	-	-	0.19	-	-	-	-	-	-	0.17	0.28	-	-	-	-	-	-	-	-	-
CaO	7.47	7.34	7.45	7.50	7.48	7.37	7.29	7.27	7.39	7.51	7.30	7.69	7.70	7.74	6.45	6.79	7.02	7.17	7.73	7.69	7.67
Na ₂ O	7.45	7.58	7.57	7.46	7.45	7.35	7.51	7.57	7.48	7.40	7.30	7.45	7.39	7.43	8.07	7.97	7.81	7.68	7.21	7.14	7.09
K ₂ O	-	-	-	-	-	0.14	0.10	0.09	-	0.14	0.12	-	-	0.09	0.12	-	0.10	0.12	-	0.10	0.10
Total	99.93	99.69	100.35	99.58	99.36	99.51	99.32	99.24	99.62	99.34	99.46	99.91	99.53	100.22	100.37	100.74	100.38	100.83	99.03	99.48	100.06
Number of anions on the basis of 8 oxygen atoms																					
Si ⁴⁺	2.65	2.66	2.65	2.65	2.67	2.66	2.67	2.66	2.66	2.65	2.66	2.64	2.63	2.65	2.70	2.69	2.69	2.68	2.65	2.65	2.65
Al ³⁺	1.34	1.33	1.34	1.33	1.32	1.34	1.32	1.33	1.33	1.34	1.34	1.34	1.36	1.34	1.30	1.30	1.30	1.32	1.35	1.36	1.35
Fe ²⁺	0.01	-	-	0.01	-	-	-	-	-	-	0.01	0.01	-	0.00	0.00	0.00	0.00	0.00	0.00	0.00	0.00
Ca ²⁺	0.36	0.35	0.35	0.36	0.36	0.35	0.35	0.35	0.35	0.36	0.35	0.37	0.37	0.37	0.31	0.32	0.33	0.34	0.37	0.37	0.37
Na ⁺	0.64	0.66	0.65	0.65	0.65	0.64	0.65	0.66	0.65	0.64	0.64	0.64	0.64	0.64	0.69	0.68	0.67	0.66	0.63	0.62	0.61
K ⁺	-	-	-	-	-	0.01	0.01	0.01	-	0.01	0.01	-	-	0.01	0.01	-	0.01	0.01	-	0.01	0.01
Σcat.	5.00	5.00	5.00	5.00	5.00	5.00	5.00	5.00	5.00	5.00	5.00	5.00	5.00	5.00	5.00	5.00	5.00	5.00	5.00	5.00	5.00
Anions	8.00	8.00	8.00	8.00	8.01	8.01	8.00	7.99	8.01	7.99	8.01	7.99	7.99	7.99	8.00	8.00	8.00	8.00	8.01	8.01	8.01
XAn	0.36	0.35	0.35	0.36	0.36	0.35	0.35	0.34	0.35	0.36	0.35	0.36	0.37	0.36	0.30	0.32	0.33	0.34	0.37	0.37	0.37
XAb	0.64	0.65	0.65	0.64	0.64	0.64	0.65	0.65	0.65	0.64	0.64	0.64	0.63	0.63	0.69	0.68	0.67	0.66	0.63	0.62	0.62
SrO	-	-	-	277.96	-	181.12	-	-	-	-	-	236.34	220.52	550.60	584.50	338.49	697.10	-	438.38	-	637.30

Table E: continued

Sample	CR1a	L2b	L2b	L2b	L2b	L2b	L2b	L2b	L2b	L2b	L2b	L2b	L2b	L2b	L2b	L2b	L2b	L2b	L2b	L2b	L2b
Mineral	Matrix	plag1	plag1	plag1	plag1	plag1	plag1	plag1	plag1	plag1	plag1	plag1	plag1	plag1	plag1	plag1	plag1	plag1	plag1	plag1	plag1
Generation	rim	rim	rim	rim	rim	core	core	core	core	core	core	core	core	core	core	core	core	core	core	core	core
SiO ₂	59.05	59.07	59.38	58.78	58.75	58.88	58.92	58.91	58.54	58.76	58.47	58.26	58.15	58.66	59.21	59.24	58.73	58.91	59.06	58.57	58.71
Al ₂ O ₃	25.98	25.92	25.64	25.60	25.87	25.66	25.59	26.06	25.81	26.01	25.86	26.05	25.78	25.87	26.28	26.07	25.77	26.14	25.81	26.04	25.76
FeO	-	0.29	-	-	0.19	-	-	-	-	-	-	-	-	-	-	-	-	-	-	-	-
CaO	7.69	7.89	7.81	7.84	7.75	7.92	7.95	8.13	7.78	8.06	8.00	8.13	7.98	8.08	8.09	8.16	8.20	7.95	7.99	7.95	7.95
Na ₂ O	7.21	7.30	7.03	7.15	7.11	7.20	7.12	6.88	7.13	7.08	6.97	6.95	6.91	7.16	7.11	7.16	7.14	7.03	7.09	7.24	7.06
K ₂ O	-	0.25	0.25	0.26	0.24	0.30	0.23	0.30	0.20	0.18	0.27	0.27	0.33	0.28	0.18	0.22	0.25	0.17	0.21	0.15	0.12
Total	99.94	100.71	100.10	99.63	99.92	99.95	99.81	100.28	99.46	100.10	99.57	99.65	99.15	100.04	100.87	100.84	100.08	100.20	100.16	99.95	99.60
Number of anions on the basis of 8 oxygen atoms																					
Si ⁴⁺	2.64	2.62	2.65	2.63	2.63	2.63	2.64	2.63	2.63	2.62	2.62	2.61	2.62	2.62	2.62	2.62	2.62	2.63	2.64	2.61	2.63
Al ³⁺	1.37	1.35	1.35	1.35	1.36	1.35	1.35	1.37	1.37	1.37	1.37	1.38	1.37	1.36	1.37	1.36	1.36	1.37	1.36	1.37	1.36
Fe ²⁺	-	0.01	-	-	0.01	-	-	-	-	-	-	-	-	-	-	-	-	-	-	-	-
Ca ²⁺	0.37	0.37	0.37	0.38	0.37	0.38	0.38	0.39	0.37	0.39	0.38	0.39	0.39	0.39	0.38	0.39	0.39	0.38	0.38	0.38	0.38
Na ⁺	0.63	0.63	0.61	0.62	0.62	0.62	0.62	0.60	0.62	0.61	0.61	0.60	0.60	0.62	0.61	0.61	0.62	0.61	0.61	0.63	0.61
K ⁺	-	0.01	0.01	0.01	0.01	0.02	0.01	0.02	0.01	0.01	0.02	0.02	0.02	0.02	0.01	0.01	0.01	0.01	0.01	0.01	0.01
Σcat.	5.00	5.00	5.00	5.00	5.00	5.00	5.00	5.00	5.00	5.00	5.00	5.00	5.00	5.00	5.00	5.00	5.00	5.00	5.00	5.00	5.00
Anions	8.01	7.98	8.02	7.99	7.99	7.99	8.00	8.01	7.99	8.00	8.00	7.99	8.00	7.98	8.00	7.99	7.98	8.01	8.00	7.98	8.01
XAn	0.37	0.37	0.37	0.37	0.37	0.37	0.38	0.39	0.37	0.38	0.38	0.39	0.38	0.38	0.38	0.38	0.38	0.38	0.38	0.37	0.38
XAb	0.63	0.62	0.61	0.61	0.62	0.61	0.61	0.59	0.62	0.61	0.60	0.60	0.60	0.61	0.61	0.61	0.60	0.61	0.61	0.62	0.61
SrO	512.50	-	-	-	-	-	177.55	-	198.60	-	-	-	-	-	-	-	239.69	-	276.78	-	-

Table E: continued

Sample	L2b	L2b	L2b	L2b	L2b	L2b	L2b	L2b	L2b	L2b	L2b	L2b	L2b	L2b	L2b	L2b	L2b	L2b	L2b	L2b	L2b
Mineral	plag1	plag1	plag1	plag1	plag1	plag2	plag2	plag2	plag2	plag2	plag2	plag2	plag2	plag2	plag2	plag2	plag2	plag2	plag2	plag2	plag2
Generation	core	rim	rim	rim	rim	rim	rim	core	core	core	core	core	core	core	core	core	core	core	core	core	core
SiO ₂	59.12	58.56	58.76	58.50	58.61	59.83	59.88	60.13	60.38	60.51	60.58	60.22	59.92	60.41	59.84	59.81	59.63	60.58	59.67	60.02	60.01
Al ₂ O ₃	25.71	25.37	25.66	25.83	25.50	25.18	25.07	24.82	24.80	25.41	25.12	24.72	24.67	25.09	24.89	25.05	25.02	25.35	24.74	25.11	24.79
FeO	-	-	0.19	-	0.35	0.34	0.17	-	-	-	-	-	-	-	-	-	-	-	-	-	-
CaO	7.92	8.00	7.91	7.85	7.75	7.03	6.96	7.03	6.98	6.94	6.89	6.78	6.74	6.55	6.90	7.25	7.01	6.74	6.82	6.76	6.75
Na ₂ O	6.92	7.17	7.28	7.08	7.27	7.54	7.52	7.52	7.69	7.66	7.92	7.56	7.83	7.75	7.49	7.65	7.72	7.93	7.56	7.86	7.65
K ₂ O	0.16	0.15	0.12	-	-	0.29	0.34	0.32	0.35	0.30	0.32	0.34	0.36	0.32	0.19	0.20	0.14	0.22	0.19	0.18	0.29
Total	99.83	99.25	99.91	99.25	99.49	100.22	99.94	99.81	100.20	100.82	100.83	99.61	99.53	100.11	99.30	99.97	99.53	100.82	98.98	99.93	99.49
Number of anions on the basis of 8 oxygen atoms																					
Si ⁴⁺	2.65	2.63	2.63	2.63	2.63	2.66	2.67	2.69	2.68	2.67	2.67	2.70	2.68	2.69	2.69	2.67	2.67	2.67	2.69	2.67	2.69
Al ³⁺	1.36	1.35	1.35	1.37	1.35	1.32	1.32	1.31	1.30	1.32	1.31	1.30	1.30	1.31	1.32	1.32	1.32	1.32	1.31	1.32	1.31
Fe ²⁺	-	-	0.01	-	0.01	0.01	0.01	-	-	-	-	-	-	-	-	-	-	-	-	-	-
Ca ²⁺	0.38	0.39	0.38	0.38	0.37	0.34	0.33	0.34	0.33	0.33	0.33	0.33	0.32	0.31	0.33	0.35	0.34	0.32	0.33	0.32	0.32
Na ⁺	0.60	0.63	0.63	0.62	0.63	0.65	0.65	0.65	0.66	0.66	0.68	0.66	0.68	0.67	0.65	0.66	0.67	0.68	0.66	0.68	0.66
K ⁺	0.01	0.01	0.01	-	-	0.02	0.02	0.02	0.02	0.02	0.02	0.02	0.02	0.02	0.01	0.01	0.01	0.01	0.01	0.01	0.02
Σcat.	5.00	5.00	5.00	5.00	5.00	5.00	5.00	5.00	5.00	5.00	5.00	5.00	5.00	5.00	5.00	5.00	5.00	5.00	5.00	5.00	5.00
Anions	8.02	7.99	7.98	8.01	7.99	7.99	8.00	8.01	7.99	8.00	7.98	8.01	7.98	8.00	8.01	7.99	7.99	7.99	8.01	7.99	8.00
XAn	0.38	0.38	0.37	0.38	0.37	0.33	0.33	0.33	0.33	0.33	0.32	0.33	0.32	0.31	0.33	0.34	0.33	0.32	0.33	0.32	0.32
XAb	0.61	0.61	0.62	0.62	0.63	0.65	0.65	0.65	0.65	0.66	0.66	0.66	0.66	0.67	0.66	0.65	0.66	0.67	0.66	0.67	0.66
SrO	-	-	-	-	-	338.34	259.66	209.77	193.30	235.01	337.85	300.15	201.75	197.80	267.68	276.15	0.00	268.22	325.33	202.19	246.99

Table E: continued

Sample	L2b	L2b	L2b	L2b	L2b	L2b	L2b	L2b	L2b	L2b	L2b	L2b	L2b	L2b	L2b	L2b	L2b	L2b	L2b	L2b	L2b
Mineral	plag3	plag3	plag3	plag3	plag3	plag3	plag3	plag3	plag3	plag3	plag3	plag4	plag4	plag4	plag4	plag4	plag4	plag4	plag4	plag4	plag4
Generation	core	core	core	core	core	rim	rim	rim	rim	core	core	core	core	core	core	core	core	core	core	core	core
SiO ₂	59.98	59.85	59.62	59.98	60.02	59.64	59.36	58.14	58.39	58.46	58.84	58.57	58.89	58.66	58.84	59.36	59.06	59.38	58.68	59.20	58.83
Al ₂ O ₃	24.72	24.70	24.74	24.58	24.77	24.51	24.87	25.59	25.48	25.53	25.60	25.49	25.87	25.77	26.06	25.82	25.78	25.84	25.92	25.73	25.83
FeO	-	-	-	-	-	-	0.26	0.40	0.27	0.26	-	-	-	-	-	-	-	-	-	-	0.19
CaO	6.84	6.71	6.60	6.95	6.78	6.92	6.87	7.74	7.63	7.62	7.77	7.63	7.85	7.80	7.90	7.86	7.96	8.01	7.98	7.84	7.95
Na ₂ O	7.82	7.86	7.73	7.64	7.87	7.77	7.62	6.96	6.89	7.19	7.26	7.16	7.11	6.91	7.16	7.04	6.90	7.16	7.10	7.09	7.15
K ₂ O	0.26	0.29	0.29	0.31	0.25	0.28	0.27	0.35	0.34	0.32	0.35	0.35	0.35	0.33	0.38	0.30	0.33	0.34	0.32	0.42	0.22
Total	99.62	99.41	98.98	99.47	99.69	99.11	99.24	99.18	99.00	99.38	99.82	99.19	100.07	99.48	100.34	100.38	100.02	100.74	100.00	100.28	100.16
Number of anions on the basis of 8 oxygen atoms																					
Si ⁴⁺	2.68	2.68	2.68	2.69	2.68	2.68	2.67	2.62	2.64	2.63	2.63	2.64	2.63	2.64	2.62	2.64	2.64	2.63	2.62	2.64	2.62
Al ³⁺	1.30	1.30	1.31	1.30	1.30	1.30	1.32	1.36	1.36	1.35	1.35	1.35	1.36	1.37	1.37	1.36	1.36	1.35	1.36	1.35	1.36
Fe ²⁺	-	-	-	-	-	-	0.01	0.02	0.01	0.01	-	-	-	-	-	-	-	-	-	-	0.01
Ca ²⁺	0.33	0.32	0.32	0.33	0.32	0.33	0.33	0.37	0.37	0.37	0.37	0.37	0.38	0.38	0.38	0.38	0.38	0.38	0.38	0.37	0.38
Na ⁺	0.68	0.68	0.67	0.66	0.68	0.68	0.66	0.61	0.60	0.63	0.63	0.62	0.62	0.60	0.62	0.61	0.60	0.62	0.62	0.61	0.62
K ⁺	0.01	0.02	0.02	0.02	0.01	0.02	0.02	0.02	0.02	0.02	0.02	0.02	0.02	0.02	0.02	0.02	0.02	0.02	0.02	0.02	0.01
Σcat.	5.00	5.00	5.00	5.00	5.00	5.00	5.00	5.00	5.00	5.00	5.00	5.00	5.00	5.00	5.00	5.00	5.00	5.00	5.00	5.00	5.00
Anions	7.98	7.98	7.99	7.99	7.98	7.98	7.98	7.99	8.01	7.98	7.98	7.99	7.99	8.01	7.98	8.01	8.01	7.99	7.99	8.00	7.99
XAn	0.32	0.32	0.32	0.33	0.32	0.32	0.33	0.37	0.37	0.36	0.36	0.36	0.37	0.38	0.37	0.38	0.38	0.37	0.38	0.37	0.38
XAb	0.66	0.67	0.67	0.65	0.67	0.66	0.66	0.61	0.61	0.62	0.62	0.62	0.61	0.60	0.61	0.61	0.60	0.61	0.61	0.61	0.61
SrO	0.00	317.19	248.52	252.12	202.89	289.57	0.00	-	-	-	-	-	-	240.87	-	-	-	186.74	253.56	-	-

Table E: continued

Sample	L2b	L2b	L2b	L2b	L2b	L2b	L2b	L2b	L2b	L2b	L2b	L2b	L2b	L2b	L2b	L2b	L2b	L2b	L2b	L2b	L2b
Mineral	plag4	plag4	plag4	plag4	plag4	plag4	plag5	plag5	plag5	plag5	plag5	plag5	plag5	plag5	plag5	plag5	plag5	Matrix	Matrix	Matrix	Matrix
Generation	core	core	core	core	rim	rim	rim	rim	core	core	core	core	core	core	core	rim	rim	rim	rim	core	core
SiO₂	58.83	58.91	59.18	59.11	58.88	58.60	58.56	57.68	58.47	58.51	58.59	58.73	58.55	58.43	58.79	58.00	58.64	60.41	60.35	61.25	60.75
Al₂O₃	25.64	25.82	25.50	25.61	25.69	25.81	25.99	25.86	25.90	26.02	26.47	25.96	25.67	25.92	25.83	25.94	25.65	24.40	24.32	24.64	24.26
FeO	-	-	-	0.18	-	0.25	0.29	0.32	0.31	0.37	0.23	0.19	0.24	0.27	0.28	0.22	0.22	-	-	-	-
CaO	8.06	7.89	7.92	7.91	7.63	7.98	7.84	8.04	8.01	8.04	8.18	8.20	8.09	8.13	8.10	7.94	7.94	6.33	6.22	6.28	6.50
Na₂O	7.12	7.19	7.10	7.09	7.01	7.01	6.92	6.94	6.80	7.03	7.03	7.12	7.00	6.90	7.06	6.91	7.03	7.90	8.03	8.16	7.92
K₂O	0.30	0.28	0.22	0.18	0.25	0.27	0.22	0.20	0.21	0.24	0.22	0.24	0.28	0.25	0.30	0.30	0.24	0.25	0.39	0.31	0.35
Total	99.96	100.09	99.92	100.08	99.46	99.93	99.82	99.04	99.70	100.21	100.72	100.44	99.84	99.89	100.37	99.31	99.73	99.29	99.30	100.64	99.78
Number of anions on the basis of 8 oxygen atoms																					
Si⁴⁺	2.63	2.63	2.65	2.64	2.65	2.62	2.63	2.60	2.63	2.61	2.60	2.61	2.62	2.62	2.62	2.61	2.63	2.71	2.70	2.71	2.71
Al³⁺	1.35	1.36	1.34	1.35	1.36	1.36	1.37	1.38	1.37	1.37	1.38	1.36	1.36	1.37	1.36	1.38	1.36	1.29	1.28	1.28	1.27
Fe²⁺	-	-	-	0.01	-	0.01	0.01	0.01	0.01	0.01	0.01	0.01	0.01	0.01	0.01	0.01	0.01	-	-	-	-
Ca²⁺	0.39	0.38	0.38	0.38	0.37	0.38	0.38	0.39	0.39	0.38	0.39	0.39	0.39	0.39	0.39	0.38	0.38	0.30	0.30	0.30	0.31
Na⁺	0.62	0.62	0.62	0.61	0.61	0.61	0.60	0.61	0.59	0.61	0.61	0.61	0.61	0.60	0.61	0.60	0.61	0.69	0.70	0.70	0.68
K⁺	0.02	0.02	0.01	0.01	0.01	0.02	0.01	0.01	0.01	0.01	0.01	0.01	0.02	0.01	0.02	0.02	0.01	0.01	0.02	0.02	0.02
Σcat.	5.00	5.00	5.00	5.00	5.00	5.00	5.00	5.00	5.00	5.00	5.00	5.00	5.00	5.00	5.00	5.00	5.00	5.00	5.00	5.00	5.00
Anions	7.99	7.99	8.01	8.00	8.01	7.99	8.00	7.98	8.01	7.98	7.98	7.98	7.99	8.00	7.98	7.99	7.99	8.00	7.98	7.99	7.99
XAn	0.38	0.37	0.38	0.38	0.37	0.38	0.38	0.39	0.39	0.38	0.39	0.38	0.38	0.39	0.38	0.38	0.38	0.30	0.29	0.29	0.31
XAb	0.60	0.61	0.61	0.61	0.62	0.60	0.61	0.60	0.60	0.60	0.60	0.60	0.60	0.60	0.60	0.60	0.61	0.68	0.69	0.69	0.67
SrO	203.37	-	-	-	-	-	303.78	-	-	-	-	-	-	-	-	-	-	105.21	358.40	306.50	208.21

Table E: continued

Sample	L2b	L2b	L2b	L2b	L2b
Mineral	Matrix	Matrix	Matrix	Matrix	Matrix
Generation	core	core	core	rim	rim
SiO₂	60.55	60.55	61.59	59.99	60.11
Al₂O₃	24.13	24.37	24.75	24.41	24.63
FeO	-	-	-	-	-
CaO	6.32	6.24	6.37	6.48	6.67
Na₂O	8.03	7.81	7.82	7.78	7.69
K₂O	0.25	0.30	0.30	0.36	0.29
Total	99.27	99.26	100.82	99.02	99.38
Number of anions on the basis of 8 oxygen atoms					
Si⁴⁺	2.71	2.72	2.72	2.70	2.69
Al³⁺	1.27	1.29	1.29	1.29	1.30
Fe²⁺	-	-	-	-	-
Ca²⁺	0.30	0.30	0.30	0.31	0.32
Na⁺	0.70	0.68	0.67	0.68	0.67
K⁺	0.01	0.02	0.02	0.02	0.02
∑cat.	5.00	5.00	5.00	5.00	5.00
Anions	7.99	8.01	8.02	7.99	8.00
XAn	0.30	0.30	0.31	0.31	0.32
XAb	0.69	0.68	0.68	0.67	0.67
SrO	316.04	229.50	367.76	257.22	184.64

APPENDIX F

Table F: Detailed electron microprobe analysis of garnet across individual plagioclase inclusions in the stromatolitic leucosomes. The dashed lines represent values below the detection limit of the analytical routine

Sample	L2t-7	L2t-7	L2t-7	L2t-7	L2t-7	L2t-7	L2t-7	L2t-7	L2t-7	L2t-7	L2t-7	L2t-7	L2t-7	L2t-7	L2t-7	L2t-7	L2t-7	L2t-7	L2t-7	L2t-7	L2t-7
Mineral	Grt	Grt	Grt	Grt	Grt	Grt	Grt	Grt	Grt	Grt	Grt	Grt	Grt	Grt	Grt	Grt	Grt	Grt	Grt	Grt	Grt
Generation	A-2	A-2	A-2	A-2	A-2	A-2	A-2	A-2	A-2	A-2	A-2	A-2	A-2	A-2	A-2	A-2	A-2	A-2	A-2	A-2	A-2
SiO ₂	38.84	39.15	39.30	39.03	38.90	39.27	39.40	39.51	39.37	39.48	39.22	39.23	39.14	39.16	39.12	39.21	40.01	39.88	39.71	39.09	39.46
Al ₂ O ₃	22.32	22.26	22.52	21.98	22.28	22.30	22.08	21.95	22.19	22.29	22.29	22.21	22.04	22.50	22.25	22.33	22.53	22.40	22.45	22.12	22.31
Cr ₂ O ₃	0.21	0.16	0.14	0.14		0.20	0.15	0.17	0.13		0.18	0.16	0.20	0.24	0.13	0.22	0.26	0.30	0.32	0.21	0.33
Fe ₂ O ₃	0.03	0.07	-	0.18	0.34	-	-	-	0.37	-	0.31	0.35	0.31	0.31	0.16	-	-	-	-	-	0.26
FeO	25.05	25.06	25.13	24.78	24.84	24.66	25.03	25.15	24.96	25.00	24.72	24.77	24.67	24.61	24.88	24.66	24.42	25.18	24.84	24.50	24.74
MnO	0.90	0.93	0.83	0.85	0.84	0.71	0.81	0.75	0.74	0.86	0.85	0.80	0.75	0.82	0.71	0.82	0.87	0.78	0.79	0.75	0.77
MgO	9.85	10.03	10.03	9.96	9.85	9.83	9.83	9.86	9.83	9.66	9.67	9.64	9.59	9.54	9.45	9.27	10.59	10.50	10.57	10.27	10.67
CaO	2.29	2.28	2.38	2.57	2.55	2.71	2.85	2.89	3.00	3.16	3.18	3.24	3.35	3.42	3.39	3.45	2.29	2.19	2.13	2.15	2.06
Total	99.49	99.96	100.33	99.48	99.59	99.67	100.15	100.27	100.59	100.46	100.44	100.39	100.04	100.61	100.08	99.97	100.96	101.23	100.79	99.08	100.61
Number of anions on the basis of 12 oxygen atoms																					
Si ⁴⁺	2.98	2.99	2.99	3.00	2.98	3.01	3.01	3.01	2.99	3.00	2.99	2.99	2.99	2.98	2.99	3.00	3.01	3.00	3.00	3.01	2.99
Al ³⁺	2.02	2.00	2.02	1.99	2.01	2.01	1.99	1.97	1.99	2.00	2.00	1.99	1.99	2.02	2.00	2.01	2.00	1.99	2.00	2.00	1.99
Cr ³⁺	0.01	0.01	0.01	0.01	0.00	0.01	0.01	0.01	0.01	0.00	0.01	0.01	0.01	0.01	0.01	0.01	0.02	0.02	0.02	0.01	0.02
Fe ³⁺	-	-	-	0.01	0.02	-	-	-	0.02	-	0.02	0.02	0.02	0.02	0.02	0.01	-	-	-	-	0.01
Fe ²⁺	1.61	1.60	1.60	1.59	1.59	1.58	1.60	1.60	1.59	1.59	1.57	1.58	1.58	1.56	1.59	1.58	1.54	1.59	1.57	1.58	1.57
Mn ²⁺	0.06	0.06	0.05	0.05	0.05	0.05	0.05	0.05	0.05	0.06	0.06	0.05	0.05	0.05	0.05	0.05	0.06	0.05	0.05	0.05	0.05
Mg ²⁺	1.13	1.14	1.14	1.14	1.13	1.12	1.12	1.12	1.11	1.10	1.10	1.09	1.09	1.08	1.08	1.06	1.19	1.18	1.19	1.18	1.20
Ca ²⁺	0.19	0.19	0.19	0.21	0.21	0.22	0.23	0.24	0.24	0.26	0.26	0.26	0.27	0.28	0.28	0.28	0.18	0.18	0.17	0.18	0.17
Σcat	8.00	8.00	8.00	8.00	8.00	8.00	8.00	8.00	8.00	8.00	8.00	8.00	8.00	8.00	8.00	8.00	8.00	8.00	8.00	8.00	8.00
Anion	12.00	12.00	12.00	12.00	12.00	12.02	12.00	12.00	12.00	12.00	12.00	12.00	12.00	12.00	12.00	12.01	12.02	12.01	12.01	12.01	12.00
XGrss	0.06	0.06	0.07	0.07	0.07	0.07	0.08	0.08	0.08	0.09	0.09	0.09	0.09	0.09	0.09	0.10	0.06	0.06	0.06	0.06	0.06
XAlm	0.54	0.54	0.54	0.53	0.53	0.53	0.53	0.53	0.53	0.53	0.53	0.53	0.53	0.53	0.53	0.53	0.52	0.53	0.53	0.53	0.52
XPyrr	0.38	0.38	0.38	0.38	0.38	0.38	0.37	0.37	0.37	0.37	0.37	0.37	0.37	0.36	0.36	0.36	0.40	0.39	0.40	0.40	0.40

XSpss	0.02	0.02	0.02	0.02	0.02	0.02	0.02	0.02	0.02	0.02	0.02	0.02	0.02	0.02	0.02	0.02	0.02	0.02	0.02	0.02	0.02
D	0.00	0.00	0.00	0.00	0.00	0.02	0.02	0.02	0.02	0.02	0.04	0.04	0.04	0.06	0.06	0.06	0.08	0.08	0.08	0.11	0.11

Table F: continued

Sample	L2t-7	L2t-7	L2t-7	L2t-7	L2t-7	L2t-7	L2t-7	L2t-7	L2t-7	L2t-7	L2t-7	L2t-7	L2t-7	L2t-7	L2t-7	L2t-7	L2t-7	L2t-7	L2t-7	L2t-7	L2t-7
Mineral	Grt	Grt	Grt	Grt	Grt	Grt	Grt	Grt	Grt	Grt	Grt	Grt	Grt	Grt	Grt	Grt	Grt	Grt	Grt	Grt	Grt
Generation	A-2	A-2	A-2	A-2	A-2	A-2	A-2	A-2	A-2	A-2	A-2	A-2	A-2	A-2	A-2	A-2	A-2	A-2	A-1	A-1	A-1
SiO ₂	38.47	39.27	39.27	39.53	39.32	39.66	39.58	39.47	39.16	39.15	39.53	39.51	39.55	39.13	39.79	39.55	39.33	39.45	39.38	39.17	39.41
Al ₂ O ₃	22.02	22.45	22.30	22.52	22.51	22.14	22.50	22.53	22.26	22.33	22.36	22.18	22.13	22.32	22.45	22.29	22.54	22.42	22.53	22.36	22.13
Cr ₂ O ₃	0.23	0.25	0.19	0.20	0.20	0.32	0.24	0.28	0.29	0.36	0.36	0.40	0.46	0.23	0.15	0.19	0.22	-	-	0.13	0.20
Fe ₂ O ₃	0.51	0.63	-	-	-	-	0.19	-	0.63	0.25	0.28	-	-	-	-	-	0.37	-	-	0.04	0.47
FeO	24.18	24.50	24.92	25.21	24.68	25.08	25.00	24.82	24.64	24.65	24.86	25.17	25.29	24.89	25.29	25.14	24.70	25.00	24.78	24.91	24.37
MnO	0.75	0.70	0.78	0.72	0.77	0.75	0.79	0.80	0.87	0.81	0.90	0.75	0.72	0.87	0.77	0.71	0.87	0.79	0.89	0.83	0.86
MgO	10.39	10.78	10.48	10.55	10.70	10.56	10.92	10.81	10.79	10.85	11.00	10.82	10.93	10.71	10.75	10.95	11.02	9.37	9.19	9.28	9.57
CaO	1.98	1.98	1.96	1.81	1.86	1.76	1.60	1.68	1.61	1.56	1.47	1.36	1.35	1.27	1.38	1.37	1.42	3.65	3.75	3.66	3.76
Total	98.53	100.56	99.89	100.53	100.04	100.26	100.83	100.39	100.26	99.97	100.75	100.19	100.43	99.41	100.59	100.20	100.47	100.68	100.52	100.38	100.77

Number of anions on the basis of 12 oxygen atoms

Si ⁴⁺	2.97	2.97	2.99	3.00	2.99	3.01	2.99	2.99	2.98	2.98	2.99	3.00	3.00	3.00	3.01	3.00	2.98	2.99	3.00	2.98	2.99
Al ³⁺	2.01	2.00	2.00	2.01	2.02	1.98	2.00	2.01	1.99	2.00	1.99	1.99	1.98	2.01	2.00	1.99	2.01	2.01	2.02	2.01	1.98
Cr ³⁺	0.01	0.01	0.01	0.01	0.01	0.02	0.01	0.02	0.02	0.02	0.02	0.02	0.03	0.01	0.01	0.01	0.01	0.00	0.00	0.01	0.01
Fe ³⁺	0.03	0.04	-	-	-	-	0.01	-	0.04	0.01	0.02	-	-	-	-	-	0.02	-	-	-	0.03
Fe ²⁺	1.56	1.55	1.59	1.60	1.57	1.59	1.58	1.57	1.57	1.57	1.57	1.60	1.60	1.59	1.60	1.60	1.56	1.59	1.58	1.59	1.55
Mn ²⁺	0.05	0.04	0.05	0.05	0.05	0.05	0.05	0.05	0.06	0.05	0.06	0.05	0.05	0.06	0.05	0.05	0.06	0.05	0.06	0.05	0.06
Mg ²⁺	1.20	1.22	1.19	1.19	1.21	1.20	1.23	1.22	1.22	1.23	1.24	1.23	1.24	1.22	1.21	1.24	1.24	1.06	1.04	1.05	1.08
Ca ²⁺	0.16	0.16	0.16	0.15	0.15	0.14	0.13	0.14	0.13	0.13	0.12	0.11	0.11	0.10	0.11	0.11	0.12	0.30	0.31	0.30	0.31
Σcat	8.00	8.00	8.00	8.00	8.00	8.00	8.00	8.00	8.00	8.00	8.00	8.00	8.00	8.00	8.00	8.00	8.00	8.00	8.01	7.99	8.01
Anion	12.00	12.00	12.00	12.01	12.00	12.02	12.00	12.01	12.00	12.00	12.00	12.01	12.00	12.01	12.02	12.00	12.00	12.00	12.01	12.00	12.00
XGrss	0.06	0.05	0.05	0.05	0.05	0.05	0.04	0.05	0.04	0.04	0.04	0.04	0.04	0.04	0.04	0.04	0.04	0.10	0.10	0.10	0.10
XAlm	0.53	0.52	0.53	0.54	0.53	0.53	0.53	0.53	0.53	0.53	0.53	0.54	0.54	0.54	0.54	0.53	0.53	0.53	0.53	0.53	0.52

XPyr	0.40	0.41	0.40	0.40	0.41	0.40	0.41	0.41	0.41	0.41	0.41	0.41	0.41	0.41	0.41	0.41	0.42	0.35	0.35	0.35	0.36
XSpss	0.02	0.02	0.02	0.02	0.02	0.02	0.02	0.02	0.02	0.02	0.02	0.02	0.02	0.02	0.02	0.02	0.02	0.02	0.02	0.02	0.02
D	0.11	0.33	0.35	0.35	0.35	0.35	0.37	0.37	0.37	0.40	0.40	0.40	0.42	0.42	0.42	0.44	0.44	0.00	0.00	0.00	0.02

Table F: continued

Sample	L2t-7	L2t-7	L2t-7	L2t-7	L2t-7	L2t-7	L2t-7	L2t-7	L2t-7	L2t-7	L2t-7	L2t-7	L2t-7	L2t-7	L2t-7	L2t-7	L2t-7	L2t-7	L2t-7	L2t-7	L2t-7
Mineral	Grt	Grt	Grt	Grt	Grt	Grt	Grt	Grt	Grt	Grt	Grt	Grt	Grt	Grt	Grt	Grt	Grt	Grt	Grt	Grt	Grt
Generation	A-1	A-1	A-1	A-1	A-1	A-1	A-1	A-1	A-1	A-1	A-1	A-1	A-1	A-1	A-1	A-1	A-1	A-1	A-1	A-1	A-1
SiO ₂	39.42	39.30	39.23	39.09	39.46	39.57	39.72	39.31	39.23	39.24	39.27	39.55	39.43	39.40	39.48	39.45	39.55	39.43	39.27	39.35	39.26
Al ₂ O ₃	22.23	22.36	22.31	22.40	22.32	22.31	22.69	22.29	22.28	22.44	22.43	22.42	22.34	22.37	22.28	22.24	22.13	22.40	22.24	22.48	22.59
Cr ₂ O ₃	-	0.15	0.22	0.21	0.19	0.17	0.25	0.23	0.13	0.14	0.24	0.19	0.18	0.14	-	0.18	0.26	0.21	0.27	0.14	0.24
Fe ₂ O ₃	0.37	0.17	0.41	0.09	-	0.04	0.48	-	-	0.23	0.49	-	0.22	-	0.04	0.32	0.07	-	-	0.12	0.21
FeO	24.60	24.75	24.79	24.92	25.02	24.96	24.86	24.49	24.75	24.49	24.62	24.72	24.81	25.14	25.08	24.71	25.06	24.72	24.67	25.20	24.89
MnO	0.87	0.82	0.85	0.73	0.79	0.87	0.78	0.70	0.76	0.85	0.89	0.77	0.80	0.85	0.88	0.86	0.78	0.78	0.94	0.88	0.83
MgO	9.51	9.42	9.30	9.24	9.39	9.44	9.68	9.25	9.47	9.54	9.44	9.36	9.61	9.38	9.64	9.80	9.86	9.81	9.78	9.89	10.06
CaO	3.66	3.61	3.66	3.60	3.58	3.61	3.58	3.57	3.45	3.56	3.59	3.51	3.43	3.36	3.16	3.22	3.02	3.02	2.69	2.60	2.56
Total	100.66	100.58	100.77	100.28	100.75	100.97	102.04	99.84	100.07	100.49	100.97	100.52	100.82	100.64	100.56	100.78	100.73	100.37	99.86	100.66	100.64
Number of anions on the basis of 12 oxygen atoms																					
Si ⁴⁺	2.99	2.99	2.98	2.98	3.00	3.00	2.98	3.01	3.00	2.98	2.98	3.01	2.99	3.00	3.00	2.99	3.00	3.00	3.00	2.99	2.98
Al ³⁺	1.99	2.00	2.00	2.02	2.00	1.99	2.00	2.01	2.01	2.01	2.00	2.01	2.00	2.00	2.00	1.99	1.98	2.01	2.00	2.01	2.02
Cr ³⁺	0.00	0.01	0.01	0.01	0.01	0.01	0.01	0.01	0.01	0.01	0.01	0.01	0.01	0.01	0.00	0.01	0.02	0.01	0.02	0.01	0.01
Fe ³⁺	0.02	0.01	0.02	0.01	-	-	0.03	-	-	0.01	0.03	-	0.01	-	-	0.02	-	-	-	0.01	0.01
Fe ²⁺	1.56	1.57	1.58	1.59	1.59	1.58	1.56	1.57	1.58	1.56	1.56	1.57	1.57	1.60	1.59	1.57	1.59	1.57	1.58	1.60	1.58
Mn ²⁺	0.06	0.05	0.05	0.05	0.05	0.06	0.05	0.05	0.05	0.05	0.06	0.05	0.05	0.05	0.06	0.06	0.05	0.05	0.06	0.06	0.05
Mg ²⁺	1.08	1.07	1.05	1.05	1.06	1.07	1.08	1.06	1.08	1.08	1.07	1.06	1.09	1.06	1.09	1.11	1.12	1.11	1.12	1.12	1.14
Ca ²⁺	0.30	0.29	0.30	0.29	0.29	0.29	0.29	0.29	0.28	0.29	0.29	0.29	0.28	0.27	0.26	0.26	0.25	0.25	0.22	0.21	0.21
Σ_{cat}	8.00	7.99	7.99	8.00	8.00	8.00	8.00	8.00	8.01	7.99	8.00	8.00	8.00	7.99	8.00	8.01	8.01	8.00	8.00	8.01	8.00
Anion	12.00	12.00	12.00	12.00	12.00	12.00	12.00	12.02	12.00	12.00	12.00	12.02	12.00	12.00	12.00	12.00	12.00	12.01	12.01	12.00	12.00
XGrss	0.10	0.10	0.10	0.10	0.10	0.10	0.10	0.10	0.09	0.10	0.10	0.10	0.09	0.09	0.09	0.09	0.08	0.08	0.07	0.07	0.07
XAlm	0.52	0.53	0.53	0.53	0.53	0.53	0.52	0.53	0.53	0.52	0.52	0.53	0.53	0.53	0.53	0.52	0.53	0.53	0.53	0.54	0.53
XPyrr	0.36	0.36	0.35	0.35	0.36	0.36	0.36	0.36	0.36	0.36	0.36	0.36	0.36	0.36	0.36	0.37	0.37	0.37	0.37	0.37	0.38
XSpss	0.02	0.02	0.02	0.02	0.02	0.02	0.02	0.02	0.02	0.02	0.02	0.02	0.02	0.02	0.02	0.02	0.02	0.02	0.02	0.02	0.02
D	0.02	0.02	0.03	0.03	0.03	0.05	0.05	0.05	0.07	0.07	0.07	0.09	0.09	0.09	0.10	0.10	0.12	0.12	0.14	0.14	0.16

Table F: continued

Sample	L2t-7	L2t-7	L2t-7	L2t-7	L2t-7	L2t-7	L2t-7	L2t-7	L2t-7	L2t-7	L2t-7	L2t-7	L2t-7	L2t-7	L2t-7	L2t-7	L2t-7	L2t-7	L2t-7	L2t-7	L2t-7
Mineral	Grt	Grt	Grt	Grt	Grt	Grt	Grt	Grt	Grt	Grt	Grt	Grt	Grt	Grt	Grt	Grt	Grt	Grt	Grt	Grt	Grt
Generation	A-1	A-1	A-1	A-1	A-1	A-1	A-1	A-1	A-1	A-1	A-1	A-1	A-1	A-1	A-1	A-1	A-1	A-1	A-1	A-1	A-1
SiO ₂	39.47	39.22	39.13	38.75	39.57	39.61	39.84	39.81	39.65	39.75	39.55	39.63	39.76	39.29	39.51	39.61	39.57	39.60	39.52	39.64	39.69
Al ₂ O ₃	22.30	22.39	22.41	22.10	22.36	22.54	22.27	22.37	22.33	22.34	22.16	22.35	22.49	22.51	22.50	22.44	22.42	22.57	22.50	22.46	22.44
Cr ₂ O ₃	0.13	0.16	0.19	0.14	0.29	0.26	0.20	0.22	0.26	0.14	0.14	0.19	0.23	0.21	0.21	0.14	0.16	0.24	0.27	-	0.21
Fe ₂ O ₃	0.01	-	0.28	-	-	-	-	-	-	-	0.12	-	-	0.64	0.22	0.41	0.02	0.41	-	-	-
FeO	24.98	25.13	25.00	24.17	24.64	24.93	24.80	24.80	25.14	24.97	24.90	24.88	24.91	24.72	24.81	25.21	25.01	24.68	24.68	24.99	24.88
MnO	0.81	0.88	0.82	0.78	0.69	0.78	0.74	0.70	0.74	0.87	0.82	0.76	0.75	0.78	0.86	0.77	0.91	0.83	0.84	0.79	0.89
MgO	10.32	9.95	10.10	10.08	10.44	10.21	10.57	10.59	10.39	10.48	10.50	10.38	10.44	10.45	10.47	10.41	10.39	10.59	10.53	10.40	10.37
CaO	2.34	2.35	2.31	2.51	2.19	2.19	2.22	2.13	2.12	2.21	2.22	2.22	2.22	2.22	2.26	2.20	2.24	2.31	2.25	2.23	2.26
Total	100.36	100.08	100.24	98.53	100.18	100.52	100.64	100.62	100.63	100.76	100.41	100.41	100.80	100.82	100.84	101.19	100.72	101.23	100.59	100.51	100.74
Number of anions on the basis of 12 oxygen atoms																					
Si ⁴⁺	3.00	2.99	2.98	3.00	3.01	3.01	3.01	3.01	3.00	3.01	3.00	3.01	3.00	2.97	2.99	2.99	2.99	2.98	2.99	3.00	3.00
Al ³⁺	2.00	2.01	2.01	2.01	2.00	2.02	1.99	1.99	1.99	1.99	1.98	2.00	2.00	2.01	2.00	1.99	2.00	2.00	2.01	2.01	2.00
Cr ³⁺	0.01	0.01	0.01	0.01	0.02	0.02	0.01	0.01	0.02	0.01	0.01	0.01	0.01	0.01	0.01	0.01	0.01	0.01	0.02	0.00	0.01
Fe ³⁺	-	-	0.02	-	-	-	-	-	-	-	0.01	-	-	0.04	0.01	0.02	-	0.02	-	-	-
Fe ²⁺	1.59	1.60	1.59	1.56	1.57	1.58	1.57	1.57	1.59	1.58	1.58	1.58	1.57	1.56	1.57	1.59	1.58	1.55	1.56	1.58	1.57
Mn ²⁺	0.05	0.06	0.05	0.05	0.04	0.05	0.05	0.04	0.05	0.06	0.05	0.05	0.05	0.05	0.06	0.05	0.06	0.05	0.05	0.05	0.06
Mg ²⁺	1.17	1.13	1.15	1.16	1.18	1.15	1.19	1.19	1.17	1.18	1.19	1.17	1.18	1.18	1.18	1.17	1.17	1.19	1.19	1.17	1.17
Ca ²⁺	0.19	0.19	0.19	0.21	0.18	0.18	0.18	0.17	0.17	0.18	0.18	0.18	0.18	0.18	0.18	0.18	0.18	0.19	0.18	0.18	0.18
Σ_{cat}	8.01	7.99	8.00	8.00	8.00	8.01	8.00	7.98	7.99	8.01	8.00	8.00	7.99	8.00	8.00	8.00	7.99	7.99	8.00	7.99	7.99
Anion	12.00	12.00	12.00	12.01	12.02	12.02	12.01	12.02	12.01	12.01	12.00	12.01	12.01	12.00	12.00	12.00	12.00	12.00	12.00	12.01	12.01
XGrss	0.06	0.06	0.06	0.07	0.06	0.06	0.06	0.06	0.06	0.06	0.06	0.06	0.06	0.06	0.06	0.06	0.06	0.06	0.06	0.06	0.06
XAlm	0.53	0.54	0.53	0.52	0.53	0.53	0.53	0.53	0.53	0.53	0.53	0.53	0.53	0.53	0.53	0.53	0.53	0.52	0.52	0.53	0.53
XPyrr	0.39	0.38	0.38	0.39	0.40	0.39	0.40	0.40	0.39	0.39	0.40	0.39	0.39	0.40	0.40	0.39	0.39	0.40	0.40	0.39	0.39
XSpss	0.02	0.02	0.02	0.02	0.01	0.02	0.02	0.02	0.02	0.02	0.02	0.02	0.02	0.02	0.02	0.02	0.02	0.02	0.02	0.02	0.02
D	0.16	0.16	0.17	0.17	0.29	0.29	0.29	0.31	0.31	0.33	0.33	0.34	0.34	0.34	0.36	0.36	0.36	0.38	0.38	0.38	0.40

Table F: continued

Sample	L2t-7	L2t-7	L2t-7	L2t-7	L2t-7	L2t-7	L2t-7	L2t-7	L2t-7	L2t-7	L2t-7	L2t-7	L2t-7	L2t-7	L2t-7	L2t-7	L2t-7	L2t-7	L2t-7	L2t-7	L2t-7	
Mineral	Grt	Grt	Grt	Grt	Grt	Grt	Grt	Grt	Grt	Grt	Grt	Grt	Grt	Grt	Grt	Grt	Grt	Grt	Grt	Grt	Grt	
Generation	A-1	A-1	A-1	A-1	A-1	A-1	A-1	A-1	A-1	A-1	A-1	A-1	A-1	A-1	A-1	A-1	A-1	A-1	A-1	A-1	B-1	B-1
SiO ₂	39.54	39.40	39.49	39.49	39.55	39.33	39.80	39.56	39.80	39.43	39.76	39.38	39.37	39.62	39.72	39.72	39.47	39.39	39.21	39.34	39.41	
Al ₂ O ₃	22.51	22.60	22.33	22.61	22.37	22.60	22.67	22.60	22.66	22.48	22.57	22.21	22.72	22.46	22.33	22.38	22.40	22.13	22.43	22.22	22.34	
Cr ₂ O ₃	0.20	0.16	0.22	-	0.19	0.15	0.14	-	-	0.19	0.22	0.19	0.14	0.13	0.14	0.26	0.20	0.25	0.30	0.13	0.18	
Fe ₂ O ₃	0.05	0.14	0.00	0.31	-	0.46	0.04	-	0.06	0.11	0.02	0.13	0.30	0.12	-	-	-	0.18	-	0.17	-	
FeO	24.90	24.76	24.43	24.69	24.52	24.58	25.08	24.91	24.87	24.70	24.90	24.88	24.79	25.17	24.90	25.13	25.44	24.98	25.25	24.85	25.36	
MnO	0.65	0.82	0.82	0.88	0.86	0.89	0.91	0.84	0.83	0.80	0.74	0.70	0.82	0.73	0.76	0.85	0.68	0.89	0.82	0.88	0.81	
MgO	10.52	10.41	10.51	10.51	10.49	10.44	10.53	10.42	10.75	10.54	10.78	10.64	10.61	10.74	10.93	10.78	10.71	10.89	10.65	10.34	10.19	
CaO	2.30	2.32	2.29	2.26	2.29	2.29	2.20	2.23	2.13	2.22	2.09	1.99	1.99	1.81	1.68	1.61	1.52	1.42	1.33	2.24	2.16	
Total	100.67	100.61	100.09	100.75	100.27	100.74	101.37	100.56	101.10	100.47	101.08	100.12	100.74	100.78	100.46	100.73	100.42	100.13	99.99	100.17	100.45	
Number of anions on the basis of 12 oxygen atoms																						
Si ⁴⁺	2.99	2.98	3.00	2.98	3.00	2.98	2.99	3.00	2.99	2.99	2.99	3.00	2.98	2.99	3.01	3.00	2.99	3.00	2.99	2.99	2.99	
Al ³⁺	2.01	2.02	2.00	2.01	2.00	2.01	2.01	2.02	2.01	2.01	2.00	1.99	2.02	2.00	1.99	1.99	2.00	1.98	2.01	1.99	2.00	
Cr ³⁺	0.01	0.01	0.01	0.00	0.01	0.01	0.01	0.00	0.00	0.01	0.01	0.01	0.01	0.01	0.01	0.02	0.01	0.02	0.02	0.01	0.01	
Fe ³⁺	-	0.01	-	0.02	-	0.03	-	-	-	0.01	-	0.01	0.02	0.01	-	-	-	0.01	-	0.01	-	
Fe ²⁺	1.57	1.57	1.55	1.56	1.56	1.55	1.58	1.58	1.56	1.57	1.57	1.58	1.57	1.59	1.58	1.59	1.61	1.59	1.61	1.58	1.61	
Mn ²⁺	0.04	0.05	0.05	0.06	0.06	0.06	0.06	0.05	0.05	0.05	0.05	0.04	0.05	0.05	0.05	0.05	0.04	0.06	0.05	0.06	0.05	
Mg ²⁺	1.19	1.17	1.19	1.18	1.19	1.18	1.18	1.18	1.20	1.19	1.21	1.21	1.20	1.21	1.23	1.21	1.21	1.23	1.21	1.17	1.15	
Ca ²⁺	0.19	0.19	0.19	0.18	0.19	0.19	0.18	0.18	0.17	0.18	0.17	0.16	0.16	0.15	0.14	0.13	0.12	0.12	0.11	0.18	0.18	
Σ_{cat}	8.00	8.00	7.99	7.99	8.01	8.01	8.01	8.01	7.98	8.01	8.00	8.00	8.01	8.01	8.01	7.99	7.98	8.01	8.00	7.99	7.99	
Anion	12.00	12.00	12.01	12.00	12.01	12.00	12.00	12.00	12.00	12.00	12.00	12.00	12.00	12.00	12.01	12.01	12.00	12.00	12.00	12.00	12.00	
XGrss	0.06	0.06	0.06	0.06	0.06	0.06	0.06	0.06	0.06	0.06	0.06	0.05	0.05	0.05	0.05	0.04	0.04	0.04	0.04	0.06	0.06	
XAlm	0.53	0.53	0.52	0.52	0.52	0.52	0.53	0.53	0.52	0.52	0.52	0.53	0.53	0.53	0.53	0.53	0.54	0.53	0.54	0.53	0.54	
XPyr	0.40	0.39	0.40	0.40	0.40	0.40	0.39	0.39	0.40	0.40	0.40	0.40	0.40	0.40	0.41	0.41	0.40	0.41	0.41	0.39	0.39	
XSpss	0.01	0.02	0.02	0.02	0.02	0.02	0.02	0.02	0.02	0.02	0.02	0.01	0.02	0.02	0.02	0.02	0.01	0.02	0.02	0.02	0.02	
D	0.40	0.40	0.42	0.43	0.43	0.45	0.45	0.47	0.47	0.48	0.50	0.50	0.52	0.52	0.55	0.55	0.57	0.57	0.59	0.00	0.00	

Table F: continued

Sample	L2t-7	L2t-7	L2t-7	L2t-7	L2t-7	L2t-7	L2t-7	L2t-7	L2t-7	L2t-7	L2t-7	L2t-7	L2t-7	L2t-7	L2t-7	L2t-7	L2t-7	L2t-7	L2t-7	L2t-7	L2t-7
Mineral	Grt	Grt	Grt	Grt	Grt	Grt	Grt	Grt	Grt	Grt	Grt	Grt	Grt	Grt	Grt	Grt	Grt	Grt	Grt	Grt	Grt
Generation	B-1	B-1	B-1	B-1	B-1	B-1	B-1	B-1	B-1	B-1	B-1	B-1	B-1	B-1	B-1	B-1	B-1	B-1	B-1	B-1	B-1
SiO ₂	39.39	39.54	39.28	39.12	39.09	39.13	39.01	38.96	38.81	39.10	39.04	39.24	38.84	39.18	39.45	39.73	39.41	39.62	39.61	39.23	39.28
Al ₂ O ₃	22.36	22.37	22.43	22.47	22.33	21.97	22.10	22.43	22.14	22.16	22.10	22.43	22.36	21.85	22.47	22.87	22.27	22.34	22.70	22.45	22.57
Cr ₂ O ₃	0.17	0.16	0.15	0.17	0.15	0.15	0.16		0.20	0.13	0.14	0.18	0.18	0.24	0.21	0.22	0.23	0.13	0.21	0.00	0.16
Fe ₂ O ₃	-	-	0.34	0.45	0.40	0.27	-	-	-	-	-	-	-	-	-	-	-	0.02	-	-	-
FeO	25.22	25.05	25.31	25.02	24.98	25.02	24.82	26.56	25.95	25.44	25.09	24.90	24.65	24.67	24.71	24.71	24.81	24.95	24.81	24.73	24.51
MnO	0.78	0.85	0.89	0.75	0.83	0.81	0.75	0.80	0.75	0.72	0.76	0.73	0.69	0.74	0.79	0.73	0.67	0.81	0.83	0.88	0.76
MgO	10.22	10.35	10.23	10.33	10.24	10.09	10.02	8.90	9.23	9.82	10.24	10.30	10.40	10.53	10.59	10.58	10.48	10.51	10.53	10.37	10.43
CaO	2.13	2.10	1.97	2.02	2.08	2.31	2.42	2.13	2.03	1.94	1.92	1.90	1.97	1.96	2.05	2.13	2.15	2.25	2.21	2.13	2.19
Total	100.27	100.42	100.60	100.33	100.10	99.75	99.28	99.78	99.11	99.31	99.29	99.68	99.09	99.17	100.27	100.97	100.02	100.63	100.90	99.79	99.90
Number of anions on the basis of 12 oxygen atoms																					
Si ⁴⁺	3.00	3.00	2.98	2.98	2.98	3.00	3.00	3.00	3.00	3.01	3.00	3.00	2.98	3.01	2.99	2.99	3.00	3.00	2.99	2.99	2.99
Al ³⁺	2.00	2.00	2.01	2.01	2.01	1.98	2.00	2.04	2.02	2.01	2.00	2.02	2.02	1.98	2.01	2.03	2.00	1.99	2.02	2.02	2.03
Cr ³⁺	0.01	0.01	0.01	0.01	0.01	0.01	0.01		0.01	0.01	0.01	0.01	0.01	0.01	0.01	0.01	0.01	0.01	0.01		0.01
Fe ³⁺	-	-	0.02	0.03	0.02	0.02	-	-	-	-	-	-	-	-	-	-	-	-	-	-	-
Fe ²⁺	1.60	1.59	1.61	1.59	1.59	1.60	1.59	1.71	1.68	1.64	1.61	1.59	1.58	1.58	1.57	1.56	1.58	1.58	1.57	1.58	1.56
Mn ²⁺	0.05	0.05	0.06	0.05	0.05	0.05	0.05	0.05	0.05	0.05	0.05	0.05	0.05	0.05	0.05	0.05	0.04	0.05	0.05	0.06	0.05
Mg ²⁺	1.16	1.17	1.16	1.17	1.16	1.15	1.15	1.02	1.07	1.13	1.17	1.17	1.19	1.21	1.20	1.19	1.19	1.19	1.18	1.18	1.18
Ca ²⁺	0.17	0.17	0.16	0.16	0.17	0.19	0.20	0.18	0.17	0.16	0.16	0.16	0.16	0.16	0.17	0.17	0.18	0.18	0.18	0.17	0.18
Σ_{cat}	7.99	7.99	8.01	8.00	7.99	8.00	8.00	8.00	8.00	8.01	8.00	8.00	7.99	8.00	8.00	8.00	8.00	8.00	8.00	8.00	8.00
Anion	12.00	12.01	12.00	12.00	12.00	12.00	12.00	12.02	12.02	12.02	12.00	12.02	12.00	12.01	12.01	12.01	12.01	12.00	12.00	12.00	12.01
XGrss	0.06	0.06	0.05	0.06	0.06	0.06	0.07	0.06	0.06	0.05	0.05	0.05	0.05	0.05	0.06	0.06	0.06	0.06	0.06	0.06	0.06
XAlm	0.54	0.53	0.54	0.53	0.53	0.53	0.53	0.58	0.57	0.55	0.54	0.54	0.53	0.53	0.53	0.53	0.53	0.53	0.52	0.53	0.53
XPyrr	0.39	0.39	0.39	0.39	0.39	0.38	0.38	0.35	0.36	0.38	0.39	0.40	0.40	0.40	0.40	0.40	0.40	0.40	0.40	0.39	0.40
XSpss	0.02	0.02	0.02	0.02	0.02	0.02	0.02	0.02	0.02	0.02	0.02	0.02	0.02	0.02	0.02	0.02	0.01	0.02	0.02	0.02	0.02
D	0.00	0.00	0.00	0.00	0.02	0.02	0.02	0.16	0.16	0.16	0.16	0.16	0.16	0.18	0.18	0.18	0.20	0.20	0.20	0.22	0.22

Table F: continued

Sample	L2t-7	L2t-7	L2t-7	L2t-7	L2t-7	L2t-7	L2t-7	L2t-7	L2t-7	L2t-7	L2t-7	L2t-7	L2t-7	L2t-7	L2t-7	L2t-7	L2t-7	L2t-7	L2t-7	L2t-8	L2t-9
Mineral	Grt	Grt	Grt	Grt	Grt	Grt	Grt	Grt	Grt	Grt	Grt	Grt	Grt	Grt	Grt	Grt	Grt	Grt	Grt	Grt	Grt
Generation	B-1	B-2	B-2	B-2	B-2	B-2	B-2	B-2	B-2	B-2	B-2	B-2	B-2	B-2	B-2	B-2	B-2	B-2	B-2	B-2	B-2
SiO ₂	39.46	39.34	39.41	39.39	39.54	39.28	39.12	39.09	39.13	39.01	38.96	38.81	39.10	39.04	39.24	38.84	39.18	39.45	39.73	39.41	39.62
Al ₂ O ₃	22.45	22.22	22.34	22.36	22.37	22.43	22.47	22.33	21.97	22.10	22.43	22.14	22.16	22.10	22.43	22.36	21.85	22.47	22.87	22.27	22.34
Cr ₂ O ₃	0.20	0.13	0.18	0.17	0.16	0.15	0.17	0.15	0.15	0.16	0.00	0.20	0.13	0.14	0.18	0.18	0.24	0.21	0.22	0.23	0.13
Fe ₂ O ₃	-	0.17	-	-	-	0.34	0.45	0.40	0.27	-	-	-	-	-	-	-	-	-	-	-	-
FeO	24.70	24.85	25.36	25.22	25.05	25.31	25.02	24.98	25.02	24.82	26.56	25.95	25.44	25.09	24.90	24.65	24.67	24.71	24.71	24.81	24.95
MnO	0.69	0.88	0.81	0.78	0.85	0.89	0.75	0.83	0.81	0.75	0.80	0.75	0.72	0.76	0.73	0.69	0.74	0.79	0.73	0.67	0.81
MgO	10.38	10.34	10.19	10.22	10.35	10.23	10.33	10.24	10.09	10.02	8.90	9.23	9.82	10.24	10.30	10.40	10.53	10.59	10.58	10.48	10.51
CaO	2.09	2.24	2.16	2.13	2.10	1.97	2.02	2.08	2.31	2.42	2.13	2.03	1.94	1.92	1.90	1.97	1.96	2.05	2.13	2.15	2.25
Total	99.97	100.17	100.45	100.28	100.41	100.59	100.33	100.09	99.75	99.28	99.78	99.12	99.32	99.28	99.68	99.09	99.17	100.26	100.98	100.03	100.63
Number of anions on the bases of 12 oxygen atoms																					
Si ⁴⁺	3.01	2.99	2.99	3.00	3.00	2.98	2.98	2.98	3.00	3.00	3.00	3.00	3.01	3.00	3.00	2.98	3.01	2.99	2.99	3.00	3.00
Al ³⁺	2.02	1.99	2.00	2.00	2.00	2.01	2.01	2.01	1.98	2.00	2.04	2.02	2.01	2.00	2.02	2.02	1.98	2.01	2.03	2.00	1.99
Cr ³⁺	0.01	0.01	0.01	0.01	0.01	0.01	0.01	0.01	0.01	0.01	0.00	0.01	0.01	0.01	0.01	0.01	0.01	0.01	0.01	0.01	0.01
Fe ³⁺	-	0.01	-	-	-	0.02	0.03	0.02	0.02	-	-	-	-	-	-	-	-	-	-	-	-
Fe ²⁺	1.57	1.58	1.61	1.60	1.59	1.61	1.59	1.59	1.60	1.59	1.71	1.68	1.64	1.61	1.59	1.58	1.58	1.57	1.56	1.58	1.58
Mn ²⁺	0.04	0.06	0.05	0.05	0.05	0.06	0.05	0.05	0.05	0.05	0.05	0.05	0.05	0.05	0.05	0.05	0.05	0.05	0.05	0.04	0.05
Mg ²⁺	1.18	1.17	1.15	1.16	1.17	1.16	1.17	1.16	1.15	1.15	1.02	1.07	1.13	1.17	1.17	1.19	1.21	1.20	1.19	1.19	1.19
Ca ²⁺	0.17	0.18	0.18	0.17	0.17	0.16	0.16	0.17	0.19	0.20	0.18	0.17	0.16	0.16	0.16	0.16	0.16	0.17	0.17	0.18	0.18
Σ_{cat}	8.00	8.00	8.00	8.00	8.00	8.00	8.00	8.00	8.00	8.00	8.00	8.00	8.00	8.00	8.00	8.00	8.00	8.00	8.00	8.00	8.00
Anion	12.02	12.00	12.00	12.00	12.01	12.00	12.00	12.00	12.00	12.00	12.02	12.02	12.02	12.00	12.02	12.00	12.01	12.01	12.01	12.01	12.00
XGrss	0.06	0.06	0.06	0.06	0.06	0.05	0.06	0.06	0.06	0.07	0.06	0.06	0.05	0.05	0.05	0.05	0.05	0.06	0.06	0.06	0.06
XAlm	0.53	0.53	0.54	0.54	0.53	0.54	0.53	0.53	0.53	0.53	0.58	0.57	0.55	0.54	0.54	0.53	0.53	0.53	0.53	0.53	0.53
XPyr	0.40	0.39	0.39	0.39	0.39	0.39	0.39	0.39	0.38	0.38	0.35	0.36	0.38	0.39	0.40	0.40	0.40	0.40	0.40	0.40	0.40
XSpss	0.02	0.02	0.02	0.02	0.02	0.02	0.02	0.02	0.02	0.02	0.02	0.02	0.02	0.02	0.02	0.02	0.02	0.02	0.02	0.01	0.02
D	0.22	0.00	0.00	0.00	0.00	0.00	0.00	0.02	0.02	0.02	0.16	0.16	0.16	0.16	0.16	0.16	0.18	0.18	0.18	0.20	0.20

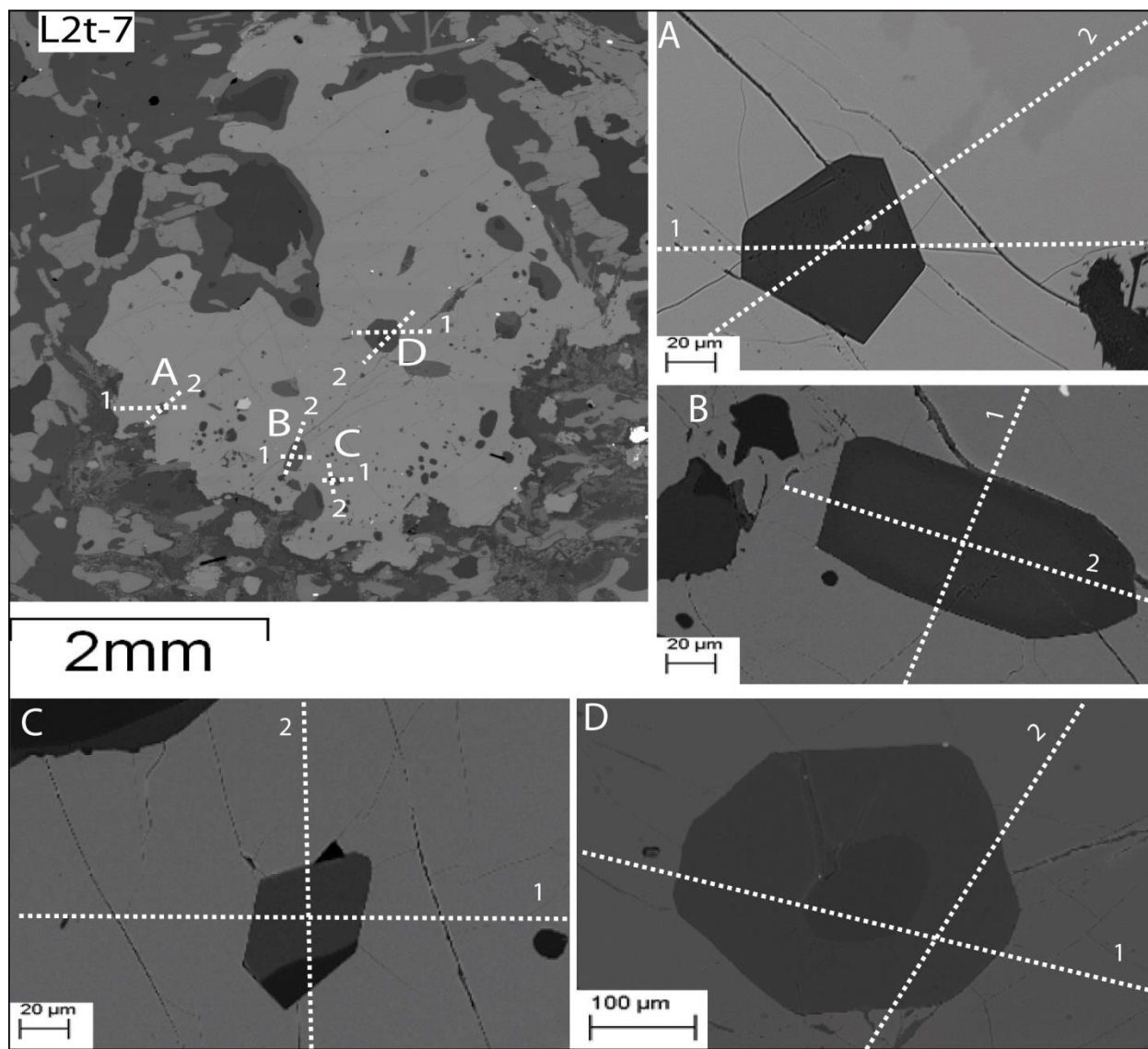


Figure 1: BSE images illustrating the detailed electron microprobe analyses of cross-sections (dotted white lines) through the plagioclase inclusions into garnet host in sample L2t-7. (A-D) Show magnified inclusions within garnet.

